SIMULATION OF REGIONAL GROUND-WATER FLOW IN THE CAMBRIAN–ORDOVICIAN AQUIFER SYSTEM IN THE NORTHERN MIDWEST, UNITED STATES

U. S. GEOLOGICAL SURVEY PROFESSIONAL PAPER 1405–C

AVAILABILITY OF BOOKS AND MAPS OF THE U.S. GEOLOGICAL SURVEY

Instructions on ordering publications of the U.S. Geological Survey, along with prices of the last offerings, are given in the current-year issues of the monthly catalog "New Publications of the U.S. Geological Survey." Prices of available U.S. Geological Survey publications released prior to the current year are listed in the most recent annual "Price and Availability List." Publications that are listed in various U.S. Geological Survey catalogs (**see back inside cover**) but not listed in the most recent annual "Price and Availability List" are no longer available.

Prices of reports released to the open files are given in the listing "U.S. Geological Survey Open-File Reports," updated monthly, which is for sale in microfiche from U.S. Geological Survey Book and Open-File Report Sales, Box 25286, Denver, CO 80225. Reports released through the NTIS may be obtained by writing to the National Technical Information Service, U.S. Department of Commerce, Springfield, VA 22161; please include NTIS report number with inquiry.

Order U.S. Geological Survey publications **by mail** or **over the counter** from the offices given below.

BY MAIL

Books

Professional Papers, Bulletins, Water-Supply Papers, Techniques of Water-Resources Investigations, Circulars, publications of general interest (such as leaflets, pamphlets, booklets), single copies of Earthquakes & Volcanoes, Preliminary Determination of Epicenters, and some miscellaneous reports, including some of the foregoing series that have gone out of print at the Superintendent of Documents, are obtainable by mail from

U.S. Geological Survey, Book and Open-File Report Sales
Box 25286
Denver, CO 80225

Subscriptions to periodicals (Earthquakes & Volcanoes and Preliminary Determination of Epicenters) can be obtained ONLY from the

Superintendent of Documents
Government Printing Office
Washington, D.C. 20402

(Check or money order must be payable to Superintendent of Documents.)

Maps

For maps, address mail orders to

U.S. Geological Survey, Map Sales
Box 25286
Denver, CO 80225

Residents of Alaska may order maps from

U.S. Geological Survey, Map Sales
101 Twelfth Ave. - Box 12
Fairbanks, AK 99701

OVER THE COUNTER

Books

Books of the U.S. Geological Survey are available over the counter at the following U.S. Geological Survey Offices, all of which are authorized agents of the Superintendent of Documents:

- **ANCHORAGE, Alaska**—Rm. 101, 4230 University Dr.
- **LAKEWOOD, Colorado**—Federal Center, Bldg. 810
- **MENLO PARK, California**—Bldg. 3 (Stop 533), Rm. 3128, 345 Middlefield Rd.
- **RESTON, Virginia**—503 National Center, Rm. 1C402, 12201 Sunrise Valley Dr.
- **SALT LAKE CITY, Utah**—Federal Bldg., Rm. 8105, 125 South State St.
- **SPOKANE, Washington**—U.S. Post Office Bldg., Rm. 135, West 904 Riverside Ave.
- **WASHINGTON, D.C.**—Main Interior Bldg., 2600 corridor, 18th and C Sts., NW.

Maps

Maps may be purchased over the counter at the U.S. Geological Survey offices where books are sold (all addresses in above list) and at the following U.S. Geological Survey offices:

- **DENVER, Colorado**—Map Distribution, Bldg. 810, Federal Center
- **FAIRBANKS, Alaska**—New Federal Bldg., 101 Twelfth Ave.
- **ROLLA, Missouri**—1400 Independence Rd.

Simulation of Regional Ground-Water Flow in the Cambrian-Ordovician Aquifer System in the Northern Midwest, United States

By R.J. MANDLE and A.L. KONTIS

REGIONAL AQUIFER-SYSTEM ANALYSIS—NORTHERN MIDWEST

U.S. GEOLOGICAL SURVEY PROFESSIONAL PAPER 1405-C

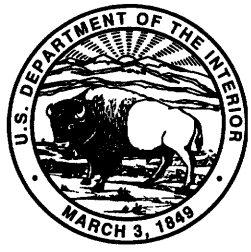

UNITED STATES GOVERNMENT PRINTING OFFICE, WASHINGTON: 1992

U.S. DEPARTMENT OF THE INTERIOR

MANUEL LUJAN, Jr., *Secretary*

U.S. GEOLOGICAL SURVEY

Dallas L. Peck, *Director*

Library of Congress Cataloging in Publication Data

Mandle, Richard J.
Simulation of regional ground-water flow in the Cambrian-Ordovician aquifer system in the northern Midwest, United States.

(Regional aquifer-system analysis) (U.S. Geological Survey professional paper ; 1405–C)
Bibliography; p.
Supt. of Docs. no.: I 19.16:1405–C
1. Groundwater flow—Middle West—Simulation methods. 2. Aquifers—Middle West—Simulation methods. I. Kontis, A.L. II. Title. III. Series. IV. Series: Geological Survey professional paper ; 1405–C
GB1197.7.M36 1991 551.49'0977 86–607911

For sale by Book and Open-File Report Sales, U.S. Geological Survey, Federal Center, Box 25286, Denver, CO 80225

FOREWORD

THE REGIONAL AQUIFER-SYSTEM ANALYSIS PROGRAM

The Regional Aquifer-System Analysis (RASA) Program was started in 1978 following a congressional mandate to develop quantitative appraisals of the major ground-water systems of the United States. The RASA Program represents a systematic effort to study a number of the Nation's most important aquifer systems, which in aggregate underlie much of the country and which represent an important component of the Nation's total water supply. In general, the boundaries of these studies are identified by the hydrologic extent of each system and accordingly transcend the political subdivisions to which investigations have often arbitrarily been limited in the past. The broad objective for each study is to assemble geologic, hydrologic, and geochemical information, to analyze and develop an understanding of the system, and to develop predictive capabilities that will contribute to the effective management of the system. The use of computer simulation is an important element of the RASA studies, both to develop an understanding of the natural, undisturbed hydrologic system and the changes brought about in it by human activities, and to provide a means of predicting the regional effects of future pumping or other stresses.

The final interpretive results of the RASA Program are presented in a series of U.S. Geological Survey Professional Papers that describe the geology, hydrology, and geochemistry of each regional aquifer system. Each study within the RASA Program is assigned a single Professional Paper number, and where the volume of interpretive material warrants, separate topical chapters that consider the principal elements of the investigation may be published. The series of RASA interpretive reports begins with Professional Paper 1400 and thereafter will continue in numerical sequence as the interpretive products of subsequent studies become available.

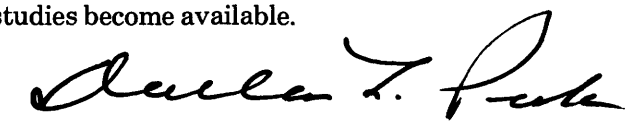

Dallas L. Peck
Director

CONTENTS

ILLUSTRATIONS

TABLE

CONVERSION FACTORS AND VERTICAL DATUM

For readers who wish to convert measurements from the inch-pound system of units to the metric system of units, the conversion factors are listed below:

Multiply inch-pound units	By	To obtain metric units
	Length	
inch (in)	25.40	millimeter (mm)
foot (ft)	0.3048	meter (m)
mile (mi)	1.609	kilometer (km)
	Area	
square foot (ft^2)	0.09290	square meter (m^2)
square mile (mi^2)	2.590	square kilometer (km^2)
	Volume	
gallon (gal)	0.003785	cubic meter (m^3)
million gallons (Mgal)	3,785	cubic meter (m^3)
cubic foot (ft^3)	0.02832	cubic meter (m^3)
	Flow	
foot per second (ft/s)	0.3048	meter per second (m/s)
foot per day (ft/d)	0.3048	meter per day (m/d)
cubic foot per second (ft^3/s)	0.02832	cubic meter per second (m^3/s)
cubic foot per second per square mile [$(ft^3/s)/mi^2$]	0.01093	cubic meter per second per square kilometer [$(m^3/s)/km^2$]
inch per year (in/yr)	25.4	millimeter per year (mm/yr)
million gallons per day (Mgal/d)	0.04381	cubic meter per second (m^3/s)
	Temperature	
degree Fahrenheit (°F)	°C=0.5556(°F-32)	degree Celsius (°C)
	Hydraulic conductivity	
foot per day (ft/d)	0.3048	meter per day (m/d)
foot per second (ft/s)	26,330	meter per day (m/d)
	Transmissivity	
square foot per day (ft^2/d)	0.09290	square meter per day (m^2/d)
	Pressure	
bar	100	kilopascal (kPa)
pound per square inch (lb/in^2)	6.895	kilopascal (kPa)
pound per square inch (lb/in^2)	703.1	kilogram-force per square meter (kgf/m^2)
	Dynamic viscosity	
pound-force-second per square foot ($lbf{\cdot}s/ft^2$)	47.88	pascal-second (Pa·s)
slug per foot-second (slug/ft·s)	47.88	pascal-second (Pa·s)
	Specific weight	
pound-force per cubic foot (lbf/ft^3)	157.1	newton per cubic meter (N/m^3)
	Acceleration	
foot per second squared (ft/s^2)	0.3048	meter per second squared (m/s^2)
	Density	
slug per cubic foot ($slug/ft^3$)	515.4	kilogram per cubic meter (kg/m^3)
	EQUIVALENTS	
	Inch-pound unit	*Metric unit*
Acceleration of gravity	32.17 ft/s^2	9.806 m/s^2
Density of pure water (68 °F, 20 °C)	1.936 $slug/ft^3$	997.6 kg/m^3
Specific weight of water (59 °F, 15 °C)	62.4 lb/ft^3	9,800 N/m^3
Standard atmosphere	14.70 lb/in^2	101.325 kPa

Sea level: In this report "sea level" refers to the National Geodetic Vertical Datum of 1929 (NGVD of 1929)—a geodetic datum derived from a general adjustment of the first-order level nets of both the United States and Canada, formerly called Sea Level Datum of 1929.

SIMULATION OF REGIONAL GROUND-WATER FLOW IN THE CAMBRIAN-ORDOVICIAN AQUIFER SYSTEM IN THE NORTHERN MIDWEST, UNITED STATES

By R.J. MANDLE and A.L. KONTIS

ABSTRACT

A six-State area in the northern Midwest of the United States has become increasingly dependent on ground water from the Cambrian-Ordovician aquifer system, which consists of a sequence of sandstones, carbonate rocks, and shales. Ground-water withdrawals from the aquifer system began in the late 1800's and increased to approximately 684 million gallons per day (1,058 cubic feet per second) by 1980. This withdrawal has caused more than 900 feet of decline in the potentiometric surface of the aquifer system in parts of the Chicago, Ill., area. Pumping in Minneapolis-St. Paul, Minn., Milwaukee, Wis., and central Iowa has produced a few hundreds of feet of water-level decline.

A quasi-three-dimensional ground-water flow model was developed to improve understanding of the regional ground-water flow system by simulating the aquifer system under the conditions that existed before and during ground-water development. The Cambrian-Ordovician aquifer system and the overlying rocks were incorporated in the conceptual model as five aquifer layers with four intervening confining layers. The aquifer layers, from top to bottom, are as follows: Quaternary deposits and Cretaceous rocks (aquifer layer 5); basal Devonian carbonate rocks and underlying Silurian carbonate rocks (aquifer layer 4); Middle Ordovician St. Peter Sandstone, Lower Ordovician Prairie du Chien Group, and Upper Cambrian Jordan Sandstone (aquifer layer 3); Upper Cambrian Ironton and Galesville Sandstones (aquifer layer 2); and Upper Cambrian Mount Simon Sandstone and Precambrian Hinckley Sandstone (aquifer layer 1).

The effects on the flow system of ground water having variable density and the individual aquifer layer contribution of flow to wells open to several aquifer layers were simulated by incorporating appropriate terms in the ground-water flow equation and corresponding modifications in the ground-water flow model.

Results of steady-state simulations are shown as maps of freshwater head and as flow-rate vectors. A comparison was made of available predevelopment head data and simulated predevelopment heads for the Mount Simon, St. Peter-Prairie du Chien-Jordan, and Silurian-Devonian aquifers. The root mean square of the differences between observed and simulated heads for these aquifers was 53, 36, and 44 feet, respectively.

Steady-state model simulation indicates that regional recharge areas are located in northwestern Iowa, southeastern Minnesota, much of Wisconsin, northern Illinois, and central Missouri. Regional discharge areas are located near the Mississippi River and its tributaries, the Missouri River, Lake Michigan, and the Illinois basin.

Results of a transient simulation of the period 1861 to 1980 are shown as maps of freshwater head and freshwater-head decline. The root mean square of the differences between observed and simulated heads for the St. Peter-Prairie du Chien-Jordan aquifer was 63 feet. In addition, hydrographs of simulated hydraulic head were compared with hydrographs of observed head in wells open to various combinations of aquifers. The numerous head measurements within a model node display a wide range in magnitude; however, their historical trend generally follows the trend of the simulated heads.

The simulated recharge from the glacial drift to the immediately underlying bedrock aquifers averages 0.03, 0.06, 0.24, and 0.02 inch per year, respectively, to the Mount Simon, Ironton-Galesville, St. Peter-Prairie du Chien-Jordan, and Silurian-Devonian aquifers for predevelopment conditions and 0.03, 0.07, 0.45, and 0.07 inch per year, respectively, to the same aquifers for 1976–80. These recharge rates are less than 1.5 percent of average annual precipitation of about 30 inches per year. Most of the recharge from precipitation discharges to streams as base flow through local and intermediate ground-water flow systems. Only a small fraction of the precipitation recharges the deeper, regional flow system. The simulated predevelopment recharge of 571 cubic feet per second is balanced by an equivalent discharge. For the period 1976–80, simulated recharge increased to 1,398 cubic feet per second. Total discharge, including pumpage from the four bedrock aquifers, increased to 1,619 cubic feet per second. The difference in recharge and discharge during this period is from aquifer storage.

Results of variable-density simulations indicate that the rate of ground-water movement is small in areas where ground water is highly mineralized. The rates and directions are controlled by the intrinsic permeability of the rock, freshwater head gradients, and gravitational force.

INTRODUCTION

Sandstone and carbonate strata of Cambrian and Ordovician age make up much of the sedimentary bedrock overlying the Precambrian basement in the northern Midwest and form the major aquifer system of the area. Many metropolitan areas depend on the aquifer system for all or part of their water supplies. The potentiometric head in the aquifer system has declined hundreds of feet since the late 1800's in the heavily pumped Chicago-Milwaukee area and to a somewhat lesser extent in other major metropolitan areas, such as Minneapolis-St. Paul, Minn., Green Bay, Wis., and Des Moines, Mason City, and Cedar Rapids, Iowa. Projections of future water needs indicate steady or increasing demands and, therefore, continuing water-level declines.

The aquifer system contains highly mineralized water in several places, especially in its deepest parts. These generally coincide with regional discharge or structurally low areas and are located mainly in the southwestern, southern, and eastern parts of the study area. Water from the highly mineralized zones may be induced into freshwater zones by large withdrawals of freshwater in some areas, such as northeastern Illinois, eastern Wisconsin, and central Iowa.

Protection and management of the aquifer system are important concerns of State and local planning, regulatory, and water-management agencies. Sound management decisions require a thorough understanding of the aquifer system—its physical dimensions, hydrologic and geologic characteristics, water availability and quality, and the effects of past and future pumping from the aquifer system.

In October 1978, the U.S. Geological Survey began a regional assessment of the Cambrian-Ordovician aquifer system (Steinhilber and Young, 1979) as part of the national Regional Aquifer-System Analysis (RASA) program (Bennett, 1979). The primary goal of the RASA program is to gain an understanding of the hydrogeologic system in each region, including the nature of the hydrogeologic units, ground-water flow system, and chemical quality of the water. This goal is accomplished through compilation and collection of hydrogeologic data, development and use of ground-water flow models, and interpretation of geochemical data.

This report describes the development and results of a computer-based model of three-dimensional ground-water flow used to improve understanding of the regional ground-water flow system, with emphasis on the aquifer units of the Cambrian and Ordovician rocks. Also described are modifications to the ground-water flow equation to incorporate effects of spatially varying ground-water density and of wells open to more than one aquifer.

Prior to this investigation, several two-dimensional flow models of the Cambrian-Ordovician aquifer system in parts of the study area were developed, including the Chicago area (Prickett and Lonnquist, 1971), southeastern Wisconsin (Young, 1976), and the Madison, Wis., area (McLeod, 1975a, 1975b). Concurrent with this study, three-dimensional models were prepared for the Twin Cities, Minn. (Guswa and others, 1982), northeastern Wisconsin (Emmons, 1987), and Brown County, Wis. (Krohelski, 1986). In addition, two-dimensional models were prepared for northeastern Missouri (Imes, 1985) and for the Jordan aquifer of Iowa (M.R. Burkart and R.C. Buchmiller, U.S. Geological Survey, written commun., 1988).

Other Northern Midwest RASA reports on the aquifer system also are to be published as chapters of U.S. Geological Survey Professional Paper 1405. They include chapter A, a summary of the Northern Midwest RASA (H.L. Young, U.S. Geological Survey, written commun., 1988), chapter B, which describes the regional hydrogeology and water quality (Young, in press), chapter D, which describes the regional geochemistry (Siegel, 1989), and chapter E, which presents a detailed three-dimensional ground-water flow model of the Chicago-Milwaukee area (H.L. Young and A.J. MacKenzie, U.S. Geological Survey, written commun., 1988).

The Northern Midwest RASA study covers about 161,000 mi^2 and includes northern Illinois, northwestern Indiana, most of Iowa, southeastern Minnesota, northern Missouri, and most of Wisconsin (fig. 1). The border of the study area delimits either the natural physical or hydrologic boundaries of the system or places where the aquifer is not used because of poor water quality. The northern boundary, from northwestern Iowa to northeastern Wisconsin, delineates the erosional edge of Cambrian rocks overlying crystalline basement rocks of Precambrian age. The Missouri River is a discharge line and forms the western and southwestern boundary. Beyond the eastern and southeastern boundary in Michigan, Illinois, and Indiana, water in the aquifer system is too highly mineralized to be used. The ground-water flow model covers an area larger than the study area—378,880 mi^2 compared with 161,000 mi^2—in order to reduce the effect of the model boundary on simulations within the study area.

Although the major aquifer system is composed of rocks of Cambrian and Ordovician age, other rocks are locally important. The major secondary aquifers consist of Silurian and Devonian carbonate rocks and Quaternary sand and gravel. These rocks as well as rocks of Mississippian and Pennsylvanian age are included in the study because they have a major influence on the amount and distribution of recharge and discharge for the Cambrian-Ordovician aquifer system. In addition, some

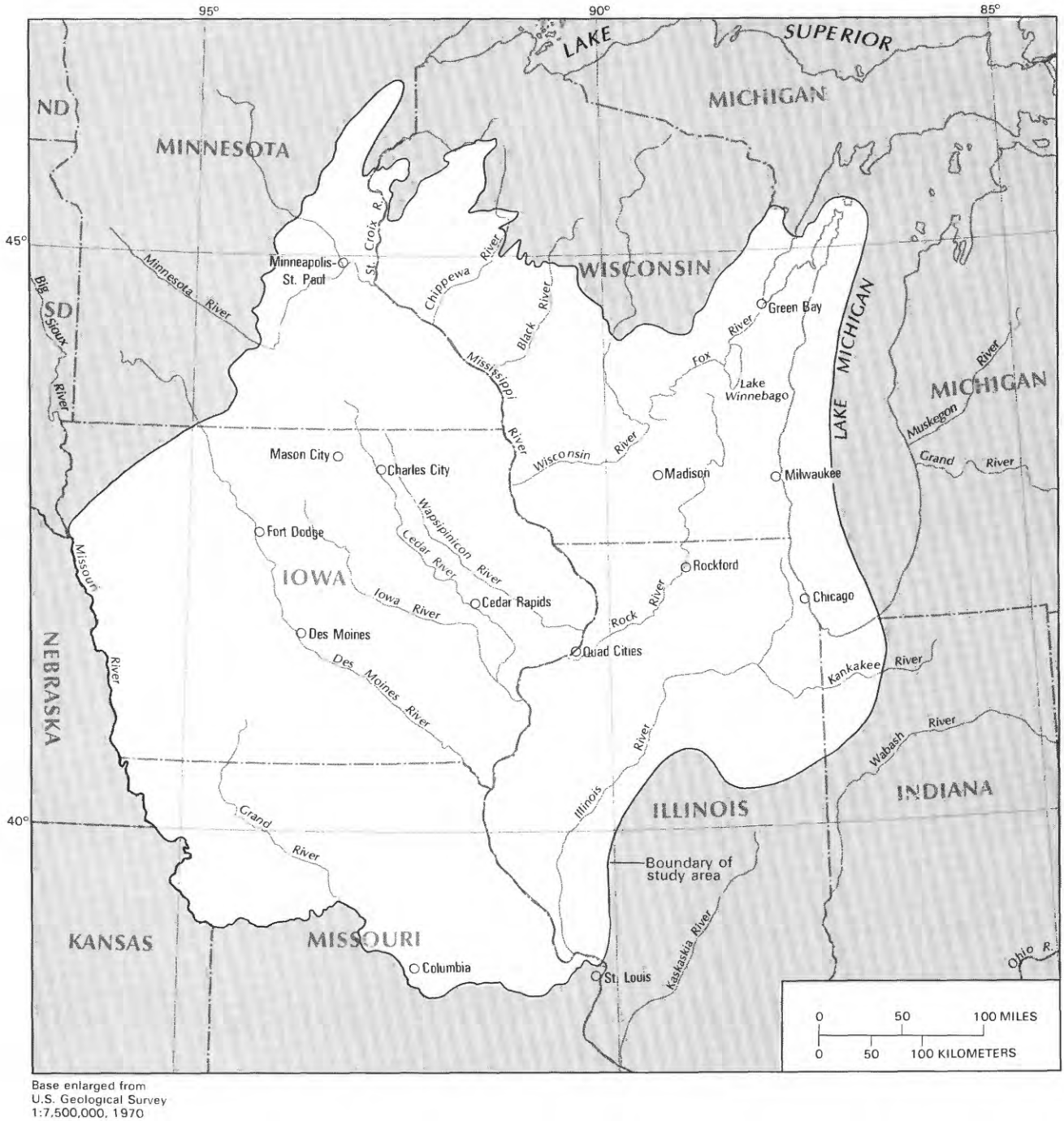

Base enlarged from
U.S. Geological Survey
1:7,500,000, 1970

FIGURE 1.—Location and general features of the Northern Midwest Regional Aquifer-System Analysis area.

of the wells developed in the Cambrian-Ordovician aquifer system are open to the Silurian-Devonian aquifer.

The hydrologic data needed for the model were generated from existing files, publications, and newly gathered and interpreted data from several State agencies and the U.S. Geological Survey District Offices in each State. Composite regional thickness maps of model aquifer and confining layers and a water-table map were prepared from individual hand-drawn State maps.

Thickness arrays and water-table elevations required for the ground-water flow model were developed from the composite maps by manual estimation of the average thickness or elevation over the areal extent of each finite difference model block (256 square miles). Because the composite thickness maps were based on limited data and because of the averaging process, isopachs of aquifer and confining layers (figs. 4–11) are highly generalized representations of actual thickness. As discussed in the

section on hydraulic properties to follow, the thickness arrays were used, together with hydraulic conductivity and specific storage values, to calculate model input arrays of thickness-dependent hydraulic properties such as transmissivity, vertical leakance, and storativity. Consequently, isopachs of the model units are presented primarily to document the development of these hydraulic properties.

Structure contour maps of the tops of the aquifer and confining units are given in Chapter B of Professional Paper 1405 on the hydrogeology of the Cambrian-Ordovician aquifer system (Young, in press). These maps are based on altitudes generated at a uniform spacing of 8 miles, derived from a computerized two-dimensional interpolation technique (Kontis and Mandle, 1980), applied to digitized hand-drawn regional structure contours. Thicknesses obtained from these computer-generated structure maps may differ somewhat from the isopachs presented herein because of the different grid spacing and procedure used in their development.

Because collection of data for model parameters in Michigan and eastern Indiana was not part of the original project plan, generalized data were later obtained to extend the model coverage into Indiana and Michigan to satisfy boundary condition restraints. Very little hydrostratigraphic data existed in western Michigan on which to base model layering, and trends were continued into the Michigan basin using these sparse data. The data and model results in this extended area, therefore, are not necessarily valid.

HYDROGEOLOGIC SETTING

The following is a regional synopsis of the structural, lithologic, and hydrologic features of the geologic formations in the study area and a description of the vertical discretization of geologic units into model layers. Detailed accounts of the geology and hydrology of each of the States in the study area can be found in publications of State agencies and the U.S. Geological Survey referenced in Professional Paper 1405-B (Young, in press). The nomenclature used in this report was established for the Northern Midwest RASA and does not necessarily coincide with that previously accepted by the U.S. Geological Survey. It follows usage prevalent in the majority of the study area, or the usage of a particular State, where appropriate.

GEOLOGIC STRUCTURE

The consolidated sedimentary rocks in the northern Midwest consist of sandstone, carbonate, and shale sequences that range in age from Precambrian to Cretaceous (fig. 2). They overlie the eroded surface of the Precambrian basement complex. The highest areas of the Precambrian surface are the Transcontinental and Wisconsin arches in the north. Other structural highs are the Kankakee arch and the Nemaha uplift. The major structurally low areas are the Illinois, Michigan, and Forest City basins. Subsidence of the Illinois and Michigan basins began during Early Cambrian time, and, as a result, the Cambrian rocks, especially the Mount Simon Sandstone, increase in thickness toward these basins. The formations thin toward and lap onto the Wisconsin and Transcontinental arches and dip gently to the south and east toward the basins. They also dip gently away from the Ozark uplift in southeastern Missouri toward the Illinois and Forest City basins. Overlying the Cambrian and Ordovician rocks are progressively younger rocks of Silurian, Devonian, Mississippian, and Pennsylvanian age. Cretaceous rocks directly overlie the Cambrian and Ordovician rocks in northwestern Iowa and southwestern Minnesota. Throughout most of the study area, a blanket of unconsolidated Quaternary deposits covers the consolidated sedimentary rocks. The spatial relationship between the rocks is shown in figure 3, a geologic section typical of much of the study area.

STRATIGRAPHY AND CONCEPTUAL AQUIFER AND CONFINING LAYERS

On the basis of their general hydraulic properties, geologic formations in the study area are grouped into five regional aquifer layers and four regional confining layers, as shown in table 1. Formations that have a recognized higher permeability are grouped as aquifer layers, and those that have relatively low permeabilities are grouped as confining layers. These layers are numbered from deepest (layer 1) to shallowest (layer 5). The regional Cambrian-Ordovician aquifer system consists of aquifer layers 1, 2, and 3 and their confining layers. Rock-stratigraphic nomenclature for the Cambrian and Ordovician in the following discussion is derived primarily from the outcrop area in the northern part of the study area. The equivalent rocks in most of Missouri, Illinois, and Indiana contain more carbonates and generally are less important as aquifers. Model layer boundaries in this report may differ from the geologic unit boundaries available from more recent geologic investigations and interpretation, especially in extreme northwestern Iowa and southwestern Minnesota and in northwestern Missouri and northeastern Kansas.

Aquifer layer 1 consists primarily of the Mount Simon Sandstone and its equivalents, which rest on the Precambrian basement. This layer contains the Precambrian Hinckley Sandstone in Minnesota, which directly underlies the Mount Simon Sandstone. In Illinois, the lowermost member of the Eau Claire Formation, the Elmhurst

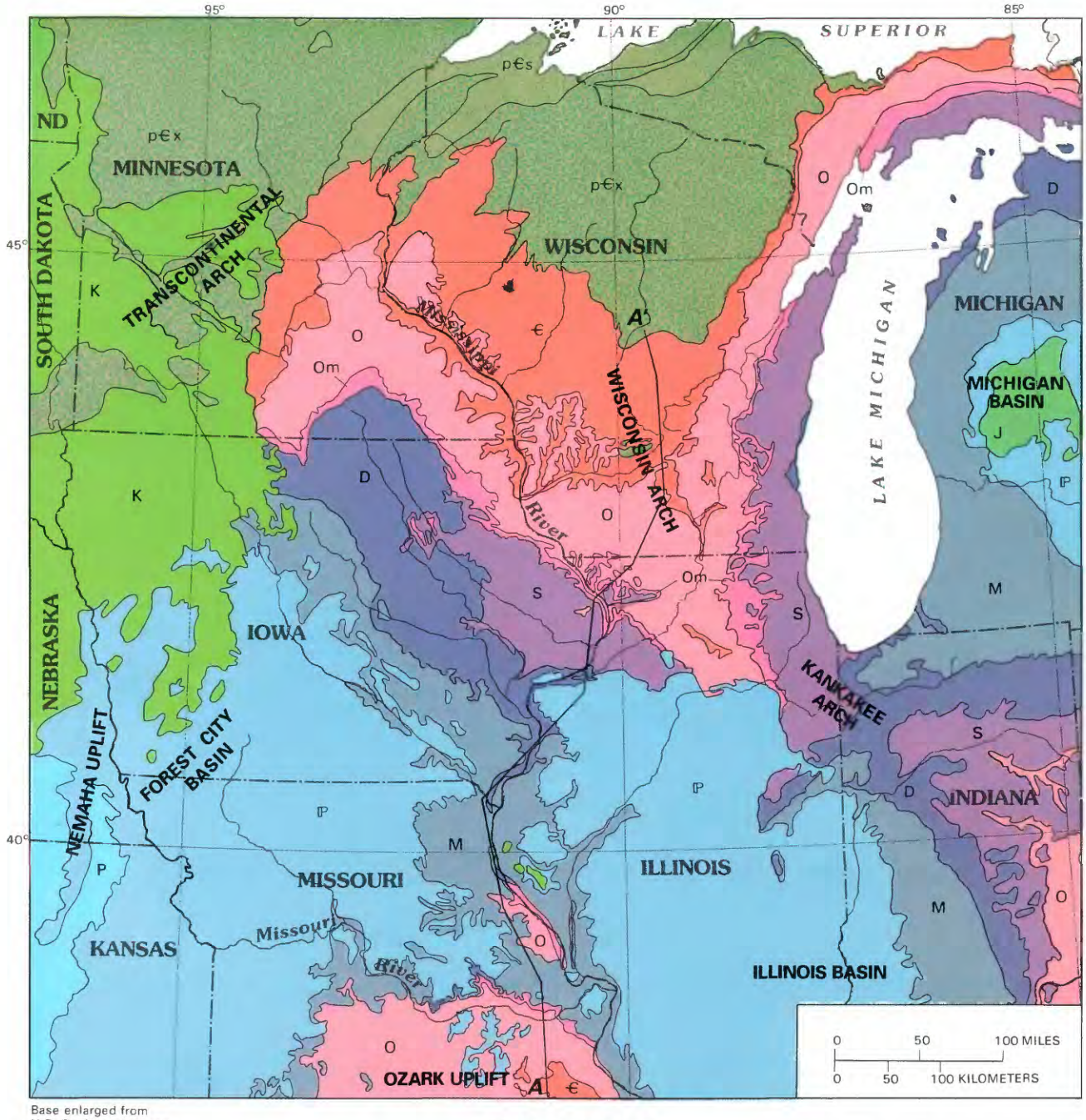

Base enlarged from
U.S. Geological Survey
1:7,500,000, 1970

EXPLANATION

GEOLOGIC UNITS

K	Cretaceous rocks	M	Mississippian rocks	O	Ordovician rocks older than the Maquoketa Shale
J	Jurassic rocks	D	Devonian rocks	Є	Cambrian rocks
P	Permian rocks	S	Silurian rocks	pЄs	Precambrian sandstone
IP	Pennsylvanian rocks	Om	Ordovician Maquoketa Shale	pЄx	Precambrian crystalline rocks

CONTACT

A—A' LINE OF HYDROGEOLOGIC SECTION — Section shown in figure 3

FIGURE 2.—General bedrock geology of the northern Midwest. (Modified from Young, in press.)

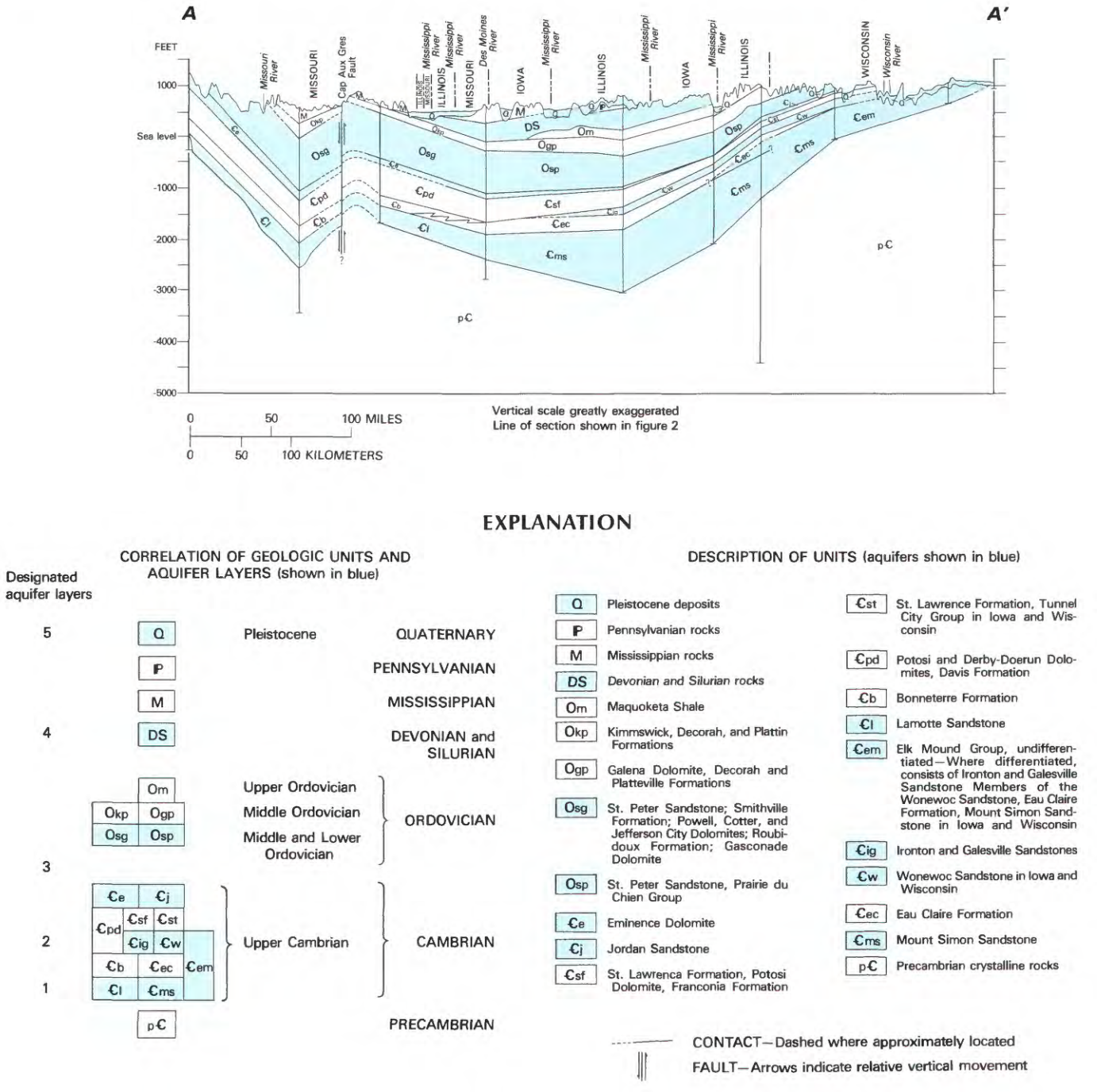

FIGURE 3.—Geologic section from Missouri to Wisconsin. (Modified from Young, in press.)

Sandstone, is included in this layer. The Mount Simon Sandstone consists of fine- to coarse-grained sandstone. It crops out and laps onto the Precambrian basement in Wisconsin and Minnesota and thickens to more than 2,500 ft on the northern edge of the Illinois basin (fig. 4).

Confining layer 1–2 separates aquifer layers 1 and 2 and consists of shaly dolomitic sandstones, siltstones, and carbonates of the Eau Claire Formation. It ranges in thickness from zero in its outcrop area in Wisconsin and Minnesota to more than 1,000 ft in the Illinois basin (fig. 5). In most of Wisconsin, the Eau Claire Formation consists mainly of sandstone and is generally a poor aquifer. It is not easily distinguished from the underlying Mount Simon Sandstone or the overlying Ironton and Galesville Sandstones. As a result, some of the Eau Claire Formation is included in aquifer layers 1 and 2.

The Ironton and Galesville Sandstones and their equivalents form aquifer layer 2. This layer is generally

TABLE 1.—*Stratigraphic configuration of simulated aquifer and confining layers*

Geologic system	*Hydrogeologic unit*		*Aquifer layer*	*Confining layer*
Quaternary	Drift		5	
Cretaceous	Cretaceous aquifer—only in Minnesota and Iowa			
Pennsylvanian	Pennsylvanian-Mississippian-Devonian confining unit			4–5
Mississippian				
Devonian				
Silurian	Silurian-Devonian aquifer—Includes basal Devonian in Illinois, Indiana, and Iowa		4	
Ordovician	Maquoketa confining unit—Consists of the Maquoketa Shale, and the Galena Dolomite and Decorah, Platteville, and Glenwood Formations, where overlain by the Maquoketa. Equivalents in Missouri and southern Illinois are the sequence of the Maquoketa Shale through the Joachim Dolomite			3–4
	St. Peter-Prairie du Chien-Jordan aquifer—In Missouri and Illinois, consists of the sequence of the St. Peter Sandstone through Eminence Dolomite		3	
Cambrian	St. Lawrence-Franconia confining unit—In Missouri and Illinois, consists of the sequence of the Potosi Dolomite through Davis Formation			2–3
	Ironton-Galesville aquifer—Not present in southern Illinois, western and southwestern Iowa, and Missouri		2	
	Eau Claire confining unit—Bonneterre Formation is the equivalent in Missouri and western Iowa			1–2
	Mount Simon aquifer	Includes overlying Elmhurst Sandstone Member of the Eau Claire Formation in Illinois	1	
		Mount Simon Sandstone is main component. Equivalent in Missouri is the Lamotte Sandstone		
		Includes underlying Hinckley Sandstone in Minnesota		
Precambrian	Crystalline basement rock			

less than 100 ft thick, except in Illinois, where it is more than 200 ft thick on the northern edge of the Illinois basin (fig. 6). It grades from a calcareous to dolomitic sandstone in the north (Minnesota, Wisconsin, northeastern Iowa, and northern Illinois) to carbonate rocks in the south (southwestern Iowa, Missouri, and southern Illinois).

Overlying aquifer layer 2 are shaly sandstones, limestones, and dolomites of the Franconia and St. Lawrence Formations, which form confining layer 2–3. They thicken from their eroded outcrop area in Minnesota and Wisconsin to more than 800 ft in the Illinois basin (fig. 7). In most of their extent in Minnesota, Iowa, and northern Illinois, they range from 100 to 300 ft in thickness.

The Jordan Sandstone, the Prairie du Chien Group and equivalents, and the overlying St. Peter Sandstone make up aquifer layer 3. The Jordan Sandstone is a medium- to coarse-grained, quartzose to dolomitic sandstone in Minnesota, Wisconsin, and Iowa and grades into dolomite and sandy dolomite in southern Iowa, Missouri, and most of Illinois. The Prairie du Chien and its equivalents consist of fossiliferous, cherty limestone and dolomite interbedded with thin, discontinuous layers of sandstone, siltstone, and shale. The St. Peter Sandstone is a very clean quartzose sandstone throughout the study area and is deposited on an erosional surface that dissects many of the Cambrian rocks. Aquifer layer 3 is generally 200 to 600 ft thick in the northern half of the study area but thickens to more than 1,750 ft in the Illinois basin (fig. 8).

Overlying aquifer layer 3 is a confining layer formed by the Glenwood, Platteville, and Decorah Formations, the Galena Dolomite, and the Maquoketa Shale. The Glenwood Formation is a poorly sorted sandstone with interbedded layers of dolomite and shale. The Platteville is predominantly a fossiliferous limestone with some cherty dolomite. The Decorah is a shaly limestone and dolomite and is overlain by the Galena Dolomite, which is mostly limestone and dolomite. The principal confining unit in

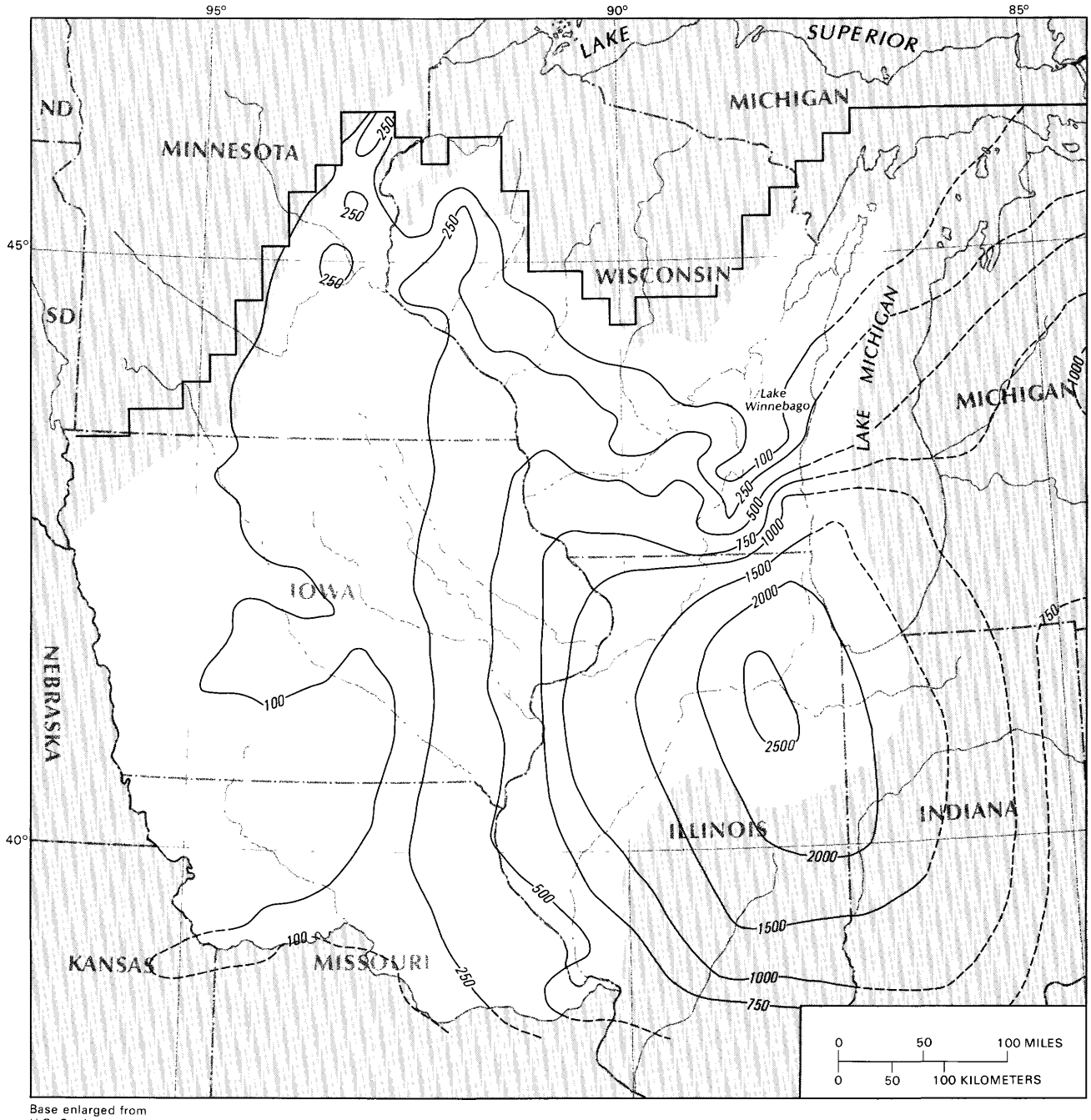

Base enlarged from
U.S. Geological Survey
1:7,500,000, 1970

EXPLANATION

—500— LINE OF EQUAL THICKNESS OF THE MOUNT SIMON AQUIFER (LAYER 1)—Dashed where inferred. Interval, in feet, is variable

MODELED LAYER BOUNDARY

FIGURE 4.—Generalized thickness of the Mt. Simon aquifer used to compute transmissivities and storage coefficients for model layer 1.

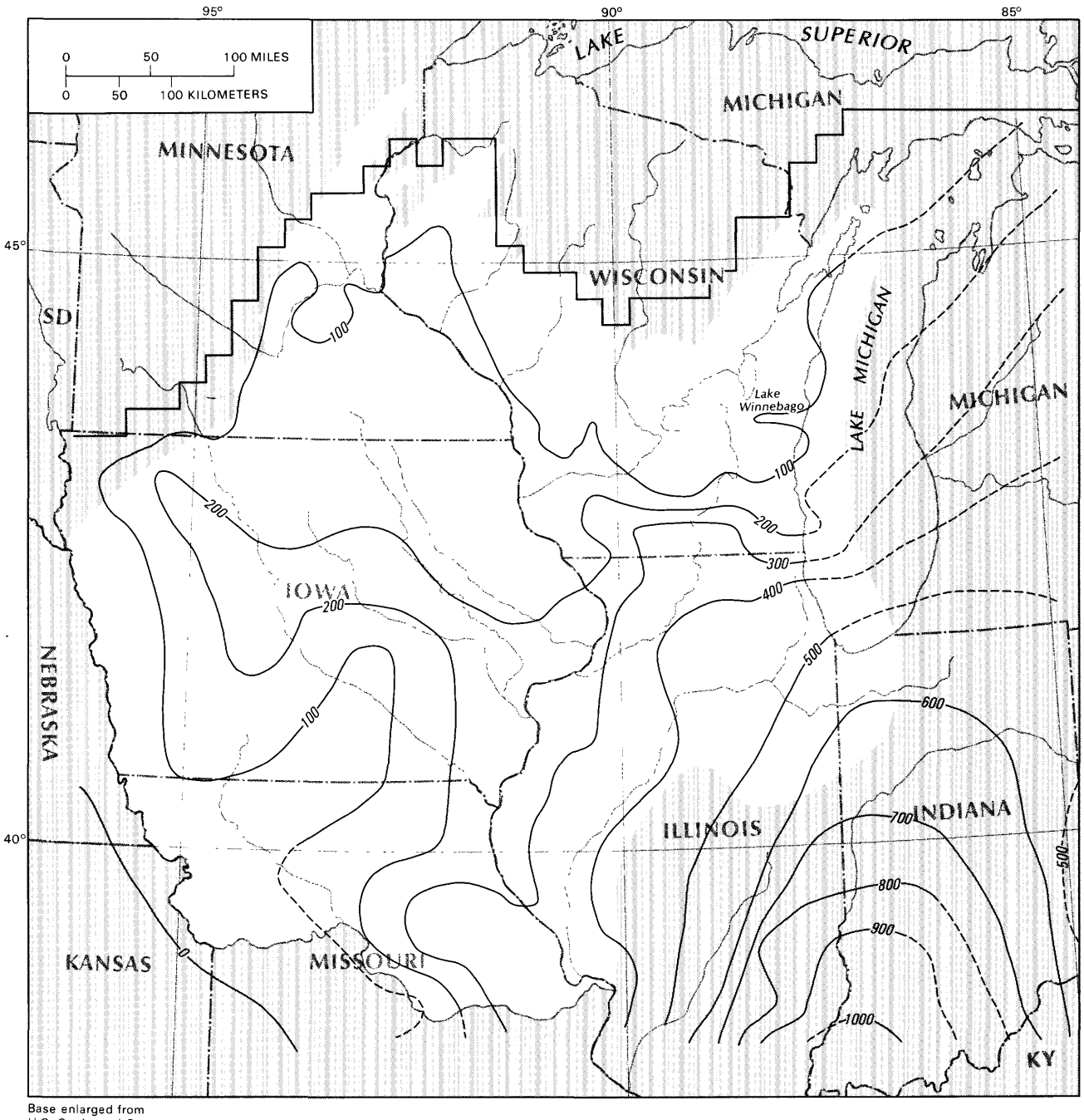

Base enlarged from
U.S. Geological Survey
1:7,500,000, 1970

EXPLANATION

——300—— LINE OF EQUAL THICKNESS OF THE EAU CLAIRE CONFINING UNIT (LAYER 1-2)—Dashed where inferred. Interval 100 feet

MODELED LAYER BOUNDARY

FIGURE 5.—Generalized thickness of the Eau Claire confining unit used to compute vertical leakance between model layers 1 and 2.

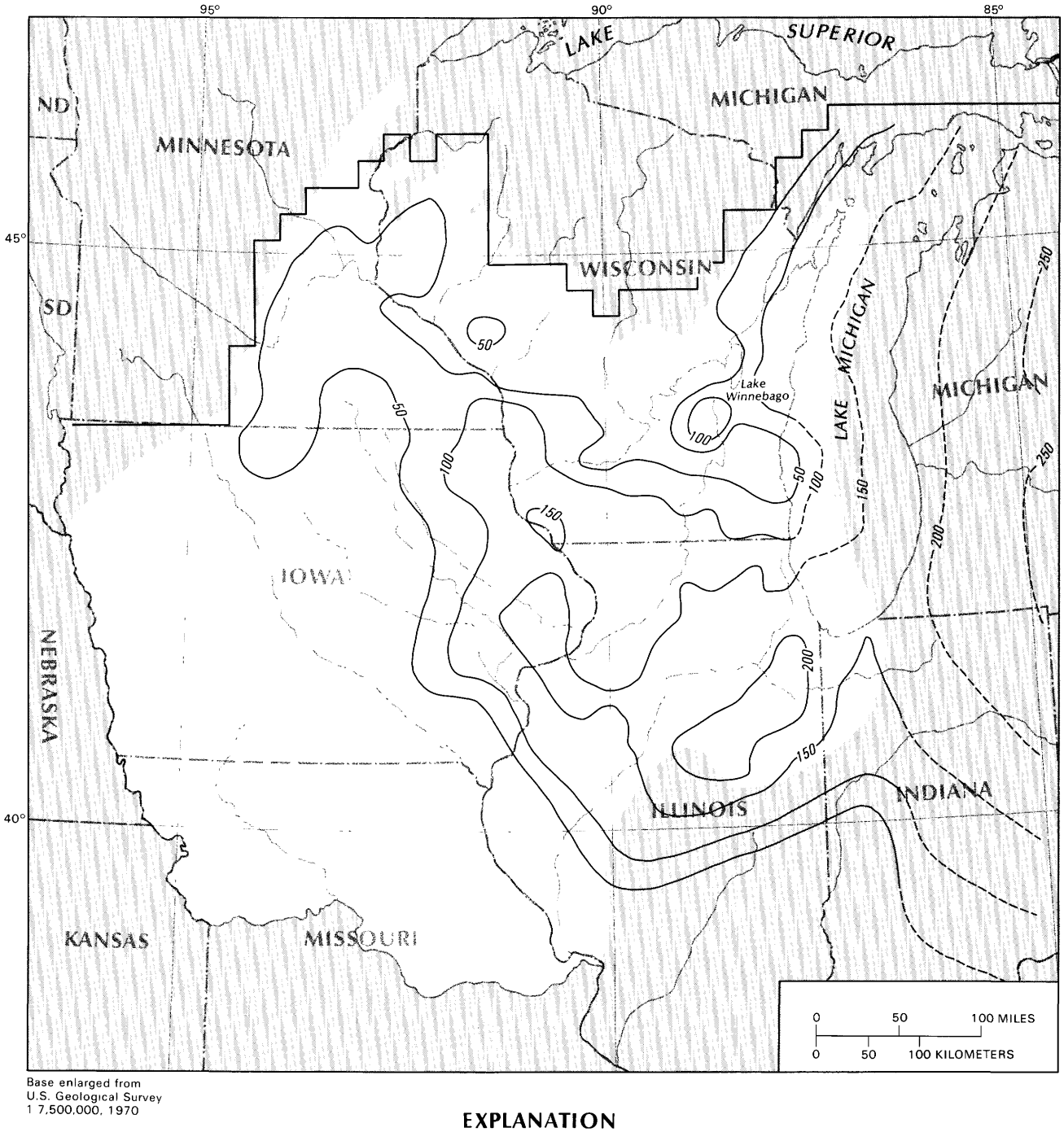

FIGURE 6.—Generalized thickness of the Ironton-Galesville aquifer used to compute transmissivities and storage coefficients for model layer 2.

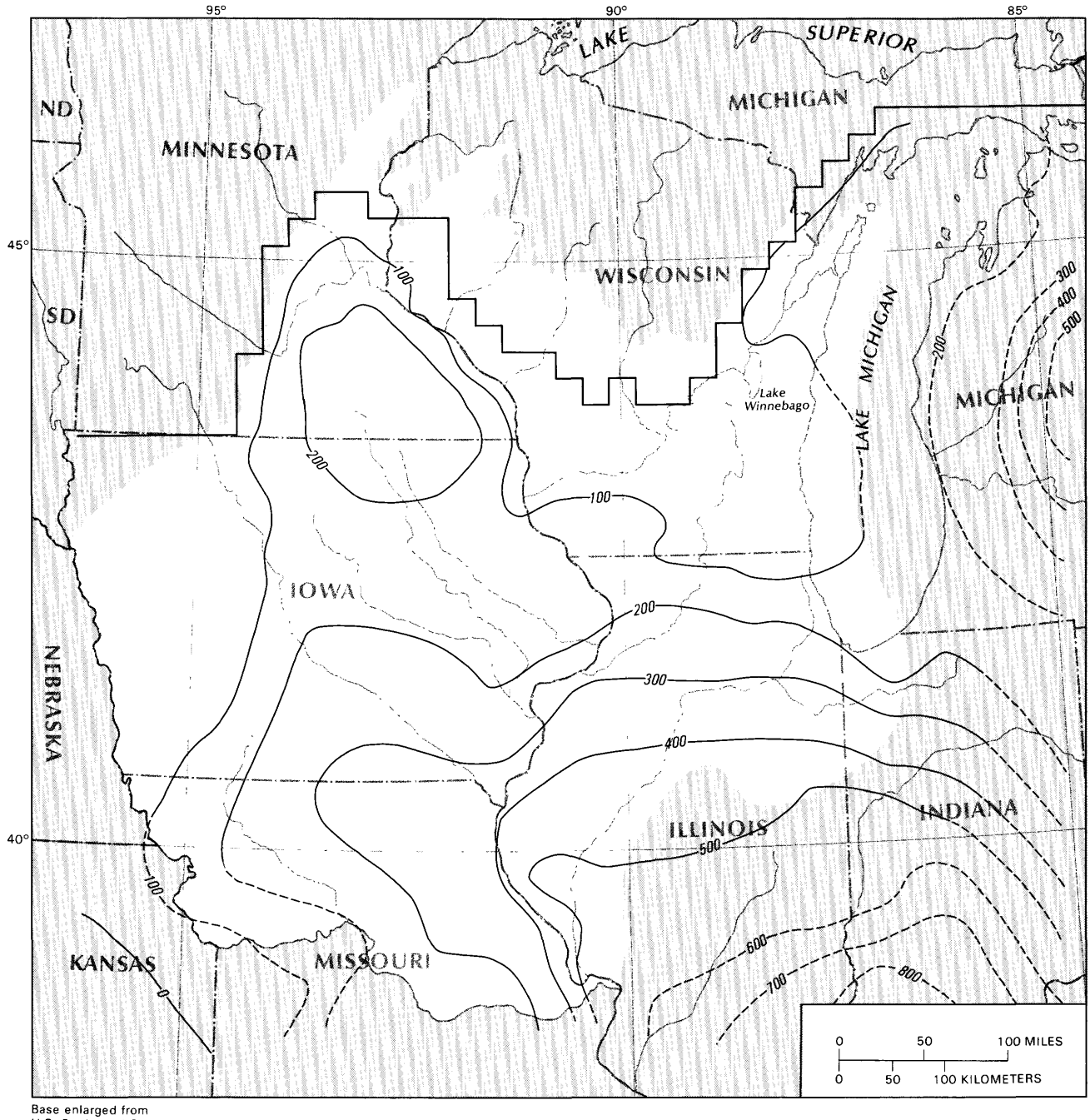

EXPLANATION

——200– – LINE OF EQUAL THICKNESS OF THE ST.LAWRENCE-FRANCONIA CONFINING UNIT (LAYER 2-3)—Dashed where inferred. Interval 100 feet

MODELED LAYER BOUNDARY

FIGURE 7.—Generalized thickness of the St. Lawrence-Franconia confining unit used to compute vertical leakance between model layers 2 and 3.

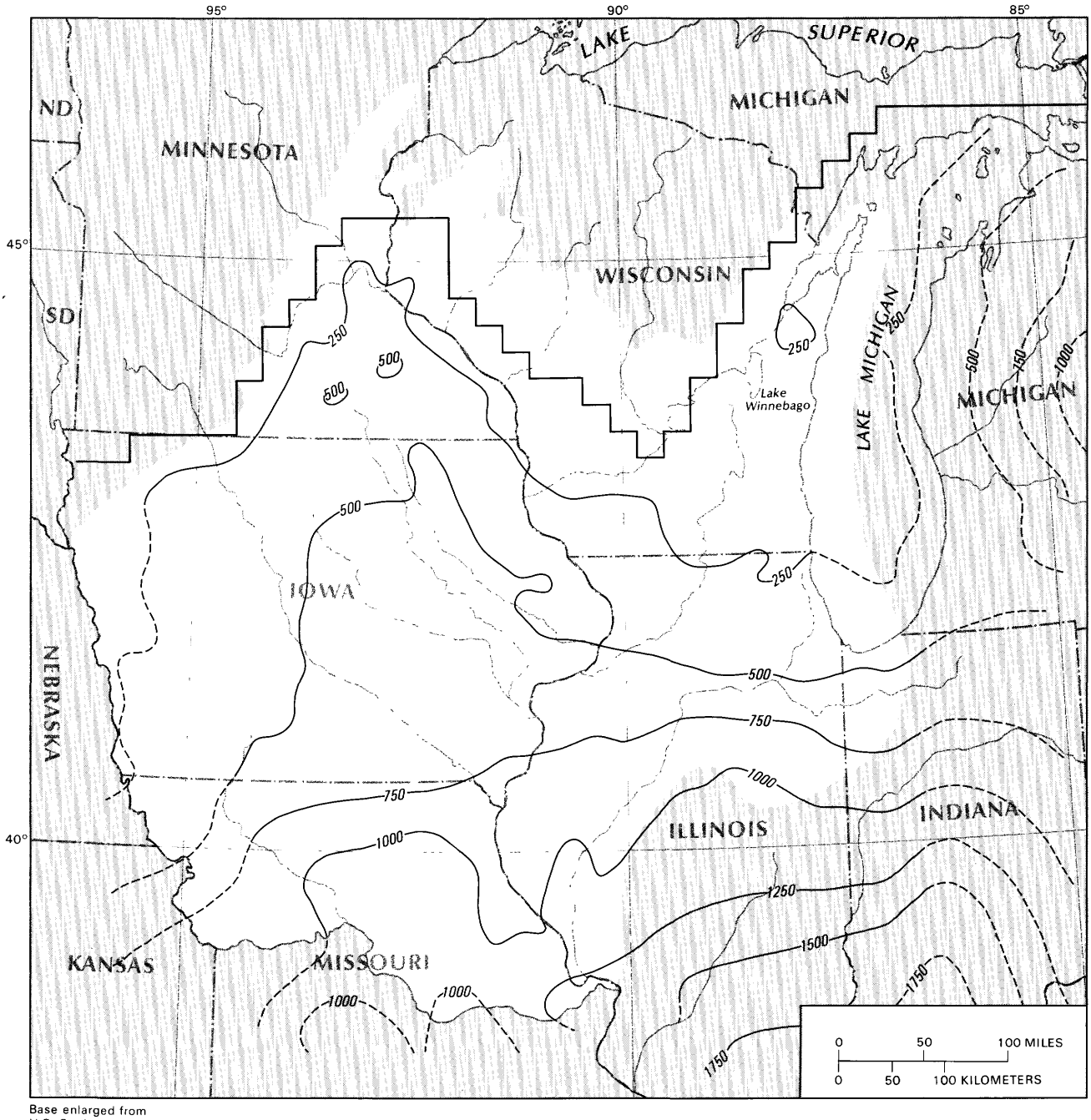

EXPLANATION

500 — LINE OF EQUAL THICKNESS OF THE ST. PETER-PRAIRIE DU CHIEN-JORDAN AQUIFER (LAYER 3)—Dashed where inferred. Interval 250 feet

MODELED LAYER BOUNDARY

FIGURE 8.—Generalized thickness of the St. Peter-Prairie du Chien-Jordan aquifer used to compute transmissivities and storage coefficients for model layer 3.

Minnesota, Wisconsin, northern Illinois, and northeastern Iowa is the Maquoketa Shale, which consists mostly of thick shales but includes some interbedded limestones and dolomites. Where the Maquoketa is absent and the Galena and Platteville crop out or subcrop, they are weathered, are less effective as a confining unit, and commonly produce moderate amounts of water to wells. Where the confining layer has not been eroded, it generally is 400 to 600 ft thick (fig. 9).

Aquifer layer 4 consists of carbonate rocks of Silurian and Early Devonian age. These are dominantly limestone and dolomite, with some shale and siltstone, especially in the Devonian rocks. In much of the study area, where it has not been exposed by erosion, aquifer layer 4 ranges in thickness from 200 to 600 ft (fig. 10). However, it is more than 1,000 ft thick in the Illinois and Michigan basins.

Rocks of Middle Devonian through Pennsylvanian age overlie layer 4 and form regional confining layer 4–5, even though the intervening Mississippian rocks yield small amounts of ground water. This confining layer consists of limestone, shale, sandstone, siltstone, and coal; it is essentially nonexistent in Minnesota and Wisconsin. Its thickness increases from the eroded edge in northern Iowa and Illinois to more than 4,000 ft in the Illinois and Michigan basins (fig. 11).

The uppermost layer, aquifer layer 5, includes all Quaternary unconsolidated sediments (Holocene surficial deposits and Pleistocene glacial drift) and Cretaceous rocks in the study area. The Pleistocene drift is present everywhere except in extreme southern and northwestern Illinois, southwestern Wisconsin, northeastern Iowa, and south of the Missouri River in Missouri. Cretaceous rocks overlie the Cambrian and Ordovician rocks in southwestern Minnesota and northwestern Iowa and consist of marine shales, siltstones, and lignitic sandstones of the Dakota Formation. The thickness of aquifer layer 5 ranges from zero to more than 500 ft.

HYDROLOGY

Ground-water recharge in the area is from precipitation. Ground water is stored in and moves through pores and fractures in the sandstone and carbonate rocks in response to hydraulic gradients. The hydraulic-head distribution in an aquifer system is controlled, in part, by the configuration of the water table and surface drainage features. Study of these features can provide a preliminary understanding of the local and regional ground-water flow system.

Figure 12 represents the smoothed water-table configuration in the regional ground-water flow model. It was prepared from published and unpublished water-table maps and data for the study area, but where data were lacking, the water table was constructed by following trends in land-surface topography.

To gain a preliminary appreciation of regional flow patterns, the ground-water regime may be viewed initially as an unconfined two-dimensional isotropic system in which movement occurs at right angles to the regional water-table contours (see fig. 12). Areas in which the water table is relatively high are inferred to be ground-water recharge areas, and areas in which the water table is low or where surface-drainage features exist are considered to be ground-water discharge areas. The development of local, intermediate, and regional flow patterns depends, in part, on the amount of local and regional relief of the water table and topography. Local and intermediate ground-water flow systems are closely related to the relief of the water table and the presence of a surface-drainage network. The pattern of deeper flow is influenced less by local water-table features and more by major regional topographic features (Freeze and Witherspoon, 1967).

The major surface-water features in the northern Midwest are the Mississippi and Missouri Rivers and Lake Michigan. The Mississippi River flows from north to south, generally bisecting the study area. Its drainage basin comprises most of the study area. The Missouri River flows from north to south where it bounds the study area on the west and then flows from west to east across central Missouri to form the southern boundary of the study area. Lake Michigan forms the northern half of the eastern boundary. Tributaries to Lake Michigan are very short because of the narrow width of its drainage area.

Water-table contours indicate overall directions of movement in the ground-water regime and can also show the patterns of shallow ground-water circulation in local flow systems; in the same way, maps of potentiometric head in deeper aquifers can indicate the general direction of regional ground-water movement in those units. Measured head data for predevelopment conditions are sparse in many areas, especially for the Mount Simon and Ironton-Galesville aquifers (layers 1 and 2), but are sufficient to prepare a reasonable regional approximation of head distribution for the St. Peter-Prairie du Chien-Jordan and Silurian-Devonian aquifers (layers 3 and 4) (figs. 14 and 13, respectively). Data used to prepare these maps are not necessarily from the same time period (Norton and others, 1912; Weidman and Schultz, 1915; Suter and others, 1959; Bond, 1972; Norvitch and others, 1973; Imes, 1985); however, most are representative of early heads that were not affected by ground-water withdrawals. For southeastern Minnesota, Iowa, and northern Missouri, most of the data are from wells open only to the units making up an individual aquifer. However, because of a lack of data for northern Illinois and

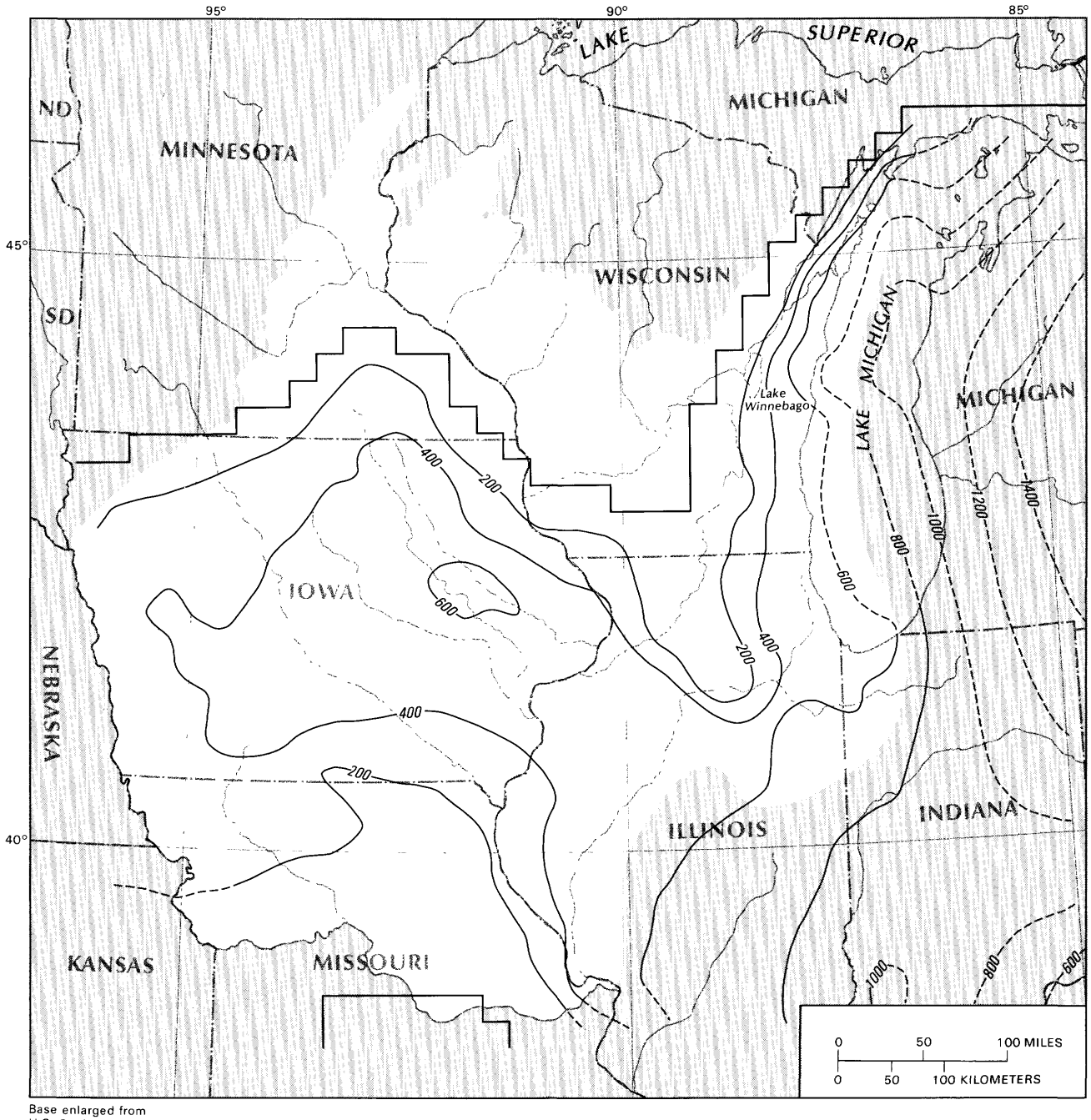

FIGURE 9.—Generalized thickness of the Maquoketa confining unit used to compute vertical leakance between model layers 3 and 4.

Wisconsin, data from wells open to more than one aquifer layer were used to develop the estimated predevelopment heads.

The generalized distribution of predevelopment head in the Silurian-Devonian aquifer (layer 4) (fig. 13) shows the distinctly irregular pattern of the water table in

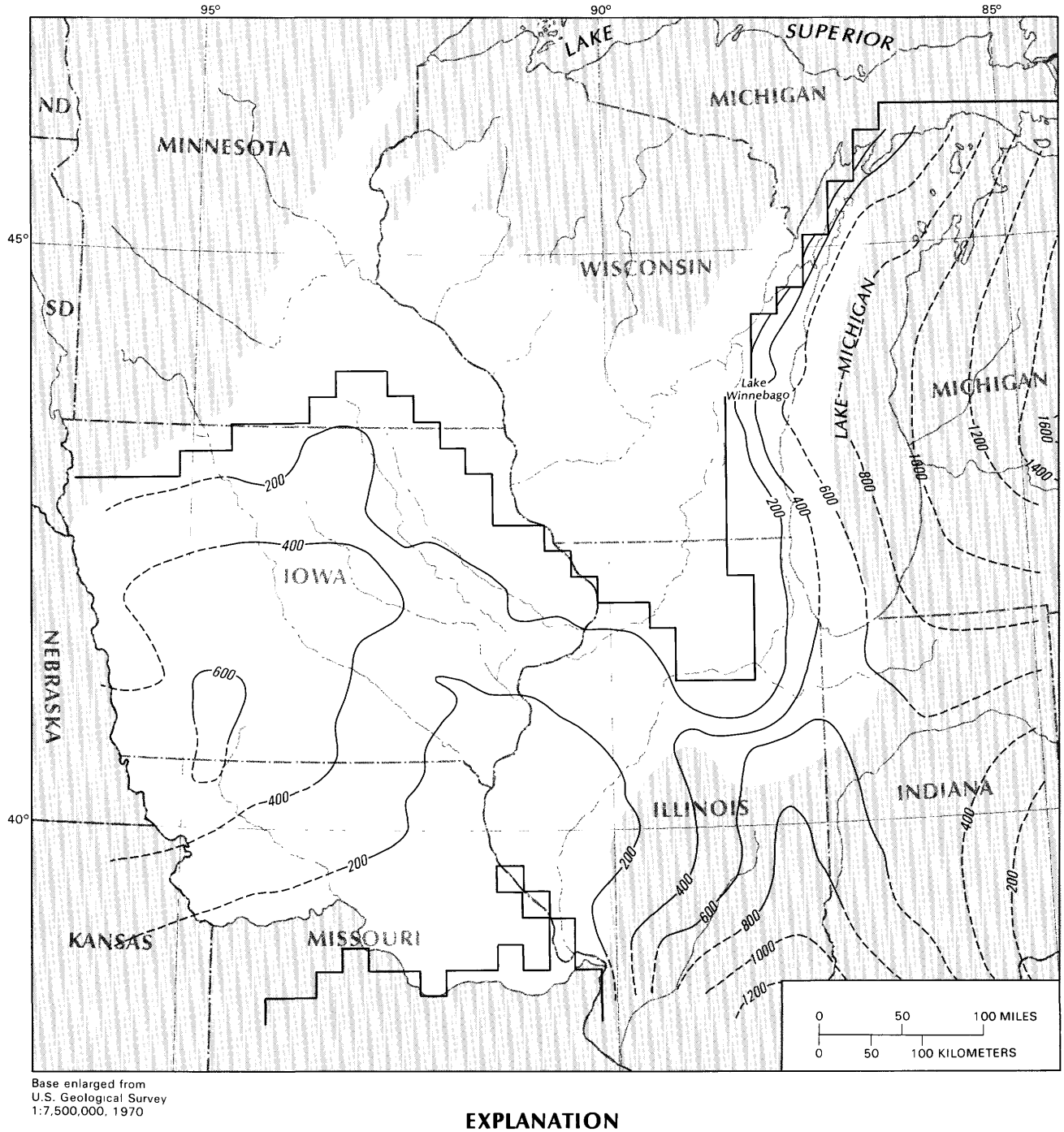

FIGURE 10.—Generalized thickness of the Silurian-Devonian aquifer used to compute transmissivities and storage coefficients for model layer 4.

unconfined areas and the smoother regional gradient in confined areas. Where it is unconfined, layer 4 receives recharge directly from precipitation. The confined area receives ground water by lateral flow from the unconfined area and by vertical leakage through its confining layers. Most discharge from aquifer layer 4 is through

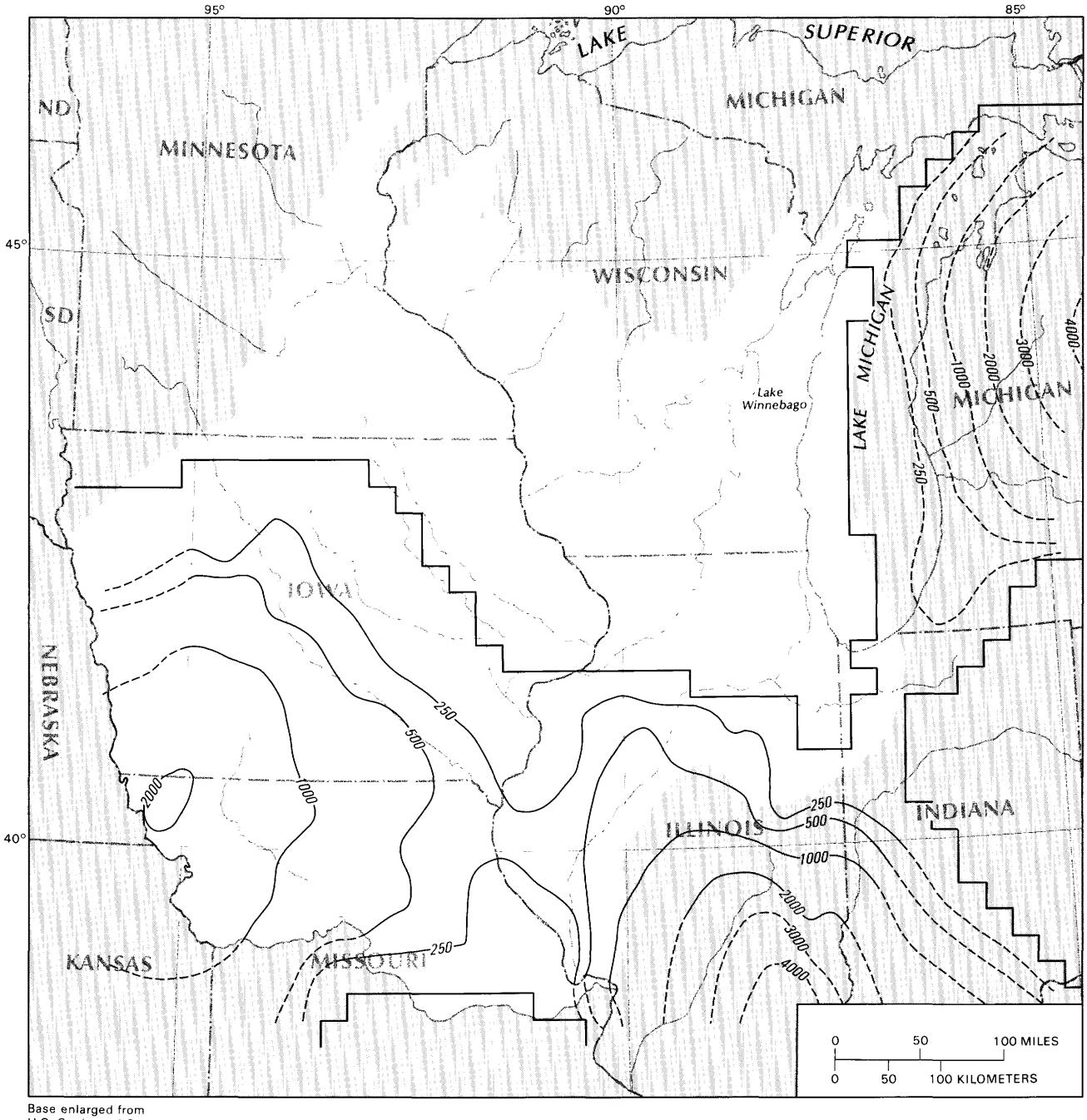

FIGURE 11.—Generalized thickness of the Pennsylvanian-Mississippian-Devonian confining unit used to compute vertical leakance between model layers 4 and 5.

local and intermediate flow systems. Upward leakage from aquifer layer 4 occurs primarily near main surface-drainage features.

The generalized predevelopment potentiometric head in the St. Peter-Prairie du Chien-Jordan aquifer (layer 3) is presented in figure 14. In central Wisconsin, east-

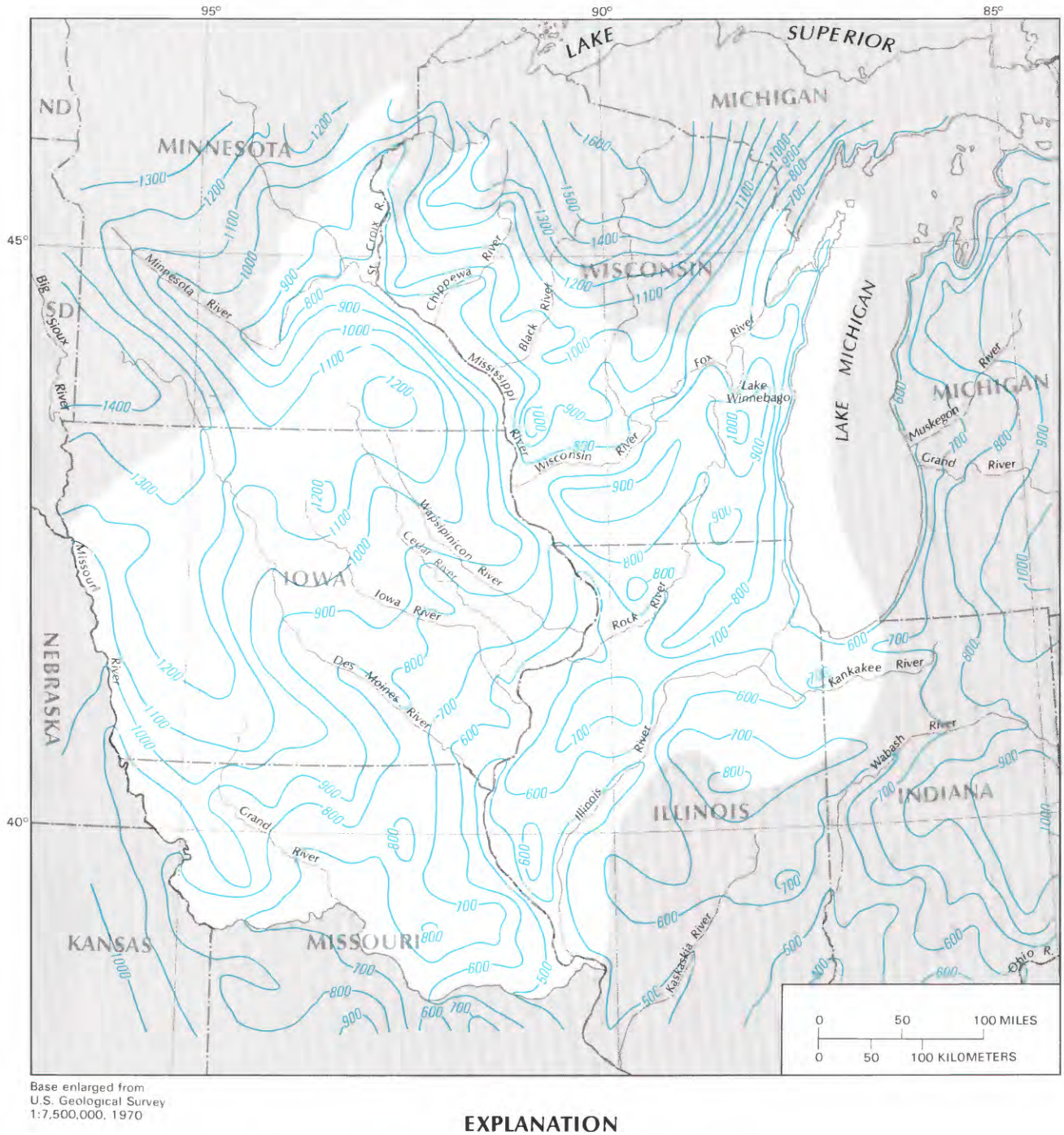

Base enlarged from
U.S. Geological Survey
1:7,500,000, 1970

EXPLANATION

—600— WATER-TABLE CONTOUR—Shows altitude of generalized water table, 1980. Contour interval 100 feet. Datum is sea level

FIGURE 12.—Generalized water table and major surface-water drainage network.

central Minnesota, northeastern Iowa, and northern Illinois, where the aquifer subcrops directly beneath glacial drift, head distribution in this aquifer is similar to the water table. Consequently, ground water flows from recharge to discharge areas over relatively short distances. Where the Maquoketa confining unit (layer 3–4) is less than 200 to 300 ft thick (fig. 9), it consists primarily of weathered carbonates of the Galena Dolomite and the Platteville Formation. These weathered rocks do not provide the same degree of confinement as the

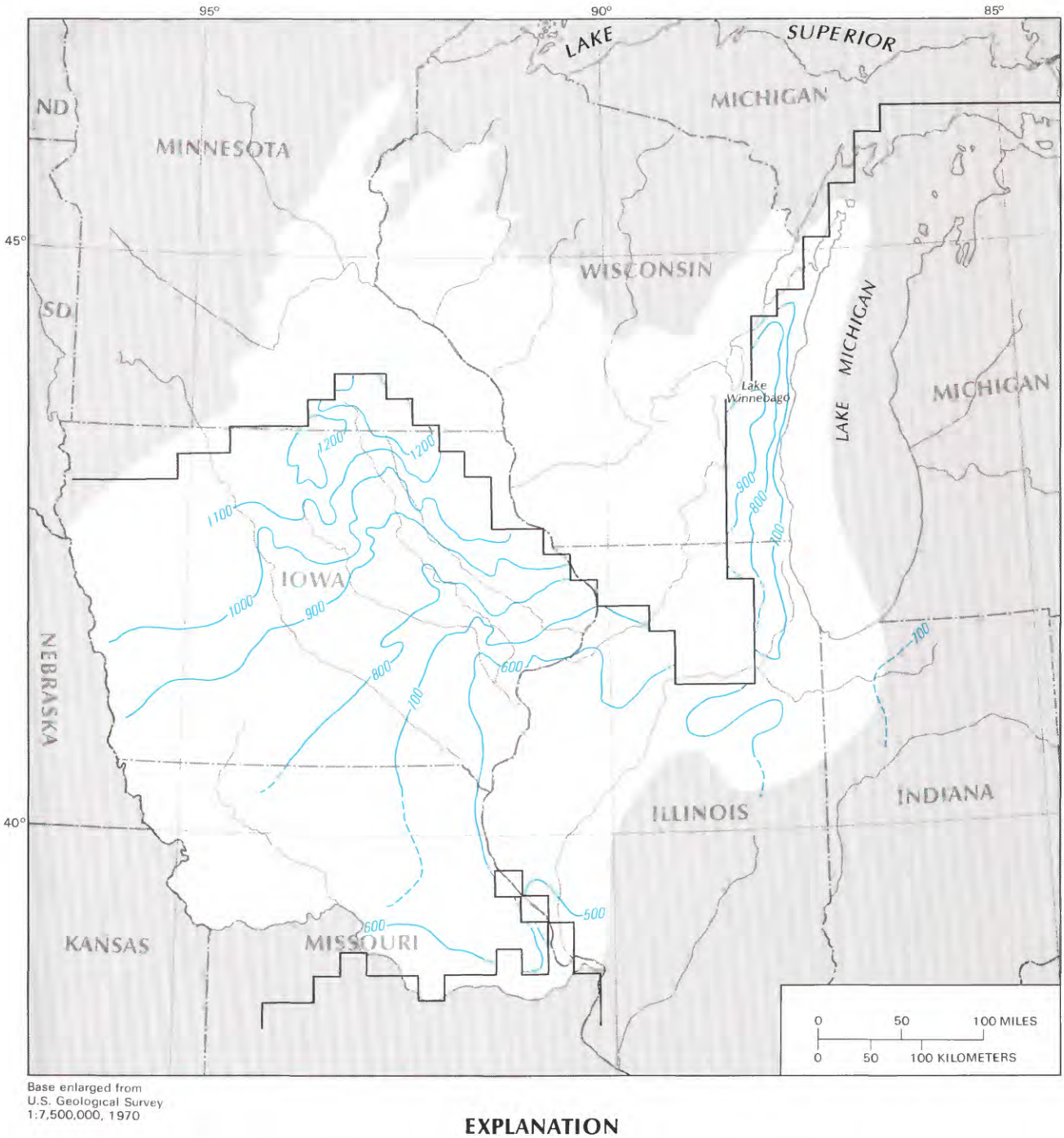

FIGURE 13.—Predevelopment potentiometric surface for the Silurian-Devonian aquifer (layer 4).

Maquoketa Shale; thus, in areas where the Maquoketa Shale is absent, the potentiometric head distribution in aquifer layer 3 is similar to the water table. Contours of potentiometric head beneath the Maquoketa Shale (fig.

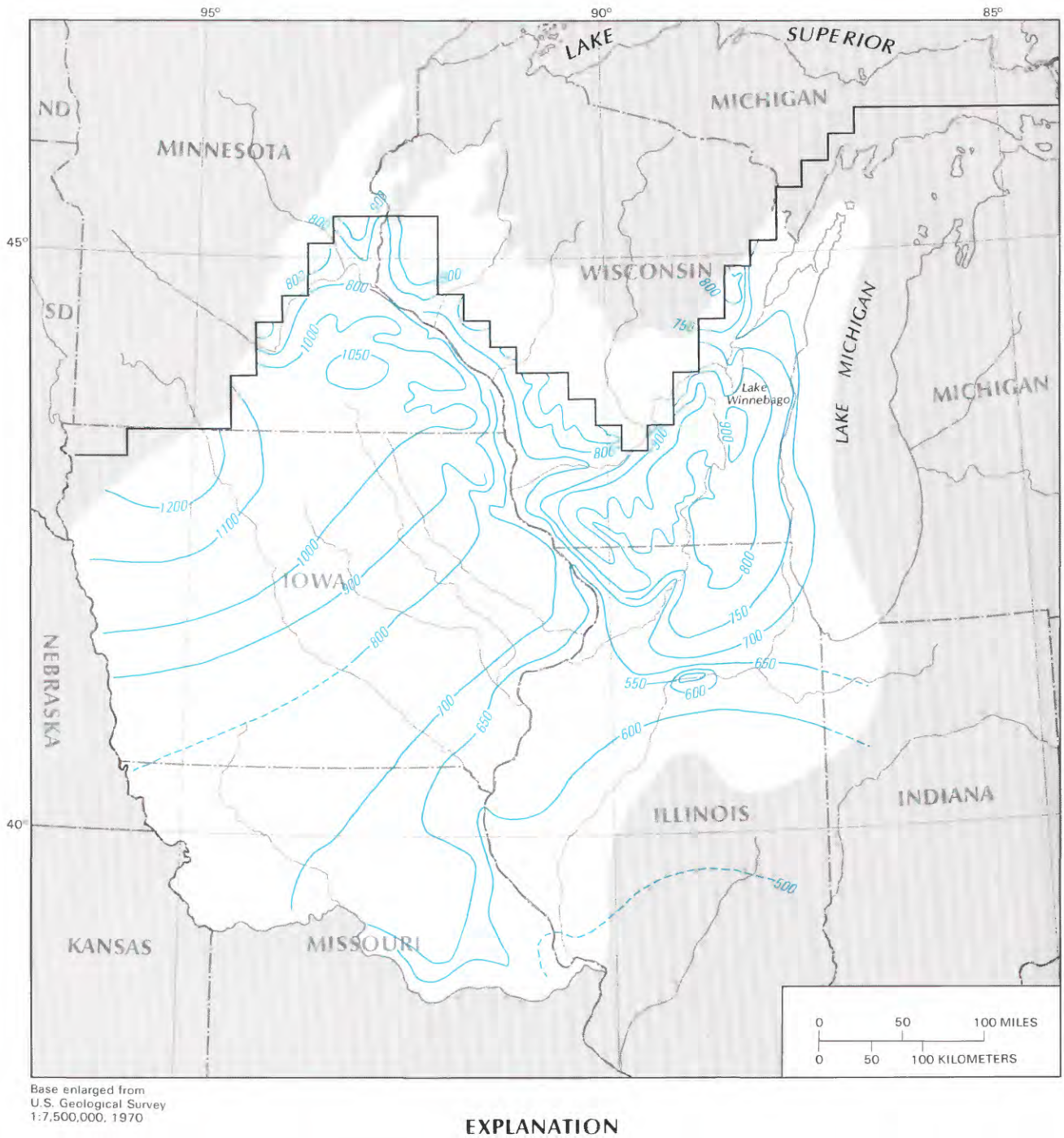

FIGURE 14.—Predevelopment potentiometric surface for the St. Peter-Prairie du Chien-Jordan aquifer (layer 3).

14) show a pattern of long regional flow paths in Iowa, northern Missouri, and Illinois to the structural basins.

Measurements of predevelopment head for the Mount Simon aquifer (layer 1) (fig. 15) are sparse over much of

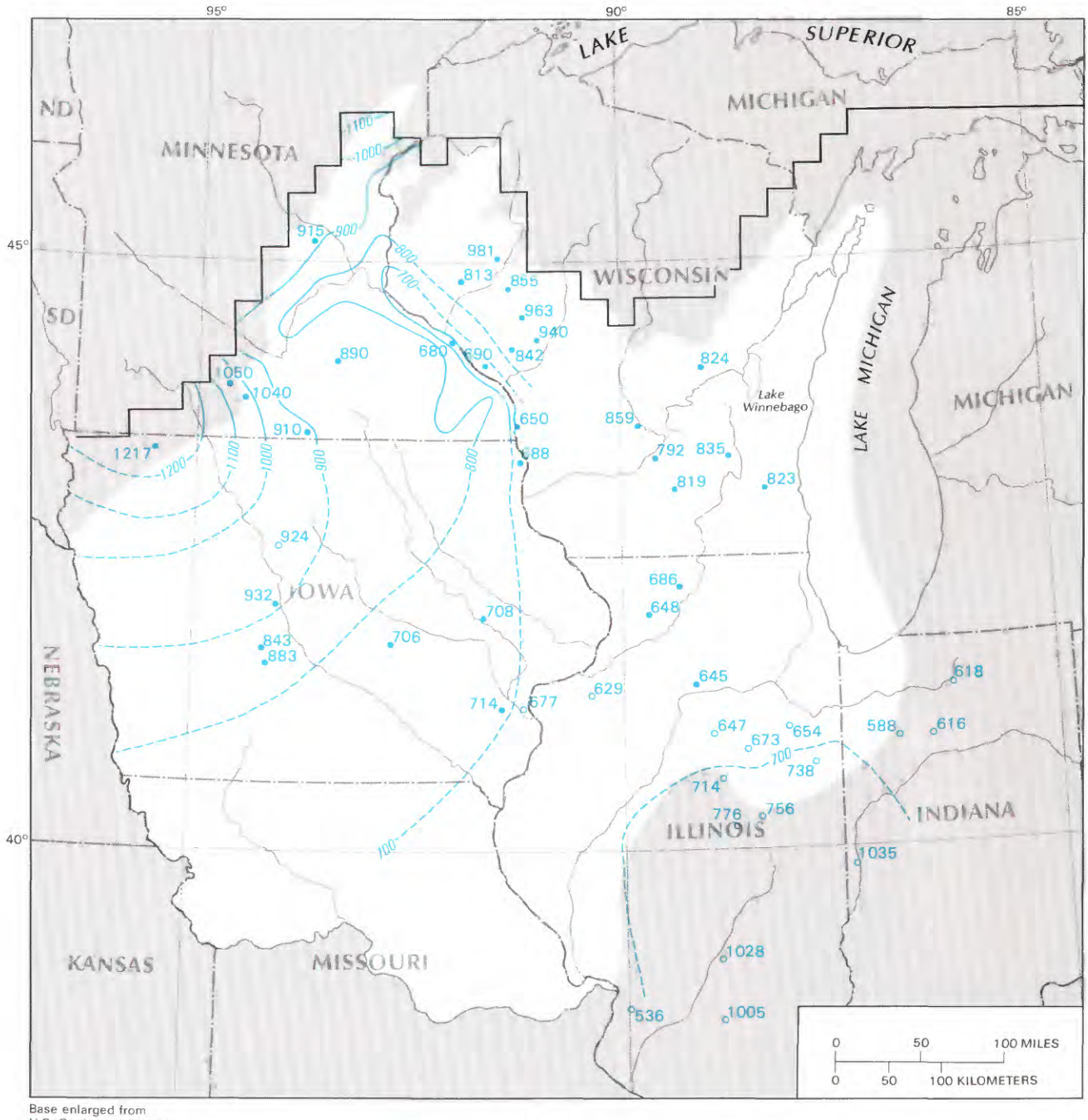

Base enlarged from
U.S. Geological Survey
1:7,500,000, 1970

EXPLANATION

900 — POTENTIOMETRIC CONTOUR—Shows approximate altitude of predevelopment potentiometric surface in the late 1800's for the Mount Simon aquifer (layer 1). Dashed where inferred. Contour interval 100 feet. Datum is sea level

932 — WELL LOCATION—Number is potentiometric head measurement, in feet. Datum is sea level

924 — WELL LOCATION—Number is density-corrected head measurement, in feet. (Bond, 1972). Datum is sea level

MODELED LAYER BOUNDARY

FIGURE 15.—Predevelopment potentiometric head data for the Mount Simon aquifer (layer 1).

the area, and only a few generalized head contours can be constructed.

When the first wells were drilled into the Cambrian-Ordovician aquifer system in the late 1800's, artesian head in the deeper buried aquifers produced flowing wells in several topographically low areas. These are primarily the Mississippi and Missouri River valleys, near Lake Michigan, and around Lake Winnebago in northeastern Wisconsin. Flowing wells also occurred in the valleys of major tributaries of the Mississippi, especially in western Wisconsin. In Iowa, flows were obtained along the major tributaries, the Cedar and Des Moines Rivers, as far upstream as Charles City and Fort Dodge. At present, heads are still adequate to support flowing wells along the Mississippi, but in most other areas pumping has lowered the head to below land surface.

Highly mineralized water is present along the fringes of the study area in the Michigan and Illinois basins. Water of somewhat lesser salinity is found in the Forest City basin, in eastern Wisconsin, and in northeastern Illinois. Dissolved-solids concentration in the Cambrian-Ordovician aquifer system exceeds 200,000 mg/L in the Michigan and Illinois basins (Meents and others, 1952; Graf and others, 1965, 1966; Clayton and others, 1966) and 35,000 mg/L in northwestern Missouri (Imes, 1985). The dissolved-solids distribution in aquifer layer 3 in the northern Midwest is summarized by Siegel (in press).

Ground-water flow directions and magnitudes in these areas undoubtedly are complex because of the spatial variation in ground-water density and aquifer permeability. A theoretical model of flow in the Illinois basin by Bredehoeft and others (1963) and a model based on geochemical data by Graf and others (1966) indicate that water moves from the basin margins, where the lowermost formations crop out, toward the center of the basin and upward through overlying shale layers. Cartwright (1970), using temperature anomaly data, and Davis (1973), studying the chemical quality of near-surface waters, also indicate an upward circulation pattern. Cartwright indicates that the magnitude of upward discharge from the underlying aquifers might be relatively high due to leakage through faults in the Illinois basin. Bond (1972) proposed similar flow patterns by analyzing hydraulic potential gradients, although he indicates that potential gradients may not be adequate to cause upward flow across shale layers in the center of the Illinois basin.

The conceptual regional flow system can be summarized as follows. Over most of Wisconsin, north-central Illinois, east-central Minnesota, and northeastern Iowa, ground water in the unconfined system flows relatively short distances, originating as recharge at water table highs and discharging to dissecting rivers. Ground water in the confined Cambrian-Ordovician aquifer system is derived from lateral flow from the unconfined areas and by vertical leakage through confining units. Ground water generally flows toward the structural basins, where it discharges vertically through confining units. In eastern Wisconsin and northeastern Illinois, ground water flows from the unconfined outcrop areas, where the Cambrian-Ordovician aquifer system is recharged, toward the east, where the system is overlain by confining layer 3–4. Although the predevelopment hydraulic potential gradients indicate upward discharge to Lake Michigan, the rate of discharge was probably small due to the relative impermeability of the Maquoketa confining unit. In northwestern Iowa, ground water from overlying drift and Cretaceous deposits recharges the Cambrian-Ordovician aquifer system and flows along regional flow paths to the southeast. Gradual head loss occurs because of friction and upward leakage along the flow paths. The rate of leakage is very small because of the low vertical hydraulic conductivity of the Maquoketa Shale and the great thickness of the Devonian, Mississippian, and Pennsylvanian rock sequence (figs. 9, 11).

SIMULATION OF THE AQUIFER SYSTEM

A quasi-three-dimensional model of the Cambrian-Ordovician aquifer system was developed to estimate the direction and magnitude of regional ground-water flow and to refine the conceptualization of the regional flow system.

The computer code for the model used in this study is documented in Trescott (1975) and Trescott and Larson (1976). In its quasi-three-dimensional form, the program simulates horizontal flow within aquifers and vertical leakage through confining units between aquifers.

The Trescott and Larson code is based on the assumption that the aquifers are horizontal and contain ground water of uniform density. The aquifers can be nonhomogeneous and anisotropic, and the coordinate axes are assumed to be aligned with the principal directions of the hydraulic-conductivity tensor. Except for the uppermost layer, which may be simulated as unconfined, underlying aquifers are treated as confined. The confining units can be nonhomogeneous and are assumed to have negligible storage. Stresses on the aquifer system can be in the form of well discharge, well recharge, and recharge from precipitation.

The general form of the quasi-three-dimensional flow equation used in the flow model is

$$\frac{\partial}{\partial x}\left(K_{xx}b\frac{\partial h}{\partial x}\right)+\frac{\partial}{\partial y}\left(K_{yy}b\frac{\partial h}{\partial y}\right)+q_v+W=S\frac{\partial h}{\partial t}, \qquad (1)$$

where

x,y = space coordinates (L),
K_{xx} = principal component of the hydraulic-conductivity tensor in the x direction (L/T),
b = thickness of the aquifer (L),
h = hydraulic head (L),
K_{yy} = principal component of the hydraulic-conductivity tensor in the y direction (L/T),
q_v = vertical leakage through confining units (L/T),
W = volumetric flux per unit area of aquifer (L/T),
S = storage coefficient (dimensionless), and
t = time variable (T).

The source term, W, which can vary spatially and with time, accounts for all stresses on the aquifer system, including recharge from precipitation and well discharge or recharge. Vertical leakage, q_v, is described by

$$q_v = \frac{K'}{b'}(h' - h), \tag{2}$$

where

K' = vertical hydraulic conductivity of the confining unit (L/T),
b' = thickness of the confining unit (L),
h' = hydraulic head of the adjacent aquifer (L), and
h = head in the aquifer of interest (L).

In a multilayer problem, vertical leakage from adjacent aquifers can come from above or below a given aquifer. The finite-difference form of equation 1 is described by Bredehoeft and Pinder (1970). For this study, the finite-difference equations were solved by the slice-successive-over-relaxation method (SSOR). The SSOR solution scheme is described by Wattenbarger and Thurnau (1976), McDonald and Harbaugh (1983), and Kontis and Mandle (1989).

MODIFICATIONS TO THE TRESCOTT THREE-DIMENSIONAL MODEL

The effects of two conditions in the model area, the presence of brines in the Illinois and Michigan basins and the existence of wells open to more than one aquifer, cannot be simulated with the documented version of the Trescott code (Trescott, 1975; Trescott and Larson, 1976) because of the model code assumptions that ground water is of constant density and that a given well is open to only a single aquifer.

To simulate the effect of brines on the regional freshwater flow system, an approach suggested by Bennett (1980) was used wherein it is assumed that although temperature and solute concentration may vary spatially, they are invariant over the time period of simulation. Under this assumption, the ground-water finite-difference equation can be rewritten to accommodate the effects of variable density and the Trescott code can be used with only minor modification. Variable-density steady-state flow equations with resultant finite-difference approximations are also discussed by Weiss (1982b) and Kuiper (1983).

In the study area, with the exception of Minnesota, a majority of the wells are open to more than one aquifer. As discussed by Bennett and others (1982), multiaquifer wells can have a significant effect on the nature of flow between aquifers connected by the wells. The flow equation that is solved in the Trescott code (eq. 1) links the head in a given node with only the heads in the four adjacent nodes within a model layer and the two adjacent nodes in the layers above and below the node. For a well open to more than one aquifer, internal flow between the aquifers in the open well is not accounted for. In addition, most measured water levels in multiaquifer wells are a composite of generally unequal heads of the aquifers. Consequently, to simulate the effects of multiaquifer wells and to provide a means of calibrating model results, modifications were made to the flow equation and to the Trescott code.

FORMULATION OF VARIABLE-DENSITY FLOW EQUATION

For a volume element of aquifer inclined with respect to the horizontal axes x and y and with sides parallel to the axes of the α, β, γ coordinate system shown in figure 16, where α, β, and γ are assumed to be the principal axes of the permeability tensor, the specific discharge of ground water may be expressed by Darcy's Law (De Weist, 1969) as

$$\bar{q} = \frac{-\mathbf{k}}{\mu}(\nabla P + \rho_s g \nabla Z), \tag{3}$$

where

$\bar{q}$ = specific discharge (L/T), $\bar{q} = \bar{q}\ (\alpha, \beta, \gamma)$,
$\mathbf{k}$ = intrinsic permeability tensor whose principal axes are aligned with the α, β, γ axes (L^2),
μ = dynamic viscosity of the ground water (M/LT), $\mu = \mu\ (\alpha, \beta, \gamma)$,
∇ = the gradient operator in the α, β, γ coordinate system, expressed as

$$\nabla = \frac{\partial}{\partial \alpha}\bar{\alpha} + \frac{\partial}{\partial \beta}\bar{\beta} + \frac{\partial}{\partial \gamma}\bar{\gamma}, \quad \text{and}$$

$\bar{\alpha}$, $\bar{\beta}$, $\bar{\gamma}$ = unit vectors in the α, β, γ coordinate system,
P = hydraulic pressure (M/LT^2), $P = P\ (\alpha, \beta, \gamma)$,
ρ_s = density of the ground water, defined as the total mass per volume of solution (M/L^3), $\rho_s = \rho_s\ (\alpha, \beta, \gamma)$,
g = Earth's gravitational acceleration, assumed to be constant and directed along the z axis (L/T^2), and
Z = elevation above a datum (L), $Z = Z\ (\alpha, \beta, \gamma)$.

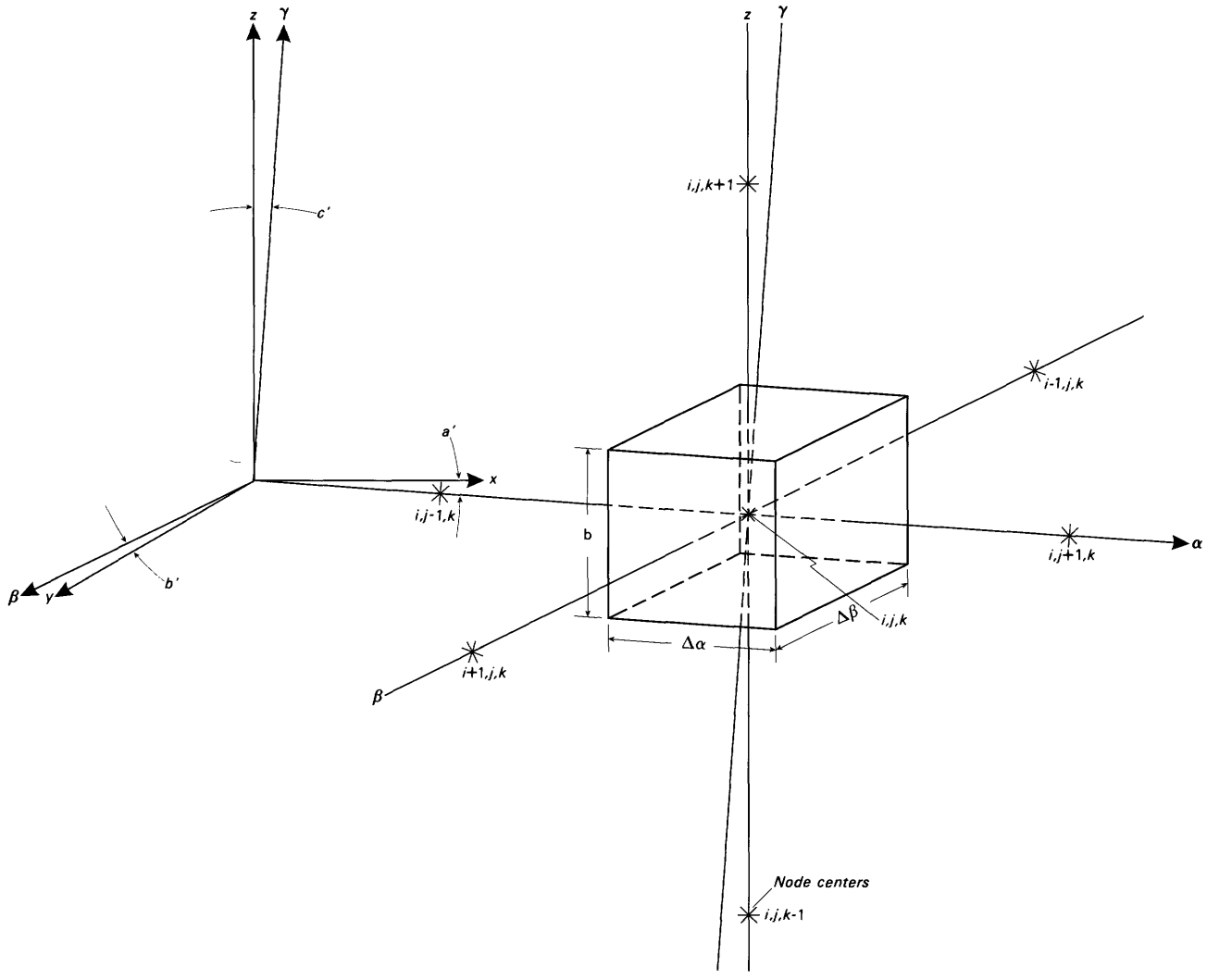

FIGURE 16.—α, β, γ coordinate system showing orientation of finite-difference node i,j,k relative to the x,y,z coordinate system.

To formulate the mass balance for ground water of variable density it is assumed that density varies spatially owing to chemical dissolution, precipitation, or other processes but is independent of time. To balance the total mass in an aquifer element it is necessary to know the sources and sinks of the solutes. Such information is difficult, if not impossible, to obtain. For this study, the mass of equivalent pure water entering and leaving an aquifer element is assumed to be balanced. In addition, the dispersion of pure water is assumed to be negligible. The pure water mass is calculated by multiplying the volumetric flux terms by a pure water density defined as

$$\rho_p = \rho_s - \rho_i \,, \tag{4}$$

where

ρ_p = density of pure water, defined as the mass of pure water per volume of solution (M/L^3), and

ρ_i = density of the solutes in the ground water, defined as the mass of solute per volume of solution (M/L^3).

Note that ρ_p is treated here as a variable in space because solute concentrations may be so large that the volume of pure water in a unit volume of solution is reduced. Thus ρ_p does not refer to the (constant) density of pure water under standard laboratory conditions, but rather to the mass of pure water in a unit volume of ground water, as observed in the field. Over most of the study area, solute concentrations are sufficiently low so that ρ_p can be taken as 1.94 slugs/ft^3; however, in some

deeper parts of the Illinois and Michigan basins, concentrations reach levels at which this assumption of a constant value is no longer valid.

Balancing the inflow and outflow of pure water mass for an aquifer element, neglecting dispersive movement of pure water, and assuming steady-state conditions yields the equation

$$\sum_{m=1}^{6}\left[-\Delta A\rho_p\frac{\mathbf{k}}{\mu}(\nabla P+\rho_s g\nabla Z)\right]_m+\rho_p Q=0, \qquad (5)$$

where the summation represents integration of mass inflow and outflow per unit time across the six faces of an aquifer element and where

ΔA = cross-sectional flow area of the mth face of an aquifer element (L^2) and

Q = a source or sink term representing addition or removal of water from an aquifer element (L^3/T).

If pressure is written in terms of freshwater head, that is, $P=\rho_f g(h_f-Z)$, then equation 5 becomes

$$\sum_{m=1}^{6}\left\{-\Delta A\rho_p\frac{\mathbf{k}\rho_f g}{\mu}\left[\nabla h_f+\left(\frac{\rho_s}{\rho_f}-1\right)\nabla Z\right]\right\}_m+\rho_p Q=0, \qquad (6)$$

where

ρ_f = density of freshwater at a temperature of 20 °C (M/L^3) and

h_f = equivalent freshwater head for water of density ρ_f (L).

Let $\mathbf{K}$ be the hydraulic-conductivity tensor of the equivalent freshwater aquifer having an intrinsic permeability tensor of $\mathbf{k}$, with ground water of density ρ_f and dynamic viscosity of μ_f, defined by

$$\mathbf{K}=\frac{\mathbf{k}\rho_f g}{\mu_f} \qquad (L/T). \qquad (7)$$

Equation 6 expressed in terms of hydraulic conductivity, $\mathbf{K}$, becomes

$$\sum_{m=1}^{6}\left\{-\Delta A\rho_p\frac{\mathbf{K}}{\mu'}[\nabla h_f+(\rho'-1)\nabla Z]\right\}_m+\rho_p Q=0, \qquad (8)$$

where

μ' = the relative viscosity, or ratio of the dynamic viscosity of the ground water of interest to the dynamic viscosity of the equivalent freshwater at 20 °C, that is, $\mu'=\mu/\mu_f$, and

ρ' = the relative density, or ratio of the density of the ground water of interest to the density of the equivalent freshwater at a temperature of 20 °C, that is, $\rho'=\rho_s/\rho_f$.

In passing to the finite-difference approximation of equation 8 it is assumed that flow through the aquifers can be described by a quasi-three-dimensional approach, that is, that flow within an aquifer is essentially parallel to the plane of the aquifer and that leakage occurs through confining layers above and below the aquifers. In addition, it is assumed that for transient conditions, changes in head over the time of simulation will not significantly alter density and viscosity, especially if transient effects are confined to areas far removed from brine areas. Using the notation of figure 16, the finite-difference approximation of equation 8 for node i,j,k applicable for transient simulations, and where hydraulic conductivity, viscosity, density, elevation, and head are now considered to be averaged in the γ direction, is

$$\begin{aligned}
&-\left(\frac{K_{\alpha\alpha}b\rho_p}{\mu'}\right)_{i,j-1/2,k}\cdot\frac{\Delta\beta}{(\alpha_{i,j,k}-\alpha_{i,j-1,k})}[h_{f_{i,j,k}}-h_{f_{i,j-1,k}}+(\rho'-1)_{i,j-1/2,k}(Z_{i,j,k}-Z_{i,j-1,k})]\\
&+\left(\frac{K_{\alpha\alpha}b\rho_p}{\mu'}\right)_{i,j+1/2,k}\cdot\frac{\Delta\beta}{(\alpha_{i,j+1,k}-\alpha_{i,j,k})}[h_{f_{i,j+1,k}}-h_{f_{i,j,k}}+(\rho'-1)_{i,j+1/2,k}(Z_{i,j+1,k}-Z_{i,j,k})]\\
&-\left(\frac{K_{\beta\beta}b\rho_p}{\mu'}\right)_{i-1/2,j,k}\cdot\frac{\Delta\alpha}{(\beta_{i,j,k}-\beta_{i-1,j,k})}[h_{f_{i,j,k}}-h_{f_{i-1,j,k}}+(\rho'-1)_{i-1/2,j,k}(Z_{i,j,k}-Z_{i-1,j,k})]\\
&+\left(\frac{K_{\beta\beta}b\rho_p}{\mu'}\right)_{i+1/2,j,k}\cdot\frac{\Delta\alpha}{(\beta_{i+1,j,k}-\beta_{i,j,k})}[h_{f_{i+1,j,k}}-h_{f_{i,j,k}}+(\rho'-1)_{i+1/2,j,k}(Z_{i+1,j,k}-Z_{i,j,k})]\\
&-\left(\frac{K_{\gamma\gamma}\rho_p}{b_L\mu'}\right)_{i,j,k-1/2}\cdot\Delta\alpha\Delta\beta\left[h_{f_{i,j,k}}-h_{f_{i,j,k-1}}+b_L(\rho'-1)_{i,j,k-1/2}\frac{(Z_{i,j,k}-Z_{i,j,k-1})}{(\gamma_{i,j,k}-\gamma_{i,j,k-1})}\right]\\
&+\left(\frac{K_{\gamma\gamma}\rho_p}{b_U\mu'}\right)_{i,j,k+1/2}\cdot\Delta\alpha\Delta\beta\left[h_{f_{i,j,k+1}}-h_{f_{i,j,k}}+b_U(\rho'-1)_{i,j,k+1/2}\frac{(Z_{i,j,k+1}-Z_{i,j,k})}{(\gamma_{i,j,k+1}-\gamma_{i,j,k})}\right]\\
&\qquad=\rho_p S\Delta\alpha\Delta\beta\frac{\Delta h_{f_{i,j,k}}}{\Delta t}-\rho_p Q, \qquad (9)
\end{aligned}$$

where unscripted terms are at i,j,k, and where

$K_{\alpha\alpha}$, $K_{\beta\beta}$, $K_{\gamma\gamma}$ = components of the hydraulic conductivity tensor in the α, β, and γ directions (L/T),

b = average thickness of aquifer at node i,j,k (L),

$\Delta\alpha$, $\Delta\beta$ = dimensions of the finite-difference block i,j,k of the aquifer (L),

b_U, b_L = average thicknesses in the γ direction of the confining units above and below node i,j,k (L),

S = storage coefficient of aquifer at node i,j,k (dimensionless),

Δt = length of time increment (T), and

Δh = head change (L) per time increment.

The relative density of the ground water ($\rho'=\rho_s/\rho_f$) at the finite-difference block faces is obtained by averaging the densities at adjacent nodes. The rate of change of elevation with respect to γ is approximated by

$$\frac{(Z_{i,j,k+1}-Z_{i,j,k})}{(\gamma_{i,j,k+1}-\gamma_{i,j,k})}\sim\cos\alpha'\cos b'|_{i,j,k}=\left.\frac{\Delta x\Delta y}{\Delta\alpha\Delta\beta}\right|_{i,j,k}, \qquad (10)$$

where

a', b' = angles between the α, β, and x,y axes, respectively (fig. 16) and

$\Delta x, \Delta y$ = horizontal dimensions of the finite-difference block i,j,k of the aquifer projected to land surface (L).

The finite-difference equation (eq. 9) may be simplified by introducing hydraulic-conductance notation, resulting in

$$\begin{aligned} &-TR_{i,j-1,k}(h_{f_{i,j,k}}-h_{f_{i,j-1,k}}) + A_{i,j-1,k} \\ &+ TR_{i,j,k}(h_{f_{i,j+1,k}}-h_{f_{i,j,k}}) - A_{i,j,k} \\ &- TC_{i-1,j,k}(h_{f_{i,j,k}}-h_{f_{i-1,j,k}}) + B_{i-1,j,k} \\ &+ TC_{i,j,k}(h_{f_{i+1,j,k}}-h_{f_{i,j,k}}) - B_{i,j,k} \\ &- TK_{i,j,k-1}(h_{f_{i,j,k}}-h_{f_{i,j,k-1}}) + \Gamma_{i,j,k-1} \\ &+ TK_{i,j,k}(h_{f_{i,j,k+1}}-h_{f_{i,j,k}}) - \Gamma_{i,j,k} \\ &= S^* \frac{\Delta h_{f_{i,j,k}}}{\Delta t} - Q^*, \end{aligned} \tag{11a}$$

where

$$\begin{aligned} TR_{i,j-1,k} &= \frac{\Delta\beta\left(\frac{K_{\alpha\alpha}b\rho_p}{\mu'}\right)_{i,j-1/2,k}}{\alpha_{i,j,k}-\alpha_{i,j-1,k}} \\ &= \frac{2\Delta\beta\left(\frac{K_{\alpha\alpha}b\rho_p}{\mu'}\right)_{i,j,k}\cdot\left(\frac{K_{\alpha\alpha}b\rho_p}{\mu'}\right)_{i,j-1,k}}{\Delta\alpha_{i,j,k}\left(\frac{K_{\alpha\alpha}b\rho_p}{\mu'}\right)_{i,j-1,k}+\Delta\alpha_{i,j-1,k}\left(\frac{K_{\alpha\alpha}b\rho_p}{\mu'}\right)_{i,j,k}}. \end{aligned} \tag{11b}$$

$TR_{i,j-1,k}$ is the harmonic mean of transmissivities at nodes i,j,k and $i,j\text{-}1,k$. Similarly, the harmonic means of transmissivities at surrounding nodes are

(11b cont.)

$$TR_{i,j,k} = \frac{2\Delta\beta\left(\frac{K_{\alpha\alpha}b\rho_p}{\mu'}\right)_{i,j,k}\cdot\left(\frac{K_{\alpha\alpha}b\rho_p}{\mu'}\right)_{i,j+1,k}}{\Delta\alpha_{i,j,k}\left(\frac{K_{\alpha\alpha}b\rho_p}{\mu'}\right)_{i,j+1,k}+\Delta\alpha_{i,j+1,k}\left(\frac{K_{\alpha\alpha}b\rho_p}{\mu'}\right)_{i,j,k}},$$

$$TC_{i-1,j,k} = \frac{2\Delta\alpha\left(\frac{K_{\beta\beta}b\rho_p}{\mu'}\right)_{i,j,k}\cdot\left(\frac{K_{\beta\beta}b\rho_p}{\mu'}\right)_{i-1,j,k}}{\Delta\beta_{i,j,k}\left(\frac{K_{\beta\beta}b\rho_p}{\mu'}\right)_{i-1,j,k}+\Delta\beta_{i-1,j,k}\left(\frac{K_{\beta\beta}b\rho_p}{\mu'}\right)_{i,j,k}},$$

$$TC_{i,j,k} = \frac{2\Delta\alpha\left(\frac{K_{\beta\beta}b\rho_p}{\mu'}\right)_{i,j,k}\cdot\left(\frac{K_{\beta\beta}b\rho_p}{\mu'}\right)_{i+1,j,k}}{\Delta\beta_{i,j,k}\left(\frac{K_{\beta\beta}b\rho_p}{\mu'}\right)_{i+1,j,k}+\Delta\beta_{i+1,j,k}\left(\frac{K_{\beta\beta}b\rho_p}{\mu'}\right)_{i,j,k}},$$

$$TK_{i,j,k-1} = \Delta\alpha\Delta\beta\left(\frac{K_{\gamma\gamma}\rho_p}{b_L\mu'}\right)_{i,j,k-1/2}, \text{ and}$$

$$TK_{i,j,k} = \Delta\alpha\Delta\beta\left(\frac{K_{\gamma\gamma}\rho_p}{b_U\mu'}\right)_{i,j,k+1/2}.$$

The remaining terms, those representing the effects of gravity forces and the variable-density form of the storage coefficient and the well term, are represented by the following expressions:

$$\begin{aligned} A_{i,j-1,k} &= -TR_{i,j-1,k}(\rho'-1)_{i,j-1/2,k}(Z_{i,j,k}-Z_{i,j-1,k}) \\ A_{i,j,k} &= -TR_{i,j,k}(\rho'-1)_{i,j+1/2,k}(Z_{i,j+1,k}-Z_{i,j,k}) \\ B_{i-1,j,k} &= -TC_{i-1,j,k}(\rho'-1)_{i-1/2,j,k}(Z_{i,j,k}-Z_{i-1,j,k}) \\ B_{i,j,k} &= -TC_{i,j,k}(\rho'-1)_{i+1/2,j,k}(Z_{i+1,j,k}-Z_{i,j,k}) \\ \Gamma_{i,j,k-1} &= -TK_{i,j,k-1}b_L(\rho'-1)_{i,j,k-1/2}\left(\frac{\Delta x\Delta y}{\Delta\alpha\Delta\beta}\right)_{i,j,k} \\ \Gamma_{i,j,k} &= -TK_{i,j,k}b_U(\rho'-1)_{i,j,k+1/2}\left(\frac{\Delta x\Delta y}{\Delta\alpha\Delta\beta}\right)_{i,j,k} \\ S^* &= (\Delta\alpha\Delta\beta\rho_p S)_{i,j,k}, \text{ and} \\ Q^* &= (\rho_p Q)_{i,j,k}. \end{aligned} \tag{11c}$$

Because the terms of the first six expressions in equation 11c are all known and are independent of head, they can be incorporated into a single term, $TS_{i,j,k}$, resulting in

$$\begin{aligned} &-TR_{i,j-1,k}(h_{f_{i,j,k}}-h_{f_{i,j-1,k}}) + TR_{i,j,k}(h_{f_{i,j+1,k}}-h_{f_{i,j,k}}) \\ &-TC_{i-1,j,k}(h_{f_{i,j,k}}-h_{f_{i-1,j,k}}) + TC_{i,j,k}(h_{f_{i+1,j,k}}-h_{f_{i,j,k}}) \\ &-TK_{i,j,k-1}(h_{f_{i,j,k}}-h_{f_{i,j,k-1}}) + TK_{i,j,k}(h_{f_{i,j,k+1}}-h_{f_{i,j,k}}) \\ &= S^* \frac{\Delta h_{f_{i,j,k}}}{\Delta t} - Q^* - TS_{i,j,k}, \end{aligned} \tag{11d}$$

where

$$TS_{i,j,k} = A_{i,j-1,k} - A_{i,j,k} + B_{i-1,j,k} - B_{i,j,k} + \Gamma_{i,j,k-1} - \Gamma_{i,j,k}. \tag{11e}$$

The form of equation 11d is now the same as that of the finite-difference equations of the Trescott code with the exception of the TS term. This term represents the net effect of gravity forces exerted on the flow system by ground-water mass in a tilted aquifer block.

In areas containing relatively fresh water, the individual terms A, B, and Γ are zero or very small so that the magnitude of flow across model block faces is propor-

tional to the head gradient and flow is essentially orthogonal to contours of freshwater head. In areas containing brines, and where aquifers are not horizontal, the flow may be significantly altered by the A, B, Γ terms of equation 11c and resultant flow directions will not be orthogonal to lines of equal freshwater head. The condition for no flow in these areas is that the freshwater head gradient in a particular direction be exactly opposed by the net effect of the gravitational forces.

The volumetric flow components for any node i,j,k are computed by

$$QR_{i,j,k} = [-TR_{i,j,k}(h_{f_{i,j+1,k}} - h_{f_{i,j,k}}) + A_{i,j,k}]/\rho_{p_{i,j+1/2,k}}, \quad (12a)$$

$$QC_{i,j,k} = [-TC_{i,j,k}(h_{f_{i+1,j,k}} - h_{f_{i,j,k}}) + B_{i,j,k}]/\rho_{p_{i+1/2,j,k}}, \text{ and} \quad (12b)$$

$$QK_{i,j,k} = [-TK_{i,j,k}(h_{f_{i,j,k+1}} - h_{f_{i,j,k}}) + \Gamma_{i,j,k}]/\rho_{p_{i,j,k+1/2}}, \quad (12c)$$

where

$QR_{i,j,k}$=flow along rows between nodes i,j,k and $i,j+1,k$ (L^3/T),

$QC_{i,j,k}$=flow along columns between nodes i,j,k and $i+1,j,k$ (L^3/T), and

$QK_{i,j,k}$=flow across confining layers between nodes i,j,k and $i,j,k+1$ (L^3/T), and

where the pure-water density term in each expression is the average value for the pair of nodes in question.

The magnitude of resultant flow, Q_n, within a layer at node i,j,k is

$$|Q_n|_{i,j,k} = \sqrt{QR^2_{i,j,k} + QC^2_{i,j,k}} \quad (12d)$$

and the angle of the resultant flow within a layer at node i,j,k is

$$A_{Q_{i,j,k}} = \tan^{-1}[QR_{i,j,k}/QC_{i,j,k}]. \quad (12e)$$

The variable-density flow formulation (eq. 11d) was tested by comparing model results (Kontis and Mandle, 1989) with the results of a cross-sectional analog model of a freshwater-saltwater interface problem discussed by Bennett and Giusti (1971). In addition, Weiss (1982b) and Kuiper (1983) achieved good agreement between model results using formulations similar to equation 11d and known analytical solutions for a variety of test cases.

To obtain the variable-density and hydraulic-conductance terms of equation 11d, a computer code, termed "VARDEN" (VARiable DENsity), was developed to compute, exterior to the Trescott code, the values of TR, TC, and TK, the variable-density terms A, B, Γ, and TS for each finite-difference node. Modifications of the Trescott code consist of insertion of statements to (1) read TR and TC directly, (2) bypass the subroutine Entry TCOF, wherein the values of TR and TC were formerly computed, and (3) increase the two-dimensional recharge array, QRE, to three dimensions to provide space for the variable-density term, TS. A description of the computer code modifications, the method of determining the geometric terms of equation 9, and a description of the VARDEN computer program are documented by Kontis and Mandle (1989).

MULTIAQUIFER WELL EFFECTS

Bennett and others (1982) outline a method of accounting approximately for the effects of multiaquifer wells in three-dimensional ground-water flow simulation. Their analysis is based on the assumptions that there is only one multiaquifer well within the area represented by any one model node, that the well is located exactly at the nodal point, and that radial symmetry prevails in the head distribution surrounding the well in each aquifer. Their finite-difference equation (for node i,j,k of a three-dimensional grid) that accounts for the effects of the single multiaquifer well can be expressed (with modified notation) as

$$L(h_{i,j,k}) - Q_{i,j,k} = 0, \quad (13)$$

where $L(h_{i,j,k})$ represents all terms of the finite-difference flow equation for node i,j,k except those describing the effects of the multiaquifer well and $Q_{i,j,k}$ is the flow between layer k and the multiaquifer well, given by

$$Q_{i,j,k} = \left\{ \frac{2\pi T_{i,j,k} h_{i,j,k}}{\ln\left(\frac{r_{a_k}}{r_w}\right)} - \frac{2\pi T_{i,j,k}}{\ln\left(\frac{r_{a_k}}{r_w}\right)} \left[\frac{\sum_{n=1}^{k_{max}} \left[\frac{T_{i,j,n} h_{i,j,n}}{\ln\left(\frac{r_{a_n}}{r_w}\right)} \right] \delta[W(n)]}{\sum_{n=1}^{k_{max}} \left[\frac{T_{i,j,n}}{\ln\left(\frac{r_{a_n}}{r_w}\right)} \right] \delta[W(n)]} \right] + \frac{T_{i,j,k} Q_{w_T}}{\ln\left(\frac{r_{a_k}}{r_w}\right) \sum_{n=1}^{k_{max}} \left[\frac{T_{i,j,n}}{\ln\left(\frac{r_{a_n}}{r_w}\right)} \right] \delta[W(n)]} \right\} \delta[W(k)], \quad (14)$$

where

T=transmissivity of aquifer layer (L^2/T),

r_{a_k}=radial distance from the well in aquifer layer k at which the head $h_{i,j,k}$ is assumed to prevail (L),

r_w=well radius (L),

k_{max}=total number of aquifer layers in the model,

r_{a_n}=radial distance from the well in aquifer layer n at which the head $h_{i,j,n}$ is assumed to prevail (L), and

Q_{w_T}=total discharge of a multiaquifer well (L^3/T).

The term W is a function that specifies the sequence of aquifer layers open to a multiaquifer well and δ is a function to isolate a particular aquifer layer if the layer is open to a well and to ensure that only those layers open to a well are included in the summation by layer. In particular, for all k (k=1,2,...k_{max}),

$$W(k)=\begin{cases} k \text{ if a well is open to layer } k \\ 0 \text{ if a well is not open to layer } k \end{cases}$$

and

$$\delta[W(k)]=\begin{cases} 1 \text{ if } W(k)=k \\ 0 \text{ if } W(k)=0 \end{cases}$$

In equation 14, $\delta[W(k)]$ specifies that there is flow between layer k and a well only if the well is open to layer k and δ $[W(n)]$ specifies that only layers open to the well are included in the summations.

A graphic representation of flow and head around a multiaquifer well open to four layers is shown in figure 17. Equation 14 is obtained by assuming that the head computed in the simulation for node i,j,k actually prevails in the aquifer along a circle of radius r_{a_k} around the well (and thus around node i,j,k itself) and that the flow from the aquifer into the well can, therefore, be calculated by the Thiem equation as

$$Q_{i,j,k} = \left[\frac{2\pi T_{i,j,k}(h_{i,j,k}-h_w)}{\ln\left(\frac{r_{a_k}}{r_w}\right)}\right]\delta[W(k)], \qquad (15)$$

where h_w is the water level in the multiaquifer well. The total discharge of the well, Q_{w_T}, is then taken as the algebraic sum of the inflows from all aquifers open to the well, that is

$$Q_{w_T} = \sum_{n=1}^{k_{max}}\left[\frac{2\pi T_{i,j,n}(h_{i,j,n}-h_w)}{\ln\left(\frac{r_{a_n}}{r_w}\right)}\right]\delta[W(n)]. \qquad (16)$$

Equation 16 is solved for h_w and the result substituted into equation 15 to obtain equation 14.

As noted previously, the finite-difference equation used in the present study was phrased in terms of the mass of pure water with density of ρ_p. To express equation 15 in these terms, transmissivity, $T_{i,j,k}$, must be replaced by the term $T^*_{i,j,k}$, where

$$T^*_{i,j,k} = \left(\frac{K_{\alpha\alpha}b\rho_p}{\mu'}\right)_{i,j,k} = \left(\frac{K_{\beta\beta}b\rho_p}{\mu'}\right)_{i,j,k}, \qquad (17)$$

and where $K_{\alpha\alpha}$, $K_{\beta\beta}$, b, and μ' are as previously defined (eqs. 8 and 9).

The assumption is made that within the region affected by an individual multiaquifer well, the dip of aquifer layers is sufficiently small so that the elevation gradient term of equation 3 can be neglected. Under these conditions, equation 15 can be written in terms of pure water mass as

$$\rho_p Q_{i,j,k} = \left[\frac{2\pi T^*_{i,j,k}(h_{f_{i,j,k}}-h_{fw})}{\ln\left(\frac{r_{a_k}}{r_w}\right)}\right]\delta[W(k)], \qquad (18)$$

where $h_{fi,j,k}$ is the head computed for the node and h_{fw} is the head in the well, both in terms of a column of water of density ρ_p and, where $\rho_p Q$ gives the rate of flow, in terms of mass of pure water per unit time, from node i,j,k to the multiaquifer well. Equation 16 can in turn be rewritten in terms of pure water mass as

$$\rho_p Q_{w_T} = \sum_{n=1}^{k_{max}}\left[\frac{2\pi T^*_{i,j,n}(h_{f_{i,j,n}}-h_{fw})}{\ln\left(\frac{r_{a_n}}{r_w}\right)}\right]\delta[W(n)], \qquad (19)$$

where $\rho_p Q_{w_T}$ represents the discharge, in terms of mass of pure water per unit time, from the multiaquifer well. Equation 14 can similarly be rewritten in terms of pure water mass as

$$\rho_p Q_{i,j,k} = \left\{\frac{2\pi T^*_{i,j,k}h_{f_{i,j,k}}}{\ln\left(\frac{r_{a_k}}{r_w}\right)} - \frac{2\pi T^*_{i,j,k}}{\ln\left(\frac{r_{a_k}}{r_w}\right)}\left[\frac{\sum_{n=1}^{k_{max}}\left[\frac{T^*_{i,j,n}h_{f_{i,j,n}}}{\ln\left(\frac{r_{a_n}}{r_w}\right)}\right]\delta[W(n)]}{\sum_{n=1}^{k_{max}}\left[\frac{T^*_{i,j,n}}{\ln\left(\frac{r_{a_n}}{r_w}\right)}\right]\delta[W(n)]}\right]\right.$$

$$\left. + \frac{T^*_{i,j,k}Q_{w_T}}{\ln\left(\frac{r_{a_k}}{r_w}\right)\sum_{n=1}^{k_{max}}\left[\frac{T^*_{i,j,n}}{\ln\left(\frac{r_{a_n}}{r_w}\right)}\right]\delta[W(n)]}\right\}\delta[W(k)]. \qquad (20)$$

Prickett (1967), in considering the relation between the computed head in a finite-difference grid of uniform spacing, a, and the water level in a single well located exactly at the nodal point, developed a rationale by which

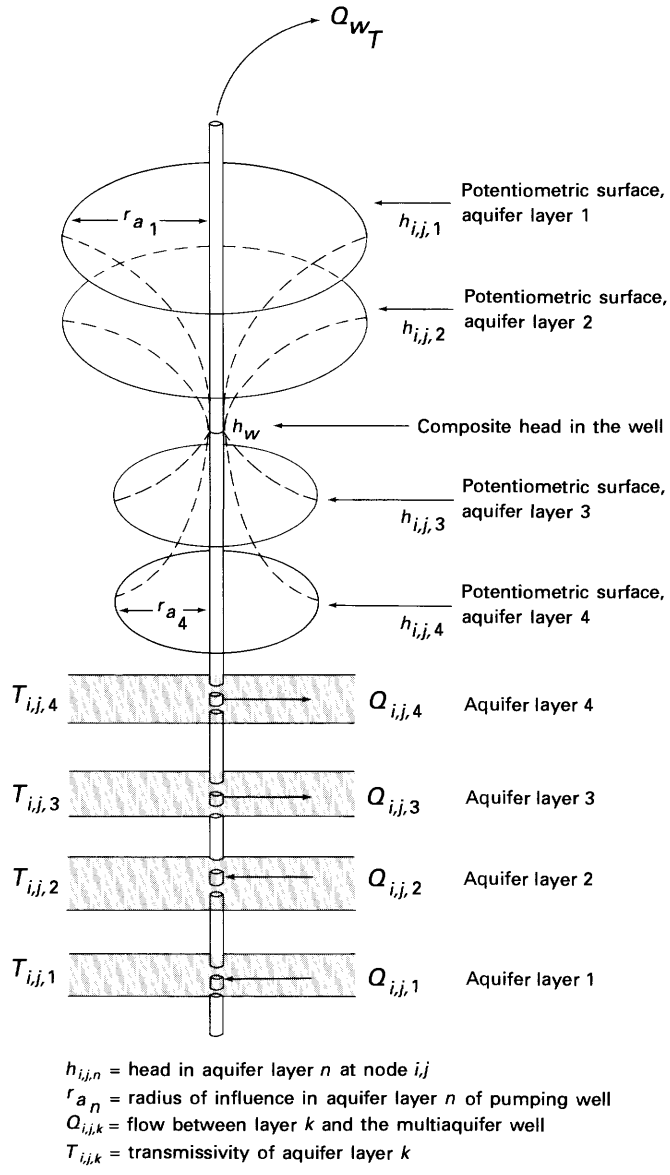

FIGURE 17.—Conditions of flow and head around a typical multiaquifer well. (Modified from Bennett and others, 1982.)

r_{a_k} can be taken as $a/4.81$. No clear rationale has yet been developed for the choice of r_{a_k} where more than one well falls in the area represented by a single node; as a result, certain more or less arbitrary assumptions must be made in dealing with such cases. In the present study, it was assumed that the wells open to a given layer, k, within the map area $\Delta x_j \Delta y_i$ (that is, the map area represented by node i,j,k) are evenly distributed over an area, s^2, where s is the smaller of Δx_j or Δy_i. Thus, each well was assumed to fall at the center of a square of area s^2/N_k and side length $\sqrt{s^2/N_k}$, where N_k is the number of wells affecting node i,j,k—that is, the total number of wells located in map area $\Delta x_j \Delta y_i$, and open to layer k. Prickett's relation was assumed to apply to these square subareas rather than to the node area, $\Delta x_j \Delta y_i$. That is, it was assumed that the head $h_{fi,j,k}$, computed in the simulation for node i,j,k, actually prevails along circles of radius r_{a_k} around each well in the node area, where r_{a_k} is given by

$$r_{a_k} = \frac{\sqrt{\frac{s^2}{N_k}}}{4.81} = \frac{s}{4.81}\sqrt{\frac{1}{N_k}}. \qquad (21)$$

This method of estimating r_{a_k} is certainly an oversimplification of the field situation; however, the objective of the analysis was to approximate the total effect of numerous multiaquifer wells on the flow system rather than to provide detailed appraisals of the performance of individual wells, and in this sense the use of equation 21 to estimate r_{a_k} seems to be justified.

To further implement the multiaquifer well analysis for the case in which numerous wells affect a single node, the wells located within map area $\Delta x_j \Delta y_i$ were segregated into categories, such that an individual category includes all of the wells open to a particular combination of aquifers. If it is assumed that each well in a given category operates at the same well discharge, Q_{w_T}, has the same well radius, r_w, and exhibits the same water level, h_{fw}, the total discharge, in terms of pure water mass, from the wells of a single category (located in map area $\Delta x_j \Delta y_i$) can be obtained by summing equation 19 over the wells of that category. Thus, if there are u_m wells in category m,

$$\rho_p Q_{T_m} = \sum_{l=1}^{u_m} \sum_{n=1}^{k_{max}} \left[\frac{2\pi T^*_{i,j,n}(h_{fi,j,n} - h_{fw})}{\ln\left(\frac{r_{a_n}}{r_w}\right)} \right] \delta[W_l(n,m)], \qquad (22)$$

where $\rho_p Q_{T_m}$ is the total discharge from all wells of the category m, in mass of pure water per unit time and for each of the u_m wells (that is, for all values of l; $1=1,2,\ldots u_m$)

$$W_1(n,m) = \begin{cases} n \text{ if a category } m \text{ well is open to layer } n \\ 0 \text{ if a category } m \text{ well is not open to layer } n \end{cases}$$

and

$$\delta[W_1(n,m)] = \begin{cases} 1 \text{ if } W(n,m) = n \\ 0 \text{ if } W(n,m) = 0 \end{cases}$$

Note that equation 22 evaluates the total discharge of the wells rather than the flow from a single layer (that is,

from node i,j,k) into the wells. Equation 22 can be expanded as follows:

$$\rho_p Q_{T_m} = \sum_{l=1}^{u_m} \left\{ \sum_{n=1}^{k_{max}} \left[\frac{2\pi T^*_{i,j,n} h_{f_{i,j,n}}}{\ln\left(\frac{r_{a_n}}{r_w}\right)} \right] \delta[W_l(n,m)] - h_{fw} \sum_{n=1}^{k_{max}} \left[\frac{2\pi T^*_{i,j,n}}{\ln\left(\frac{r_{a_n}}{r_w}\right)} \right] \delta[W_l(n,m)] \right\}, \quad (23)$$

where h_{fw} has been taken outside the summation over aquifer layers in an individual well, because the water level of a well is the same for all aquifers penetrated by the well.

Because all of the wells in a category (as indicated by the $W(n,m)$ notation) are open to the same sequence of aquifers, the interior summations are taken over the same range of aquifer layers and the terms $T^*_{i,j,k}$ and $h_{f_{i,j,k}}$ have the same sequence of values for every well. Furthermore, the use of equation 21 guarantees that r_{a_n} will also have the same sequence of values for every well. Under these conditions, the summation over u_m wells of the category m wells can be replaced with multiplication by u_m; that is,

$$\rho_p Q_{T_m} = u_m \sum_{n=1}^{k_{max}} \left[\frac{2\pi T^*_{i,j,n} h_{f_{i,j,n}}}{\ln\left(\frac{r_{a_n}}{r_w}\right)} \right] \delta[W(n,m)] - u_m h_{fw} \sum_{n=1}^{k_{max}} \left[\frac{2\pi T^*_{i,j,n}}{\ln\left(\frac{r_{a_n}}{r_w}\right)} \right] \delta[W(n,m)], \quad (24)$$

where the notation $W_1(n,m)$ has been replaced by $W(n,m)$ to stress the point that all wells of the category tap the same set of aquifers. Solving for h_{fw}, the water level common to wells of category m, yields

$$h_{fw_m} = \frac{\sum_{u=1}^{k_{max}} \left[\frac{T^*_{i,j,n} h_{f_{i,j,n}}}{\ln\left(\frac{r_{a_n}}{r_w}\right)} \right] \delta[W(n,m)]}{\sum_{n=1}^{k_{max}} \left[\frac{T^*_{i,j,n}}{\ln\left(\frac{r_{a_n}}{r_w}\right)} \right] \delta[W(n,m)]} - \frac{\rho_p Q_{T_m}}{2\pi u_m \sum_{n=1}^{k_{max}} \left[\frac{T^*_{i,j,n}}{\ln\left(\frac{r_{a_n}}{r_w}\right)} \right] \delta[W(n,m)]}, \quad (25)$$

where the notation h_{fw_m} has been introduced to associate the water level in the well with the category m.

Next consider the total mass flow $(\rho_p Q_{i,j,k})_m$ from node i,j,k into all wells of category m. This is obtained by summing equation 18 over the wells of the category:

$$(\rho_p Q_{i,j,k})_m = \sum_{l=1}^{u_m} \left[\frac{2\pi T^*_{i,j,k}(h_{f_{i,j,k}} - h_{fw_m})}{\ln\left(\frac{r_{a_k}}{r_w}\right)} \right] \delta[W_l(k,m)]. \quad (26)$$

Again, the terms of equation 26 are the same for all wells of category m, so the summation can be replaced with multiplication by u_m to obtain

$$(\rho_p Q_{i,j,k})_m = \left\{ \left[\frac{2\pi T^*_{i,j,k} h_{f_{i,j,k}}}{\ln\left(\frac{r_{a_k}}{r_w}\right)} \right] u_m - \left[\frac{2\pi T^*_{i,j,k}}{\ln\left(\frac{r_{a_k}}{r_w}\right)} \right] u_m h_{fw_m} \right\} \delta[W(k,m)]. \quad (27)$$

If there are N categories of wells in the map area $\Delta x_j \Delta y_i$, the total flow from node i,j,k into the wells of all categories can be obtained by summing equation 27 over the N categories. Therefore,

$$\rho_p Q^N_{i,j,k} = \frac{2\pi T^*_{i,j,k} h_{f_{i,j,k}}}{\ln\left(\frac{r_{a_k}}{r_w}\right)} \sum_{m=1}^{N} u_m \delta[W(k,m)] - \frac{2\pi T^*_{i,j,k}}{\ln\left(\frac{r_{a_k}}{r_w}\right)} \sum_{m=1}^{N} u_m h_{fw_m} \delta[W(k,m)], \quad (28)$$

where $Q^N_{i,j,k}$ indicates the total flow from node i,j,k to all wells of the N categories affecting the node. Substituting the expression for h_{fw_m} from equation 25 into equation 28 yields

$$\rho_p Q^N_{i,j,k} = \frac{2\pi T^*_{i,j,k} h_{f_{i,j,k}}}{\ln\left(\frac{r_{a_k}}{r_w}\right)} \sum_{m=1}^{N} u_m \delta[W(k,m)] - \frac{2\pi T^*_{i,j,k}}{\ln\left(\frac{r_{a_k}}{r_w}\right)} \sum_{m=1}^{N} \left\{ u_m \delta[W(k,m)] \frac{\sum_{n=1}^{k_{max}} \left[\frac{T^*_{i,j,n} h_{f_{i,j,n}}}{\ln\left(\frac{r_{a_n}}{r_w}\right)} \right] \delta[W(n,m)]}{\sum_{n=1}^{k_{max}} \left[\frac{T^*_{i,j,n}}{\ln\left(\frac{r_{a_n}}{r_w}\right)} \right] \delta[W(n,m)]} \right\}$$

$$+\frac{T^*_{i,j,k}}{\ln\left(\frac{r_{a_k}}{r_w}\right)}\sum_{m=1}^{N}\left\{\frac{\rho_p Q_{T_m}\delta[W(k,m)]}{\sum_{n=1}^{k_{max}}\left[\frac{T^*_{i,j,n}}{\ln\left(\frac{r_{a_n}}{r_w}\right)}\right]\delta[W(n,m)]}\right\}, \quad (29)$$

where, again, Q_{T_m} represents the total well discharge from all wells of category m in the node area $\Delta x_j\,\Delta y_i$, and the δ function provides that only wells of category m contribute to the summations over the N categories.

The generalized finite-difference form of equation 9, therefore, can be expressed as

$$L^*(h_{f_{i,j,k}}) - \rho_p Q^N_{i,j,k} = 0, \quad (30)$$

where $L^*(h_{f_{i,j,k}})$ includes all terms of equation 9 except the product of density and flow to wells, which is now represented by the term $\rho_p Q^N_{i,j,k}$. The finite-difference formulation of equation 9 allows the pure water density, ρ_p to be treated as a variable in space to accommodate areas of highly saline brine, where the percentage of dissolved salts may become so large that the mass of pure water per unit fluid volume is reduced. Most of the wells in the study area produce from zones of relatively fresh water in which spatial variation of ρ_p is minimal. Thus, a constant value of ρ_p, 1.94 slugs/ft^3, was used in all well-flow terms in this investigation.

In applying the multiaquifer-well analysis, the well radius, r_w, was taken as 0.5 ft for all wells. The method requires estimation of the total number of wells (u_m) of a given category, m, in a node area $\Delta x_j \Delta y_i$ and the total rate of pumping (Q_{T_m}) from the wells of category m in that node area. In some cases, no independent attempt was made to estimate u_m; rather, an average discharge of 0.1 ft^3/s per well was assumed, and the estimated value of Q_{T_m} was divided by this value to provide an estimate of u_m.

In equation 29, the first and second terms consist of various coefficients which multiply the heads of nodes that are linked to each other by the presence of multiaquifer wells. Because these links occur only at nodes above and below a given node, the slice-successive-over-relaxation (SSOR) method was chosen to solve the finite-difference equations to obtain the model heads. The SSOR method readily accommodates the multiaquifer terms because in this method a solution coefficient matrix is constructed for vertical slices along model rows. The nonzero terms of the matrix represent hydraulic conductances of the nodes within the slice. Consequently, to implement equation 29, the Trescott code was modified to compute the multiaquifer coefficients of the equation and to insert them in the proper location of the SSOR coefficient matrix. The last term in equation 29 is independent of head and, inserted into the well array of the Trescott code, serves as a source-sink term in the finite-difference equations. One consequence of equation 29 is that in simulation of flow systems containing multiaquifer wells, water will be withdrawn from each aquifer open to the well in proportion to the relative transmissivity of the aquifer. Without the code modification, contribution of water from each aquifer to the well discharge must be estimated and altered with each change in model transmissivity. Implementation of equation 29 eliminates the need for this step and allows rapid calculation of composite head from equation 25.

Changes to the Trescott code to accommodate the multiaquifer well terms, description of its use, and a listing of the SSOR subroutines are documented by Kontis and Mandle (1989).

MODEL DESIGN AND DEVELOPMENT

Describing a complex ground-water flow system in terms of a mathematical model requires various simplifications. The numerical representation of the regional flow system involves discretizing the aquifer system into finite-difference blocks, approximating aquifer boundaries and initial conditions in the aquifer system prior to ground-water development, and estimating appropriate values of hydrologic properties for each finite-difference block.

Approximation of hydrologic processes and properties over large finite-difference blocks can result in considerable averaging because they are assumed uniform over the entire extent of the block. If processes such as ground-water recharge and discharge vary over any finite-difference block, only the resultant flow determined by average hydraulic head differences is simulated by the model. Similarly, where hydrologic properties of the aquifer system vary over a considerable range, as is the case with differentially weathered rock, an average of this property is used in the regional model. The result of this approximation is that local anomalies will not be simulated by the regional flow models.

The process of designing the ground-water flow model of the Cambrian-Ordovician aquifer system and the methodology for estimating values of hydrologic properties are described in subsequent sections.

FINITE-DIFFERENCE GRID

The finite-difference grid (shown in figs. 19–22) selected to represent the aquifer system covers an area of 378,880 mi^2 and is subdivided into 7,400 blocks (40 columns×37 rows×5 layers). The rows and columns are

16 mi wide throughout the modeled area. The Trescott model requires that the nodes around the perimeter of each model layer be inactive; that is, there is zero flux between these nodes and the adjacent interior nodes.

A uniform rather than nonuniform spacing was used because the primary purpose of the simulation is to depict the overall characteristics of the aquifer system. In addition, the design and implementation of automated procedures is simpler if data are equally spaced. The 16-mi discretization is a compromise between the requirement that the spacing be sufficiently small to define regional predevelopment head and regional drawdown patterns on one hand, and computer storage and cost considerations on the other.

BOUNDARY AND INITIAL CONDITIONS

Two types of boundaries can be specified in the Trescott code: constant (prescribed) head and constant (prescribed) flux. Constant-head boundaries may be placed in areas where the head is known and changes due to various stresses are minimal over the period of simulation. Constant-flux boundaries are applicable where flow into or out of the system is known. Zero-flux boundaries are used where there is no flow into or out of the system, or where the distance from the boundary to areas of interest is sufficiently great so that boundary effects are not observed in the area of interest.

The upper boundary of the model consists of the drift and Cretaceous aquifers (layer 5), in which the regional water table (fig. 12) was assigned as a constant-head boundary. Although the water table generally fluctuates over a relatively small range annually and has declined a few tens of feet in some areas where water-table aquifers are heavily pumped, there are no reported long-term regional declines in the water table due to regional pumping. Nodes containing major rivers were assigned heads weighted toward the lower range of the water table in the node. In addition, where an aquifer is completely dissected by a river, the head in a node containing the river was set to the average altitude of the seepage face. This type of constant-head node was used in the northern part of the study area where the Mississippi, Minnesota, Wisconsin, and St. Croix Rivers dissect the Cambrian and Ordovician rocks and along the Mississippi River in Iowa and Illinois where the uppermost Cambrian and Ordovician rocks are dissected (see fig. 26). The lower boundary of the model, beneath the Mount Simon Sandstone, is the Precambrian complex, assumed to be impermeable.

Where each aquifer layer thins to zero thickness, the head in the adjacent node in the layer was set to the average water table of the drift or Cretaceous aquifers (layer 5) (fig. 12). These nodes mark the northern outcrop border of all layers and the outcrop of the Silurian-Devonian aquifer (layer 4) (figs. 26*A*–26*D*) near the Missouri River.

A zero-flux boundary was placed along the western edge of each layer approximately coincident with the area where strata thin toward the Nemaha uplift, west of the Missouri River (figs. 1, 2, 4–10). A zero-flux boundary was located along the southern edge of the model south of the Missouri River and passing through the center of the Illinois basin (figs. 1, 2). To the east, a zero-flux boundary was drawn through eastern Indiana and the center of the Michigan basin (figs. 1, 2). These southern and eastern boundaries do not necessarily coincide with natural zero-flow regions but are sufficiently far from the area of interest (fig. 1) that they have little effect on the simulation. Initially, the eastern edge of the model was placed along the study area boundary east of Chicago (fig. 1) to coincide with the model boundaries of Prickett and Lonnquist (1971) and Young (1976). Initial transient simulations showed that in this position, the boundary had a significant effect on drawdown patterns in and near the Chicago area. Consequently, the eastern model boundary was moved eastward to its present position.

As discussed in the conceptualization of the flow system, areas containing high dissolved-solids concentrations are probably regions of little or no flow. If so, a zero-flux boundary could simulate an interface between areas of freshwater and relatively saline water. However, with the implementation of the variable-density formulation in the flow model, it became feasible to treat the brine regions as active parts of the model and to simulate the flow in those areas. Consequently, the model includes parts of the Illinois and Michigan basins (figs. 1, 2).

DATA BASE

In order to represent the ground-water flow system in terms of the finite-difference grid, a large amount of information must be assembled and processed. The thickness and hydraulic conductivity of the four aquifer layers below the surficial drift and Cretaceous aquifer (layer 5) and the four confining layers (table 1, figs. 4–11) are required for estimation of aquifer layer transmissivity and confining layer vertical leakance. Estimates of the distribution of dissolved-solids concentration and ground-water temperature are also needed to compute viscosity and densities of ground water and of its pure water component. Storage coefficients, historical pumpage data, and the aquifer layers that are open to wells must be known in order to simulate the response of the aquifer system to stress. Finally, the configuration of the

water table (layer 5) must be known for specification of the constant-head upper boundary of the model.

With the exception of pumping rates, all of this information ultimately must be reduced to average values over the extent of each finite-difference block. A database system (Kontis and Mandle, 1980) consisting of a variety of software was designed to facilitate processing of data, efficiently generate and edit model input arrays, produce graphics of input data and model output, and, in general, provide overall management of the various steps involved in the modeling process.

Because of the large horizontal and vertical extent of the model, there are large areas for which little or no information is available. Consequently, to provide model data for these areas, a variety of procedures were used and assumptions made. These procedures are presented in the ensuing discussion of individual hydraulic properties.

HYDRAULIC PROPERTIES

Hydraulic Conductivity

Initial estimates of the hydraulic conductivity of the model aquifer layers were obtained from a variety of sources, including single aquifer tests, core analyses, drill-stem tests, packer tests, and generalized maps of formation lithology, thickness, and structure. This information was provided primarily by district offices of the U.S. Geological Survey and by State agencies within the study area. In addition, about 2,500 specific-capacity tests were analyzed using a method described in Theis and others (1963). Using this method, estimates of transmissivity were obtained from the specific-capacity data and from assumed values of the storage coefficient (0.0001), well radius (1 ft), length of test (4 hr), and a constant related to well radius (2,159). Hydraulic conductivities were then computed by dividing estimated transmissivity by aquifer thickness (figs. 4, 6, 8, 10). No corrections were made for the effects of partial penetration.

Most of the data from which hydraulic conductivity was estimated were concentrated in areas where particular rock units are relatively shallow and the degree of weathering and fracturing is highly variable. The resulting hydraulic-conductivity values range over several orders of magnitude. Although the degree of lateral anisotropy in these rocks is probably very high, no attempt was made to estimate this anisotropy. If the orientation of fractures and solution openings is random and if the density of fractures and solution openings is sufficiently great over the large extent of the finite-difference blocks, use of a laterally isotropic porous media model may not result in appreciable error.

Several investigators (Law, 1944; Warren and others, 1961; Davis, 1969; and Freeze, 1972) have observed that hydraulic-conductivity data display a log-normal distribution and that the most probable regional average hydraulic conductivity for a formation is the geometric mean of the hydraulic conductivities within that formation.

The results of the hydraulic-conductivity estimation, consisting of the distribution of hydraulic conductivities, geometric mean values, and range of values over 1 standard deviation for each of the regional aquifers, are shown in figure 18. These results indicate that the Ironton-Galesville aquifer (layer 2) is generally the most permeable, especially in the northern part of the study area where the aquifer is most productive. This is in general agreement with results obtained by Walton and Csallany (1962) for the aquifer system in northern Illinois.

Few estimates for the vertical hydraulic conductivity of confining units are available. Walton (1960), using flow-net analysis, obtained vertical hydraulic-conductivity values for the Maquoketa Shale that ranged from 4.64×10^{-11} to 1.5×10^{-10} ft/s. Young (1976), in a ground-water flow model of the Cambrian-Ordovician aquifer system in southeastern Wisconsin, used a range of vertical hydraulic conductivity for the Maquoketa Shale of 1.5×10^{-11} to 5.4×10^{-10} ft/s. In a modeling study of the Cambrian-Ordovician aquifer system in northern Missouri, Imes (1985) estimated that the vertical hydraulic conductivity of a confining unit composed of Ordovician, Devonian, and Mississippian shales and limestones ranges from 6.0×10^{-12} to 1.9×10^{-10} ft/s. In the regional model, initial values of vertical hydraulic conductivity for the confining layers were assumed to be similar to those for the Maquoketa Shale or within the range of reported representative values for tight sandstone, unweathered carbonate rocks, or shale (Freeze and Cherry, 1979).

Each of the model aquifer layers and adjoining confining layers was then subdivided into a set of distinct zones within which hydraulic parameters were assumed to be uniform. The delineation of zone boundaries was based initially on lithologic differences and an estimate of the degree of weathering and fracturing. These zones were subsequently modified, and additional zones were added as a result of the calibration process. The final model zones of hydraulic conductivity for each aquifer and confining layer are shown in figures 19*A*–19*D* and 20*A*–20*D*. Zones of relatively high hydraulic conductivity generally represent areas of outcrop or subcrop where the rocks are possibly highly weathered or fractured. Areas of relatively low hydraulic conductivity generally correspond to areas where the layer is overlain by younger bedrock.

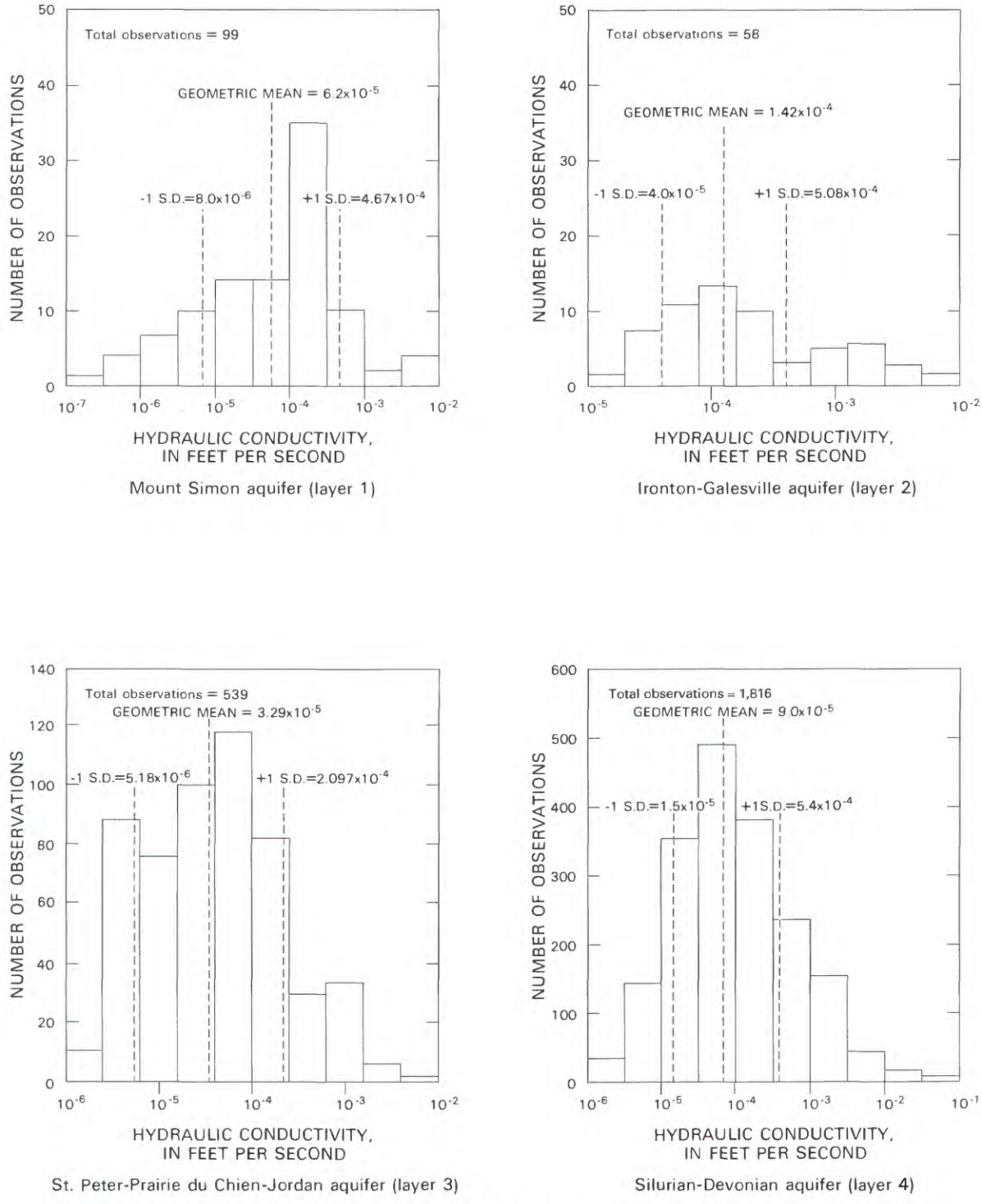

FIGURE 18.—Distribution and geometric mean of the hydraulic conductivity for each aquifer layer.

Transmissivities at each node of aquifer layers 1 through 4 were calculated by multiplying horizontal hydraulic conductivity (figs. 19*A*–19*D*) by aquifer thickness (figs. 4, 6, 8, 10). Vertical leakance for the confining layers was calculated similarly by dividing the vertical hydraulic conductivity (figs. 20*A*–20*D*) of the confining layers (figs. 5, 7, 9, 11) by their thickness.

Where an overlying bedrock confining layer is missing and an aquifer layer subcrops directly beneath glacial drift or Cretaceous rocks (aquifer layer 5), the vertical

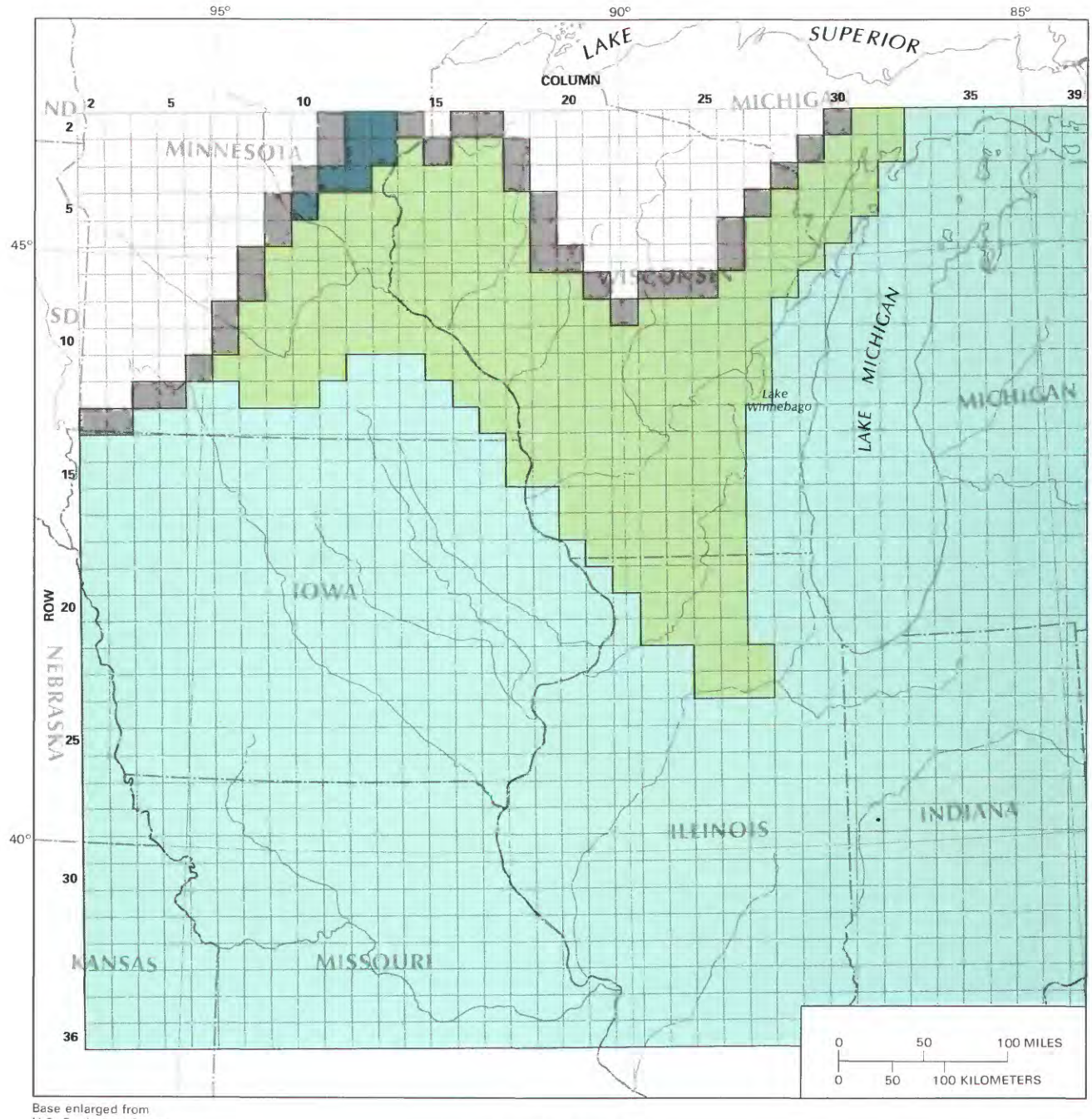

FIGURE 19A.—Horizontal hydraulic conductivity for the Mount Simon aquifer (layer 1).

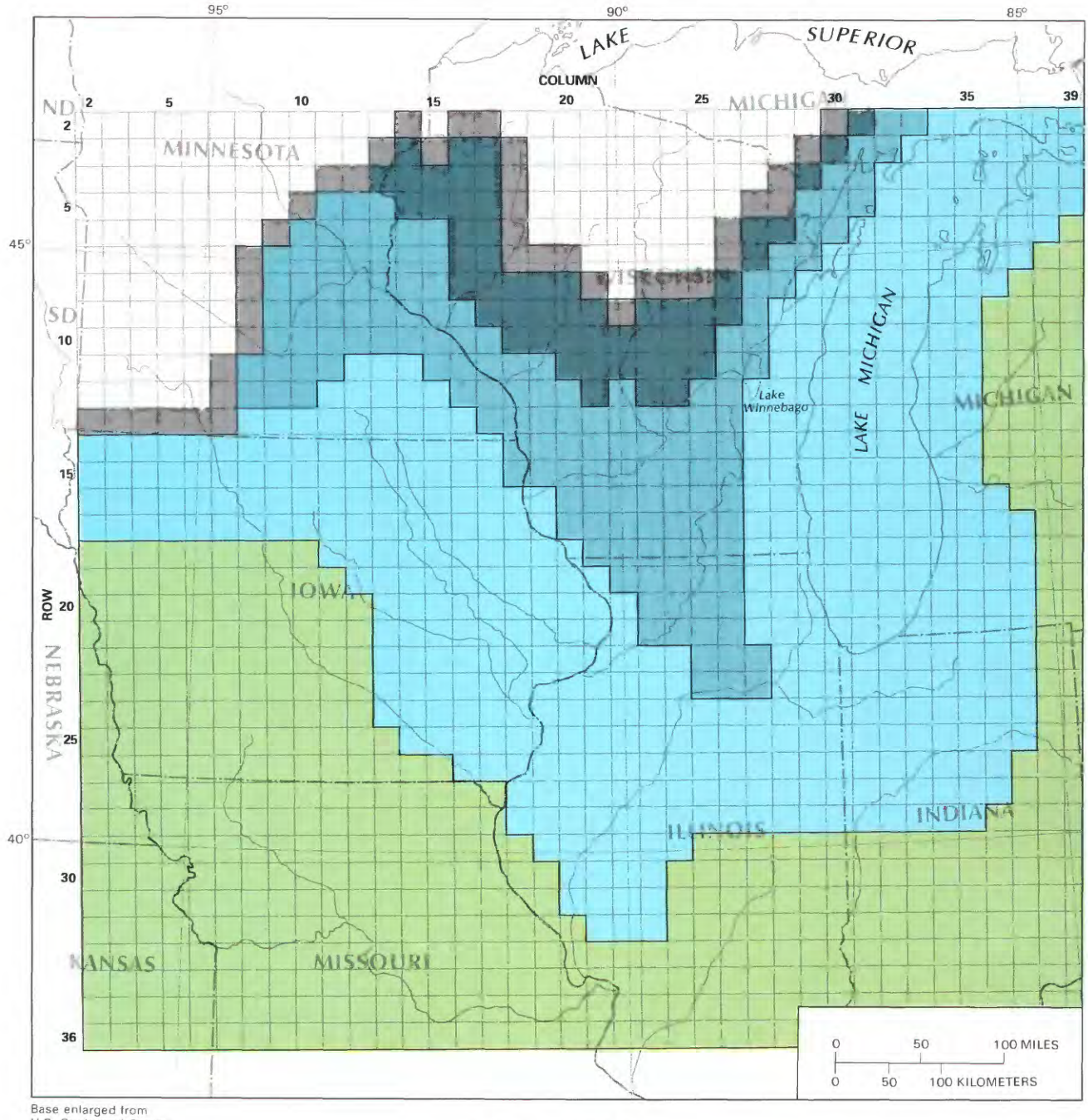

Base enlarged from U.S. Geological Survey 1:7,500,000, 1970

EXPLANATION

HORIZONTAL HYDRAULIC CONDUCTIVITY, IN FEET PER SECOND

- 1.0×10^{-4}
- 8.5×10^{-5}
- 7.0×10^{-5}
- 5.0×10^{-5}
- AQUIFER LAYER ABSENT
- MODEL CONSTANT-HEAD NODE REPRESENTING AQUIFER LAYER BOUNDARY

FIGURE 19*B*.—Horizontal hydraulic conductivity for the Ironton-Galesville aquifer (layer 2).

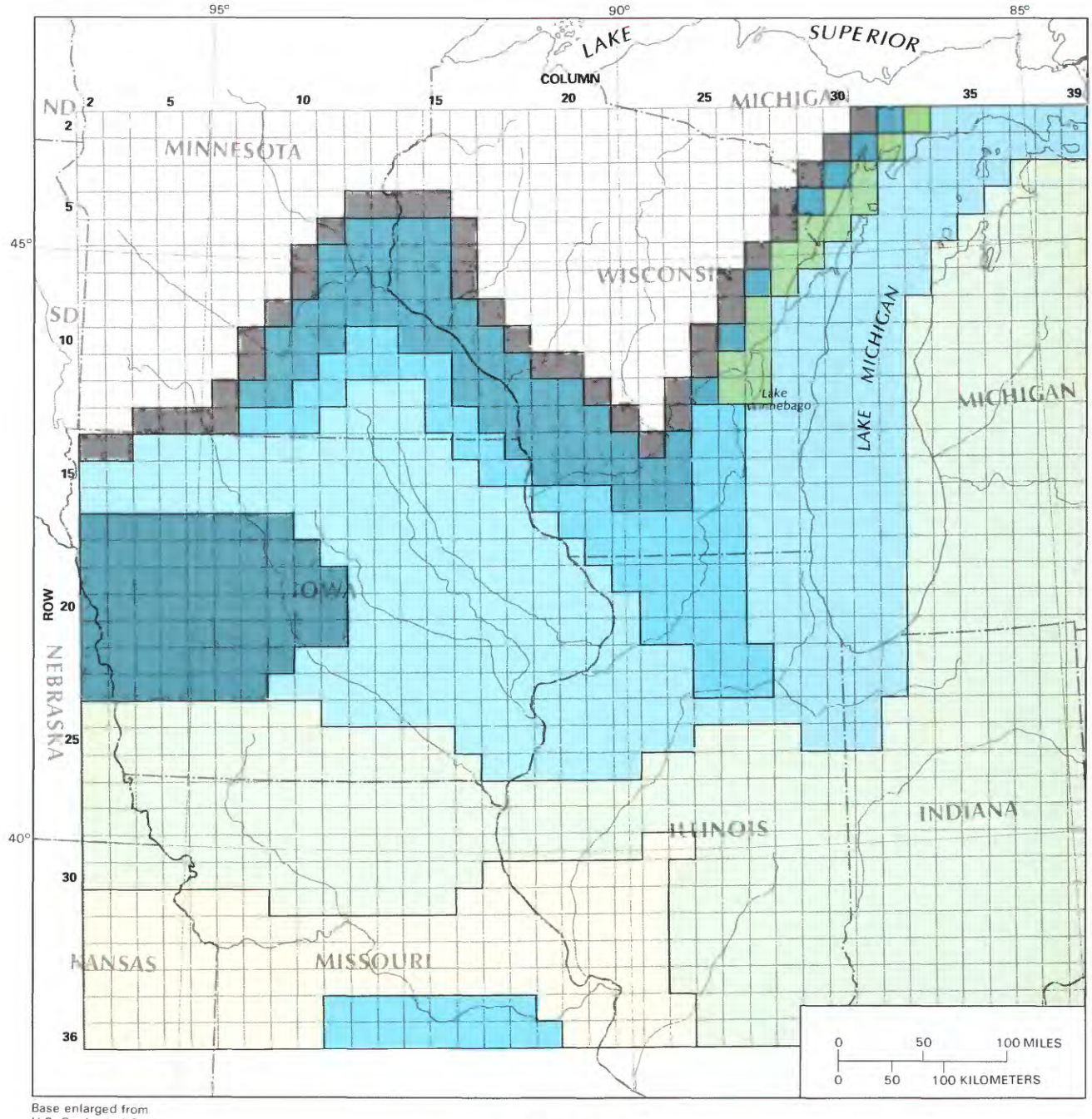

Base enlarged from
U.S. Geological Survey
1:7,500,000, 1970

EXPLANATION

HORIZONTAL HYDRAULIC CONDUCTIVITY, IN FEET PER SECOND

- 9.5×10^{-5}
- 8.5×10^{-5}
- 7.0×10^{-5}
- 6.0×10^{-5}
- 5.0×10^{-5}
- 2.0×10^{-5}
- 4.0×10^{-6}
- AQUIFER LAYER ABSENT
- MODEL CONSTANT-HEAD NODE REPRESENTING AQUIFER LAYER BOUNDARY

FIGURE 19C.—Horizontal hydraulic conductivity for the St. Peter-Prairie du Chien-Jordan aquifer (layer 3).

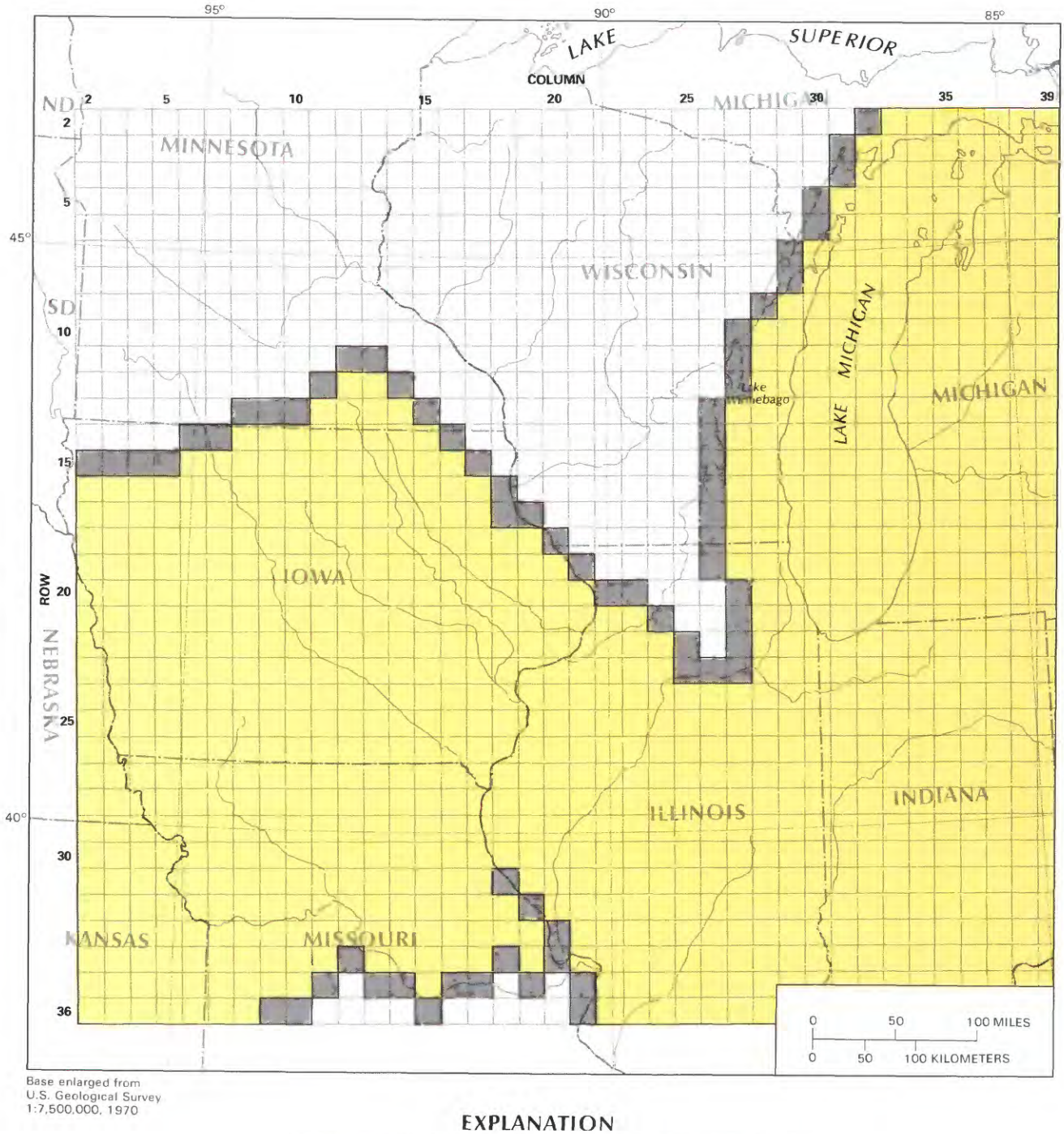

EXPLANATION

HORIZONTAL HYDRAULIC CONDUCTIVITY, IN FEET PER SECOND

- 4.5×10^{-6}
- AQUIFER LAYER ABSENT
- MODEL CONSTANT-HEAD NODE REPRESENTING AQUIFER LAYER BOUNDARY

FIGURE 19*D*.—Horizontal hydraulic conductivity for the Silurian-Devonian aquifer (layer 4).

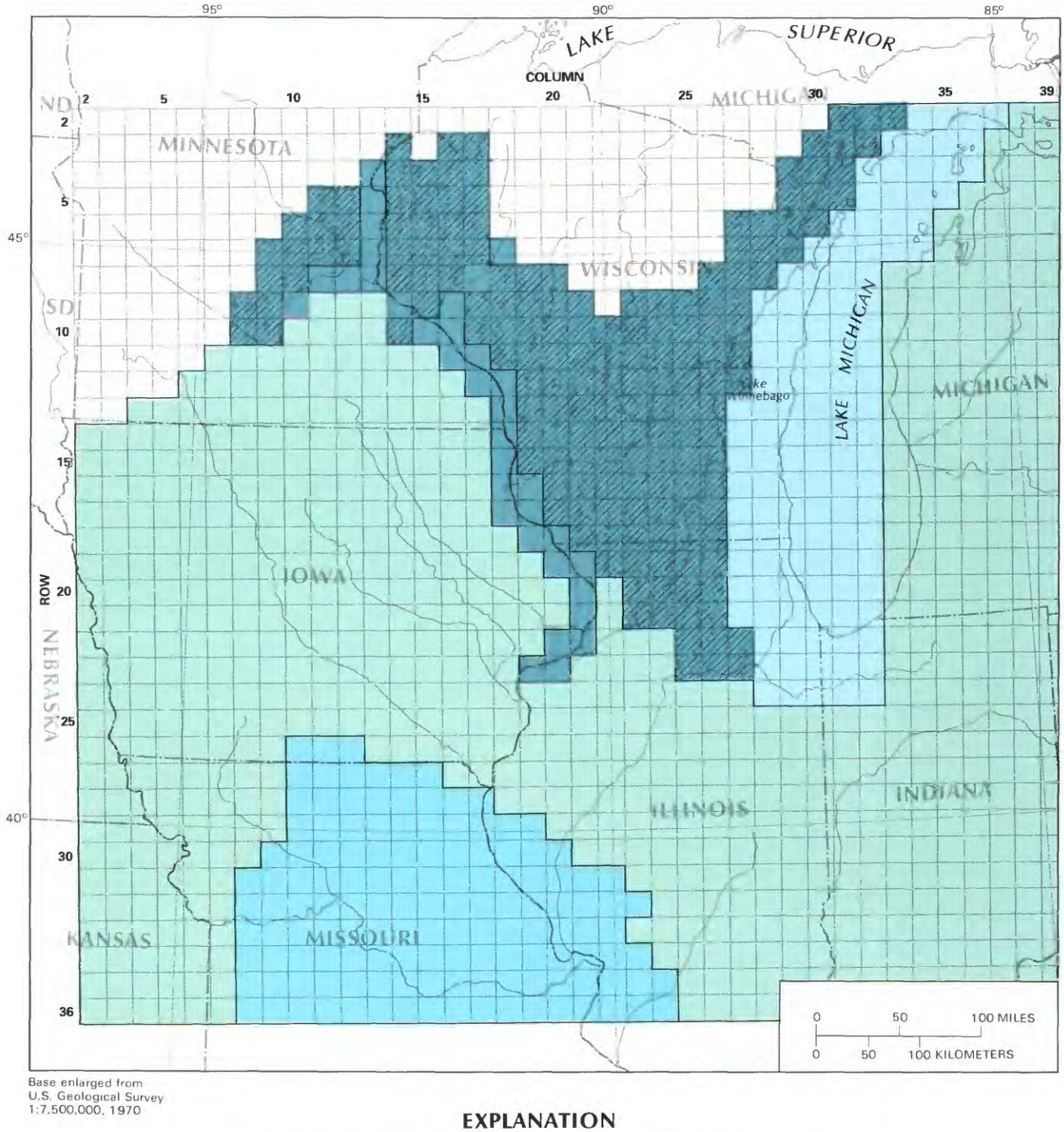

FIGURE 20A.—Vertical hydraulic conductivity for the Eau Claire confining unit (layer 1–2).

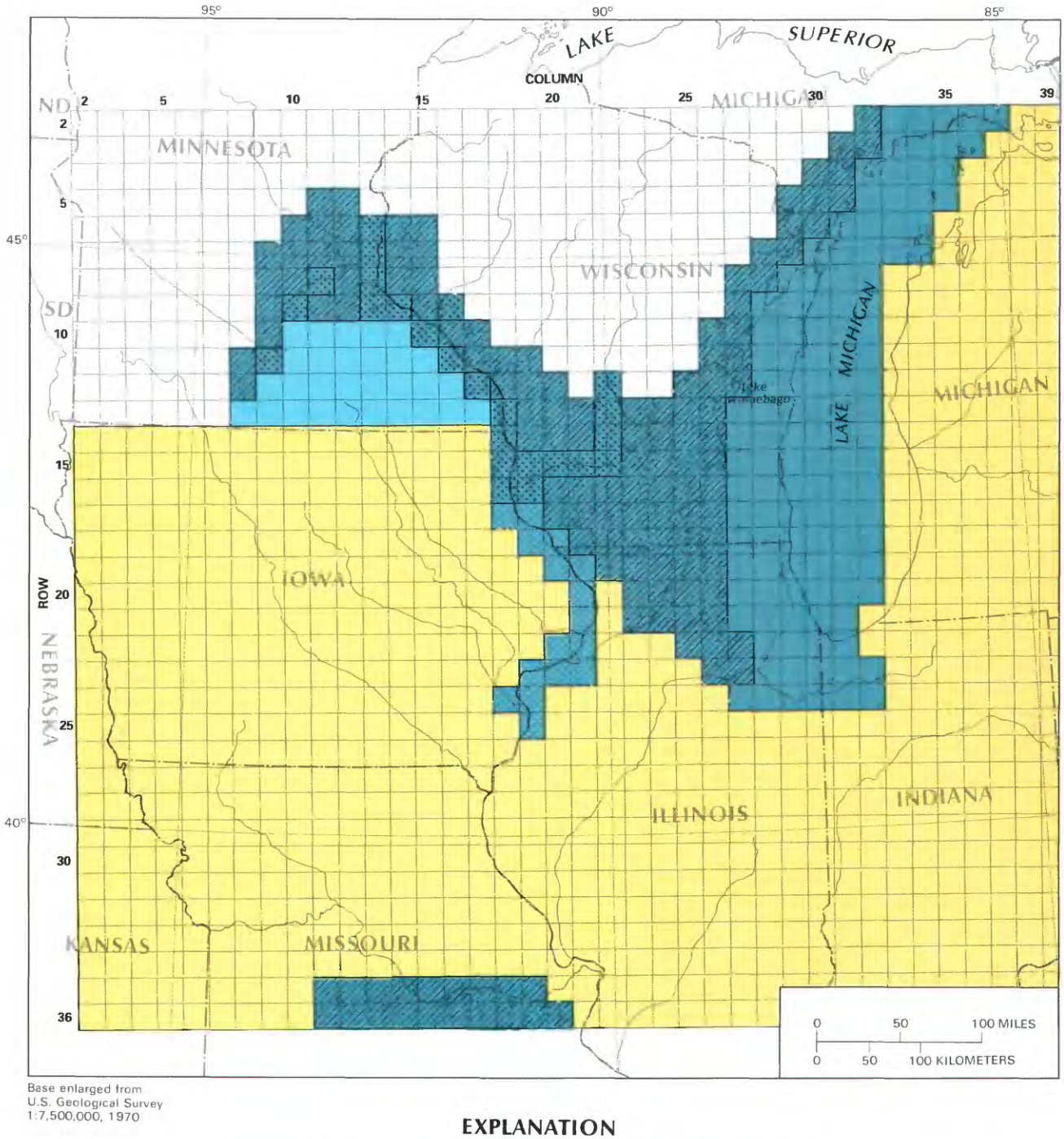

Base enlarged from
U.S. Geological Survey
1:7,500,000, 1970

EXPLANATION

VERTICAL HYDRAULIC CONDUCTIVITY, IN FEET PER SECOND

5.0×10^{-9}	1.0×10^{-9}	2.0×10^{-10}
2.5×10^{-9}	8.0×10^{-10}	1.0×10^{-11}

CONFINING LAYER ABSENT

FIGURE 20*B*.—Vertical hydraulic conductivity for the St. Lawrence-Franconia confining unit (layer 2–3).

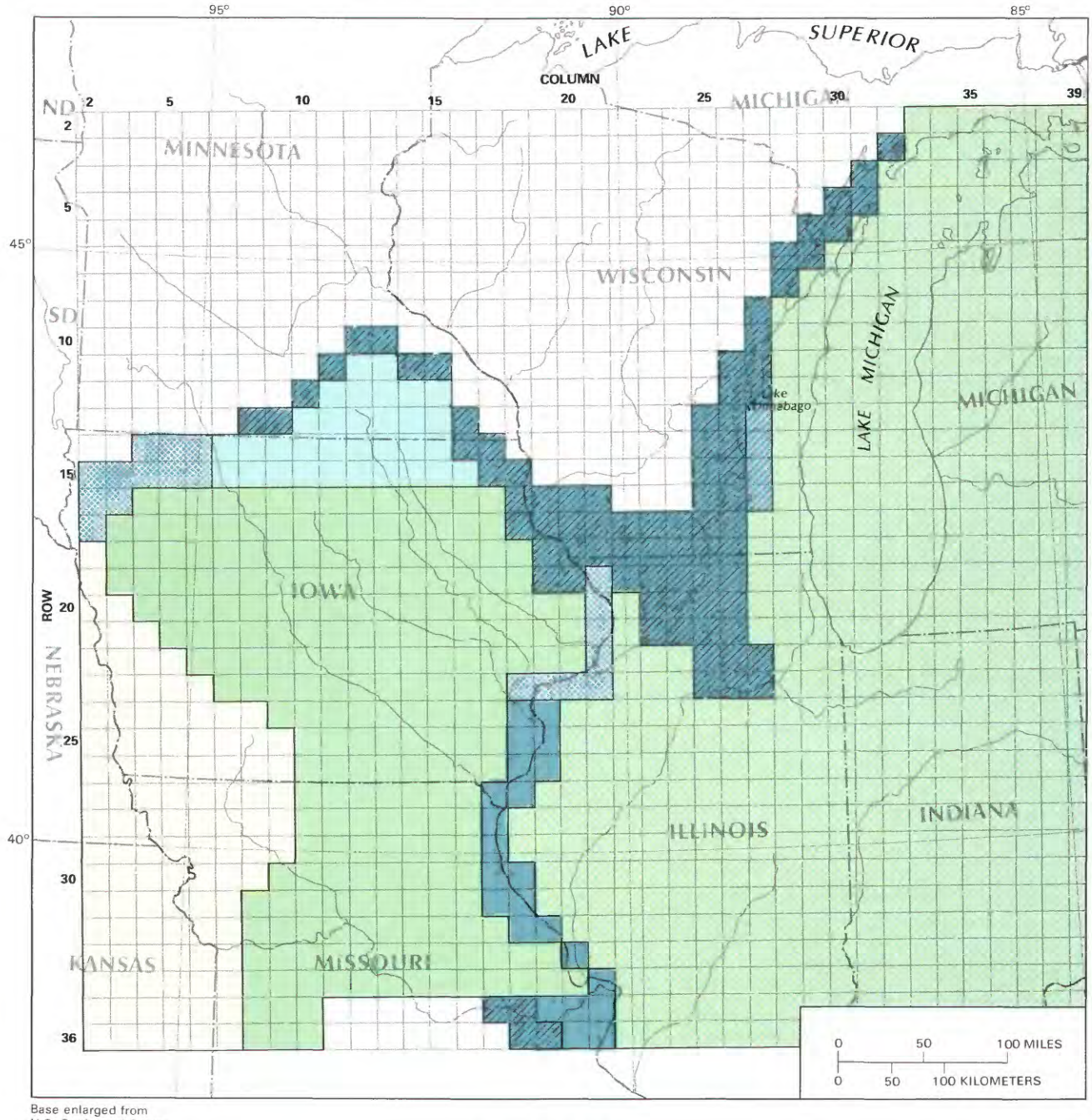

FIGURE 20C.—Vertical hydraulic conductivity for the Maquoketa confining unit (layer 3–4).

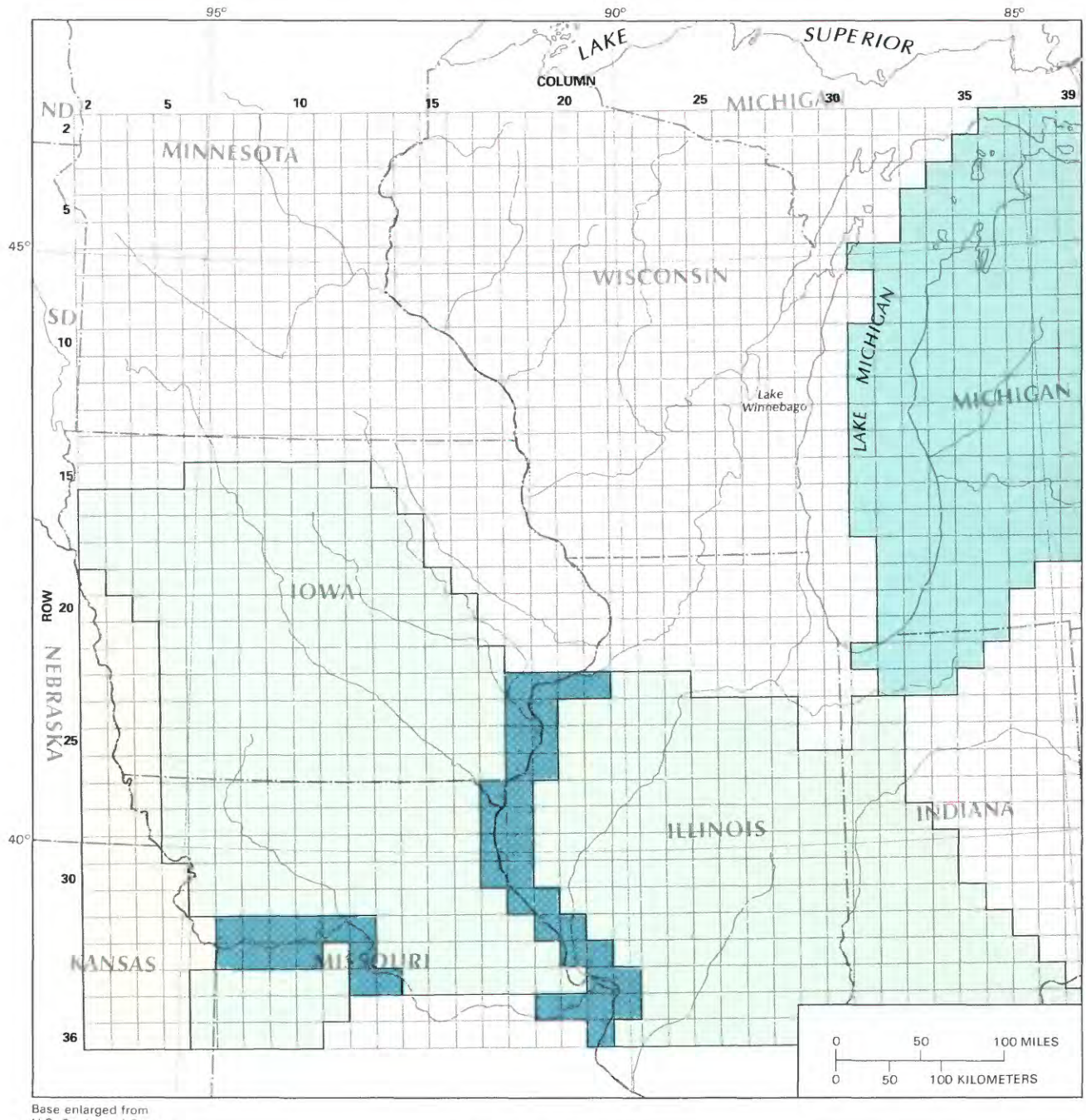

FIGURE 20*D*.—Vertical hydraulic conductivity for the Pennsylvanian-Mississippian-Devonian confining unit (layer 4–5).

hydraulic connection between layer 5 and the underlying aquifer is dependent mainly on the thickness and composition of the glacial deposits. Consequently, two additional maps were constructed to provide for variability in the vertical flow between the constant-head nodes of layer 5 and the underlying aquifer. The aquifer layer number at nodes overlain directly by glacial drift or Cretaceous rocks is shown in figure 21. Values of vertical leakance applied to these nodes are shown in figure 22.

The values of vertical leakance shown in figure 22 are of necessity generalized because they are based on surficial glacial geology and drift thickness maps of the area (Flint and others, 1959; Trotta and Cotter, 1973; Piskin and Bergstrom, 1975; Hadley and Pelham, 1976; Hobbs and Goebel, 1982; Mossler, 1983; and M.R. Burkart, U.S. Geological Survey, written commun., 1984) and do not take into account possible vertical heterogeneity in the lithology of the glacial deposits. Typical values of vertical hydraulic conductivity for glacial deposits given in Walton (1960) were used as a guide in selecting the values for vertical leakance. In assigning these values, it was presumed that vertical leakance is relatively high in driftless regions and in areas containing extensive outwash deposits and relatively low in areas containing significant amounts of till or lacustrine deposits or Cretaceous rocks.

As discussed by Davis (1969), many investigators have observed that there is a general tendency for the intrinsic permeability of rocks to decrease with increasing depth of burial. Field and laboratory measurements in northeastern Illinois (Ackermann and others, 1974) and in Ohio (Clifford, 1973) indicate that this tendency prevails in the Mount Simon Sandstone. Although no field evidence exists for rocks other than the Mount Simon Sandstone, a regionwide intrinsic permeability decrease with increasing depth of burial was assumed for all aquifer layers, thereby providing a systematic extrapolation of data from areas for which some information is available to areas for which little or no information is available.

This procedure was implemented by multiplying horizontal and vertical hydraulic conductivity values by a "Delta" factor defined as

$$Delta_{i,j,k} = \begin{cases} e^{\tau(ITH - D_{i,j,k})/1000} & \text{for } D_{i,j,k} > ITH \\ 1 & \text{for } D_{i,j,k} \leq ITH \end{cases}, \qquad (31)$$

where

$0.005 \leq Delta_{i,j,k} \leq 1.0$ (dimensionless),

$e = 2.71828$, base of Naperian logarithms,

τ = an empirical constant that controls the rate of decrease,

ITH = an initial depth of burial above which the Delta factor is taken to be unity, in feet, and

$D_{i,j,k}$ = thickness of rocks overlying layer k, in feet.

A value for ITH of 1,400 ft was chosen so that the hydraulic conductivity in relatively shallow areas, for which reasonably good estimates are available, is minimally affected by the Delta factor.

Various values of τ were tested, and on the basis of overall model results, a value of $\tau = 1$ was selected for this study. With this value, hydraulic conductivities are decreased by one order of magnitude for every 2,300 ft of increase in depth of burial. To avoid excessive reduction in hydraulic conductivity in the deep basin parts of the model, Delta was constrained to be no smaller than 0.005. The Delta factors, as computed by equation 31 for each aquifer layer, are given in figures 23*A*-23*D*. The Delta factor for vertical leakance was obtained by averaging the factors of aquifer layers above and below each confining layer.

A regression line through permeability estimates derived from 3 well tests and 38 values of specific capacity for the Mount Simon Sandstone given in Ackermann and others (1974) can be described by equation 31 with $\tau = 3.3$. Thus, the rate of decrease of intrinsic permeability with depth used in the model is considerably smaller than that indicated by field data.

In a regional study of the Dakota aquifer, Bredehoeft and others (1983) show the rate of decrease in intrinsic permeability with depth of a Cretaceous shale confining unit, as derived by numerical simulation, to be several orders of magnitude smaller than that indicated by field and laboratory data. This difference is attributed to the possibility that the numerical simulation reflects fracturing on a regional scale whereas the laboratory and field measurements are characteristic of the strata on a more local scale. A similar difference in scale may, in part, account for the difference in the rate of decrease of regionalized hydraulic conductivity used in the present study and that indicated by the aforementioned field data for the Mount Simon Sandstone.

The hydraulic conductivities assigned to aquifer layers 3 and 4 (figs. 19*C*, 19*D*) and confining layer 3–4 are not significantly reduced by the Delta factor (figs. 23*C*, 23*D*), except in the Michigan, Illinois, and Forest City basins. The hydraulic conductivities assigned to the deeper aquifer and confining layers are reduced in the major basins and in areas adjacent to the major basins (figs. 23*A*, 23*B*).

Ground-Water Density and Viscosity

The density terms ρ_s and ρ_p required for the variable-density formulation (eq. 11) were obtained from a modified version of a method developed and documented by Weiss (1982b). This method is based on the assumption that the density of ground water is equivalent to the

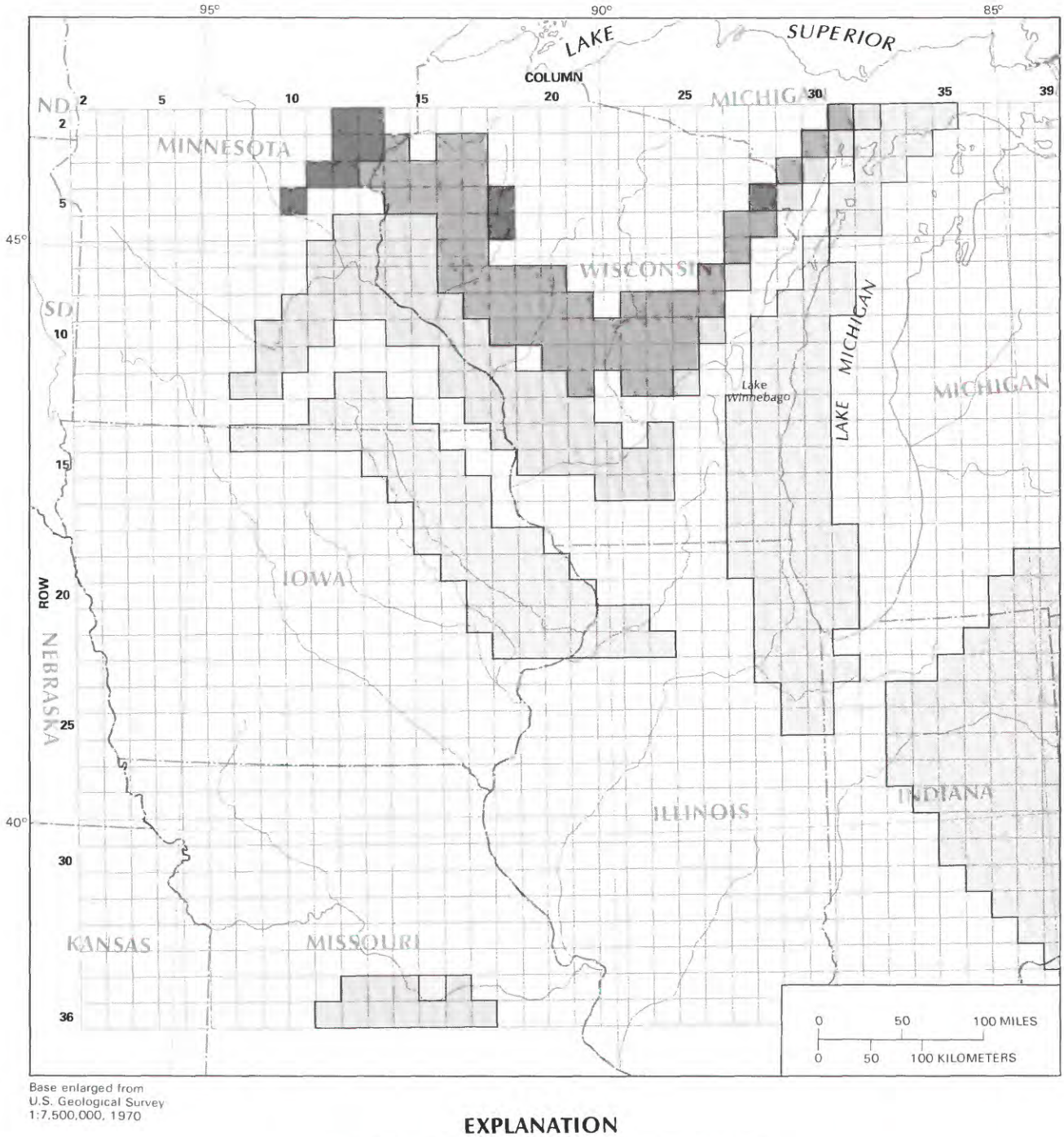

Base enlarged from
U.S. Geological Survey
1:7,500,000, 1970

EXPLANATION

AREA OF AQUIFER LAYER OUTCROP OR SUBCROP BENEATH QUATERNARY OR CRETACEOUS SEDIMENTS

- Mount Simon aquifer (layer 1)
- Ironton-Galesville aquifer (layer 2)
- St. Peter-Prairie du Chien-Jordan aquifer (layer 3)
- Silurian-Devonian aquifer (layer 4)

FIGURE 21.—Aquifer layer outcrop or subcrop beneath Quaternary or Cretaceous sediments.

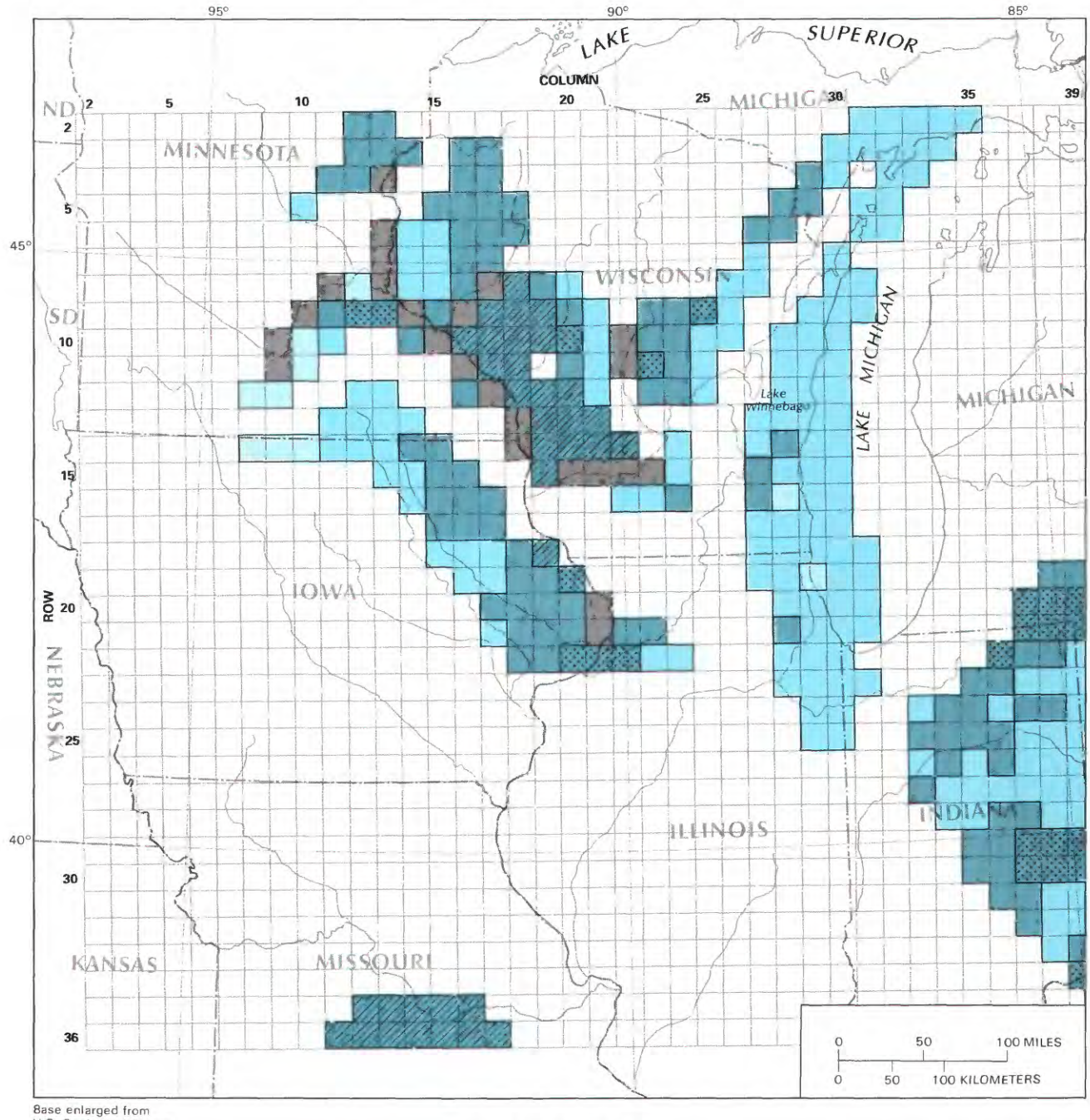

Base enlarged from U.S. Geological Survey 1:7,500,000, 1970

EXPLANATION

VERTICAL LEAKANCE (K'/b'), IN FEET PER SECOND PER FOOT, AND DESCRIPTION OF SEDIMENT OVERLYING AREA OF AQUIFER SUBCROP

- 6×10^{-9} Little or no glacial drift or much exposed bedrock
- 4×10^{-9} Primarily outwash deposits
- 2×10^{-9} Generally equal amounts of till and outwash or lacustrine deposits and outwash
- 8×10^{-10} Primarily till or lacustrine deposits
- 2×10^{-10} Relatively thick till deposits and (or) Cretaceous bedrock
- UNDERLYING AQUIFER LAYER DISSECTED BY RIVER
- NO AQUIFER LAYER DIRECTLY UNDERLYING QUATERNARY- OR CRETACEOUS-AGE SEDIMENT

FIGURE 22.—Vertical leakance (K'/b') for Quaternary or Cretaceous sediments directly overlying an aquifer layer.

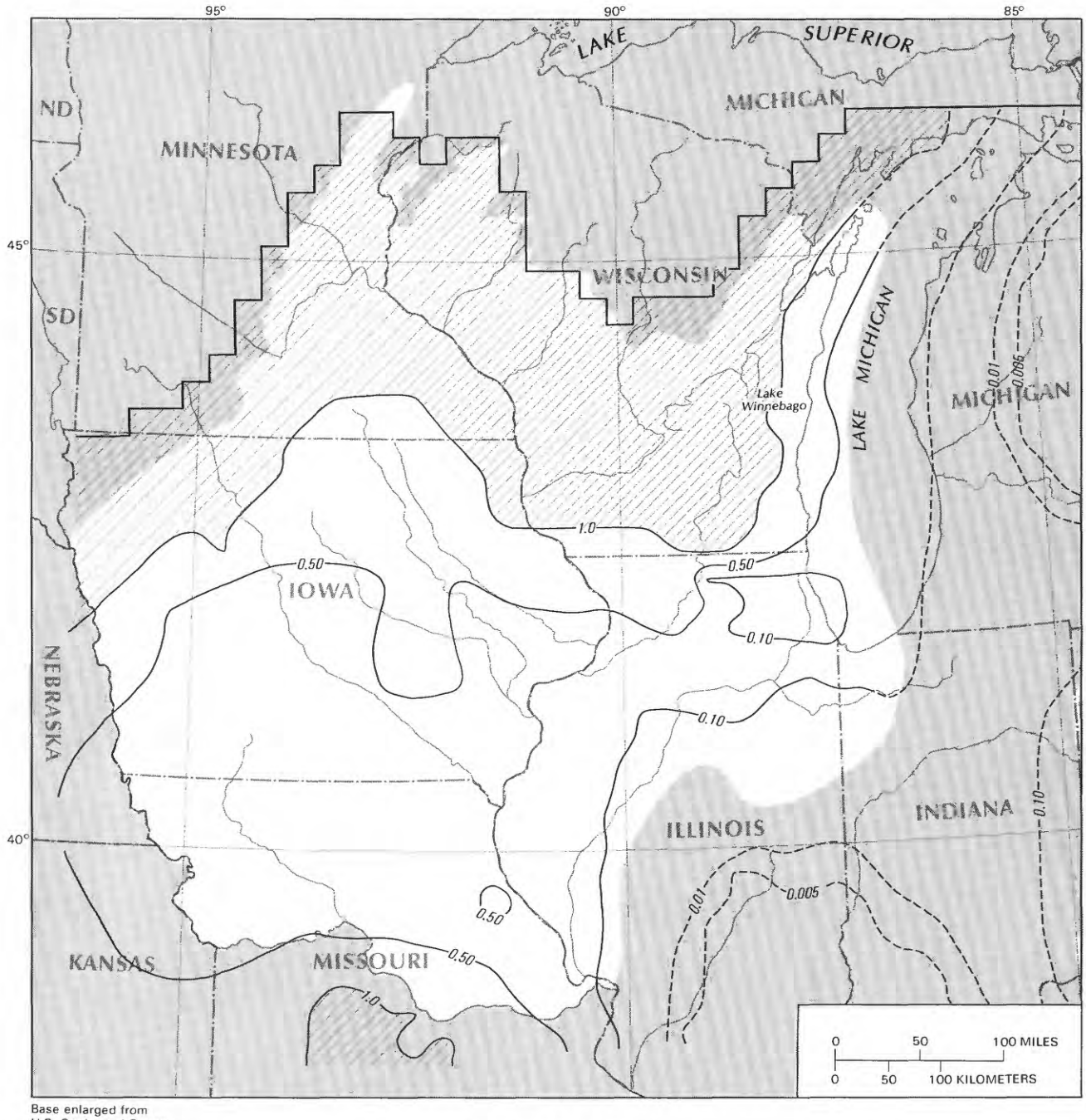

Base enlarged from
U.S. Geological Survey
1:7,500,000, 1970

EXPLANATION

—0.50— LINE OF EQUAL "DELTA" MULTIPLICATION FACTOR—Shows values used to modify hydraulic conductivity for the Mount Simon aquifer (layer 1). Dashed where based on inferred data. Interval is variable

"DELTA" FACTOR EQUAL TO UNITY

MODELED LAYER BOUNDARY

FIGURE 23A.—"Delta" multiplication factors used to modify hydraulic conductivity for the Mount Simon aquifer (layer 1).

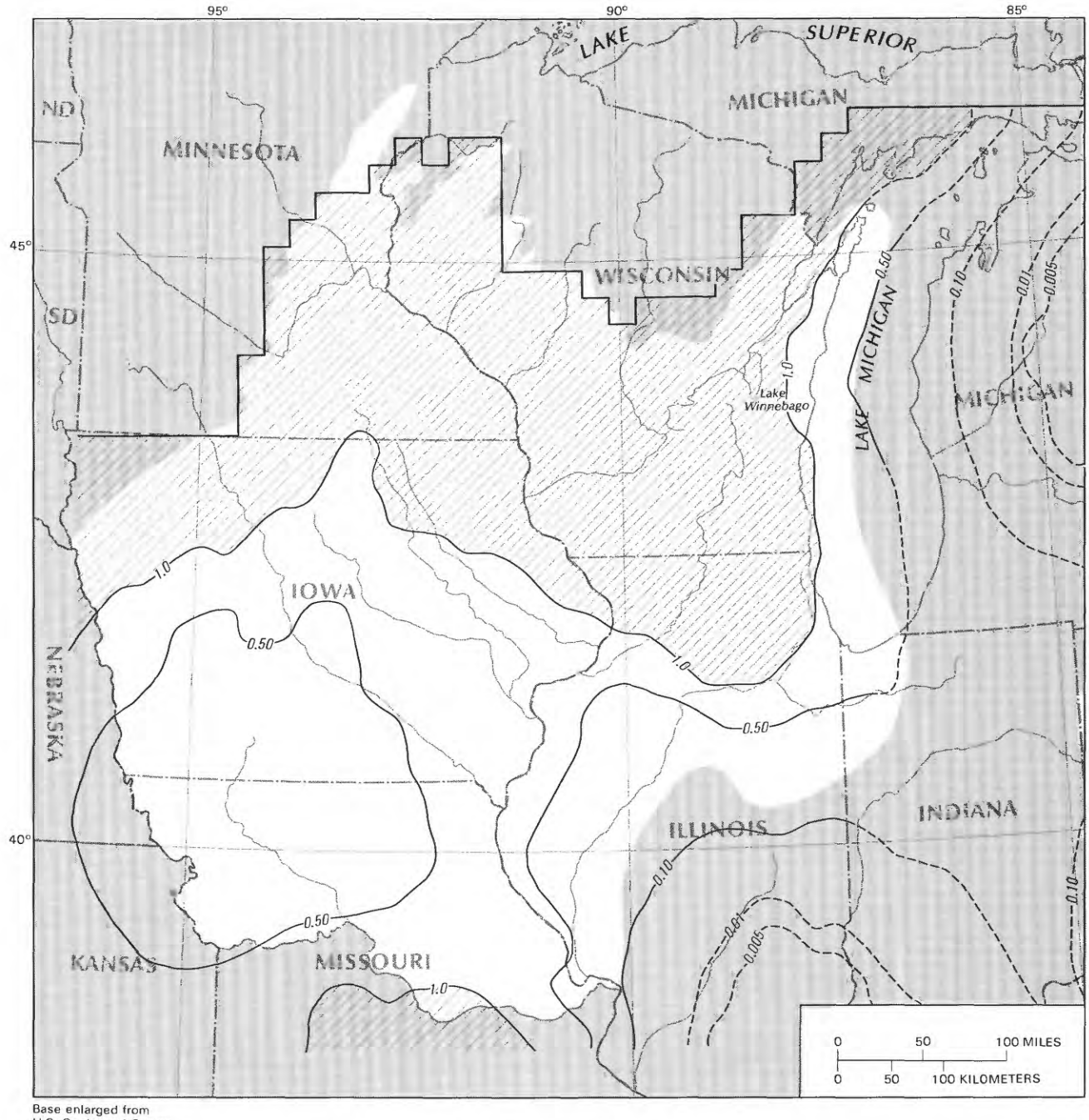

FIGURE 23*B*.—"Delta" multiplication factors used to modify hydraulic conductivity for the Ironton-Galesville aquifer (layer 2).

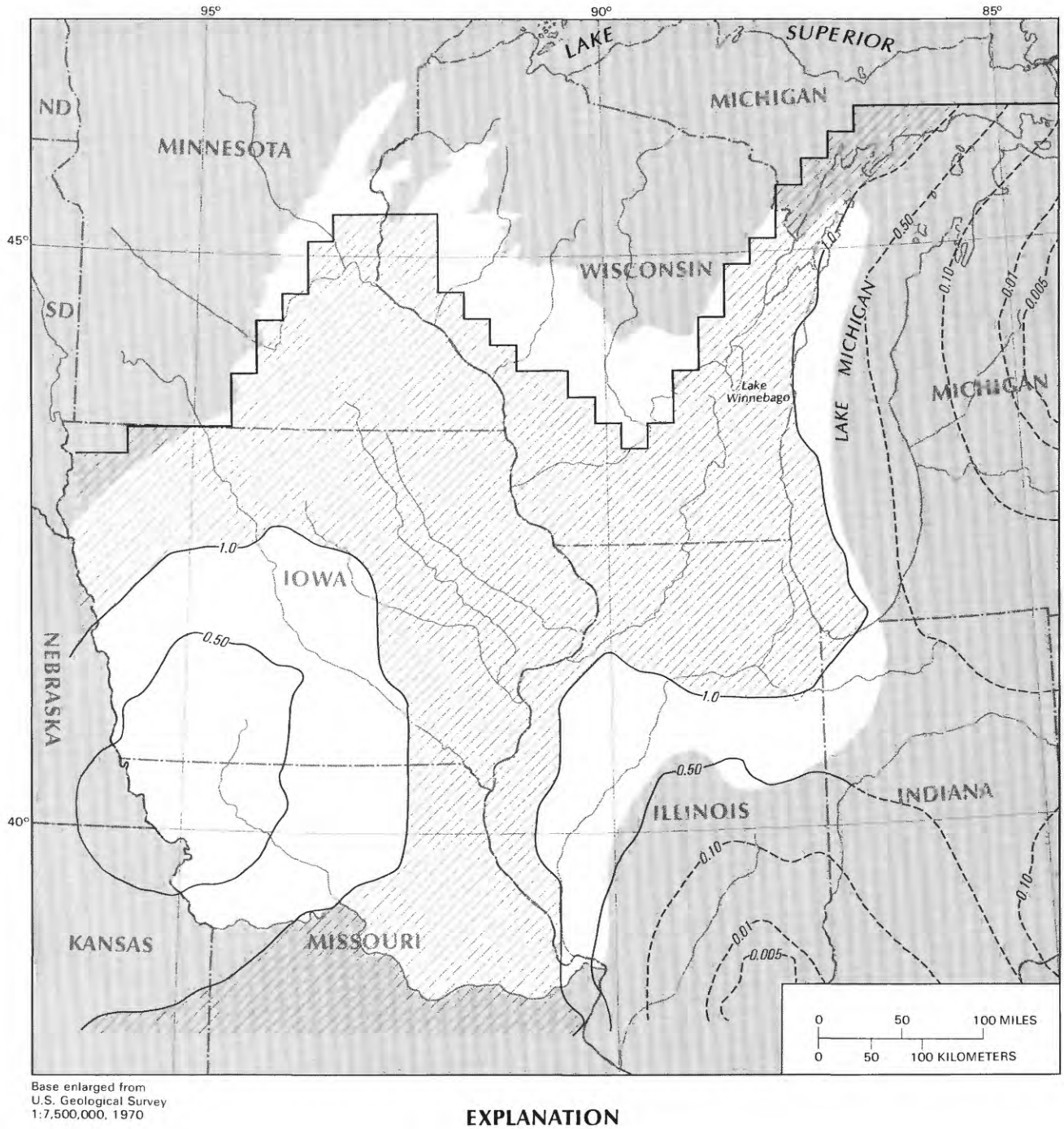

Base enlarged from
U.S. Geological Survey
1:7,500,000, 1970

EXPLANATION

—0.50— LINE OF EQUAL "DELTA" MULTIPLICATION FACTOR—Shows values used to modify hydraulic conductivity for the St. Peter-Prairie du Chien-Jordan aquifer (layer 3). Dashed where based on inferred data. Interval is variable

"DELTA" FACTOR EQUAL TO UNITY

MODELED LAYER BOUNDARY

FIGURE 23C.—"Delta" multiplication factors used to modify hydraulic conductivity for the St. Peter-Prairie du Chien-Jordan aquifer (layer 3).

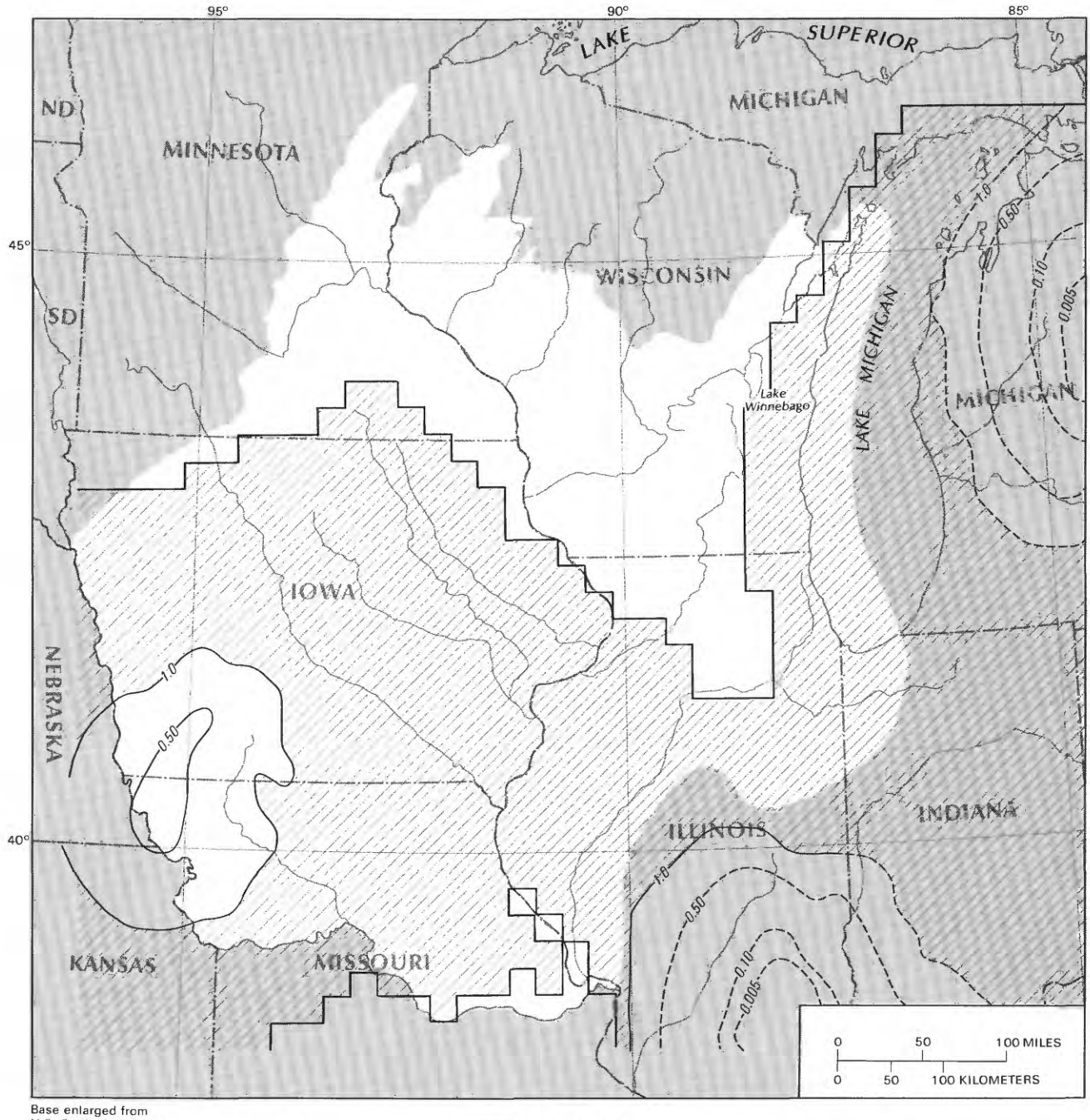

FIGURE 23*D*.—"Delta" multiplication factors used to modify hydraulic conductivity for the Silurian-Devonian aquifer (layer 4).

density of a sodium chloride solution of the same molality, temperature, and pressure. Under this assumption, the density of ground water at node i,j,k can be computed from the following relation of Potter and Brown (1977):

$$\rho_{s_{i,j,k}} = [C_a + C_b T_g + C_c T_g^2]_{i,j,k}, \quad (32)$$

where T_g is the temperature of ground water in degrees Celsius and C_a, C_b, and C_c are coefficients for sodium chloride solutions given in table 29 of Potter and Brown (1977). The coefficients are given for values of molality ranging from 0.5 to 6.0 mol/kg (mole per kilogram), in increments of 0.5 mol/kg, and for values of pressure to 2,000 bars (29,000 lb/in^2), in increments of 100 bars (1,450 lb/in^2) to 1,000 bars (14,500 lb/in^2) and in increments of 250 bars (3,625 lb/in^2) after 1,000 bars.

The molality was computed iteratively by the relation (Weiss, 1982b)

$$m = \frac{DS}{mw(\rho' - DS/1000)}, \quad (33)$$

where

m=approximate molality of ground water, in moles per kilogram,

DS=mass of dissolved solids per liter of ground water, in grams, at laboratory conditions (20° Celsius and 1 atmosphere),

mw=gram molecular weight of sodium chloride (58.4428 grams per mole), and

ρ'=density of ground water at 20° Celsius and 1 atmosphere, in grams per cubic centimeter.

Estimates of the total dissolved-solids concentration were obtained from regional data compiled by D.I. Siegel (U.S. Geological Survey, written commun., 1981), and the pressure was assumed to be hydrostatic. The temperature values used in equation 32 were obtained from a straight-line fit of temperature versus depth for the Illinois basin (Bond, 1972) given by

$$T_g = 0.0083\, Z'_{i,j,k} + 17.09°\text{C}, \quad (34)$$

where $Z'_{i,j,k}$ is the vertical distance from land surface, in feet, to the midpoint of node i,j,k. This temperature versus depth relationship was assumed to apply to the entire study area.

The procedure used by Weiss (1982b) to obtain the C_a, C_b, and C_c coefficients required for equation 32 consists of computing molality and pressure at each node and obtaining the coefficients by linear interpolation of table values. An alternate interpolation method was used for this study. Table 29 of Potter and Brown was extended to include coefficients corresponding to zero molality for pressure up to 400 bars or 5,800 lb/in^2 (R.J. Sun, U.S. Geological Survey, written commun., 1981). Viewing the tabulated coefficients as a set of uniformly spaced discrete points from three (C_a, C_b, and C_c) two-dimensional surfaces, a bicubic interpolation process (Davis and Kontis, 1970) was applied to produce bicubic coefficients that define the form of the surfaces. From these bicubic coefficients, values of C_a, C_b, and C_c can be interpolated for any value of molality between 0 and 6 mol/kg and of pressure between atmospheric and 400 bars.

Given the density of ground water, ρ_s, computed from equation 32, the pure-water component is then obtained from

$$\rho_{p_{i,j,k}} = \rho_{s_{i,j,k}} \left(1 - \frac{1}{1 + \frac{1000}{m \times mw}} \right)_{i,j,k} \quad (35)$$

The density of ground water derived by the above process for each model layer is shown in figures 24*A*–24*D*. The density of the pure-water component, ρ_p, is not shown, although its general distribution and magnitude may be inferred from figures 24*A*–24*D* and equation 35. Values of ρ_p range from about 998 kg/m^3 in freshwater areas to a low of 882 kg/m^3 in the deepest part of the Illinois basin. The elevation surfaces for each layer used in equations 9–11 and to compute temperature (eq. 34) and hydrostatic pressure are given in figures 25*A*–25*D*.

The dynamic viscosity required in equations 9–11 was obtained from an empirical relation developed by Weiss (1982a) on the basis of curves of viscosity versus temperature for various values of total dissolved-solids concentrations (Matthews and Russell, 1967). The empirical relation is

$$\mu_{i,j,k} = (38.3432/T_g^{1/2} - 14.621/T_g^{1/4} + 1.481)(1 + DS/300)_{i,j,k}, \quad (36)$$

where

$\mu_{i,j,k}$=dynamic viscosity at node i,j,k, in centipoise (M/L/T),

T_g=temperature, in degrees Fahrenheit, and

DS=total dissolved-solids concentration, in kilograms per cubic meter (M/L^3).

The resultant viscosities range from about 1.127 centipoise for cooler, relatively fresh water to a minimum of about 0.47 centipoise for the relatively warmer and more saline water in the Mount Simon Sandstone (aquifer layer 1) in the deepest parts of the Michigan and Illinois basins.

The estimates of density and viscosity and the elevation of the midpoints of the aquifer layers were not varied during the model calibrations. These estimates are an approximation of prevailing conditions and, at best, reflect the probable regionwide tendencies. The

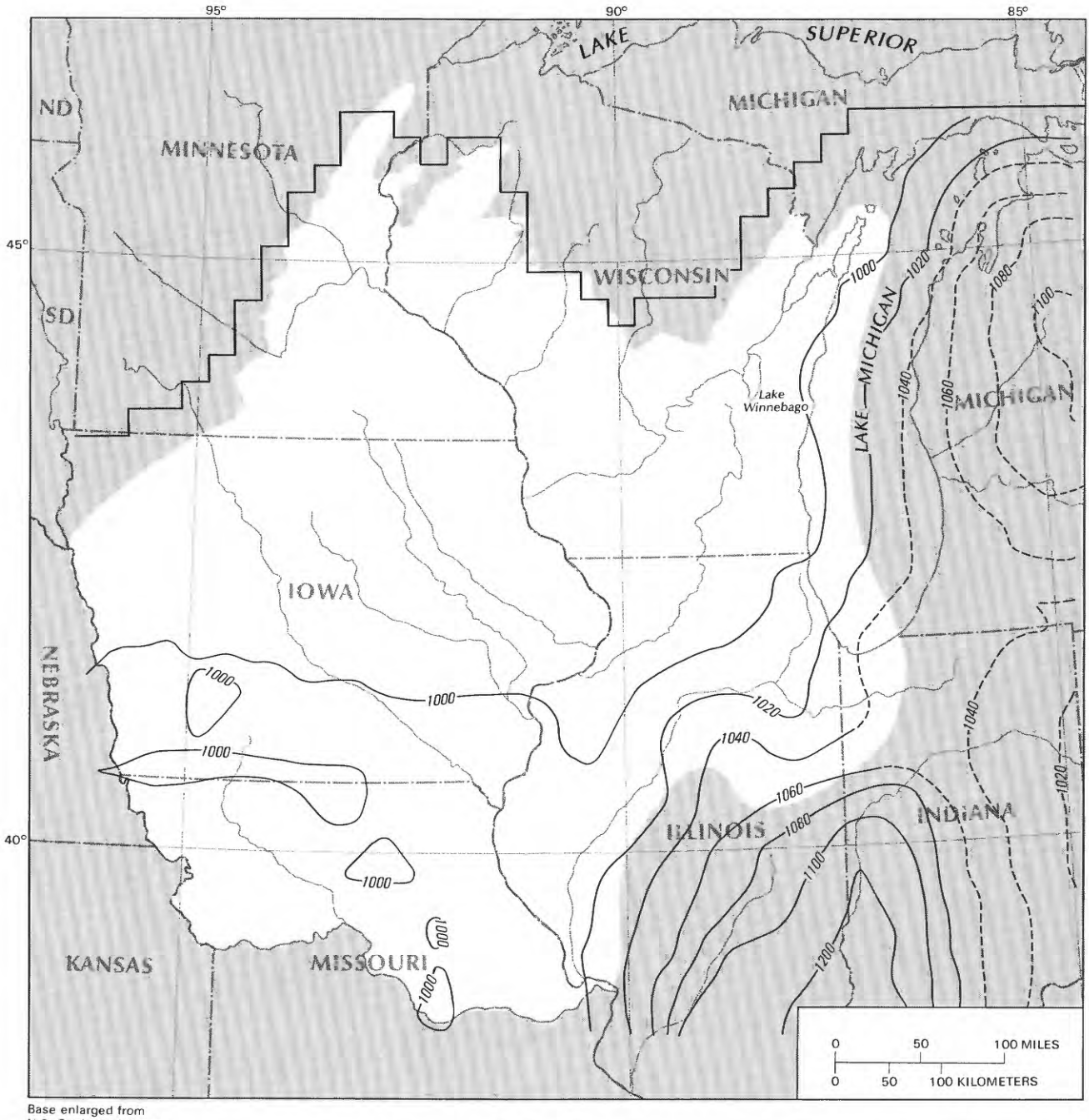

Base enlarged from
U.S. Geological Survey
1:7,500,000, 1970

EXPLANATION

—1000— LINE OF EQUAL CALCULATED GROUND-WATER DENSITY, ρ_s — Dashed where based on inferred data. Interval, in kilograms per cubic meter, is variable

MODELED LAYER BOUNDARY

FIGURE 24A.—Calculated ground-water density for the Mount Simon aquifer (layer 1).

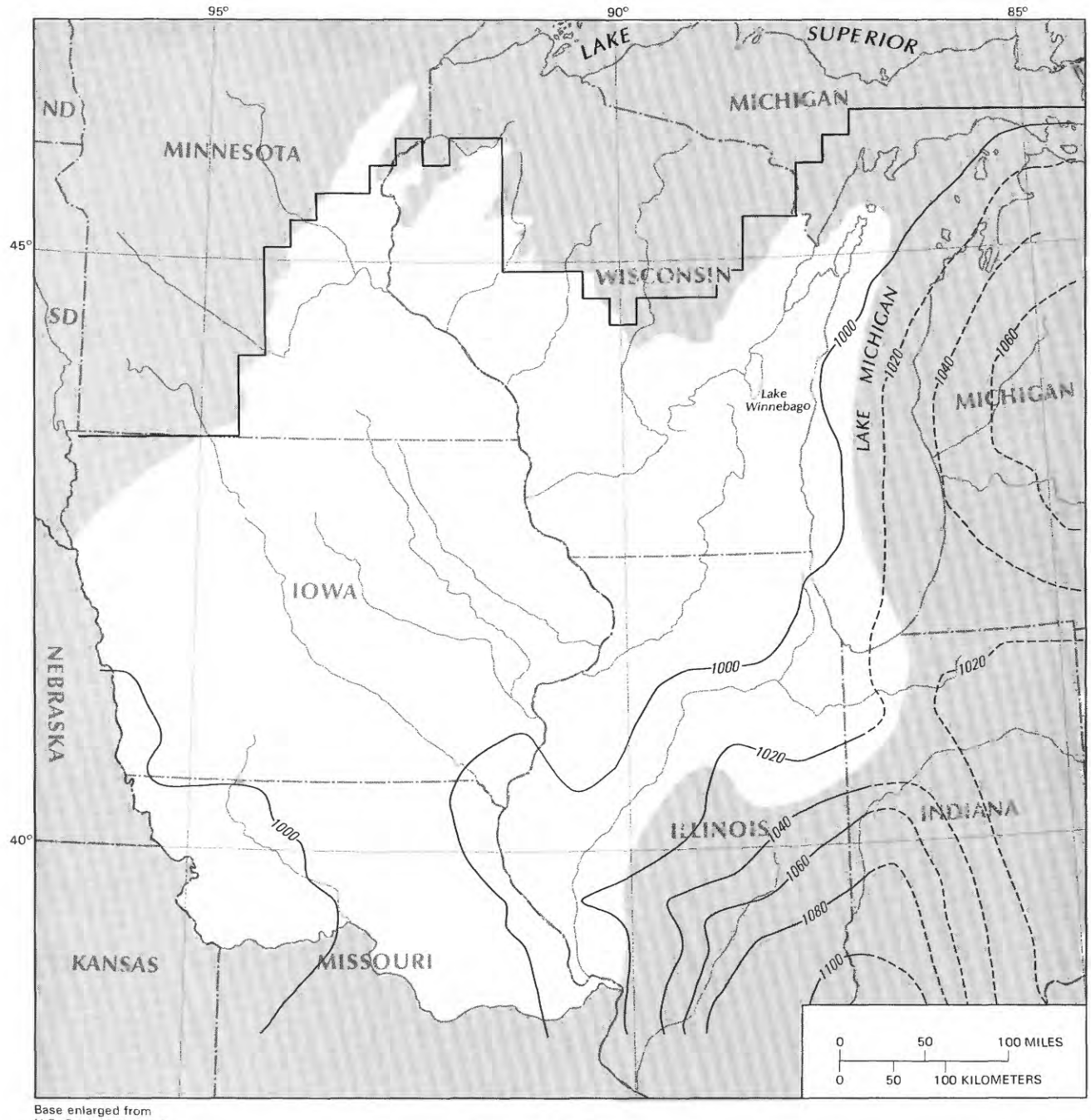

Base enlarged from
U.S. Geological Survey
1:7,500,000, 1970

EXPLANATION

—1000— LINE OF EQUAL CALCULATED GROUND-WATER DENSITY, ρ_s — Dashed where based on inferred data. Interval, 20 kilograms per cubic meter

MODELED LAYER BOUNDARY

FIGURE 24*B*.—Calculated ground-water density for the Ironton-Galesville aquifer (layer 2).

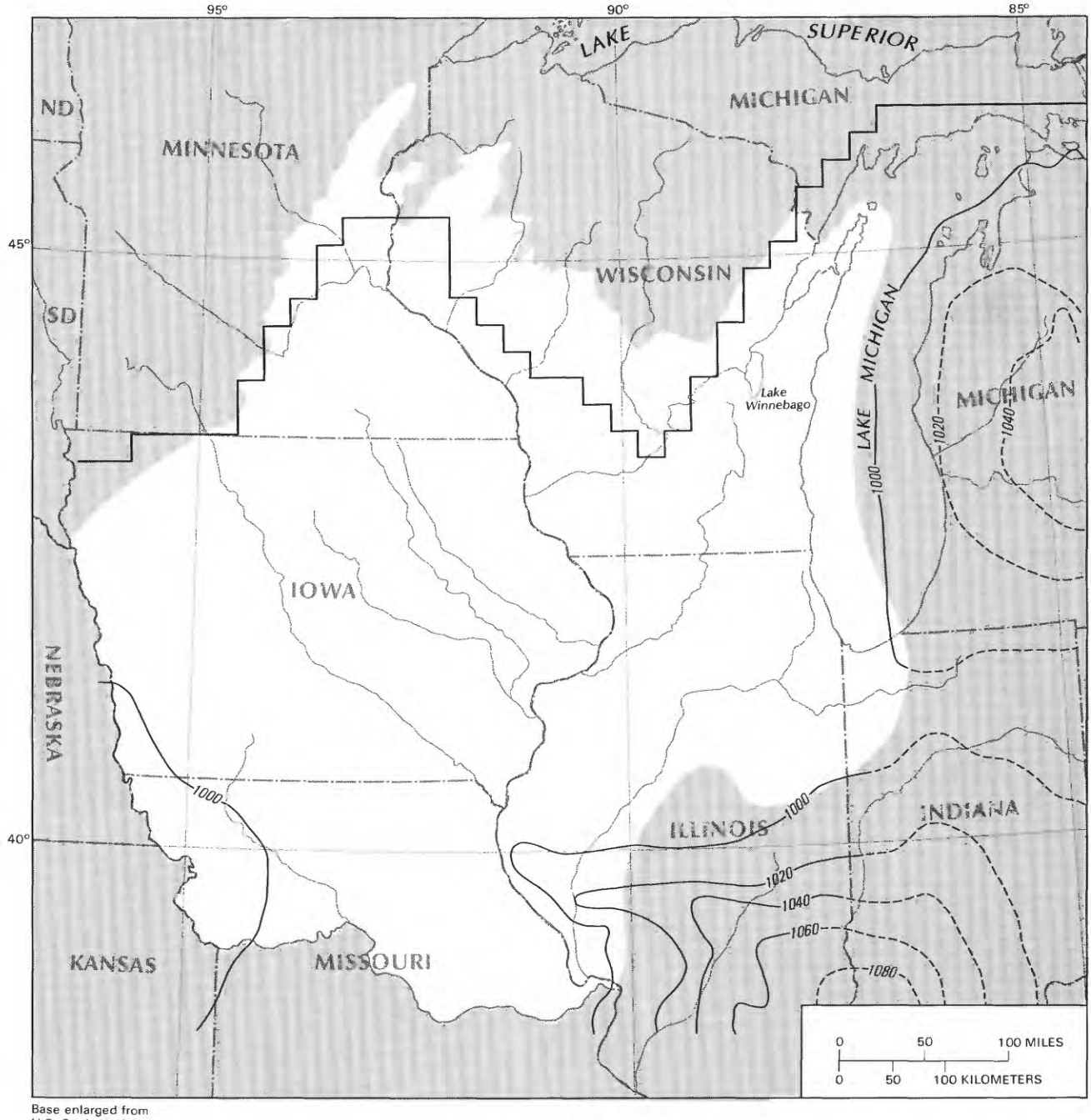

Base enlarged from
U.S. Geological Survey
1:7,500,000, 1970

EXPLANATION

—1000— LINE OF EQUAL CALCULATED GROUND-WATER DENSITY, ρ_s— Dashed where based on inferred data. Interval, 20 kilograms per cubic meter

MODELED LAYER BOUNDARY

FIGURE 24C.—Calculated ground-water density for the St. Peter-Prairie du Chien-Jordan aquifer (layer 3).

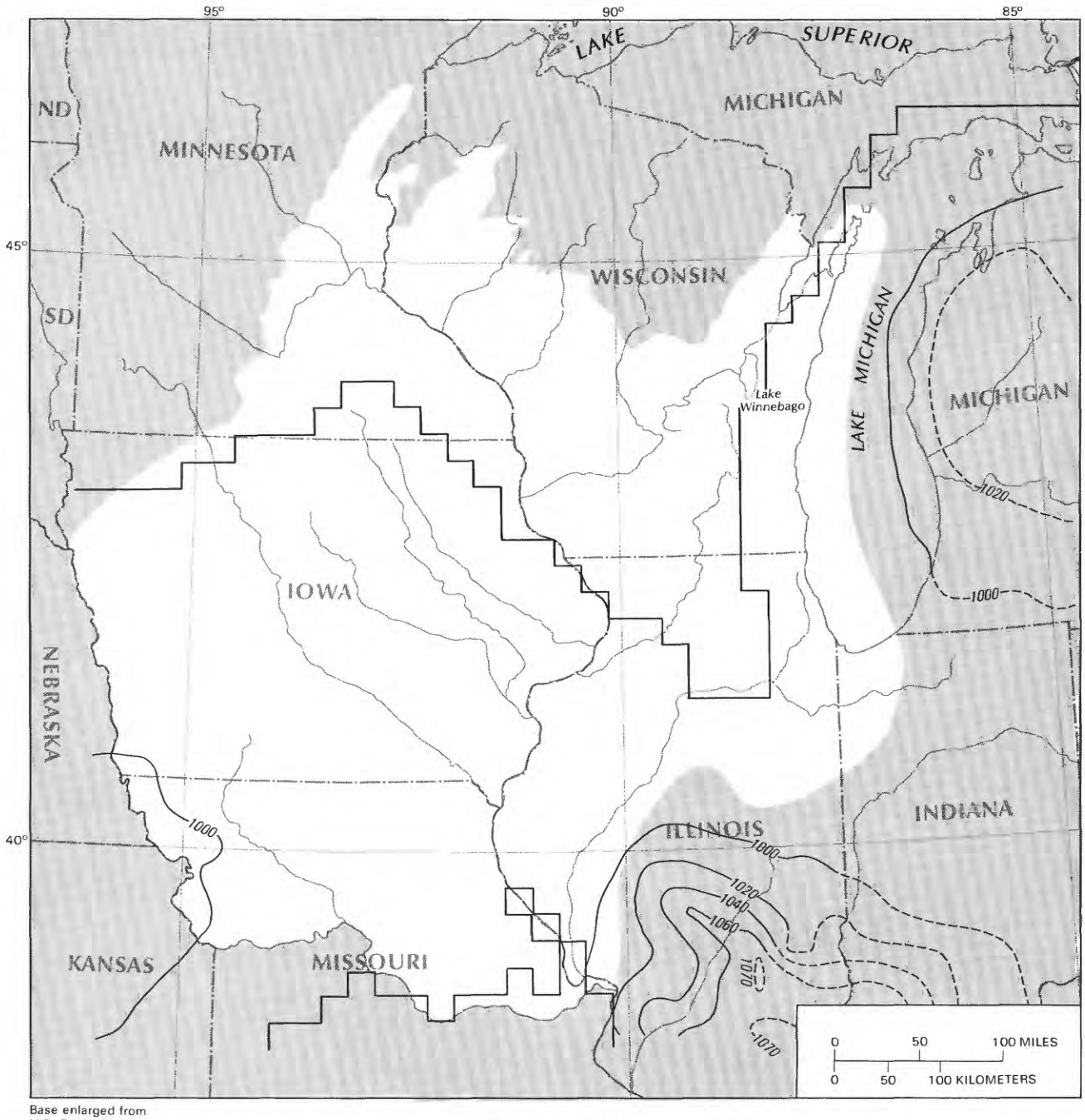

Base enlarged from
U.S. Geological Survey
1:7,500,000, 1970

EXPLANATION

—1000— LINE OF EQUAL CALCULATED GROUND-WATER DENSITY, ρ_s — Dashed where based on inferred data. Interval, in kilograms per cubic meter, is variable

MODELED LAYER BOUNDARY

FIGURE 24*D*.—Calculated ground-water density for the Silurian-Devonian aquifer (layer 4).

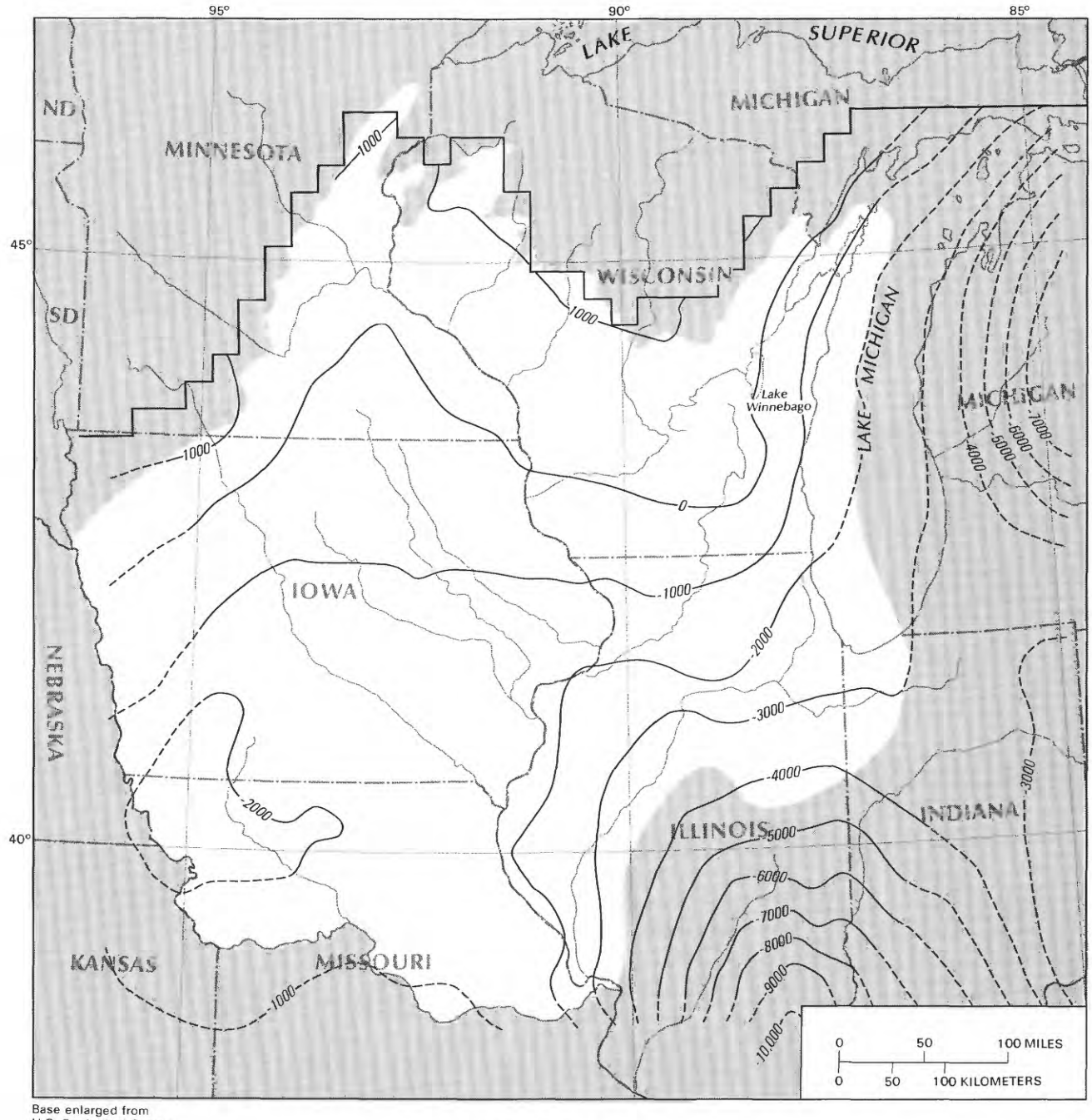

Base enlarged from
U.S. Geological Survey
1:7,500,000, 1970

EXPLANATION

—1000— CONTOUR OF MIDPOINT OF THE MOUNT SIMON AQUIFER (LAYER 1)—Dashed where inferred. Contour interval 1000 feet. Datum is sea level

MODELED LAYER BOUNDARY

FIGURE 25A.—Altitude of midpoint of the Mount Simon aquifer (layer 1).

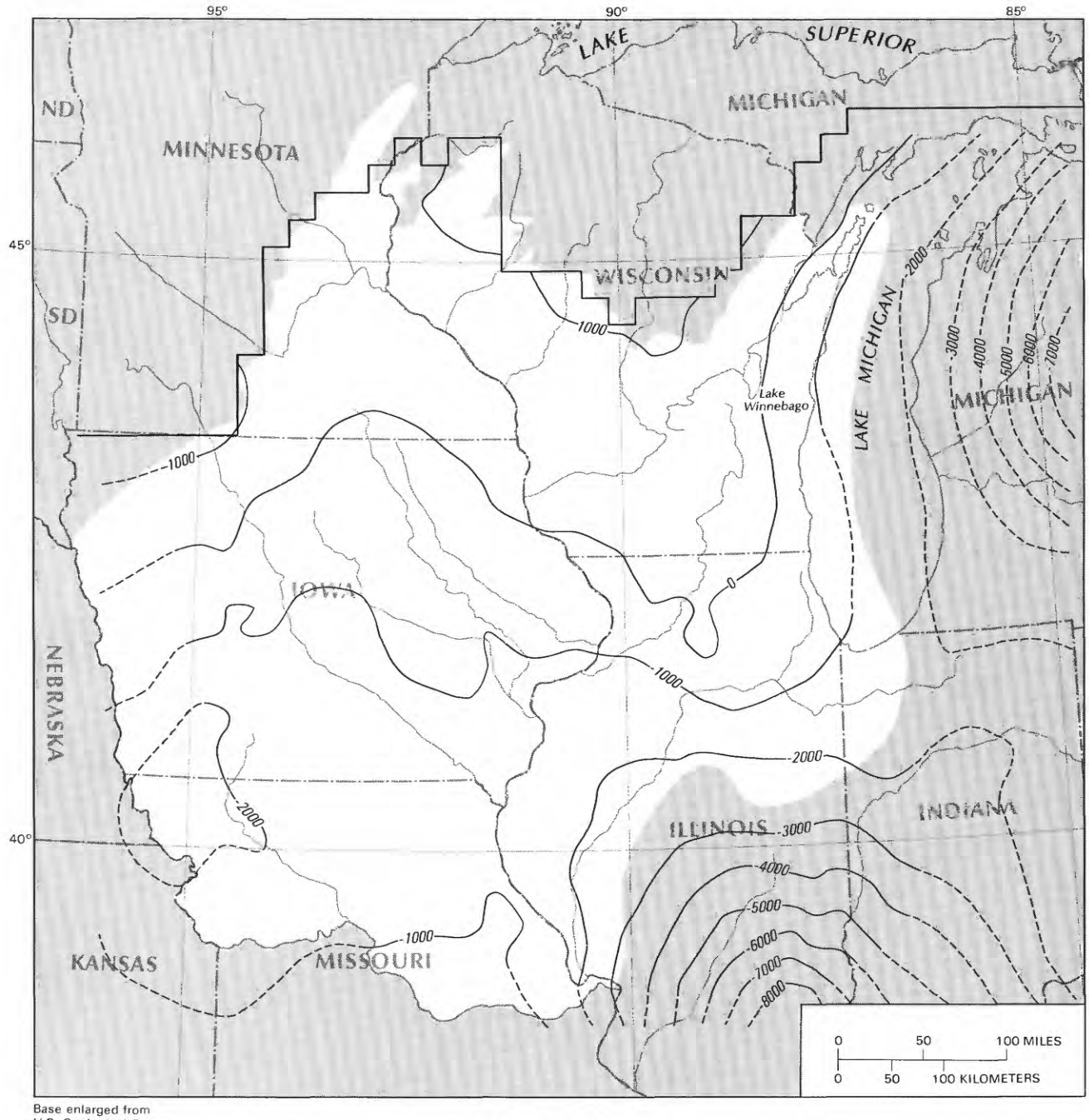

Base enlarged from
U.S. Geological Survey
1:7,500,000, 1970

EXPLANATION

—1000— CONTOUR OF MIDPOINT OF THE IRONTON-GALESVILLE AQUIFER (LAYER 2)—Dashed where inferred. Contour interval 1000 feet. Datum is sea level

MODELED LAYER BOUNDARY

FIGURE 25*B*.—Altitude of midpoint of the Ironton-Galesville aquifer (layer 2).

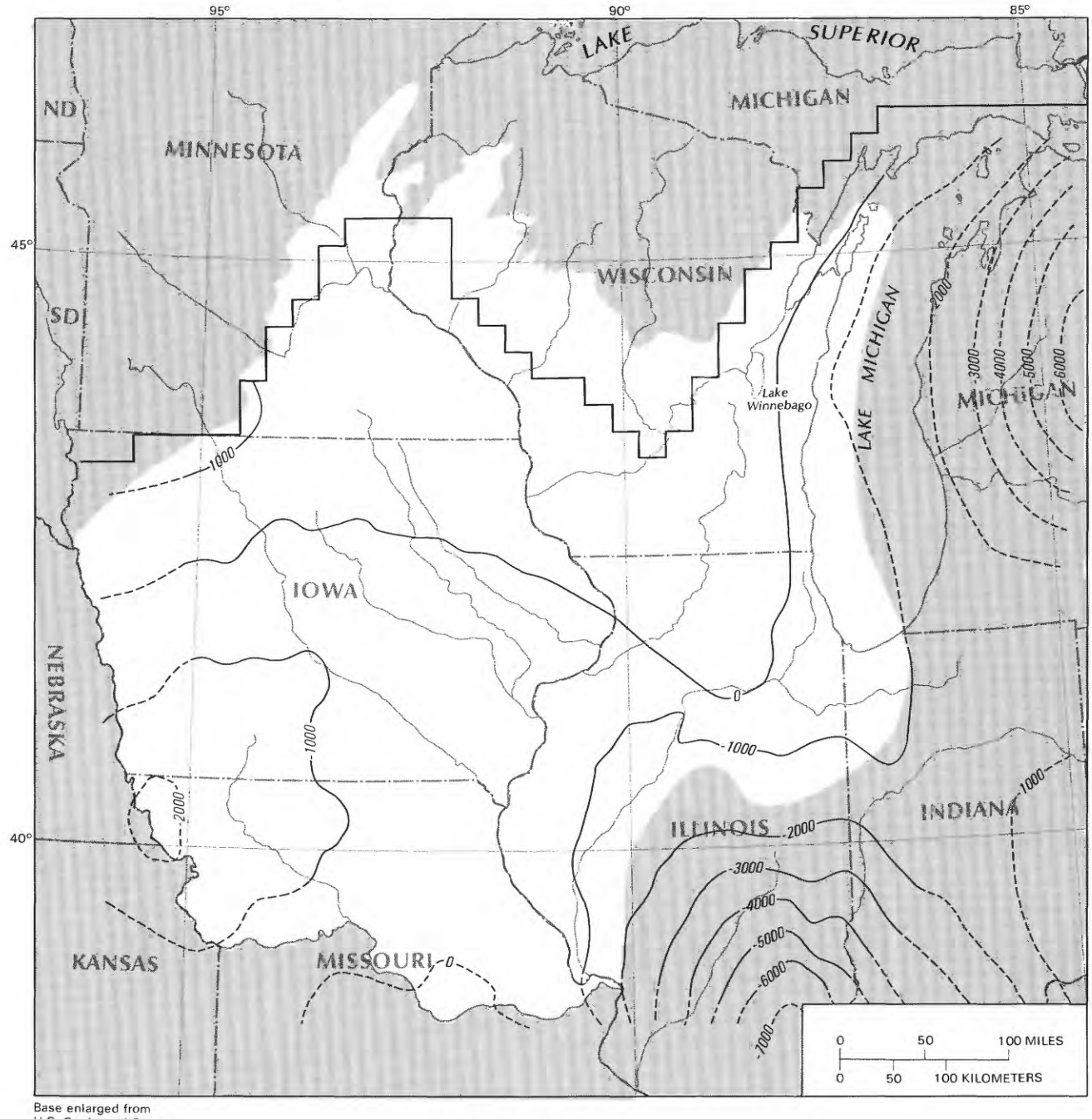

Base enlarged from
U.S. Geological Survey
1:7,500,000, 1970

EXPLANATION

—1000— CONTOUR OF MIDPOINT OF THE ST. PETER-PRAIRIE DU CHIEN-JORDAN AQUIFER (LAYER 3)—Dashed where inferred. Contour interval 1000 feet. Datum is sea level

MODELED LAYER BOUNDARY

FIGURE 25C.—Altitude of midpoint of the St. Peter-Prairie du Chien-Jordan aquifer (layer 3).

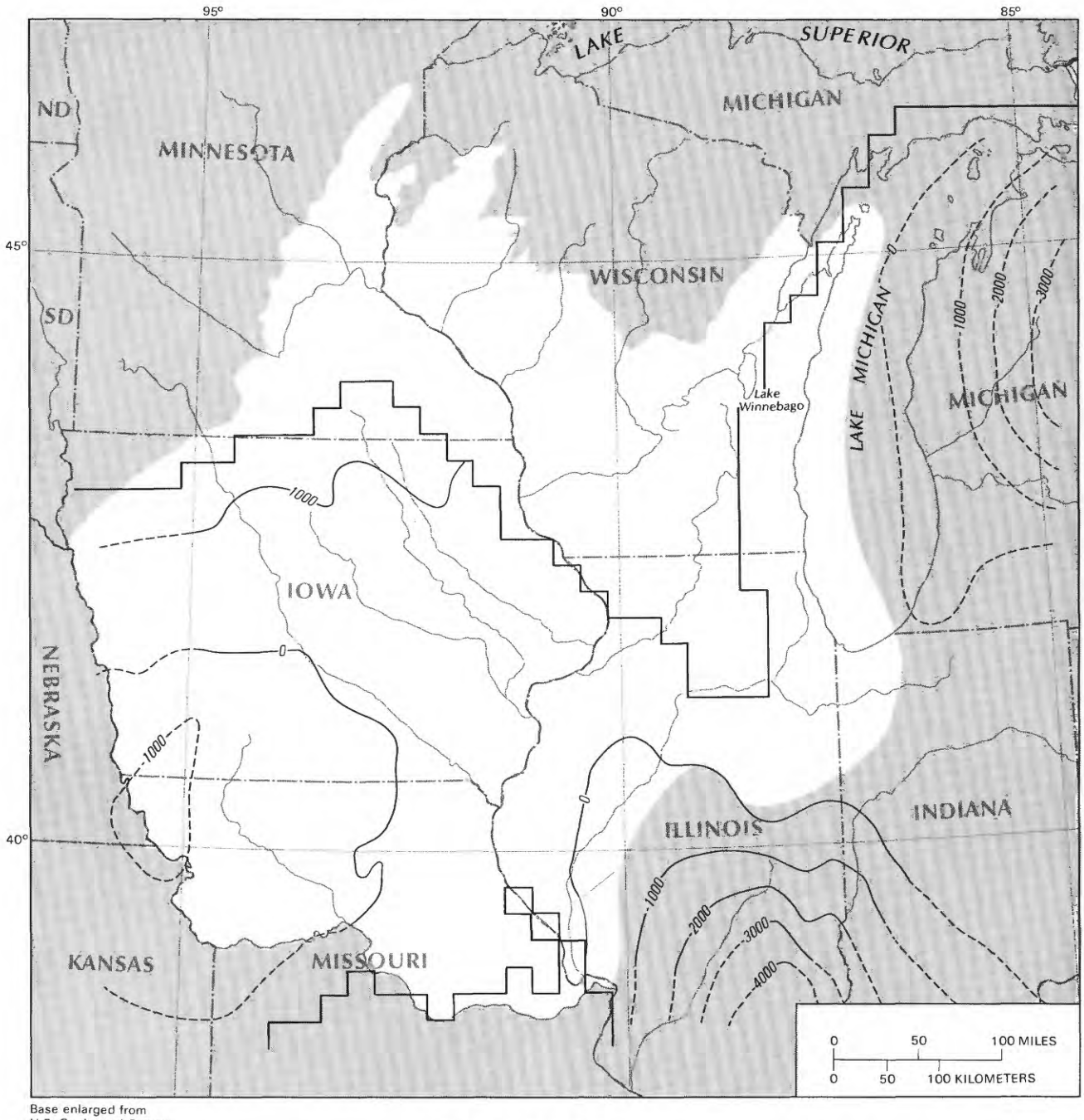

Base enlarged from
U.S. Geological Survey
1:7,500,000, 1970

EXPLANATION

—1000— CONTOUR OF MIDPOINT OF THE SILURIAN-DEVONIAN AQUIFER (LAYER 4)—Dashed where inferred. Contour interval 1000 feet. Datum is sea level

MODELED LAYER BOUNDARY

FIGURE 25*D*.—Altitude of midpoint of the Silurian-Devonian aquifer (layer 4).

procedure used to compute density and viscosity is documented by Kontis and Mandle (1989).

Storage Coefficient

Reported values of confined aquifer storage coefficients in the study area range generally from 5×10^{-5} to 6×10^{-4} (Foley and others, 1953; Suter and others, 1959; Norvitch and others, 1973; Young, 1976; and Horick and Steinhilber, 1978).

Estimates of the storage coefficient for use in the regional model were obtained by the following definition derived from Lohman (1972):

$$S_{i,j,k} = S_s b_{i,j,k} = \rho g(\alpha+n\beta)b_{i,j,k}\,, \qquad (37)$$

where

S=storage coefficient (dimensionless),
S_s=specific storage (1/L),
b=aquifer thickness (L),
ρ=density of water (M/L^3),
g=acceleration of gravity (L/T^2),
α=compressibility of the aquifer matrix (LT^2/M),
n=porosity (dimensionless), and
β=compressibility of water (LT^2/M).

For sandstones and limestones, the range of n is approximately 10 to 30 percent, and α ranges from about 1×10^{-7} to 1.3×10^{-6} in^2/lb (Clark, 1966; De Weist, 1969). For water, β is approximately 3.2×10^{-6} in^2/lb for relatively fresh water and ρg is approximately 0.434 $(lb/in^2)/ft$.

Using the above values of ρg and β and the average values of $\alpha=7\times10^{-7}$ and $n=18$ percent, the value of S_s is approximately 5.5×10^{-7}. Multiplying this specific storage by the aquifer thickness gives an initial estimate of storage coefficient for transient calibrations. Because model aquifer thicknesses range from a few feet to more than 2,000 ft, the storage coefficient was constrained to be within the range of 5×10^{-5} to 9×10^{-4} to avoid unrealistically high or low values.

Pumping Rates

Pumping-rate information is contained in a single record for each node set that contains one or more wells. A node set consists of a vertical stack of nodes at a particular row and column (i,j) that contains pumping information for wells open to at least one aquifer layer. The pumping information record contains the row and column numbers, the number of well categories, N, in the node set, a code, $W(n,m)$, for each category (see eq. 29) that specifies which layers are open to the well, and the pumping rate for each category.

Pumping rates for each aquifer or combination of aquifers were obtained from the respective district offices of the U.S. Geological Survey. Pumping data were in the form of either rate summations of individual wells over various geographic areas where well density was high, or individual well rates where well density was low.

MODEL SIMULATIONS

Model simulations included a steady-state simulation to understand the flow system under predevelopment conditions, and a transient simulation to understand the effects of ground-water development on water levels and the hydrologic budget. For the steady-state case, hydraulic conductivities were adjusted to reduce the differences between model-simulated heads and observed heads. During this process, adjustments were made on a zone basis rather than a node-by-node basis (figs. 19, 20). Because vertical hydraulic conductivity is the most uncertain hydraulic property, its values were generally varied over a larger range than were values of horizontal hydraulic conductivity.

When a generally good match between simulated and observed heads was obtained for steady-state conditions, the resultant heads were used as initial head conditions for the transient simulation, which consisted of applying reported pumping rates over the period 1861–1980 and storage coefficients computed by equation 37. The simulated transient heads were then compared with patterns of measured potentiometric head and drawdown through time. If the difference between observed and simulated heads could not be accounted for by plausible variations in storage coefficients, hydraulic conductivities were modified and the steady-state and transient simulations were repeated. This process was continued until a reasonably good fit with observed heads was achieved for both steady-state and transient conditions. Thus, in effect, the two calibration processes were carried out iteratively to obtain the best possible estimates of the hydraulic parameters.

Factors that must be considered when model output is compared with observed data are as follows: (1) model simulated heads represent the average head of blocks having an areal extent of 256 mi^2; (2) the large block size precludes simulation of local anomalies; (3) observed head data may represent local conditions and not the average head over the entire finite-difference block; (4) if vertical head differences exist within an aquifer, observed head data for partially penetrating wells may differ from the average head for the aquifer; and (5) observed head data for both developed and predevelopment conditions may be affected by undocumented local pumpage. In addition, processes that take place within the shallow ground-water system, such as in the glacial drift, are not simulated by the model. These processes

include, but are not limited to, recharge from precipitation, evapotranspiration, recharge from or discharge to streams and rivers, and nearshore recharge or discharge to Lake Michigan. Estimated budgets for local areas that account for these processes cannot be used for comparison, because in the regional model, ground-water recharge and discharge within any finite-difference block is lumped and is simulated as a net flux between the finite-difference blocks.

STEADY-STATE SIMULATION

The results of the steady-state simulation are depicted by maps of freshwater head and direction of flow between aquifer layers (figs. 26*A*–26*D*) and by maps of direction and magnitude of flow within each aquifer layer (figs. 27*A*–27*D*).

Where ground water is relatively fresh and is essentially of constant density, flow is generally in the direction of decreasing head. Where ground-water density is relatively high, as is the case in the Illinois and Michigan basins, the direction and magnitude of flow cannot be inferred from the distribution of head, but rather is determined from equations 12a–12e.

In figures 26*A*–26*D*, downward flow to an aquifer layer from an overlying aquifer layer is shown by the unshaded areas and upward flow from an aquifer layer to an overlying aquifer layer is depicted by the shaded nodes.

The steady-state simulation, which is indicative of predevelopment conditions, shows downward leakage from the Ironton-Galesville aquifer (layer 2) to the Mount Simon aquifer (layer 1) (fig. 26*A*) in areas containing relatively fresh water, primarily in southeastern Minnesota, northern and southeastern Iowa, much of Wisconsin, northeastern Missouri, and eastern Indiana. Leakage is upward to the Ironton-Galesville aquifer in the vicinity of the Mississippi and Missouri Rivers, Lake Michigan, western Michigan, most of Illinois, and southern Iowa. The patterns of leakage between the Ironton-Galesville aquifer (layer 2) and the overlying St. Peter-Prairie du Chien-Jordan aquifer (layer 3) (fig. 26*B*) are similar. The St. Peter-Prairie du Chien-Jordan aquifer (fig. 26*C*) receives downward leakage from the Silurian-Devonian aquifer (layer 4) in extreme eastern Wisconsin, the Michigan basin, eastern Indiana, central Illinois, and most of Missouri and Iowa. Leakage is upward to the Silurian-Devonian aquifer in the vicinity of the Illinois, Mississippi, and Missouri Rivers, beneath Lake Michigan, and in the Illinois basin. In addition, in their subcrop areas each of the Cambrian-Ordovician aquifers receives direct recharge from overlying glacial deposits and discharges to the major rivers.

The Silurian-Devonian aquifer (fig. 26*D*) receives downward leakage through overlying glacial deposits or Devonian, Mississippian, and Pennsylvanian rocks over most of its extent. Upward discharge occurs in the Illinois basin and beneath Lake Michigan and major rivers.

The variable-density effect of the brines on freshwater-head calculations is most evident in the Illinois and Michigan basins, where the presence of high-density ground water results in large simulated freshwater heads. The arrows in figures 27*A*–27*D* are directional vectors that represent the simulated direction of flow parallel to the α, β plane at each node in aquifer layers 1 through 4 as computed by equation 12e. In these figures, lateral flow arrows depicting flow between constant head nodes, representing glacial drift, along the northern boundary of each aquifer layer (figs. 26*A*–26*D*) and adjacent active nodes are not shown. In most cases, this flow is directed into the aquifers and is relatively small in magnitude. In addition, because of the presence of artificial zero-flux boundaries along the southern and eastern margins of the model, flow directions are not shown for the last row and column of active model nodes. The magnitude of flow rates within the aquifer layers is given by lines of equal flow rate superimposed on the directional vectors in the figures. Flow rates were computed by equation 12d and represent the net flow through the eastern and southern faces of each model block. In areas other than the Illinois and Michigan basins, the relative ground-water density is close to unity and aquifer dip is very small so that the effect of the variable-density terms is very small. Because of this small effect and the uniform spacing of the model grid, the flow rate is essentially the product of aquifer transmissivity and head difference between adjacent nodes throughout most of the study area.

The simulated steady-state direction of flow within the Mount Simon aquifer (fig. 27*A*) is to the east and southeast in southeastern Wisconsin and northeastern Illinois; toward the Mississippi River and its tributaries in central and western Wisconsin; toward the Mississippi and Minnesota Rivers in southeastern Minnesota; toward the Mississippi River from northwestern and eastern Iowa; toward the confluence of the Mississippi and Missouri Rivers from southwestern and south-central Iowa, western Illinois, and northern Missouri; and toward the Missouri River from areas south of the river. Converging radial flow in north-central Illinois coincides with a regional discharge area along the Illinois River where the St. Peter-Prairie du Chien-Jordan aquifer is at the surface and is incised by the river.

Overall, the regional flow direction for each of the other aquifers is similar to that of the Mount Simon aquifer. The primary differences are the pronounced influence of major surface-drainage features on ground-water flow directions in shallow parts of overlying aquifers.

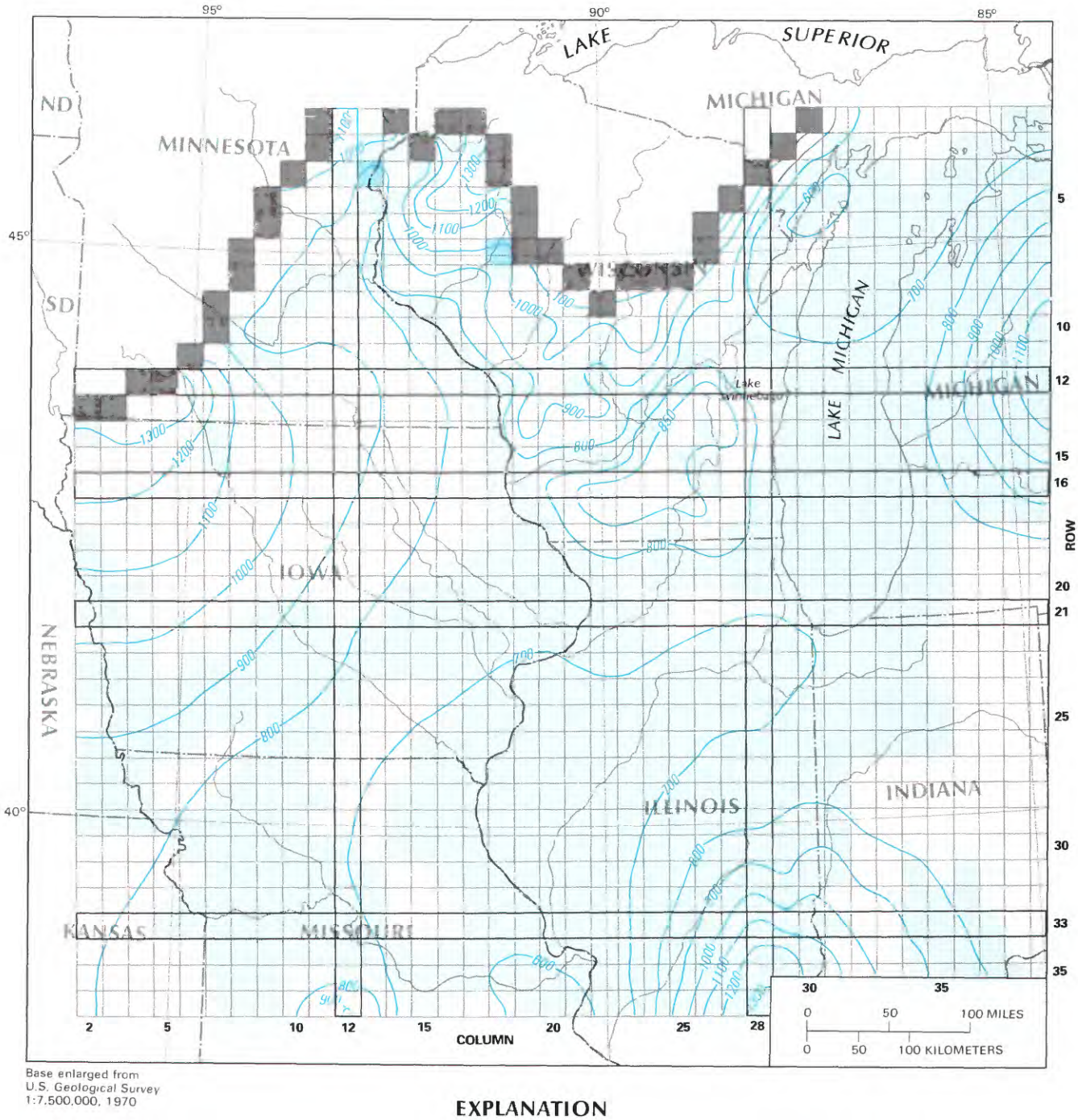

EXPLANATION

—700— POTENTIOMETRIC CONTOUR—Shows simulated predevelopment freshwater head in the Mount Simon aquifer (layer 1). Contour interval, in feet, is variable. Datum is sea level

MODEL CONSTANT-HEAD NODE DEPICTING

Aquifer layer boundary

Aquifer layer dissected by major river valley

DIRECTION OF VERTICAL FLOW THROUGH THE TOP OF THE AQUIFER

Upward

Downward

OUTLINED ROW OR COLUMN DEPICTED IN SECTIONS OF VERTICAL FLOW SHOWN IN FIGURES 29A-30D

FIGURE 26A.—Simulated predevelopment freshwater head in the Mount Simon aquifer (layer 1).

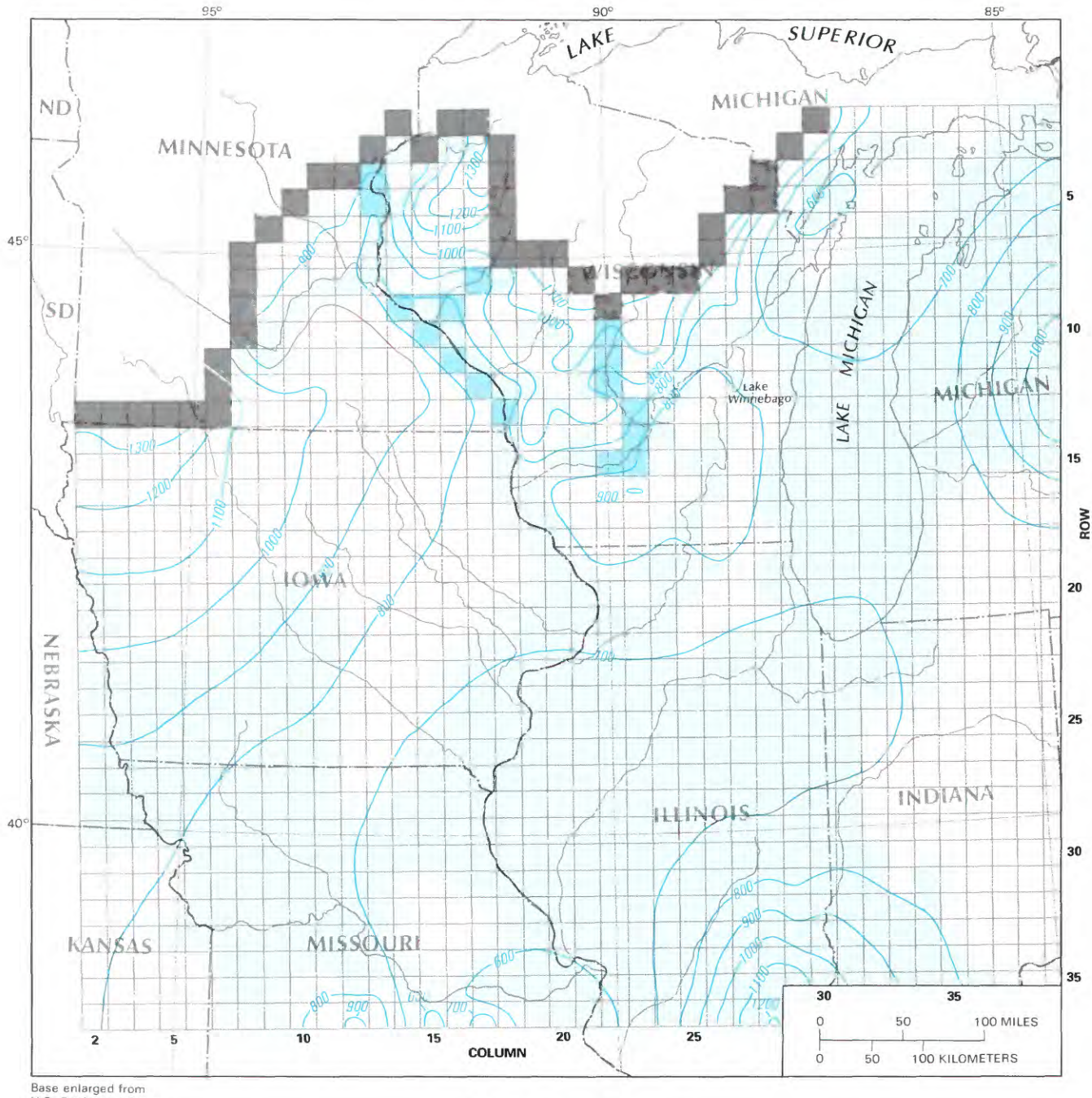

Base enlarged from U.S. Geological Survey 1:7,500,000, 1970

EXPLANATION

—700— POTENTIOMETRIC CONTOUR—Shows simulated predevelopment freshwater head in the Ironton-Galesville aquifer (layer 2). Contour interval 100 feet. Datum is sea level

MODEL CONSTANT-HEAD NODE DEPICTING

Aquifer layer boundary

Aquifer layer dissected by major river valley

DIRECTION OF VERTICAL FLOW THROUGH THE TOP OF THE AQUIFER

Upward

Downward

FIGURE 26*B*.—Simulated predevelopment freshwater head in the Ironton-Galesville aquifer (layer 2).

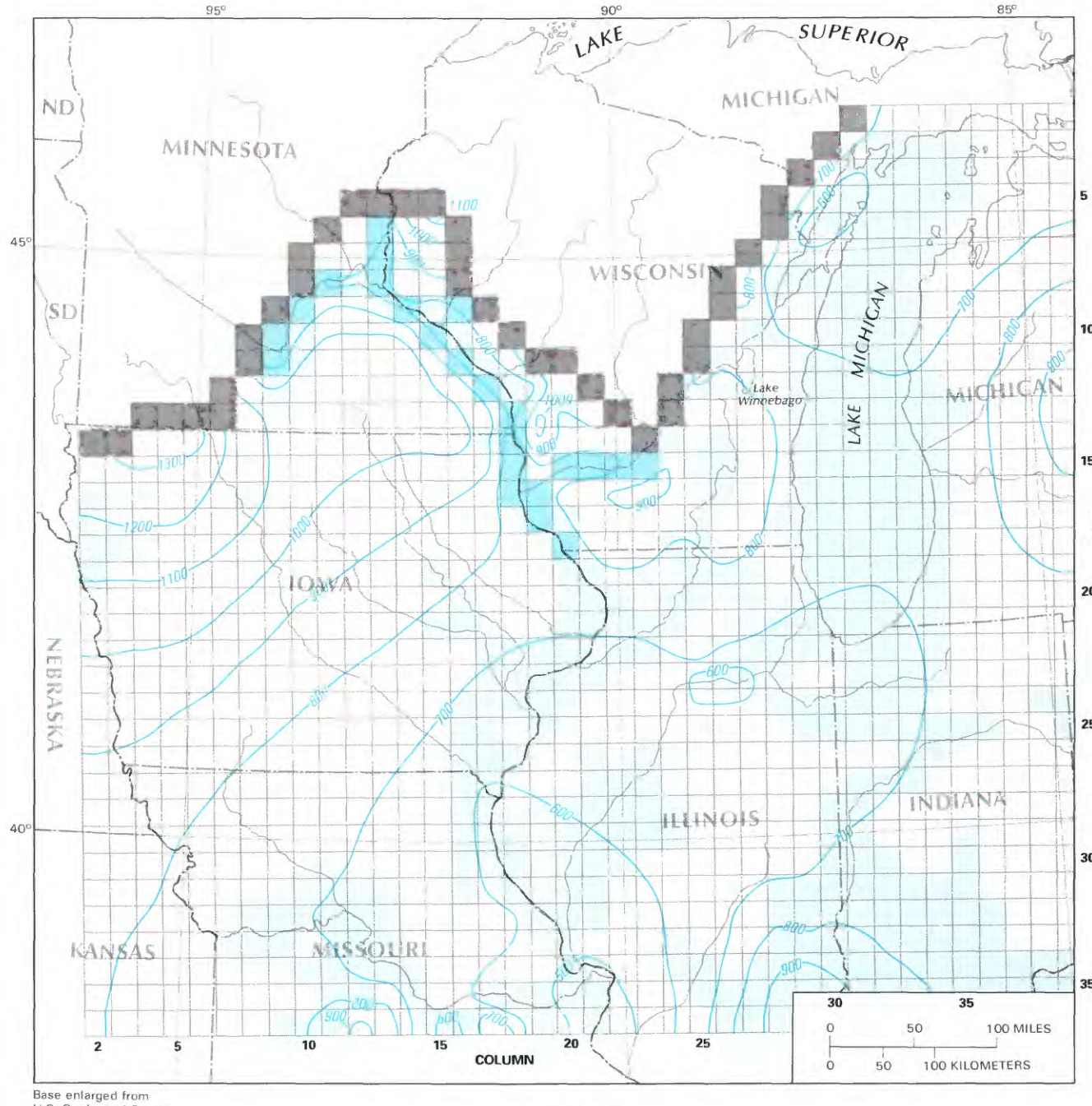

EXPLANATION

—700— POTENTIOMETRIC CONTOUR—Shows simulated predevelopment freshwater head in the St. Peter-Prairie du Chien-Jordan aquifer (layer 3). Contour interval 100 feet. Datum is sea level

MODEL CONSTANT-HEAD NODE DEPICTING

Aquifer layer boundary

Aquifer layer dissected by major river valley

DIRECTION OF VERTICAL FLOW THROUGH THE TOP OF THE AQUIFER

Upward

Downward

FIGURE 26C.—Simulated predevelopment freshwater head in the St. Peter-Prairie du Chien-Jordan aquifer (layer 3).

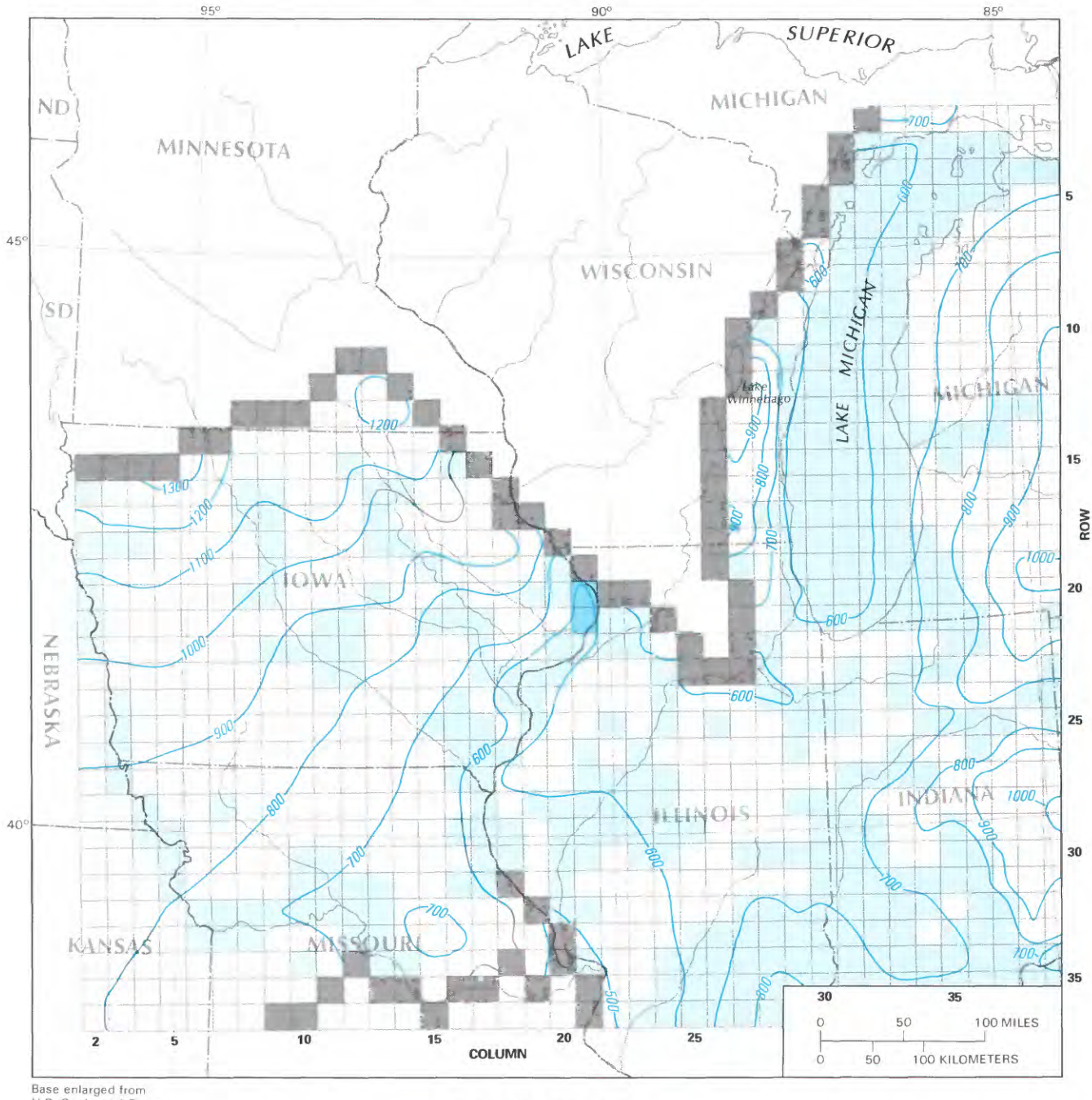

Base enlarged from
U.S. Geological Survey
1:7,500,000, 1970

EXPLANATION

—700— POTENTIOMETRIC CONTOUR—Shows simulated predevelopment freshwater head in the Silurian-Devonian aquifer (layer 4). Contour interval 100 feet. Datum is sea level

MODEL CONSTANT-HEAD NODE DEPICTING

Aquifer layer boundary

Aquifer layer dissected by major river valley

DIRECTION OF VERTICAL FLOW THROUGH THE TOP OF THE AQUIFER

Upward

Downward

FIGURE 26*D*.—Simulated predevelopment freshwater head in the Silurian-Devonian aquifer (layer 4).

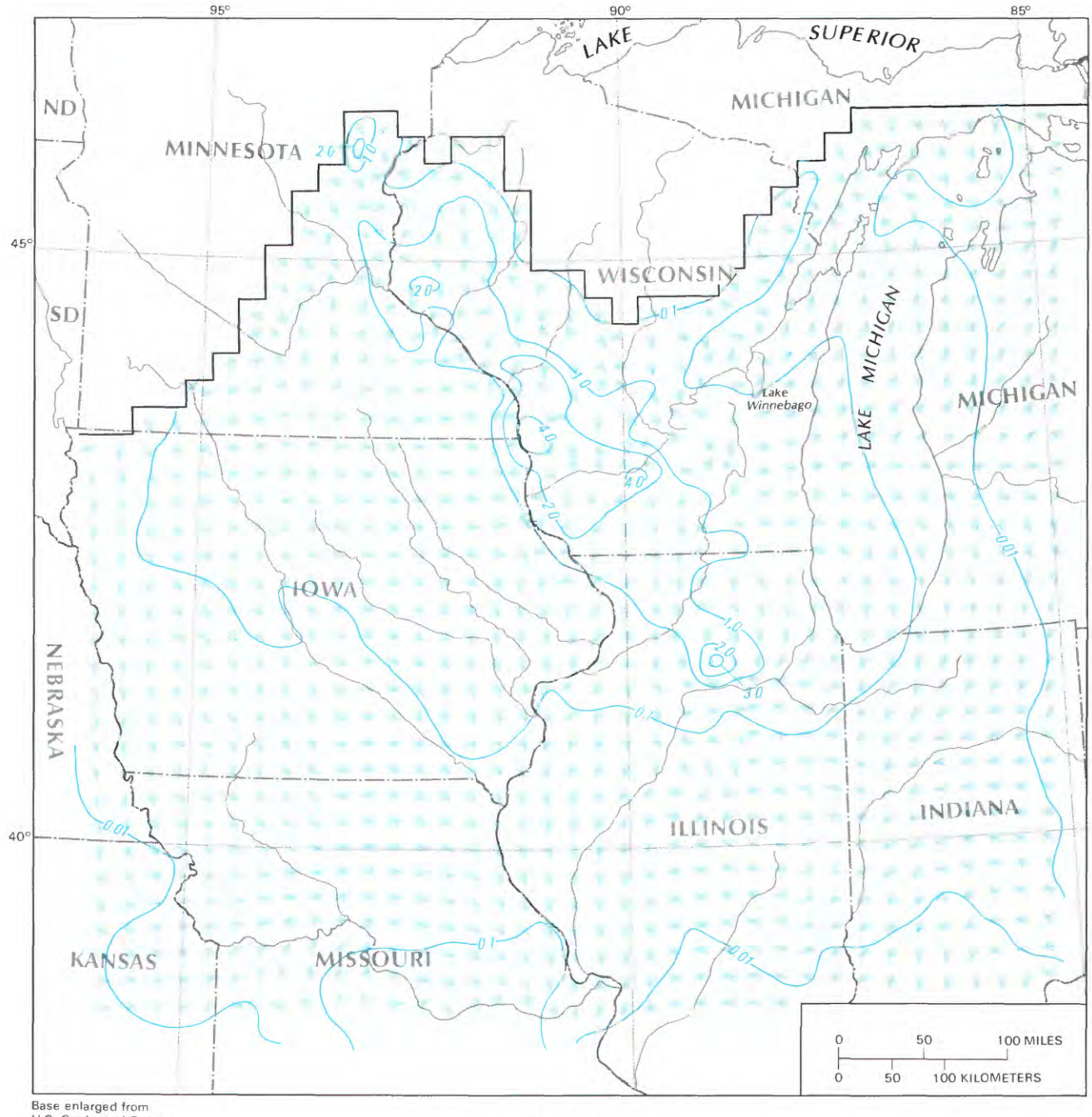

EXPLANATION

—.001— LINE OF EQUAL FLOW—Shows simulated magnitude of predevelopment horizontal flow (from equation 12d) in the Mount Simon aquifer (layer 1). Interval, in cubic feet per second, is variable

SIMULATED DIRECTION OF PREDEVELOPMENT HORIZONTAL FLOW

MODELED LAYER BOUNDARY

FIGURE 27A.—Simulated direction and magnitude of predevelopment horizontal flow in the Mount Simon aquifer (layer 1).

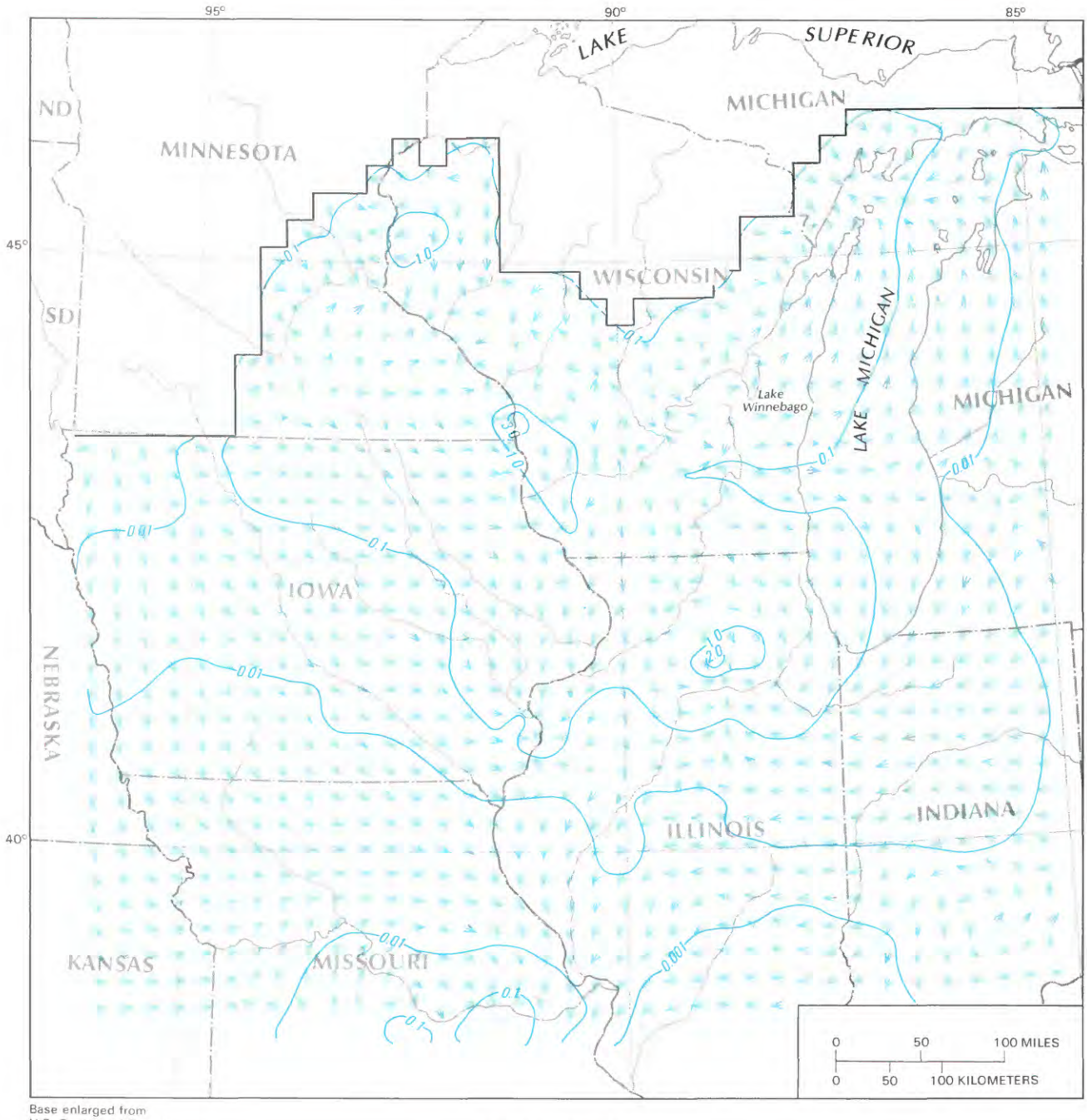

EXPLANATION

—0.01— LINE OF EQUAL FLOW—Shows simulated magnitude of predevelopment horizontal flow (from equation 12d) in the Ironton-Galesville aquifer (layer 2). Interval, in cubic feet per second, is variable

SIMULATED DIRECTION OF PREDEVELOPMENT HORIZONTAL FLOW

MODELED LAYER BOUNDARY

FIGURE 27*B*.—Simulated direction and magnitude of predevelopment horizontal flow in the Ironton-Galesville aquifer (layer 2).

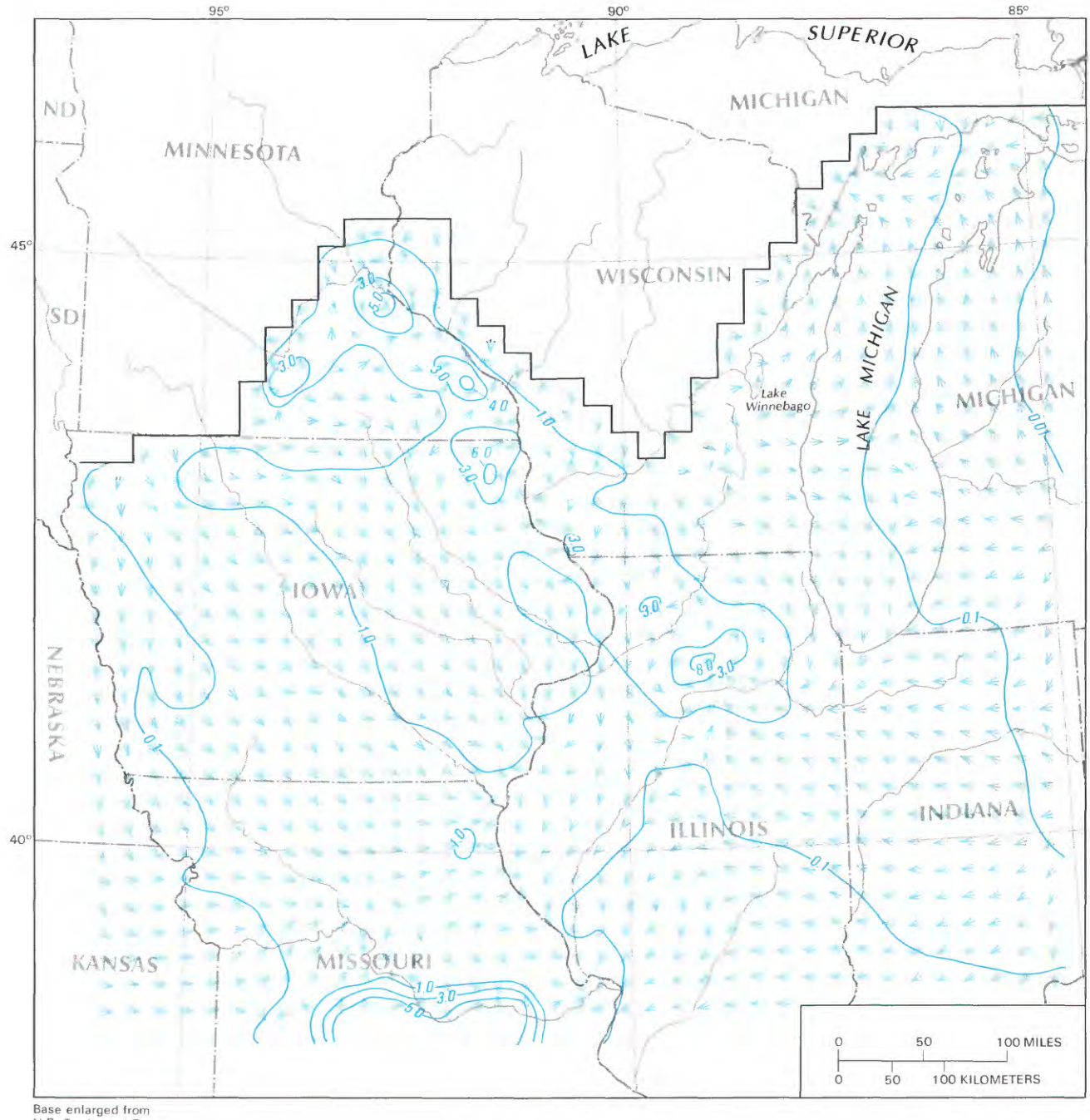

EXPLANATION

—001— LINE OF EQUAL FLOW—Shows simulated magnitude of predevelopment horizontal flow (from equation 12d) in the St. Peter-Prairie du Chien-Jordan aquifer (layer 3). Interval, in cubic feet per second, is variable

SIMULATED DIRECTION OF PREDEVELOPMENT HORIZONTAL FLOW

MODELED LAYER BOUNDARY

FIGURE 27C.—Simulated direction and magnitude of predevelopment horizontal flow in the St. Peter-Prairie du Chien-Jordan aquifer (layer 3).

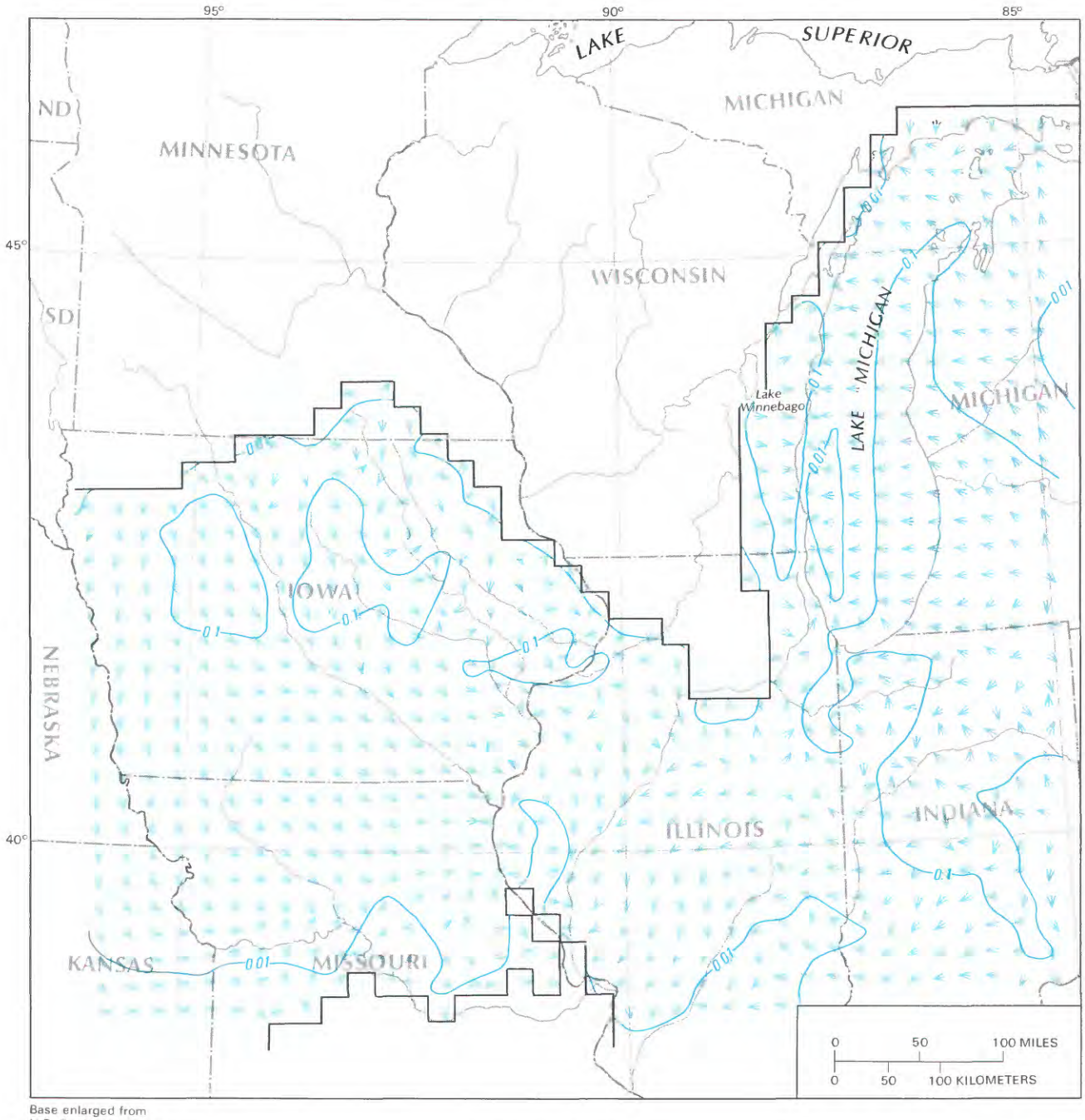

Base enlarged from U.S. Geological Survey 1:7,500,000, 1970

EXPLANATION

—.001— LINE OF EQUAL FLOW—Shows simulated magnitude of predevelopment horizontal flow (from equation 12d) in the Silurian-Devonian aquifer (layer 4). Interval, in cubic feet per second, is variable

SIMULATED DIRECTION OF PREDEVELOPMENT HORIZONTAL FLOW

MODELED LAYER BOUNDARY

FIGURE 27*D*.—Simulated direction and magnitude of predevelopment horizontal flow in the Silurian-Devonian aquifer (layer 4).

Simulated flow rates in the Mount Simon aquifer (fig. 27*A*) are less than 0.01 ft^3/s along the northern margin where the aquifer thins and in the Illinois and Michigan basins where the unit is deeply buried. The highest flow rates are in south-central and western Wisconsin, north-central Illinois, and northern Minnesota. In these areas, the aquifer is closer to land surface, has a higher hydraulic conductivity, and is partially confined.

Simulated flow rates in the Ironton-Galesville aquifer (fig. 27*B*) are less than 0.01 ft^3/s along its northern margin, in southwestern Iowa, most of Missouri, and southern Illinois, where the aquifer is primarily a carbonate rock. Flow rates also are low in the Michigan basin, where the Ironton-Galesville aquifer is deeply buried. Flow rates are highest in north-central Illinois, southwestern and northwestern Wisconsin, and south-central Minnesota.

In the St. Peter-Prairie du Chien-Jordan aquifer (fig. 27*C*), simulated flow rates are less than 0.01 ft^3/s along its margins and in the Michigan basin. Flow rates are highest where the aquifer is dissected by numerous rivers and is poorly confined in northern Illinois, western Wisconsin, south-central Minnesota, eastern Iowa, and south-central and northeastern Missouri. Flow rates in this layer are significantly higher than those in other Cambrian-Ordovician aquifers, primarily because a larger area of the aquifer is poorly confined compared with the Ironton-Galesville and Mount Simon aquifers (layers 1 and 2).

Overall, the simulated steady-state flow rates in the Silurian-Devonian aquifer (fig. 27*D*) are generally small because of the relatively low values of hydraulic conductivity. Flow rates range from less than 0.01 ft^3/s along the margins of the aquifer and in the Illinois basin to almost 1 ft^3/s in eastern Wisconsin, where the aquifer is partially confined. The elongated area of small flow rates in the center of Lake Michigan is at the junction of predominantly easterly flow from Wisconsin and westerly flow from Michigan.

The primary purpose of including the Illinois and Michigan basins as active parts of the regional model was not to simulate flow conditions in these areas, but rather as an alternative to using zero-flow boundaries to represent the freshwater-saltwater interface along the perimeter of the basins. The variable-density modifications to the Trescott code were implemented to simulate flow conditions near these boundaries more accurately. The hydrogeologic properties used in the model in the area of the basins are approximations of actual conditions and once established, except for hydraulic conductivity, were not varied during the modeling process. In addition, the southern and eastern borders of the model essentially bisect the basins. Consequently, the lack of accurate data and the presence of artificial zero-flow boundaries so as to exclude the deepest segments of the basins from the model preclude any attempt to interpret simulated flow within the basins in terms of actual flow conditions. Despite these difficulties, it may be of interest to note the effects of variable density on the simulated flow system.

The effects of variable density are manifested through the term $TS_{i,j,k}$ of equation 11d; as shown in equation 11e, $TS_{i,j,k}$ is itself a summation of the terms A, B, and Γ defined in equation 11c. The magnitude and sign of $TS_{i,j,k}$ at a given node depend on the relative magnitudes of the conductance, the degree to which the fluid density differs from unity, and the elevation gradients of node i,j,k and the nodes adjacent to it.

To examine the nature and exent of the variable-density effect, a simulation for steady-state conditions was run with the term $TS_{i,j,k}$ everywhere set to zero. This in effect introduced the assumption that the groundwater density was approximately equal to that of freshwater throughout the system. The resulting head pattern for the Mount Simon aquifer (layer 1) is shown in figure 28. For the assumed condition of uniform density, directions of flow within the layer would generally be orthogonal to the head contours of figure 28, except possibly in places where the aquifer heterogeneity as represented in the model may have generated an effective local anisotropy. For purposes of comparison, the arrows showing directions of ground-water flow in the Mount Simon aquifer (fig. 27*A*), as computed for the existing variable-density field conditions, are superimposed on the freshwater head contours of figure 28. The results indicate that along the northern margin of the Michigan basin the calculated direction of regional flow for the variable-density field condition is generally opposite to that which would be expected for freshwater conditions; within the basin, the computed flows have a stronger eastward component than would exist under freshwater conditions. In the Illinois basin, the computed variable-density flows have south-southeasterly components, whereas the simulated freshwater flow would be westward from the eastern margin. Elsewhere, the flow patterns would be generally similar for the two cases, reflecting the fact that outside the Michigan and Illinois basins, the density of ground water in the Mount Simon is generally close to that of freshwater.

As noted earlier, the eastern and southern zero-flow boundaries of the model are located just west and north of the troughs of the Michigan and Illinois basins, respectively. If the eastern boundary of the model were extended farther to the east so that the last column of active nodes would include the upward limb of the Michigan basin, then the effect of high-density ground water within the basin trough would be represented in the simulation. The result would be significantly higher

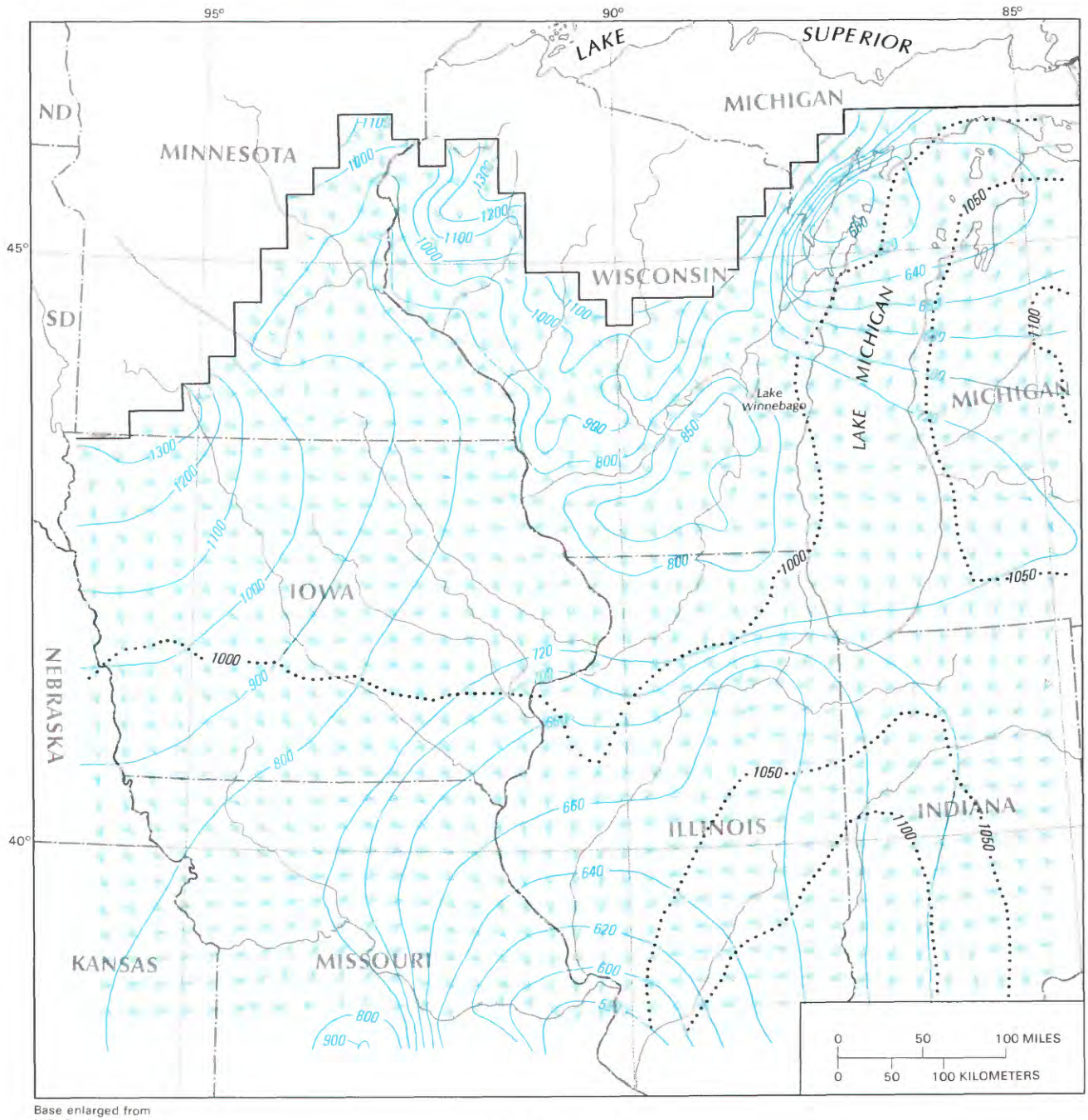

EXPLANATION

800 — POTENTIOMETRIC CONTOUR — Shows simulated steady-state head without density effects. Contour interval, in feet, is variable. Datum is sea level

1100 — LINE OF EQUAL CALCULATED GROUND-WATER DENSITY, ρ_s — Interval 50 kilograms per cubic meter

ARROW REPRESENTS DIRECTION OF SIMULATED GROUND-WATER FLOW WITH DENSITY EFFECTS

MODELED LAYER BOUNDARY

FIGURE 28.—Effects of density on ground-water flow in the Mount Simon aquifer (layer 1).

values of the term $TS_{i,j,k}$ along the north-south axis of the Michigan basin than occur along the eastern perimeter of the present model configuration. A similar effect would occur along the southern boundary if the model included the trough and southern upward limb of the Illinois basin. The net effect would be an overall increase in head, with the largest increase in the center of the respective basins. The individual terms used to compute flow (A, B, and Γ of eqs. 12a–12c) would, however, remain the same. The effect on the flow pattern depicted in figures 27*A* and 28 would be an increase in magnitude of flow components in the direction of decreasing freshwater head and a decrease in magnitude of flow components in the direction of increasing freshwater head (fig. 26*A*), especially in the vicinity of the basin centers. This would result in a greater overall deflection of the flow vectors away from regions of high ground-water density.

The general characteristics of the variable-density effects illustrated for the Mount Simon aquifer (layer 1) apply to the other aquifers as well. To the extent that the hydrogeologic properties input to the model approximate the field conditions in the deep basins, the variable-density steady-state simulation indicates that the magnitude of flow within the basins is quite small and that the areas containing high ground-water density are partial barriers to fresh ground-water flow.

To illustrate further the three-dimensional nature of ground-water flow, the horizontal and vertical components of simulated flow were computed by equations 12a-12c along selected rows and columns of the model. These components of flow are plotted as vertical sections along with a profile of the water table (figs. 29*A*, 29*B*, 30*A*–30*D*). The locations of the sections are shown in figure 26*A*. The upper section shows the simulated flow for predevelopment steady-state conditions, and the lower section shows the simulated transient flow that is discussed in a later section on calibration of the transient model. The horizontal vectors depict flow within each layer along a row or column. The cross-sectional area of flow is the product of aquifer thickness and the inclined model block width. The vertical vectors depict the direction and relative magnitude of flow through confining layers between each aquifer and the overlying aquifer. The cross-sectional area of flow, in this case, is the tilted surface area of each block and is approximately 16×16 mi^2. The vertical vectors are plotted above each node at the block face between layers, and the horizontal vectors are plotted at the block faces between nodes within an aquifer layer. In general, these cross sections are not oriented along flow lines, although in some cases segments of a given section may be approximately parallel to a flow line.

The flow vectors show the regional influence of the water-table configuration on the simulated predevelopment ground-water flow system. Except where ground-water density is high, ground water moves from areas of higher to lower water-table elevation. Areas where the water table is irregular contain numerous local flow systems, whereas areas where the water table is more regular contain regional flow systems. As illustrated on the sections, the major surface-drainage features, such as the Mississippi and Missouri Rivers, their tributaries, and Lake Michigan, serve as discharge areas to the regional ground-water flow system. The profile along column 12 (fig. 29*A*) shows overall steady-state ground-water movement downward in Minnesota, Iowa, and central Missouri. Components of ground-water flow along the column show movement downgradient toward the Mississippi and Missouri Rivers. Along column 28 (fig. 29*B*) ground water moves generally downward in Wisconsin and parts of south-central Illinois. Movement is upward along the Fox River in Wisconsin and along the Illinois River in Illinois. In the Illinois basin, low rates of lateral flow in the north-south direction and upward flow are depicted by the small arrows. The profile along row 12 (fig. 30*A*) crosses southern Minnesota and central Wisconsin. Throughout central Wisconsin the Cambrian-Ordovician aquifers are unconfined or partially confined. The water table is irregular, showing the presence of numerous local flow systems. Ground water generally moves downward from the water table and aquifer layers 4, 3, and 2 in southeastern Minnesota, upward from aquifer layers 1, 2, and 3 to the Mississippi River, and upward from aquifer layer 4 to Lake Michigan. The section along row 16 (fig. 30*B*) crosses northern Iowa and southern Wisconsin and shows that ground water moves downward to the regional aquifer system in western Iowa, with an eastward component of flow toward the Mississippi River. The Mississippi and Rock Rivers and Lake Michigan receive ground-water discharge from upward ground-water flow; in the intervening areas, ground water moves downward to recharge the regional aquifer system. A similar pattern of downward ground-water movement in western Iowa and eastward flow toward the Mississippi River is shown along row 21 (fig. 30*C*), which crosses central Iowa and northern Illinois. Also shown are eastward components of lateral flow and vertical ground-water flow toward Lake Michigan. Row 33 (fig. 30*D*) along the southern part of the model crosses several different flow systems. Ground water moves downward to the regional aquifer system in west-central Missouri south of the Missouri River and then flows toward the Missouri River, where it discharges upward. In east-central Missouri north of the Missouri River, ground water flows downward from aquifer layer 4 to recharge the regional aquifer system. In aquifer layers 3 and 4, an easterly component flows

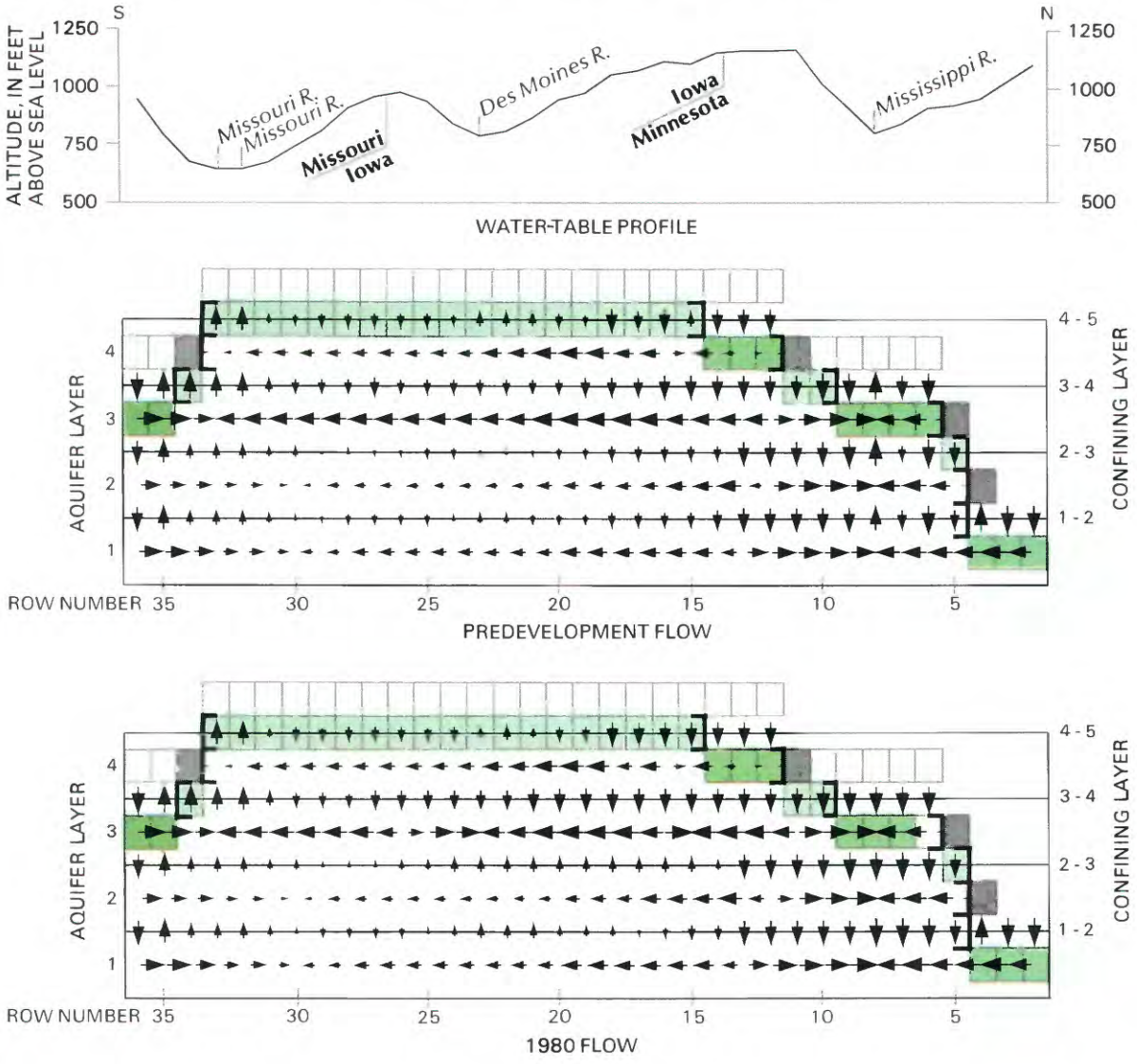

EXPLANATION

SIMULATED FLOW, IN CUBIC FEET PER SECOND—Arrows indicate the direction and magnitude of net horizontal flow across lateral boundaries of aquifer layer blocks (16 miles x aquifer thickness) or vertical flow through the upper boundary of aquifer layer blocks (16 miles x 16 miles) to or from overlying confining layers or glacial drift. Location of sections shown in figures 26*A-D*

- More than 1.0
- 0.1 to 1.0
- 0.05 to 0.1
- 0.01 to 0.05
- 0.001 to 0.01
- Less than 0.001

RELATIONSHIP OF MODEL LAYERS AND CONSTANT-HEAD NODES

- Constant-head node in glacial drift that represents the water table
- Constant-head node in glacial drift that represents the lateral boundary of an aquifer layer. Provides minimal horizontal flow at the thin, eroded edge of the layer
- Aquifer layer subcrops beneath glacial drift. Vertical flow vector above this node represents direct recharge from or discharge to a constant-head node in the glacial drift
- Confining layer subcrops beneath glacial drift. Vertical flow vector within this node represents vertical flow through that confining layer
- [ ] Brackets show extent of model layers

FIGURE 29*A*.—Simulated direction and magnitude of flow in a vertical section along column 12.

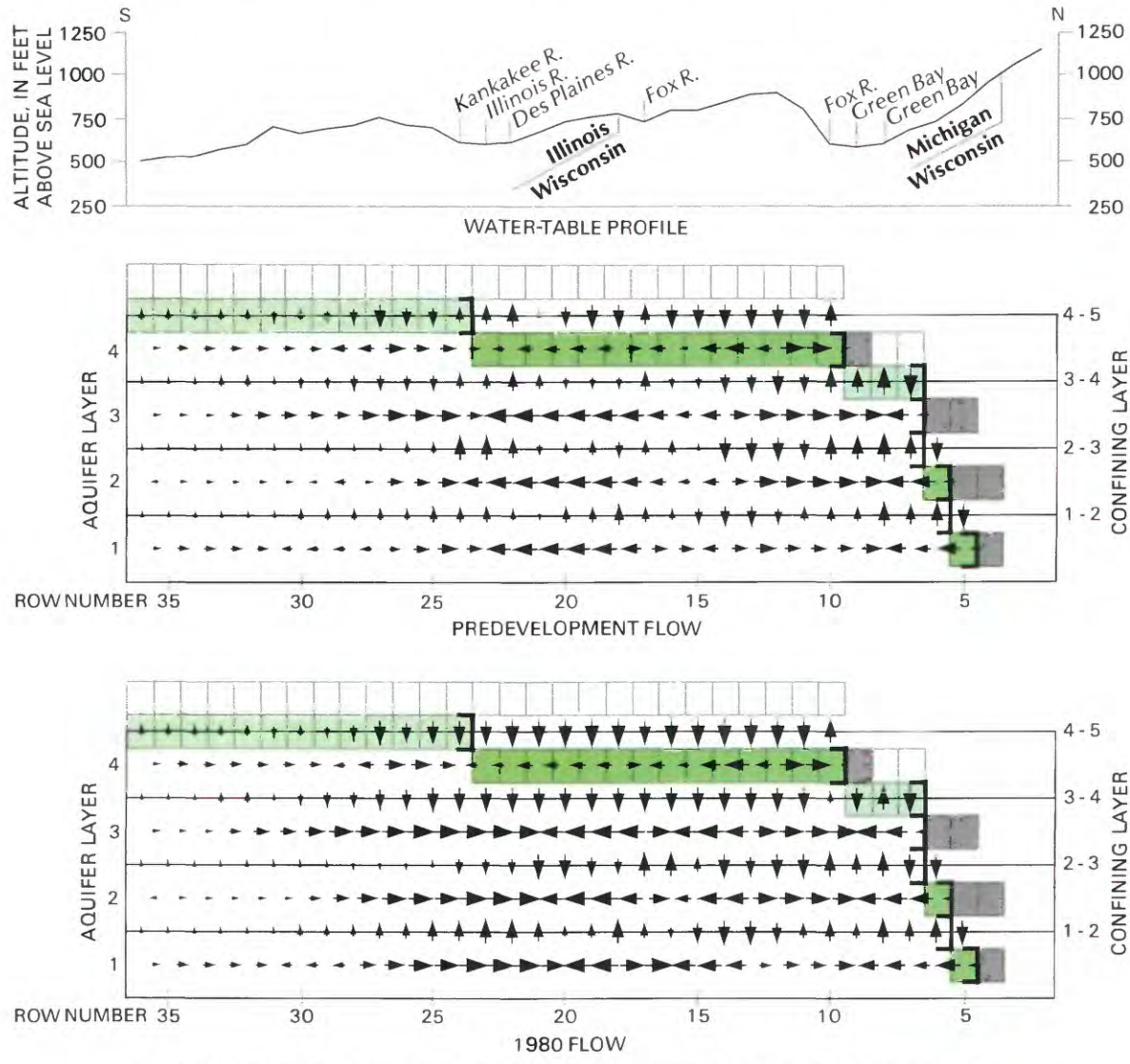

FIGURE 29*B*.—Simulated direction and magnitude of flow in a vertical section along column 28.

toward the Mississippi River and a westerly component flows toward the Missouri River.

CALIBRATION

Head data were not available in sufficient quantity and distribution to depict a predevelopment potentiometric surface for each aquifer layer. Consequently, it was possible only to compare simulated and measured potentiometric surfaces for the St. Peter-Prairie du Chien-Jordon and Silurian-Devonian aquifers (layers 3 and 4) (figs. 26*C* and 14, and figs. 26*D* and 13, respectively). Except for Minnesota, the head data were insufficient to reconstruct a predevelopment potentiometric surface for the Mount Simon aquifer, layer 1 (fig. 15). Although the observed head data are at best an approximation of predevelopment head conditions, they generally represent very early conditions and little effect of groundwater withdrawals.

Visual comparison of computed and observed steady-state potentiometric surfaces for aquifer layers 3 and 4 and for aquifer layer 1 in Minnesota shows that the general characteristics of the observed potentiometric surface are closely represented in the simulated potentiometric surfaces. Relatively large differences occur along the Mississippi River between Wisconsin and Minnesota, and between Iowa and Illinois, and in central Wisconsin, where layer 3 is at or near water-table conditions. To obtain a quantitative measure of the overall fit of the potentiometric surface, the root mean square of the differences between simulated heads and observed heads for nodes within which observed data were available (figs. 13–15) was calculated. These calculations show a root mean square difference of 53 ft for

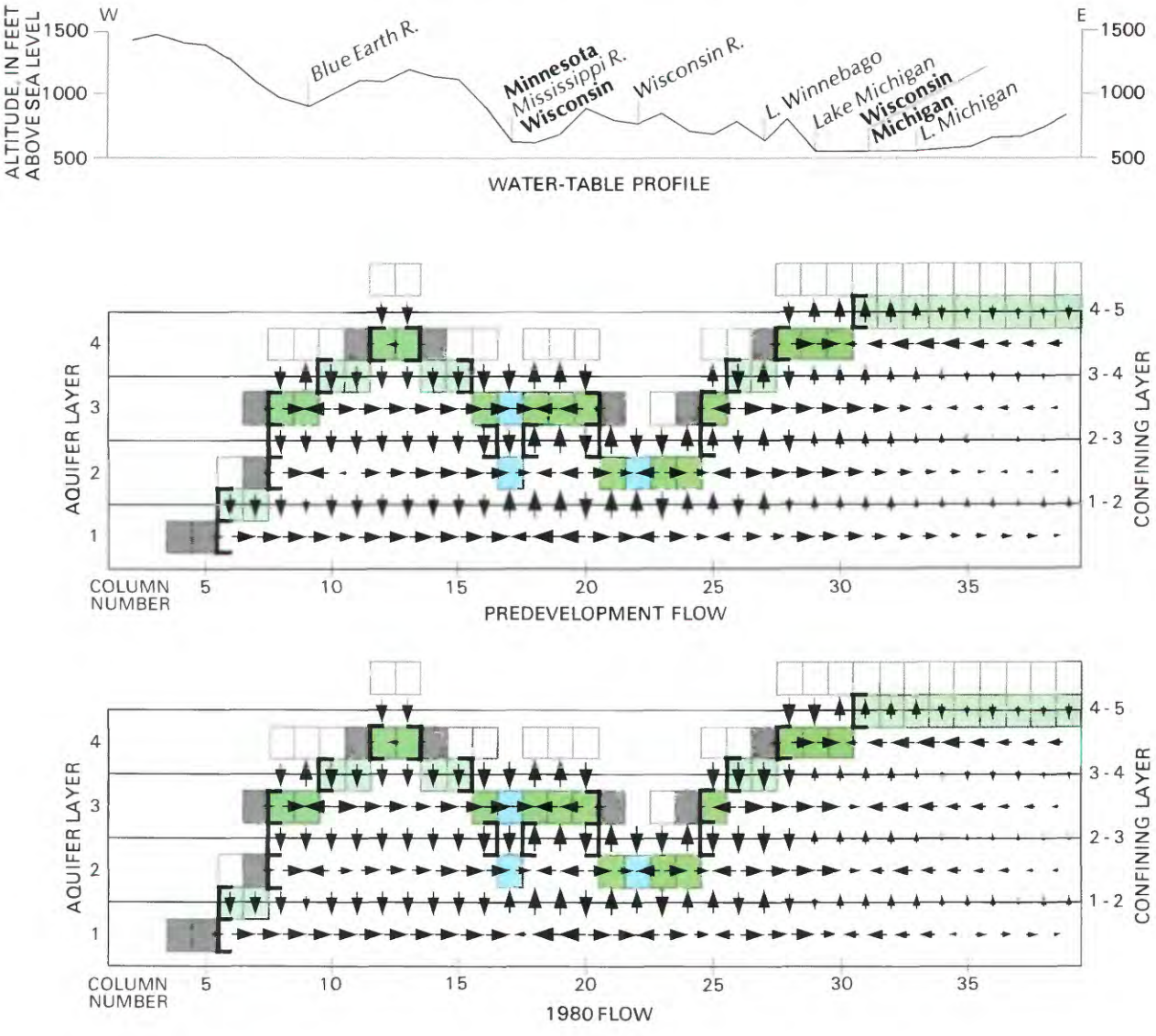

FIGURE 30A.—Simulated direction and magnitude of flow in a vertical section along row 12.

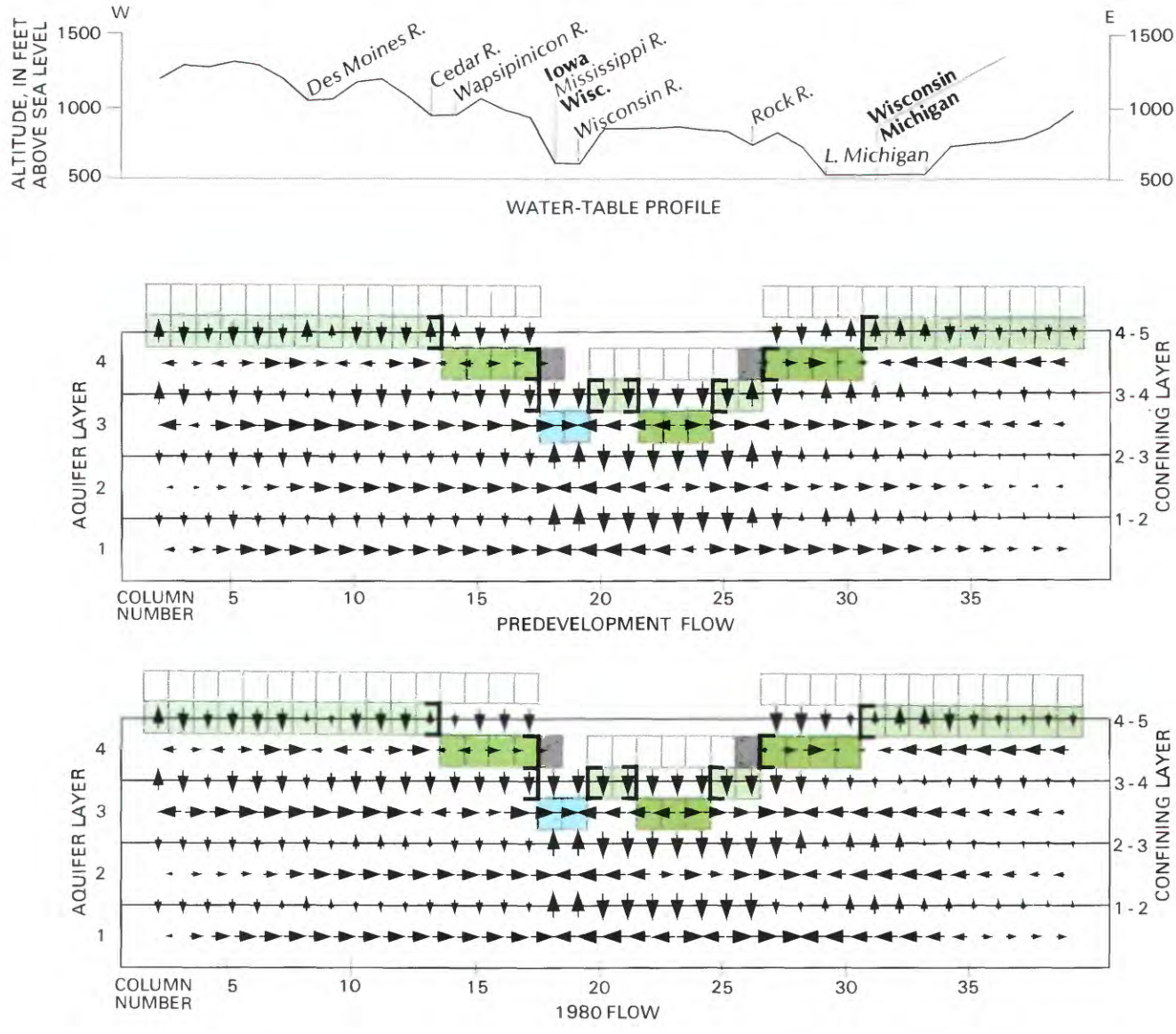

FIGURE 30*B*.—Simulated direction and magnitude of flow in a vertical section along row 16.

aquifer layer 1, 36 ft for aquifer layer 3, and 44 ft for aquifer layer 4. The differences were less than 25 ft for 42, 55, and 40 percent of the nodes containing observed values in aquifer layers 1, 3, and 4, respectively.

In part, these head differences can be attributed to problems inherent in comparing observed point values with computed values that represent the average head over the extent of a large finite-difference block (256 mi^2). Within blocks that are near water-table conditions, the observed heads may vary many tens of feet and the distribution of the observed head may not be sufficient to obtain a meaningful block average. On the other hand, if the observed heads are indicative of predevelopment conditions, the discrepancies between observed and computed heads may represent deficiencies in the steady-state simulation.

STEADY-STATE WATER BUDGET

The model indicates that under predevelopment conditions the bedrock aquifers were recharged either by direct leakage from the overlying water table in the areas covered by glacial drift or Cretaceous rocks, or by leakage through confining units. Conversely, ground water discharged either directly to streams or to the overlying glacial drift, or through confining units to adjacent aquifers. Much of the water that entered the glacial drift from precipitation was lost, either through evapotranspiration or through discharge to streams through local or intermediate flow systems, and only a small part of the infiltrated precipitation recharged the underlying aquifers. These local components of the hydrologic system and ground-water flow within the

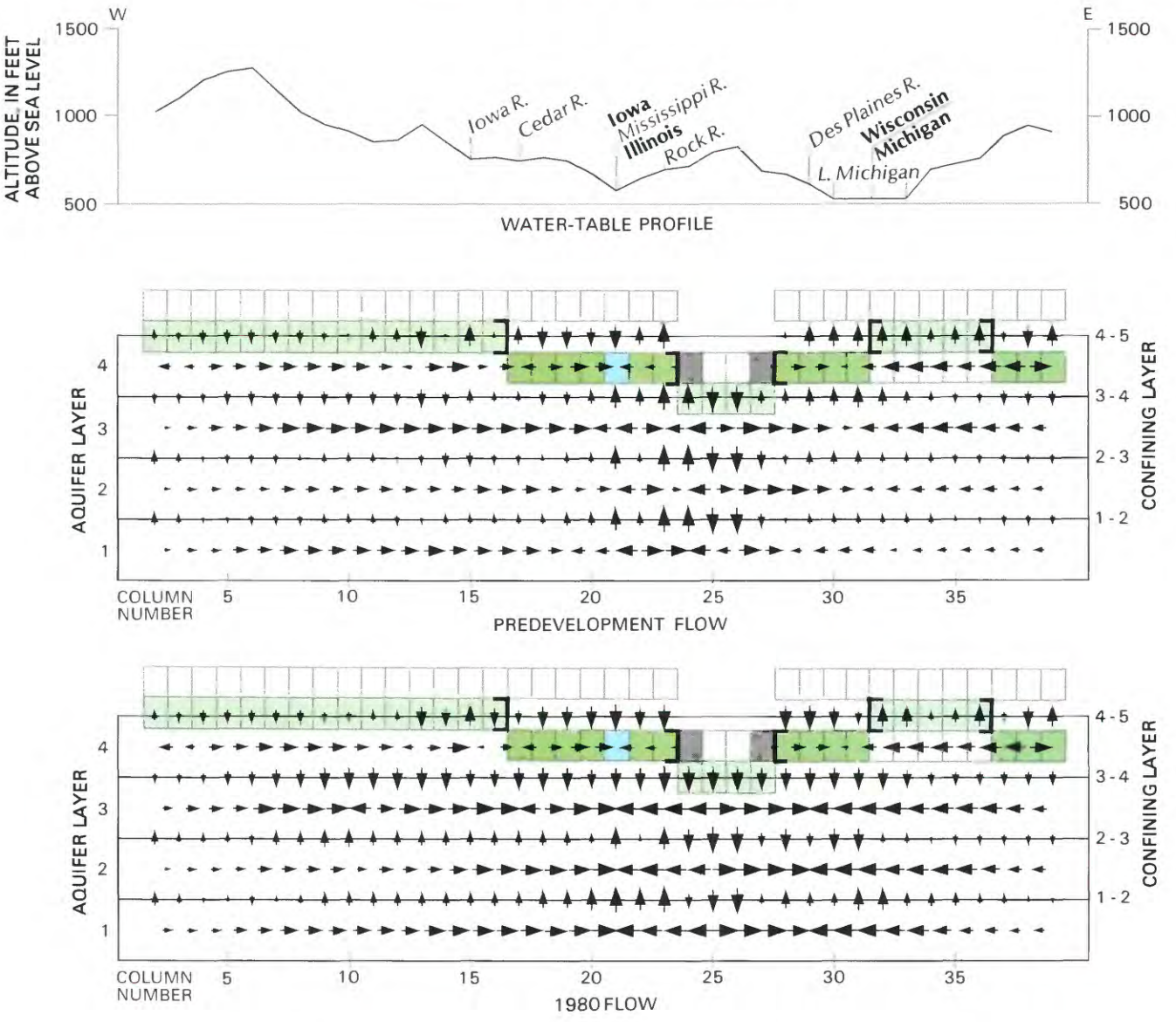

FIGURE 30C.—Simulated direction and magnitude of flow in a vertical section along row 21.

glacial drift were not simulated in the model. However, vertical flow to and from the underlying aquifers was simulated.

Simulated inflow and outflow under steady-state conditions are summarized diagrammatically in figure 31. These values represent the rates of net inflow or outflow for each finite-difference block summed for each aquifer layer. These simulated recharge or discharge rates may be lower than local estimates of inflow or outflow rates because they are averaged over a large finite-difference block.

Steady-state simulation shows that approximately 8, 47, 445, and 42 ft^3/s of direct recharge from the overlying glacial drift or Cretaceous rocks enter aquifer layers 1, 2, 3, and 4, respectively. When related to the area of subcrop of each aquifer layer, these rates are equivalent to 0.03, 0.06, 0.24, and 0.02 in/yr, respectively, for layers 1 through 4. These recharge rates are less than 1 percent of the average annual precipitation rate of about 30 in/yr in those areas. Simulated leakage to the Silurian-Devonian aquifer where it is overlain by rocks of Devonian, Mississippian, and Pennsylvanian age is calculated to be 24 ft^3/s, or 0.003 in/yr. Simulated lateral recharge from the glacial drift and Cretaceous rocks to the St. Peter-Prairie du Chien-Jordan aquifer (layer 3) is slightly more than 5 ft^3/s. Total simulated recharge to the Cambrian-Ordovician aquifer system and the Silurian-Devonian aquifer is 571 ft^3/s.

Much of the simulated recharge from the water table to the Cambrian-Ordovician aquifer system discharges to

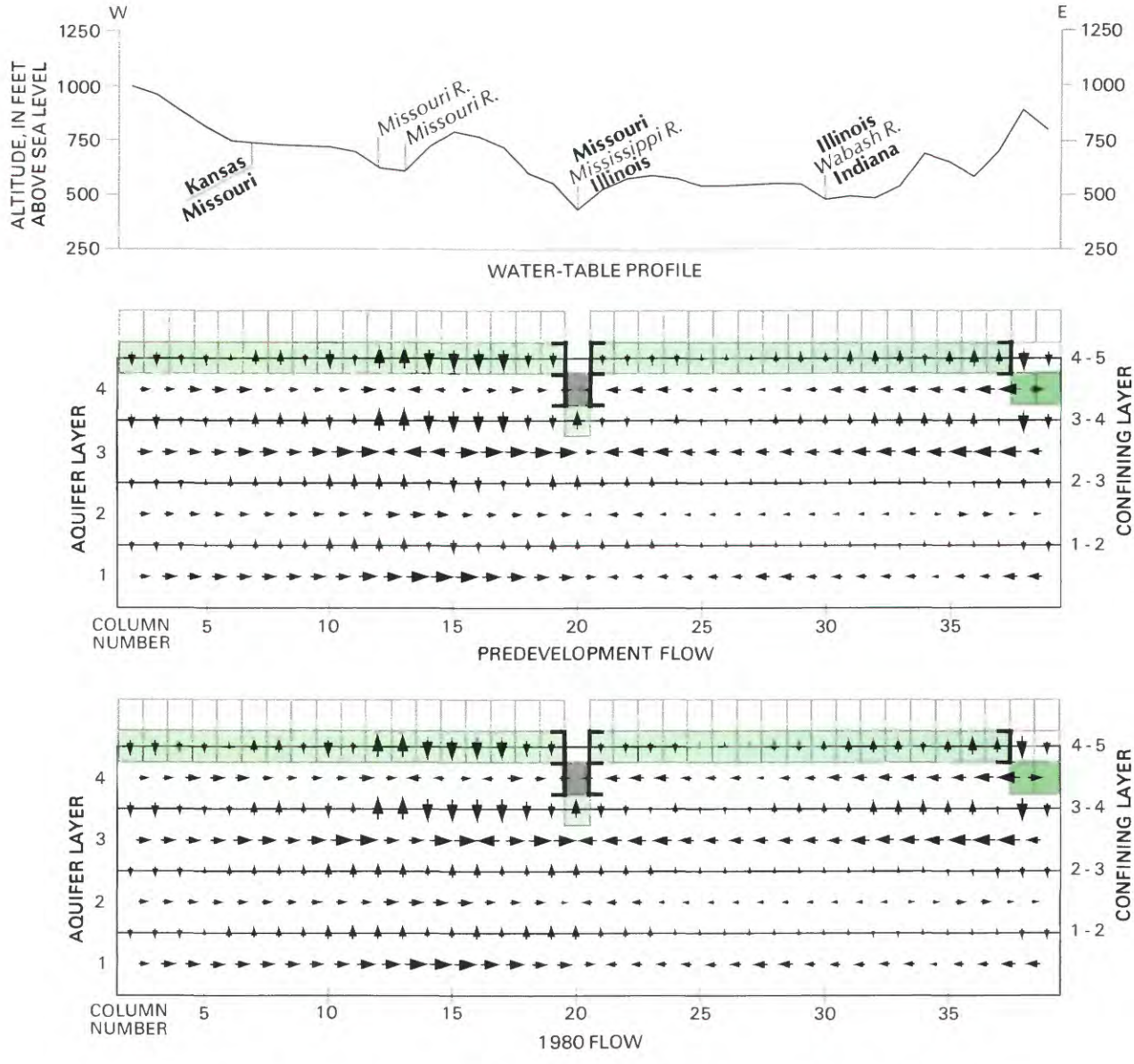

FIGURE 30*D*.—Simulated direction and magnitude of flow in a vertical section along row 33.

intersecting rivers after relatively short flow paths, or to overlying glacial drift and Cretaceous rocks, as depicted in figures 27, 29, and 30. Simulated discharge to overlying rivers and streams is 44, 75, 275, and 30 ft^3/s, or 0.13, 0.12, 0.21, and 0.02 in/yr, from aquifer layers 1 through 4, respectively. Simulated discharge from the Silurian-Devonian aquifer to the overlying younger bedrock units is 37 ft^3/s. Lateral discharge from the aquifer layers is mostly flow to rivers that dissect aquifer layers and are represented by constant-head nodes in the model. This simulated lateral discharge to rivers is 1, 14, and 95 ft^3/s from aquifer layers 1 through 3, respectively. Overall, total simulated discharge from the Cambrian-Ordovician aquifer system and the Silurian-Devonian aquifer, including lateral outflow to the glacial drift along the fringes of the subcrop areas, is 571 ft^3/s. Simulated recharge is at the same rate.

TRANSIENT SIMULATION

The transient simulation period represents the total period of ground-water development, from 1861 to 1980. Development of wells in the Cambrian-Ordovician aquifer system began in the 1860's in the Chicago metropolitan area. Total regional pumpage from the Cambrian-Ordovician aquifer system averaged 684 Mgal/d for the 1976–80 pumping period. As a result, the potentiometric surface in some areas has declined considerably. By 1980, in the heavily stressed Chicago metropolitan area, the composite potentiometric surface in the Cambrian-

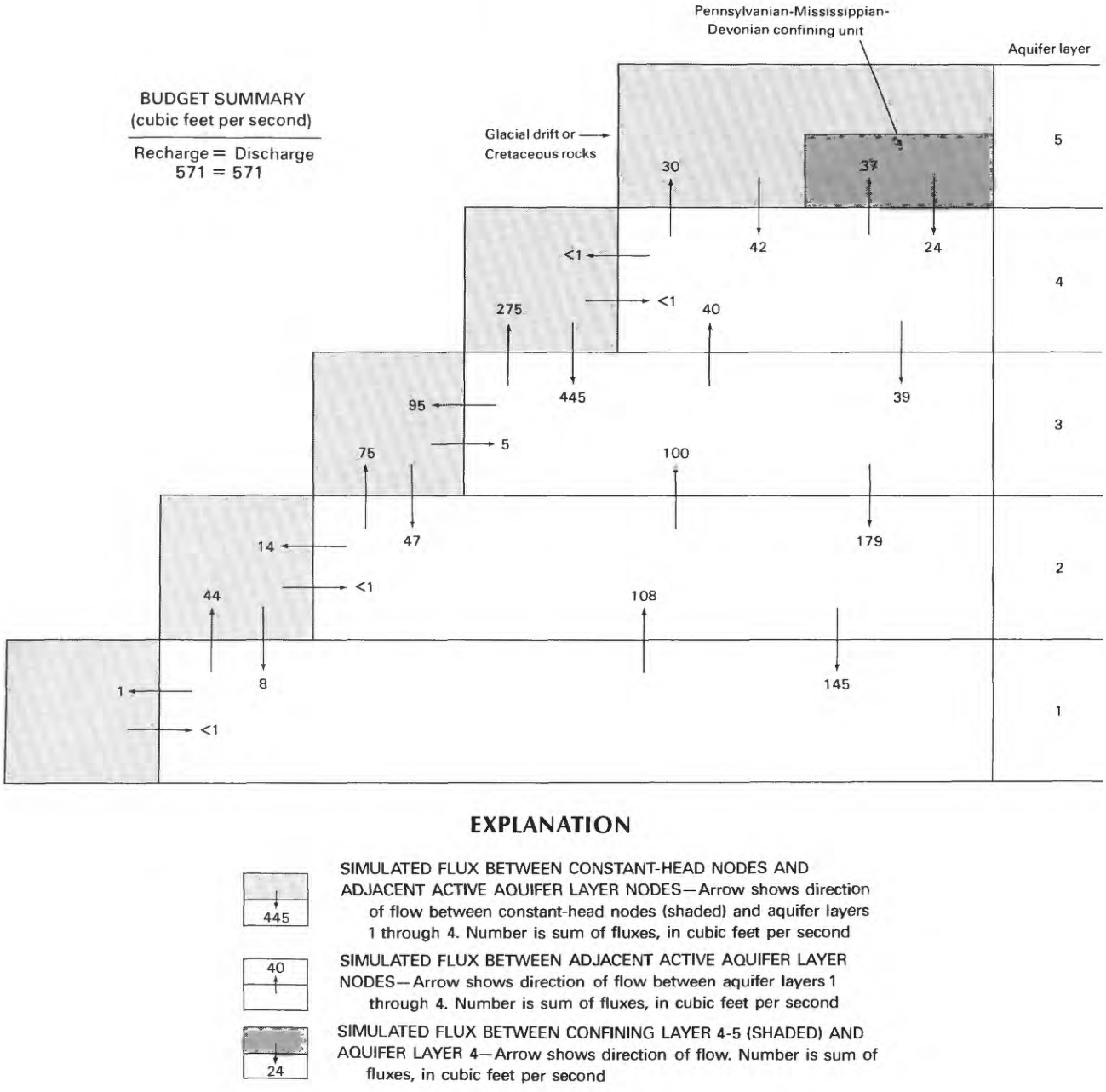

FIGURE 31.—Simulated steady-state regional ground-water budget.

Ordovician aquifer system had declined more than 900 ft since development began (Visocky, 1982). In Minneapolis-St. Paul, Mason City, Quad Cities, Des Moines, central Missouri, Green Bay, and Milwaukee, the decline of the potentiometric surface of some of the Cambrian-Ordovician aquifers ranges from 50 to 400 ft. Twelve pumping periods were used to simulate the 120 years of ground-water development from 1861 to 1980 (fig. 32). The lengths of the pumping periods are variable in order to approximate rates of change of actual pumpage as stepwise averages.

Initially, only hydraulic conductivities were varied to reduce differences between measured head data and both steady-state and transient simulated heads. After a desirable overall head fit was achieved, the initial value of specific storage used to generate the storage coefficients (eq. 37) was increased uniformly to a value of 9×10^{-7} per foot in certain parts of the modeled area. This was done to reduce simulated drawdowns that were somewhat excessive or to reduce the eastward extent of the simulated cone of depression of the Chicago-Milwaukee pumping centers. The effect of this increase

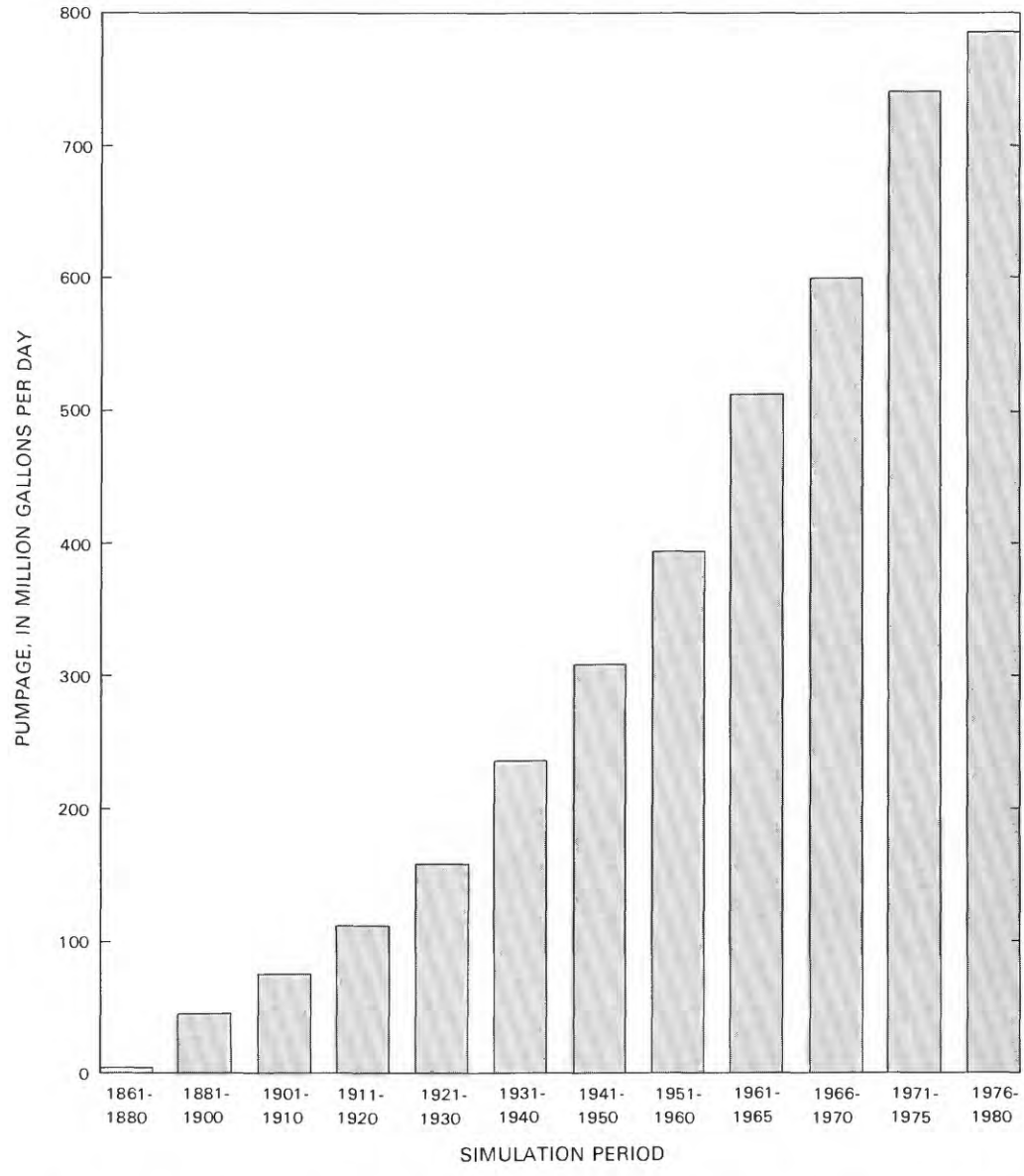

FIGURE 32.—Average ground-water pumpage from the Cambrian-Ordovician aquifer system and the Silurian-Devonian aquifer in the northern Midwest, 1861–1980.

in specific storage was to reduce simulated drawdown at the end of 1980 by, at most, 15 ft. In addition, as a result of pumping in the Chicago area, the simulated head in the St. Peter-Prairie du Chien-Jordan aquifer (layer 3) receded below the top of the layer near the end of the 1971–75 pumping period. Consequently, the Trescott code was modified to test for this condition at the end of each time step. When the condition occurred, the storage coefficient of the node in question was increased by a factor of 100 to change the storage coefficient to a specific yield. This conversion from a confined to an unconfined case occurred in two nodes in the Chicago pumping center.

Results of the transient simulation are shown as maps of freshwater head and drawdown. Simulated freshwater head surfaces for 1980 and the direction of flow between layers are shown in figures 33*A*–33*D*. Drawdown computed for the entire simulation period (1861–1980) is shown in figures 34*A*–34*C*. Simulated drawdown in the Silurian-Devonian aquifer (layer 4) is not shown because, except for a few nodes, drawdown is less than 50 ft.

Transient simulation results show the development of large depressions in the potentiometric surface in northeastern Illinois, northwestern Indiana, eastern Wisconsin, central Iowa, east-central Iowa, and central Missouri. This is in response to large-scale pumping,

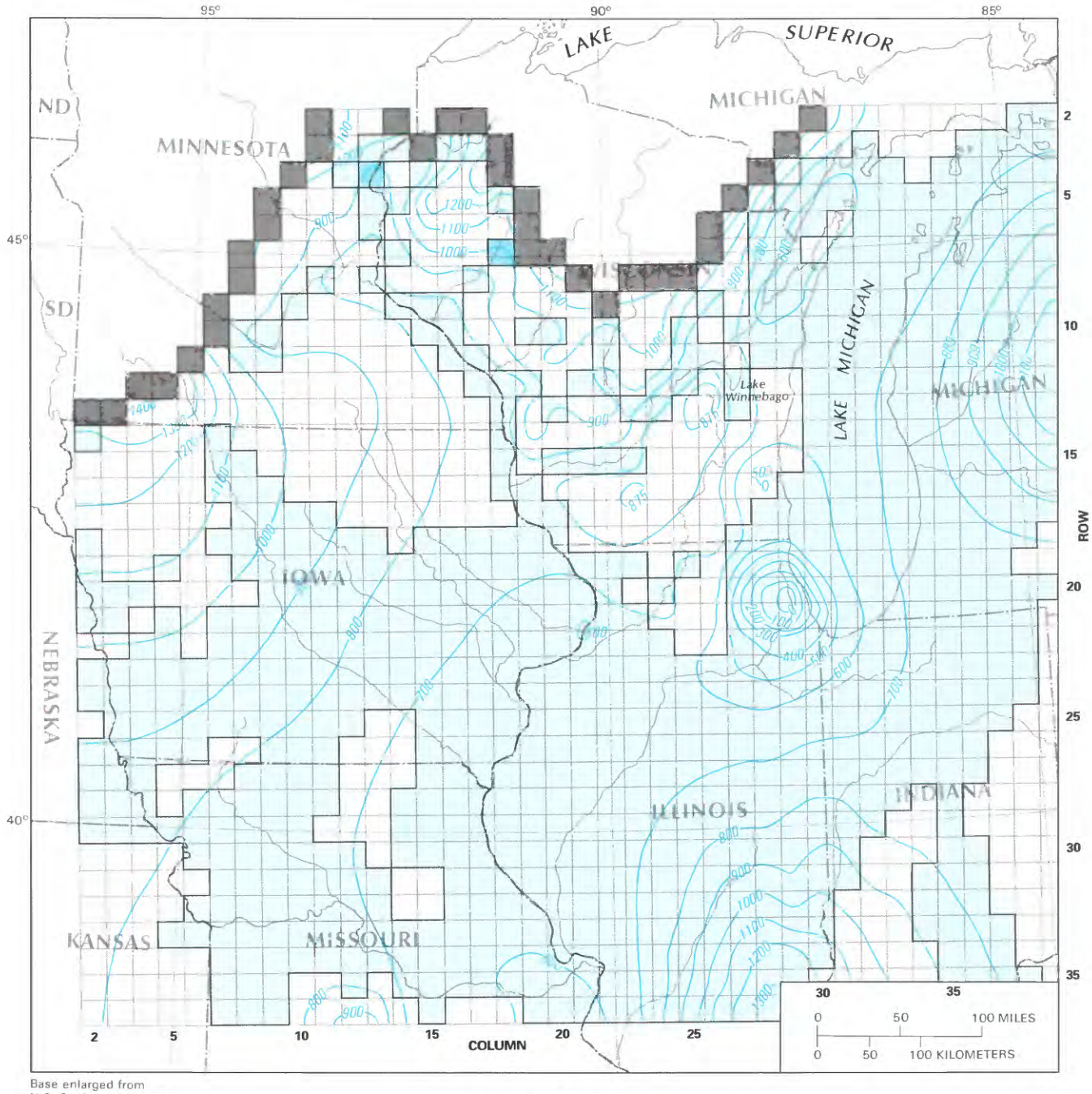

EXPLANATION

—700— POTENTIOMETRIC CONTOUR—Shows simulated 1980 freshwater head in the Mount Simon aquifer (layer 1). Contour interval 100 feet. Datum is sea level

MODEL CONSTANT-HEAD NODE DEPICTING

Aquifer layer boundary

Aquifer layer dissected by major river valley

DIRECTION OF VERTICAL FLOW THROUGH THE TOP OF THE AQUIFER

Upward

Downward

FIGURE 33A.—Simulated 1980 freshwater head in the Mount Simon aquifer (layer 1).

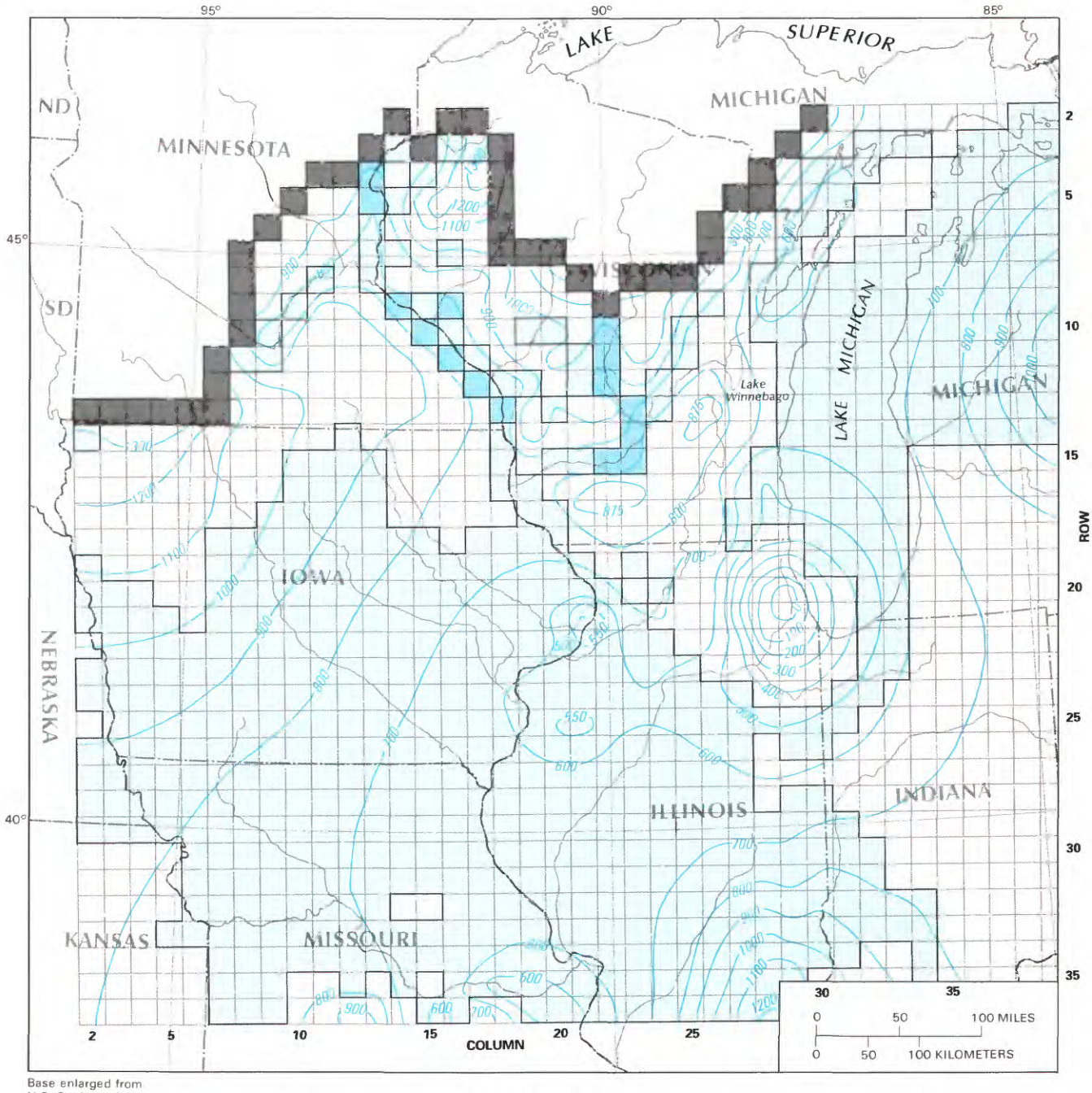

EXPLANATION

—700— POTENTIOMETRIC CONTOUR—Shows simulated 1980 freshwater head in the Ironton-Galesville aquifer (layer 2). Contour interval, in feet, is variable. Datum is sea level

MODEL CONSTANT-HEAD NODE DEPICTING

Aquifer layer boundary

Aquifer layer dissected by major river valley

DIRECTION OF VERTICAL FLOW THROUGH THE TOP OF THE AQUIFER

Upward

Downward

FIGURE 33*B*.—Simulated 1980 freshwater head in the Ironton-Galesville aquifer (layer 2).

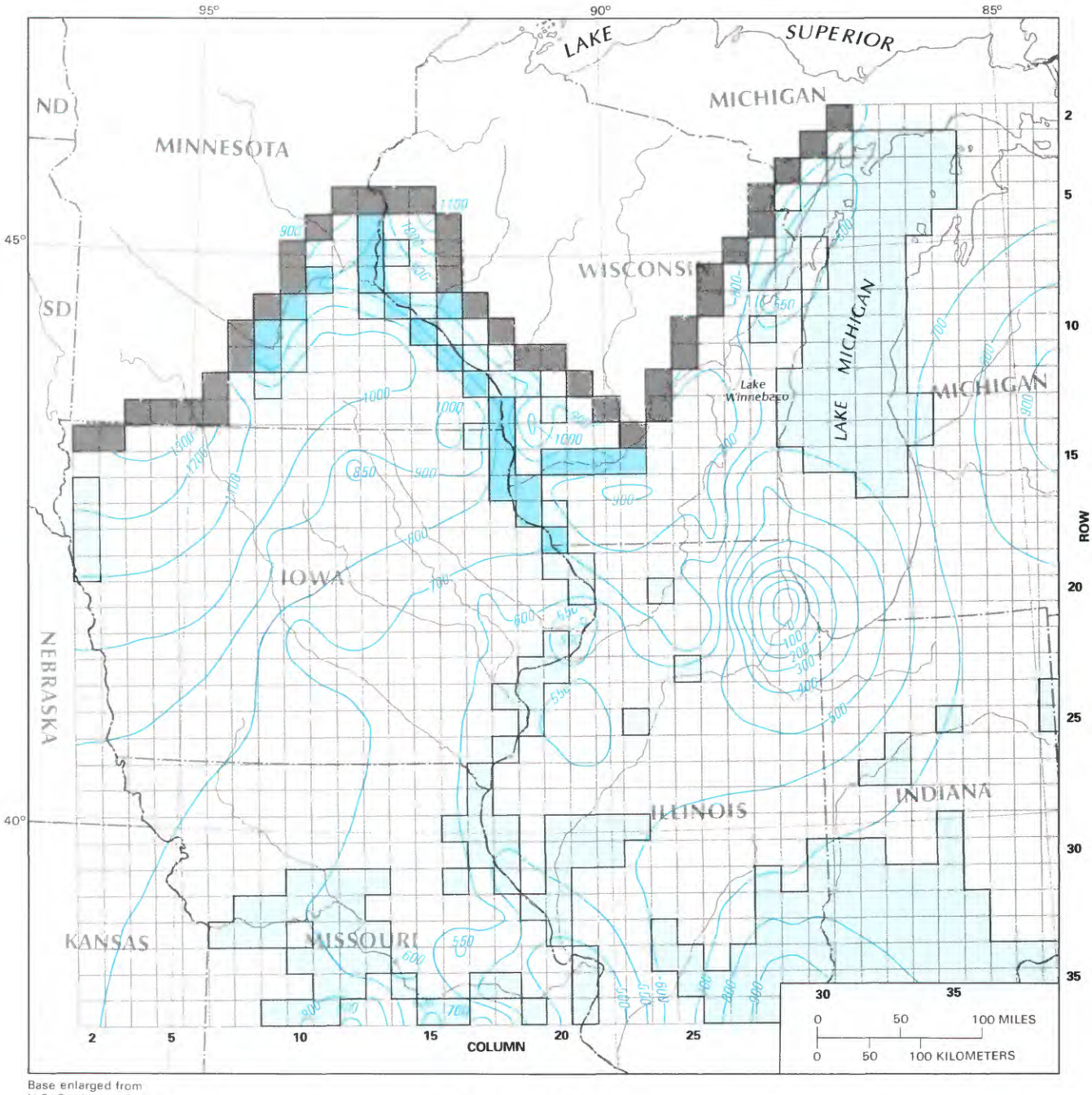

Base enlarged from U.S. Geological Survey 1:7,500,000, 1970

EXPLANATION

—700— POTENTIOMETRIC CONTOUR—Shows simulated 1980 freshwater head in the St. Peter-Prairie du Chien-Jordan aquifer (layer 3). Contour interval, in feet, is variable. Datum is sea level

MODEL CONSTANT-HEAD NODE DEPICTING

Aquifer layer boundary

Aquifer layer dissected by major river valley

DIRECTION OF VERTICAL FLOW THROUGH THE TOP OF THE AQUIFER

Upward

Downward

FIGURE 33C.—Simulated 1980 freshwater head in the St. Peter-Prairie du Chien-Jordan aquifer (layer 3).

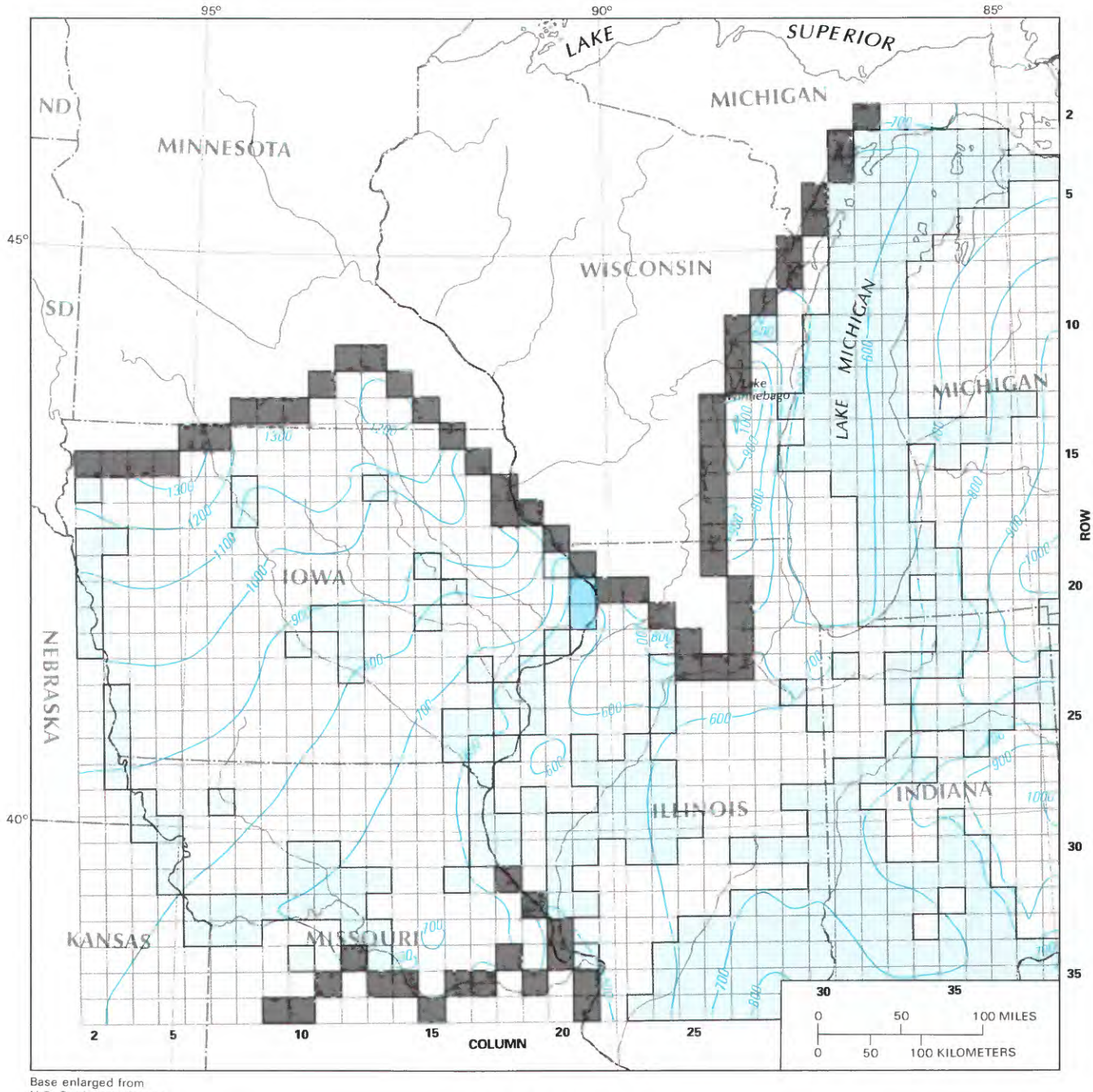

EXPLANATION

—700— POTENTIOMETRIC CONTOUR—Shows simulated 1980 freshwater head in the Silurian-Devonian aquifer (layer 4). Contour interval 100 feet. Datum is sea level

MODEL CONSTANT-HEAD NODE DEPICTING

Aquifer layer boundary

Aquifer layer dissected by major river valley

DIRECTION OF VERTICAL FLOW THROUGH THE TOP OF THE AQUIFER

Upward

Downward

FIGURE 33*D*.—Simulated 1980 freshwater head in the Silurian-Devonian aquifer (layer 4).

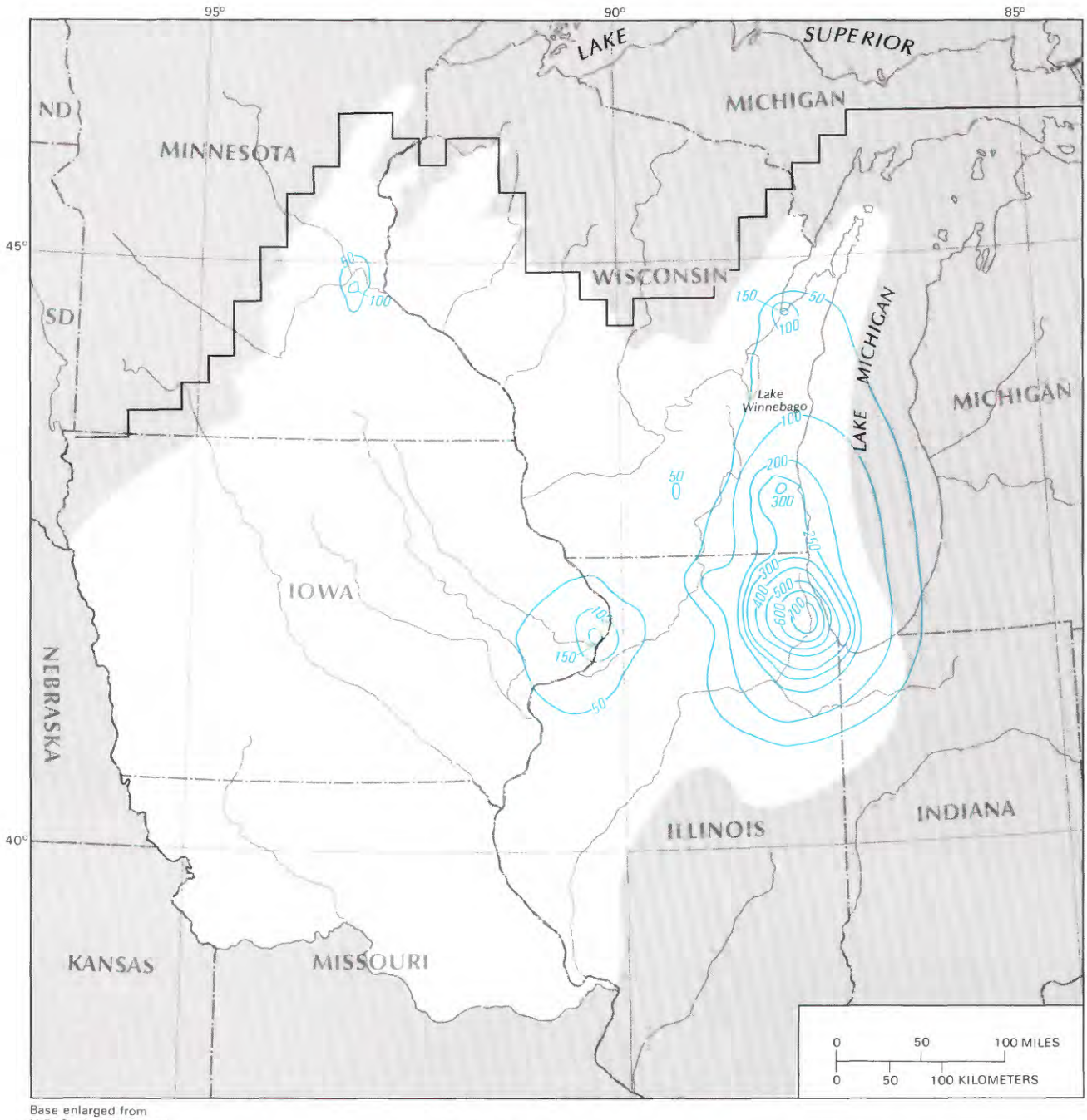

Base enlarged from U.S. Geological Survey 1:7,500,000, 1970

EXPLANATION

—100— LINE OF EQUAL FRESHWATER HEAD DECLINE IN THE MOUNT SIMON AQUIFER (LAYER 1), 1861-1980—Interval, in feet, is variable

MODELED LAYER BOUNDARY

FIGURE 34*A*.—Simulated decline in freshwater head, 1861 to 1980, in the Mount Simon aquifer (layer 1).

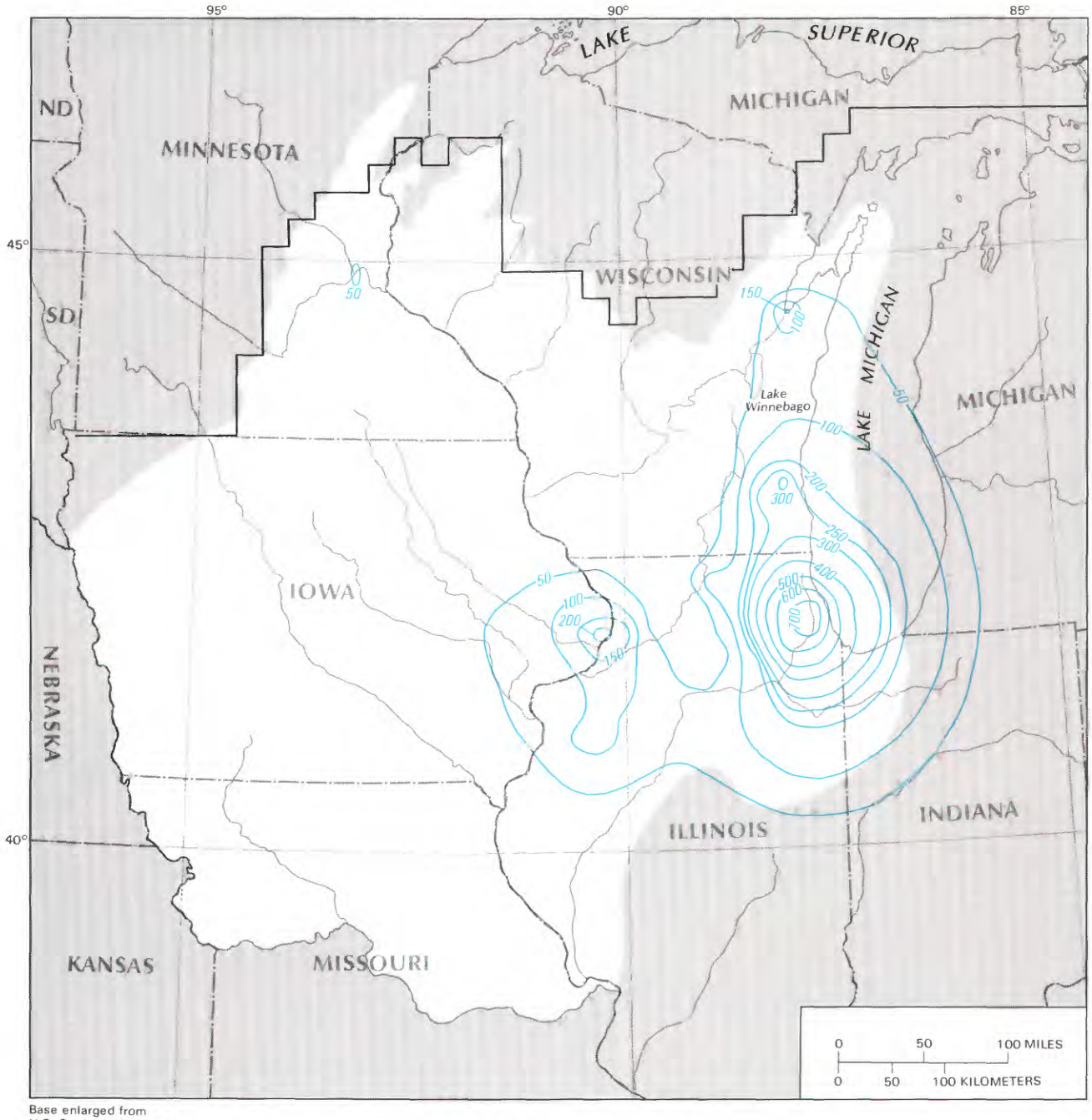

FIGURE 34*B*.—Simulated decline in freshwater head, 1861 to 1980, in the Ironton-Galesville aquifer (layer 2).

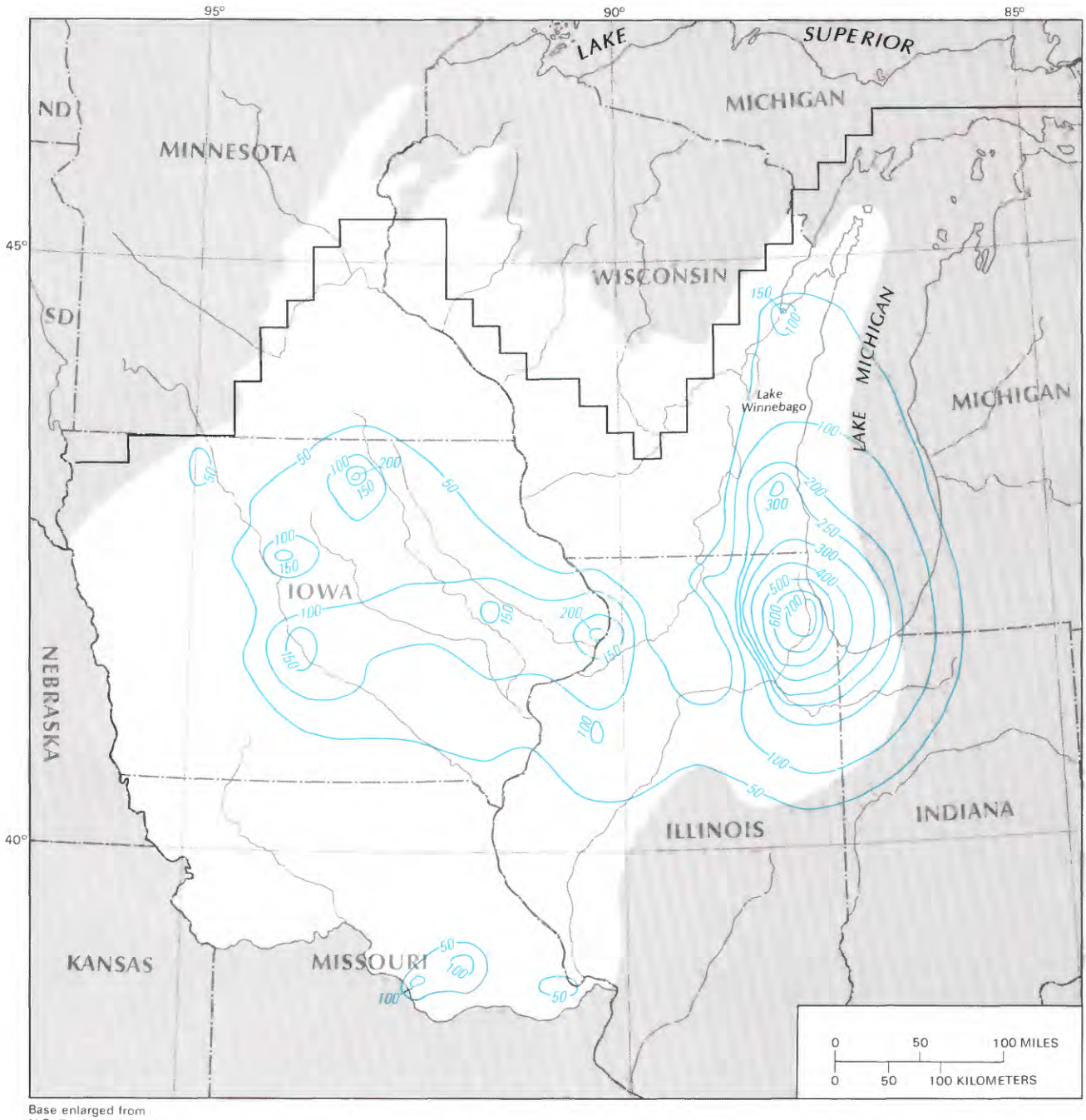

Base enlarged from U.S. Geological Survey 1:7,500,000, 1970

EXPLANATION

—100— LINE OF EQUAL FRESHWATER HEAD DECLINE IN THE ST. PETER-PRAIRIE DU CHIEN-JORDAN AQUIFER (LAYER 3), 1861-1980— Interval, in feet, is variable

MODELED LAYER BOUNDARY

FIGURE 34*C*.—Simulated decline in freshwater head, 1861 to 1980, in the St. Peter-Prairie du Chien-Jordan aquifer (layer 3).

especially near Chicago, where the potentiometric surface has declined to below sea level (figs. 33*A*–33*C*). The simulated drawdown (figs. 34*A*–34*C*) in 1980 illustrates that the Cambrian-Ordovician aquifers form a regionally continuous aquifer system. Large-scale pumping in an aquifer system that is tightly confined over much of its areal extent results in a series of coalescing drawdown cones, and this in turn imposes drawdown on all nearby pumping centers. This is especially evident in the St. Peter-Prairie du Chien-Jordan aquifer (layer 3). Several steep-sided drawdown cones in Iowa merge to form one broad cone that covers most of the State. In this tightly confined aquifer, the resultant source of ground-water pumpage is mainly storage in the aquifer.

Pumping from wells that are open to more than one aquifer results in drawdown patterns and potentiometric surfaces that are very similar for each aquifer. This is evident in figures 33 and 34. In the Chicago and Milwaukee areas, numerous multiaquifer wells pump water from the Mount Simon, Ironton-Galesville, and St. Peter-Prairie du Chien-Jordan aquifers (layers 1, 2, and 3). This is also the case in eastern Iowa and western Illinois, where wells are open primarily to aquifer layers 2 and 3. Throughout the rest of Iowa and Missouri, wells are open primarily to aquifer layer 3, and only a few wells are open to aquifer layers 2 and 4. In this case, most drawdown is restricted to aquifer layer 3.

Throughout central Wisconsin, north-central Illinois, extreme northeastern Iowa, and central Minnesota, in places where the Maquoketa Shale is absent, simulated drawdown in the Cambrian-Ordovician aquifer system is minimal (less than 50 ft) and of small areal extent. Individual aquifers in the aquifer system in these areas function as either unconfined or semiconfined aquifers. Pumping rates are relatively small and local recharge is sufficient to meet these demands.

In southeastern Wisconsin and northeastern Illinois, a deep drawdown cone extends from north of Milwaukee to the south beyond the major Chicago pumping areas. West of the north-south axis of this elongate cone, at or very near the edge of the Maquoketa Shale, the drawdown cone is very steep. This steep hydraulic gradient is due to the higher water table and leakage rate in the area west of the outer edge of the Maquoketa Shale, which is mainly a recharge area. Where the Maquoketa Shale is missing, the Maquoketa confining unit consists of weathered carbonates of the Galena Dolomite and the Decorah and Platteville Formations. Thus, ground water readily recharges the underlying St. Peter-Prairie du Chien-Jordan aquifer (layer 3). The eastern part of the drawdown cone is less steep, a typical effect of a recharge boundary on a well-confined aquifer. The zero-flux boundary to the east is placed well beyond the influence of pumping, and no boundary effects are evident from this direction. The simulation indicates, therefore, that the aquifer system is tightly confined and laterally extensive in this direction.

Simulated regional decline in head is smaller in aquifer layers 1 and 2 than in aquifer layer 3 because the latter is developed over a larger area. The drawdown cones mark the major areas of withdrawal from each aquifer. The simulated drawdown cones for aquifer layers 1 and 2 also are similar to those for aquifer layer 3, but are shallower and less extensive.

The extent to which predevelopment flow patterns between aquifers have been disrupted by pumping is shown by a comparison of simulated 1980 vertical flow patterns (figs. 33*A*–33*D*) with those from the steady-state simulation (figs. 26*A*–26*D*). Drawdown resulting from pumping has reversed the direction of vertical flow between aquifer layers in some areas. Only minimal change in the direction of flow between aquifer layers 1 and 2 is indicated, mainly in Wisconsin, north-central Iowa, and northeastern Illinois. The simulated changes in direction of flow between aquifer layer 2 and 3 are more extensive. Because of the large amount of pumping in northeastern Illinois, heads in aquifer layer 2 also declined. Ground water that would discharge to overlying aquifers under steady-state conditions is captured by the pumping centers of northeastern Illinois and southeastern Wisconsin. In Iowa, because of the drawdown in aquifer layer 3, the heads in aquifer layer 2 are now higher than in aquifer layer 3. This is shown in the simulation as a large area of upward leakage from aquifer layer 2 to 3 (fig. 33*B*). A similar reversal occurs in central Missouri. The most notable simulated head changes between aquifer layers 3 and 4 (fig. 33*C*) and between aquifer layers 4 and 5 (fig. 33*D*) are in the Chicago-Milwaukee area and eastern Iowa, where extensive drawdown has reversed the direction of flow. In both cases, the direction of predevelopment ground-water flow was upward, from aquifer layer 3 to 4 and from aquifer layer 4 to 5, to Lake Michigan and the Mississippi River. With the increase in pumping, simulated ground-water flow is reversed and leakage is now induced from aquifer layer 5 to 4 and from aquifer layer 4 to 3.

Changes in the regional flow system because of ground-water development are shown by the hydrologic cross sections of simulated steady-state and transient flow along columns and rows (figs. 26*A*, 29, and 30). The components of flow along column 12 (fig. 29*A*), which extends from Minnesota to Missouri, show that simulated discharge to the Mississippi River in the Twin Cities area ceased. This is because pumping has reversed the heads and has induced downward leakage to the aquifers. Throughout Iowa, simulated ground-water flow to the Ironton-Galesville aquifer (layer 2) from the St. Peter-Prairie du Chien-Jordan aquifer (layer 3) has

reversed because of the decline in head in the St. Peter-Prairie du Chien-Jordan aquifer. The north-south component of lateral flow within aquifer layer 3 is no longer southerly over all of Iowa. Components of lateral flow are now toward pumping centers near the Des Moines River and to the north near the Iowa-Minnesota State line. The section along column 28 (fig. 29*B*) through eastern Wisconsin and Illinois includes areas of extensive ground-water pumping. Simulated head declines in aquifer layers 2, 3, and 4 have resulted in a large downward component of flow from the glacial drift or Cretaceous rocks to aquifer layers 4 and 3. A large increase in the lateral flow component to the Chicago and Milwaukee areas is shown by the large vectors and reversed direction of flow.

The section along row 12 (fig. 30*A*) shows that simulated head declines in the vicinity of Lake Winnebago in eastern Wisconsin induce downward leakage from the water-table aquifer and the lake to the Cambrian-Ordovician aquifer system and that upward discharge to Lake Michigan is reduced. Over much of the remaining area where the Cambrian-Ordovician aquifer system is unconfined or semiconfined, change in flow direction and magnitude is negligible. Row 16 (fig. 30*B*) extends across north-central Iowa through southeastern Wisconsin. Ground-water pumping in aquifer layer 3 near the Cedar River has resulted in the capture of ground water that previously would have flowed toward the Mississippi River. General ground-water movement from recharge areas in south-central Wisconsin was toward the Mississippi, Wisconsin, and Rock Rivers under steady-state conditions. The transient simulation shows that flow is reversed to the east beneath the Rock River in aquifer layers 2 and 3. Water-level records from 1946 to the present indicate that ground water moves toward the Rock River from both sides, and there is no evidence that water levels in the Rock River basin have declined in response to the heavy pumping in the Chicago and Milwaukee areas. This discrepancy between simulated and actual conditions illustrates the limitation of the 16-mi node spacing in the regional model to depict all small-scale flow patterns.

The section along row 21 (fig. 30*C*) extends from west-central Iowa through the Chicago metropolitan area. Under steady-state conditions the direction of ground-water movement is from western Iowa toward the Mississippi River. In Iowa, the transient simulation shows an increase in leakage from aquifer layer 4 to aquifer layer 3 because of head declines in aquifer layer 3; thus the direction of leakage is reversed and now is from aquifer layer 2 to aquifer layer 3. The lateral westward flow in aquifer layer 3 to pumping centers in west and east-central Iowa is a reversal. Pumping of ground water in the Quad Cities area of Iowa and Illinois has resulted in a capture of ground water that would discharge to the Mississippi and Rock Rivers under steady-state conditions and has increased lateral flow from adjacent areas. Lateral ground-water flow toward the Chicago metropolitan area has increased, and the upward ground-water flow beneath parts of Lake Michigan now is reversed.

The section along row 33 (fig. 30*D*) passes near pumping centers in northeastern Missouri, north of the Missouri River. The simulation shows that pumping, primarily from aquifer layer 3, has induced a reversal of the former flow toward the Missouri River in aquifer layer 3 and a reversal of the previous downward flow from aquifer layer 3 to 2.

Calibration

During the transient calibration process, simulated heads were compared with hydrographs for wells that have long periods of measurement. For those cases where wells were open to more than a single aquifer, the composite model head was computed using equation 25. Figures 35*A*–35*D* show a comparison of measured and simulated heads for a representative set of nodes in areas of extensive ground-water development in northeastern Illinois, southeastern Wisconsin, and selected areas in Iowa. The hydrographs show simulated heads for a particular aquifer layer or composite heads for a combination of aquifer layers, as well as all of the available measured heads for wells penetrating a single aquifer or several aquifers. For the sake of clarity, only one simulated layer combination per node is shown. In most cases, the chosen simulated composite head is similar to the composite head for other layer combinations within the node. All the measured heads for all existing layer combinations are included to indicate the large range in measured heads that can occur within a given node. This range may not include the actual maximum and minimum head within a node because the measured wells may not be in areas where the maximum and minimum heads can be observed. In extreme cases, this range may be more than 200 to 300 ft because of the steepness of the hydraulic gradient over the large area of the nodes.

The agreement between observed and simulated composite heads in figures 35*A*–35*D* is generally good. For about half of the comparisons, the simulated heads were near the majority of the measured heads for a given node. Trends in simulated head decline are similar to trends in measured water-level decline. As a result, the amount of simulated drawdown is relatively close to the measured drawdown. Differences between simulated and measured hydraulic heads may be due to errors in estimating hydraulic properties of the different aquifer and confining units or because the particular transient water-level measurements available do not represent the

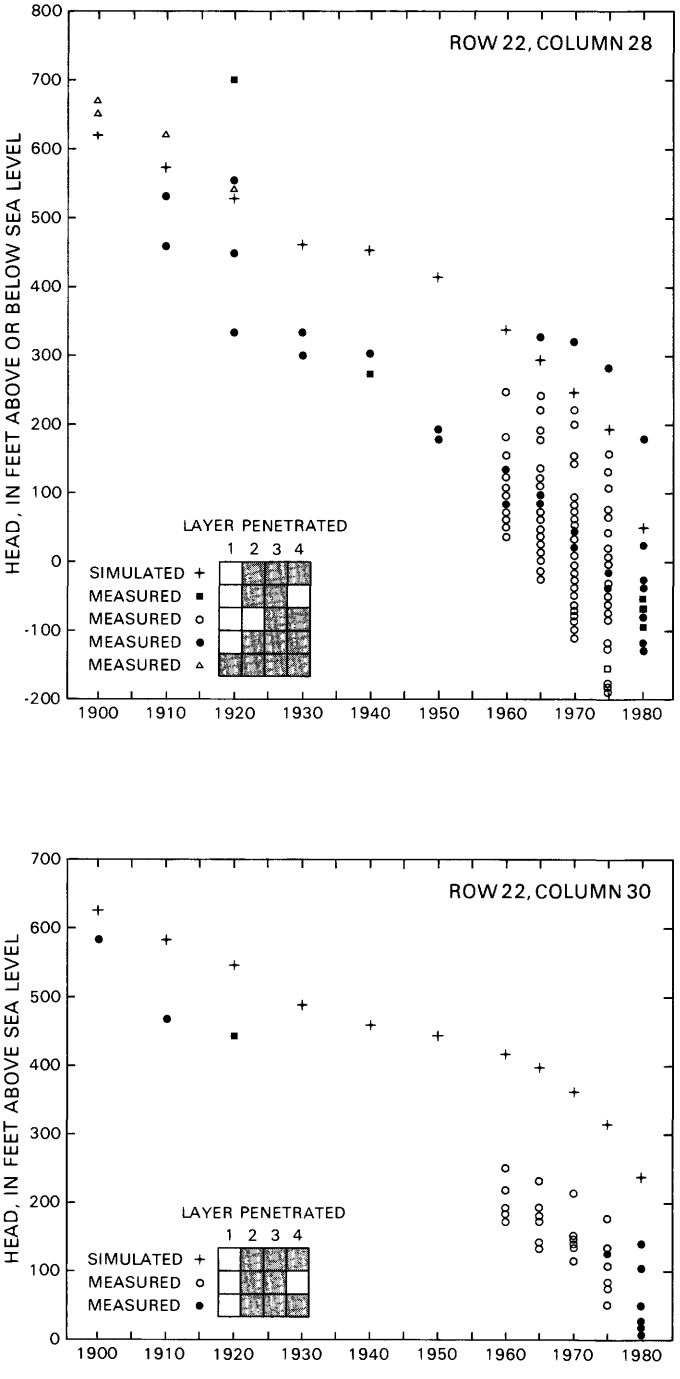

FIGURE 35A.—Comparison of simulated and measured head in northeastern Illinois.

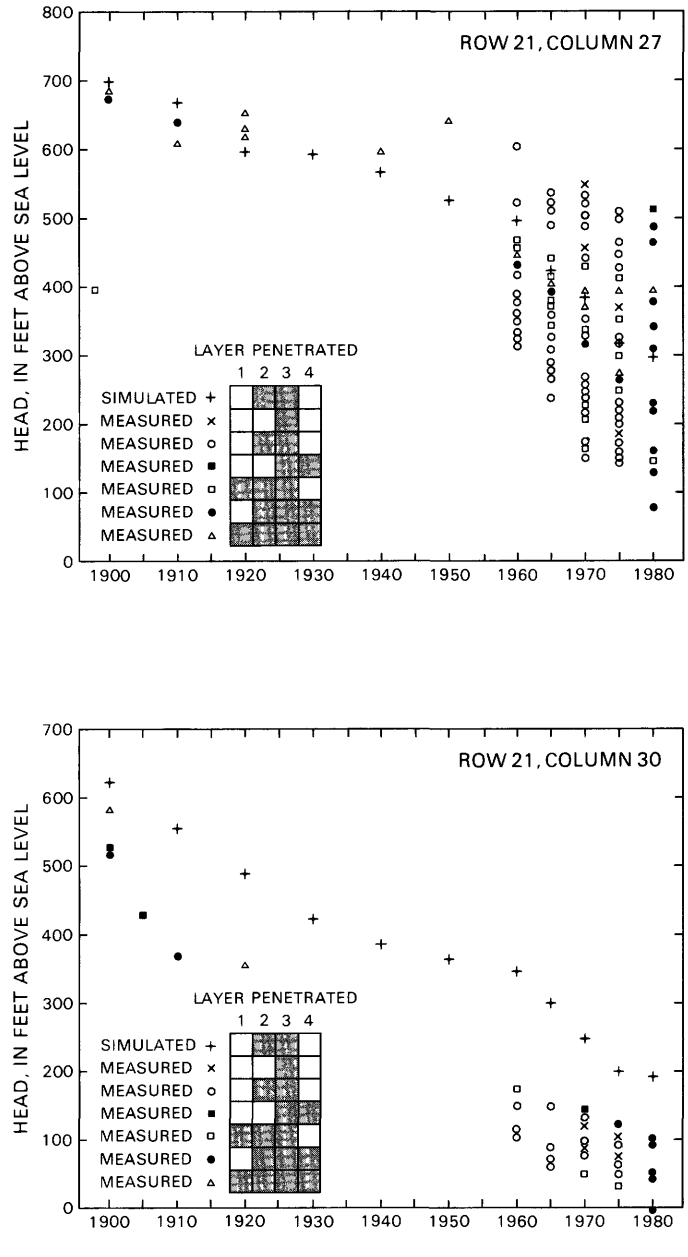

FIGURE 35A—Continued.

complete range of heads within that node during a given time period. Additionally, if measured water levels were obtained from or near pumping wells, the measured water-level declines would be greater than the average water-level decline over the area of a 256-mi^2 node.

To make an areal determination of the validity of the simulated heads, a 1980 potentiometric surface for aquifer layer 3 was constructed (fig. 36) using measured head data for wells open only to the St. Peter Sandstone, Prairie du Chien Group, or Jordan Sandstone in Minnesota, Iowa, and Missouri. In Wisconsin and Illinois, there are few wells open only to aquifer layer 3; therefore, wells penetrating aquifer layer 3 but open to other aquifer layers were also used. In general, the regional characteristics of the observed potentiometric surface are replicated in the simulated potentiometric surface of 1980 (comparing fig. 33*C* with fig. 36).

The root mean square of the differences between the simulated and observed heads for nodes within which

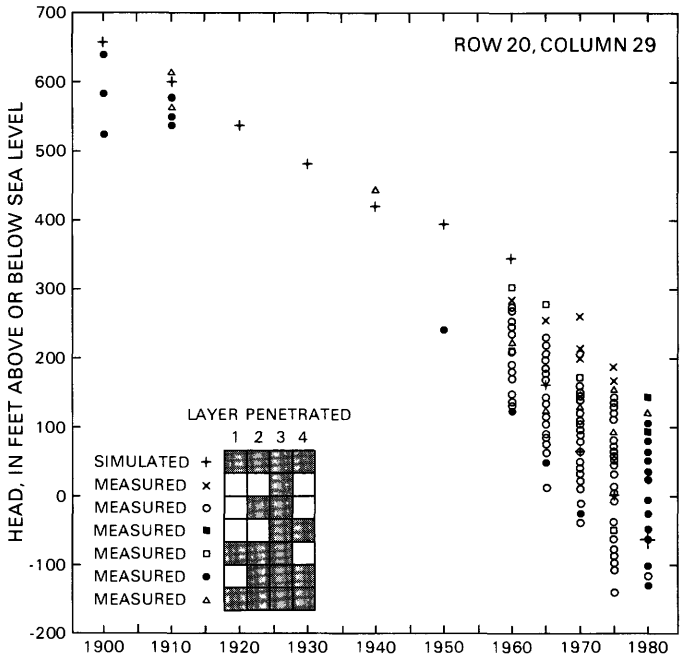

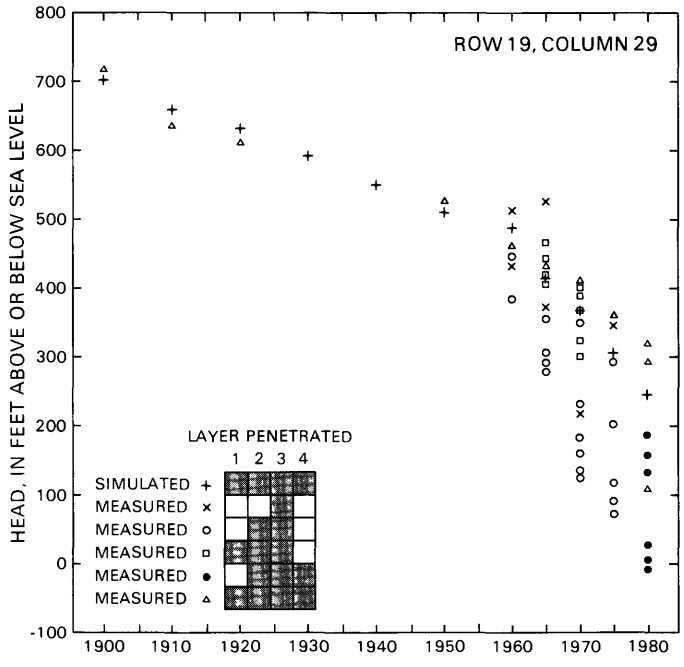

FIGURE 35*A*—Continued.

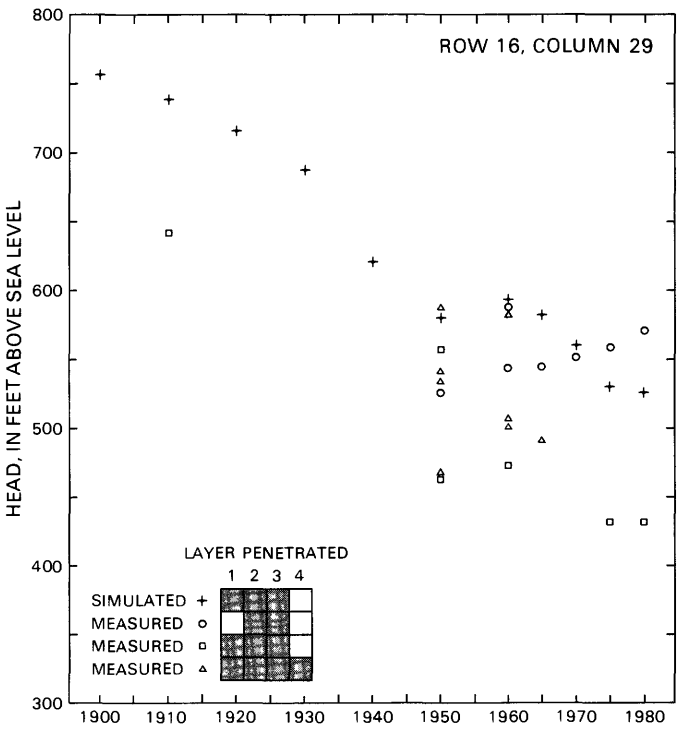

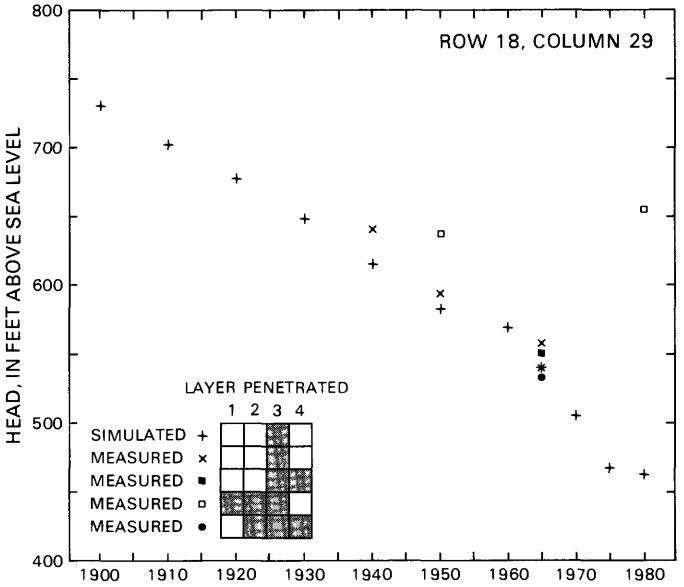

FIGURE 35*B*.—Comparison of simulated and measured head in southeastern Wisconsin.

observed heads were available is 63 ft. Of these nodes, 40 percent had differences of 25 ft or less. The largest difference between the two potentiometric surfaces is along the Mississippi River from east-central Iowa to northeastern Missouri, where simulated heads are higher than observed heads. This area also has the largest differences in the steady-state simulation. The first wells completed in the Cambrian-Ordovician aquifer system along the river in the late 1800's commonly flowed unchecked and discharged large quantities of ground water. The rates at which these wells flowed were not recorded. Many of the wells eventually stopped

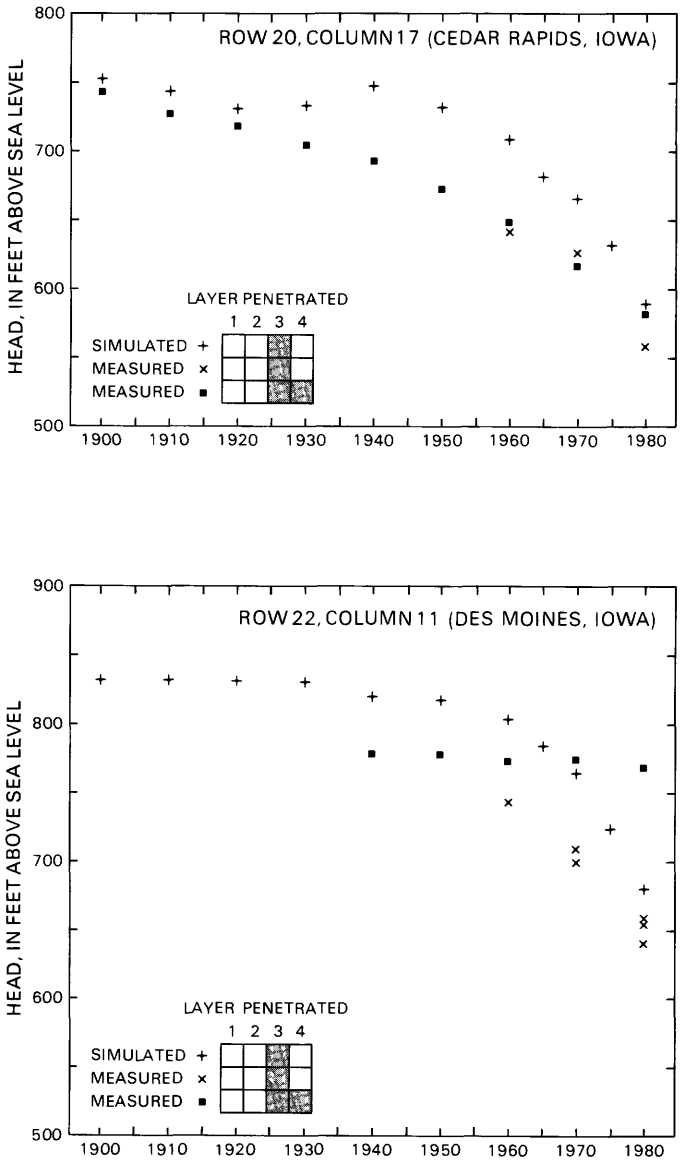

FIGURE 35*C*.—Comparison of simulated and measured head at Cedar Rapids and Des Moines, Iowa.

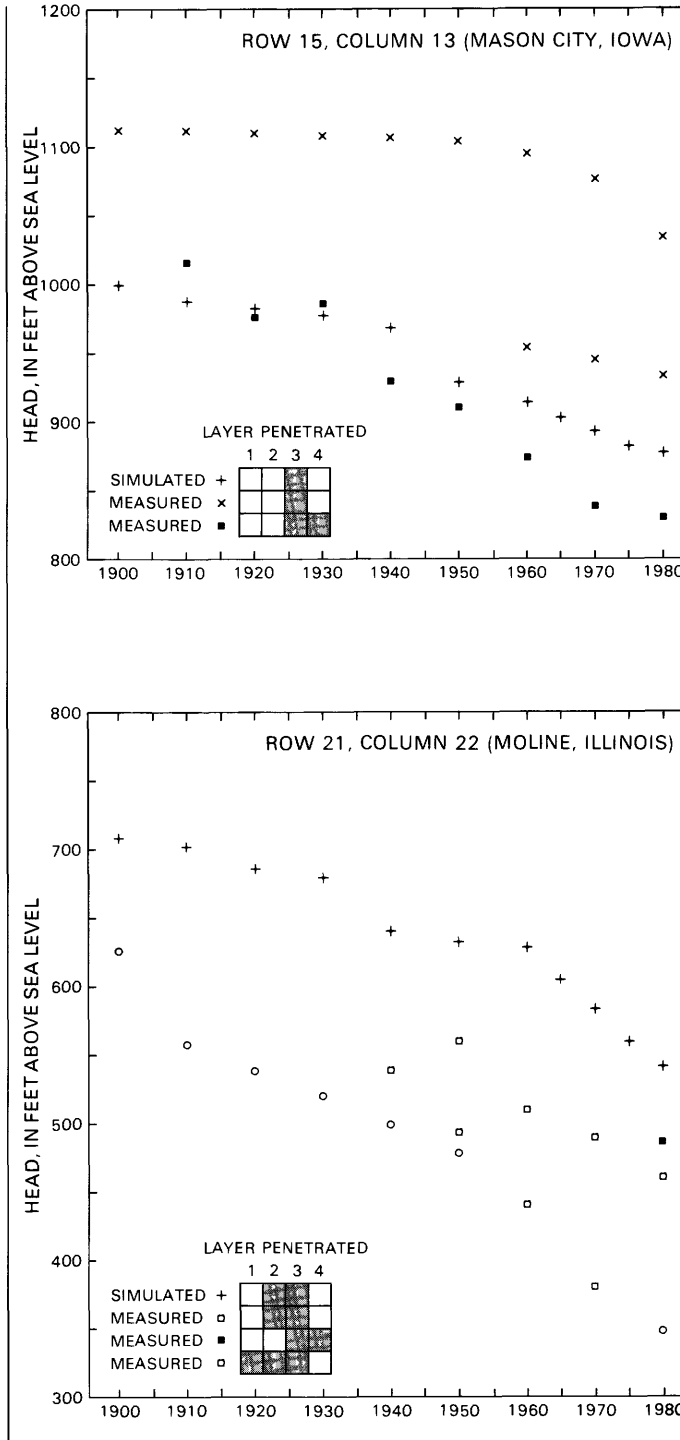

FIGURE 35*D*.—Comparison of simulated and measured head at Mason City, Iowa, and Moline, Ill.

flowing, thus requiring them to be pumped. During this period, the head probably declined several tens of feet. The quantity of this flow is not recorded in the inventory of ground-water use, and its omission from the model probably contributes to the discrepancy in head difference in the area along the river.

TRANSIENT WATER BUDGET

As illustrated by the transient simulation, the regional steady-state ground-water flow system has been altered by the extensive pumping of ground water. In response to the pumping, water levels declined, ground water was released from storage, and ground-water movement that previously was toward streams or through confining units has been diverted into the expanding cones of depression. As a result, some parts of the simulated transient ground-water budget are very different from the simulated steady-state ground-water budget (fig.

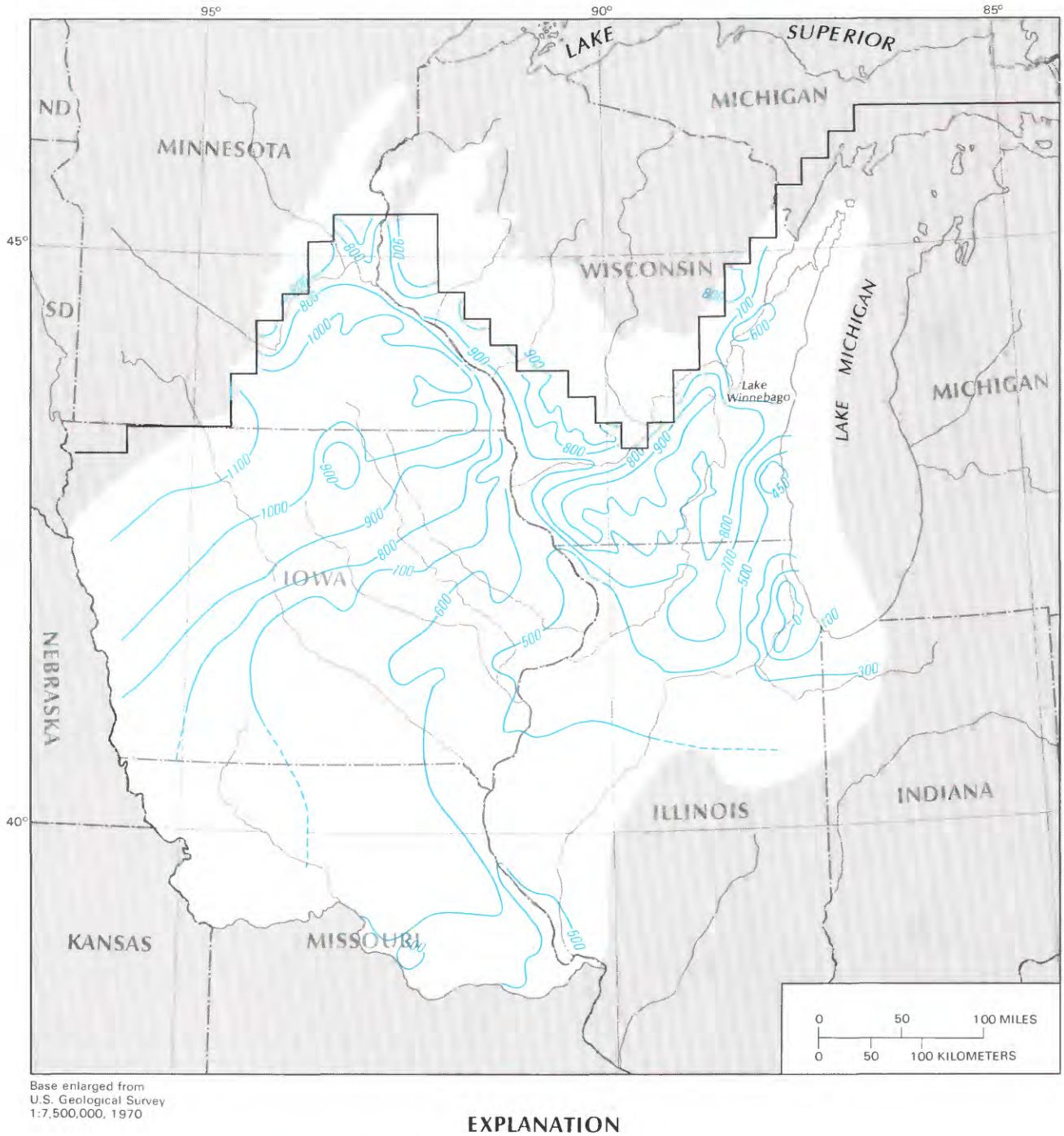

FIGURE 36.—Generalized observed potentiometric surface for the St. Peter-Prairie du Chien-Jordan aquifer (layer 3), 1980.

31). Figure 37 summarizes the simulated inflow and outflow for the period 1976–80. For this simulation period, an average of 1,208 ft^3/s (781 Mgal/d) of ground water was pumped from the Cambrian-Ordovician aquifer system and the Silurian-Devonian aquifer. Simulated direct recharge to aquifer layers 1 through 4 from the

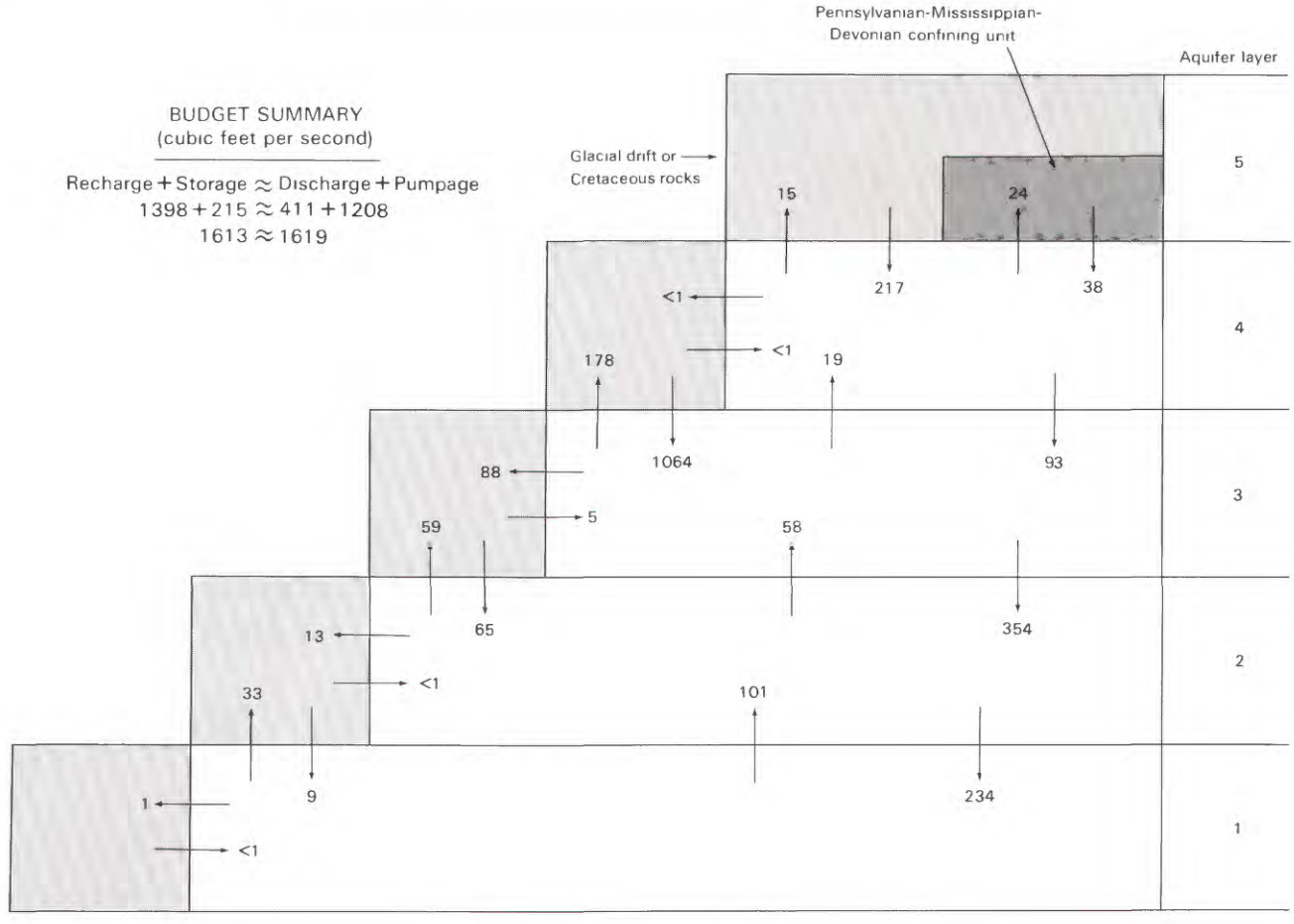

EXPLANATION

217 — SIMULATED FLUX BETWEEN CONSTANT-HEAD NODES AND ADJACENT ACTIVE AQUIFER LAYER NODES—Arrow shows direction of flow between constant-head nodes (shaded) and aquifer layers 1 through 4. Number is sum of fluxes, in cubic feet per second

65 — SIMULATED FLUX BETWEEN ADJACENT ACTIVE AQUIFER LAYER NODES—Arrow shows direction of flow between aquifer layers 1 through 4. Number is sum of fluxes, in cubic feet per second

38 — SIMULATED FLUX BETWEEN CONFINING LAYER 4-5 (SHADED) AND AQUIFER LAYER 4—Arrow shows direction of flow. Number is sum of fluxes, in cubic feet per second

FIGURE 37.—Simulated transient regional ground-water budget, 1976–80.

overlying glacial drift or Cretaceous rocks increased from the steady-state rates to 9, 65, 1,064, and 217 ft^3/s, or 0.03, 0.08, 0.45, and 0.08 in/yr, respectively. These values are less than 1.5 percent of the average annual precipitation rate of about 30 in/yr. Guswa and others (1982) estimate that in the Twin Cities area of Minnesota, less than 10 percent of the annual precipitation recharges the glacial drift. The proportion of this recharge that, in turn, reaches the deep aquifer system is undoubtedly much less. Walton (1962) estimated recharge to the Cambrian-Ordovician aquifer system to be less than 0.4 in/yr for northeastern Illinois. Simulated lateral inflow from the glacial drift or Cretaceous rocks along the fringes of the subcrop area is essentially the same, more than 5 ft^3/s. The average simulated rate of leakage for 1976–80 through confining layer 3–4, consisting of the Maquoketa Shale and the underlying Galena Dolomite and Decorah and Platteville Formations, is less than 0.01 to 0.02 in/yr in northeastern Illinois and southeastern Wisconsin. Walton (1960, 1962) estimated leakage through the Maquoketa Shale to be 0.03 to 0.04 in/yr. In addition, simulated leakage to the Silurian-Devonian

aquifer (layer 4) from overlying bedrock units increased slightly to 38 ft^3/s, or 0.005 in/yr. Total recharge, including leakage, increased to 1,398 ft^3/s. Water released from aquifer storage is 215 ft^3/s. Discharge to overlying rivers and streams from aquifer layers 1 through 4 decreased to 33, 59, 178, and 15 ft^3/s, or 0.10, 0.10, 0.23, and 0.02 in/yr, respectively. Simulated lateral discharge to dissecting rivers and streams decreased slightly to 1, 13, and 88 ft^3/s, respectively, for aquifer layers 1 through 3. Leakage from the Silurian-Devonian aquifer to the overlying rocks of Devonian, Pennsylvanian, and Mississippian age decreased to 24 ft^3/s, or 0.005 in/yr. Simulated natural discharge totals 411 ft^3/s; thus, total discharge, including pumpage (1,208 ft^3/s), is 1,619 ft^3/s. The small difference in the budget may be due to errors in accounting for the various sources of recharge or discharge or to accumulated errors in the model representation of the flow system.

SUMMARY AND CONCLUSIONS

The Cambrian-Ordovician aquifer system is the principal source of ground water in the northern Midwest of the United States. This sequence of sandstones, carbonates, and shales is confined over much of the area by the Maquoketa Shale of Ordovician age. Throughout parts of central Minnesota, Wisconsin, and north-central Illinois, the Cambrian-Ordovician aquifer system functions as an unconfined to partially confined aquifer system. Prior to extensive ground-water development, wells drilled into deeper, buried aquifers produced flowing wells. These were generally along the Mississippi and Missouri Rivers and their tributaries and along Lake Michigan. Groundwater development, which began in the mid-1860's, has resulted in as much as 900 ft of decline in the potentiometric surface in the Chicago metropolitan area. Less drawdown has occurred in other parts of the study area, notably Milwaukee, Minneapolis-St. Paul, central and eastern Iowa, and central Missouri. At present, heads are still large enough to support flowing wells along the Mississippi River, but in most other areas pumping has lowered the head to below land surface.

To investigate the nature of ground-water flow in these aquifers, a quasi-three-dimensional ground-water flow model was developed. The Trescott (1975) computer code was used and modified to simulate wells that are open to several different aquifer layers. Without this modification, estimates of the contribution of individual aquifer layers to total well discharge must be made prior to simulation. With the multiaquifer well modification, only total well discharge is required. In addition, comparison with multiaquifer water-level measurements are made possible. No detailed analysis of the effect of multiaquifer wells on the regional flow system was made because of the large size of the finite-difference blocks and uncertainties in pumping rates, number of wells, and number of aquifer layers penetrated. A detailed analysis of the effect of multiaquifer wells would be desirable as part of a small-scale study where pumping rates, number of wells, and number of aquifer layers penetrated are known with more certainty.

Another modification to the Trescott code allows simulation of ground-water flow in areas where groundwater density varies. This modification was made primarily to simulate the effects of the brines on the regional flow system near the boundary where brines and relatively fresh water coexist. The model results indicate that areas of high ground-water density are partial barriers to fresh ground-water flow and that ground water moves throughout these areas at low rates of flow.

The flow model was calibrated by comparing field-observed predevelopment heads with simulated heads, wherever possible, and by comparing measured head declines with simulated head declines. Model parameters, such as aquifer hydraulic conductivity, vertical hydraulic conductivity of confining units, and aquifer storage coefficient, were adjusted to produce a reasonable match between the measured and simulated data.

Simulated steady-state conditions indicate that the aquifer system is recharged in much of Wisconsin, southeastern Minnesota, northwestern Iowa, northern Illinois, and central Missouri. Much of the water in the aquifer system discharges locally to rivers and streams where the aquifer system is fully or partially unconfined. Regionally, ground water flows to the east and southeast from southeastern Wisconsin and northeastern Illinois, southerly from south-central Wisconsin and north-central Illinois, toward the Mississippi River from western Wisconsin, southeastern Minnesota, and northeastern Iowa, toward the Mississippi River or its confluence with the Missouri River from western Iowa and Illinois, and westerly from western Indiana. Overall, the configuration of the constant-head water table, overlying the aquifers, has a major influence on the regional flow patterns, especially on the shallower parts of the system. The principal regional discharge areas are the Mississippi and Missouri Rivers, the Illinois basin, and Lake Michigan.

The root mean square of the differences between the observed predevelopment and simulated steady-state heads for the St. Peter-Prairie du Chien-Jordan aquifer (layer 3) is 36 ft, with 55 percent of the nodes having differences of less than 25 ft. For the Silurian-Devonian aquifer (layer 4), the root mean square of the difference is 44 ft, with 40 percent of the nodes having differences of less than 25 ft. A comparison of the simulated potentiometric surface for the Mount Simon aquifer (layer 1) with measured head data obtained either from the Mount

Simon aquifer alone or from the combined Mount Simon and Ironton-Galesville aquifers indicates that the fit is generally good. The root mean square of the differences for the Mount Simon aquifer is 53 ft, with 42 percent of the nodes having differences of 25 ft or less.

Steady-state simulation indicates that predevelopment recharge from the overlying glacial drift or Cretaceous rocks to aquifer layers 1, 2, 3, and 4 was approximately 8, 47, 445, and 42 ft^3/s, or 0.03, 0.06, 0.24, and 0.02 in/yr, respectively. Much of the recharge discharges locally to overlying streams or to the glacial drift and Cretaceous rocks. This discharge amounts to 44, 75, 275, and 30 ft^3/s, or 0.13, 0.12, 0.21, and 0.02 in/yr, from aquifer layers 1, 2, 3, and 4, respectively. Simulated lateral discharge to rivers that dissect aquifer layers is 1, 14, and 95 ft^3/s from aquifer layers 1, 2, and 3, respectively. Total simulated recharge is 571 ft^3/s, balanced by an equivalent simulated discharge rate.

Simulated transient conditions show the superposition of large areas of water-level decline on the regional steady-state flow system. As a result of the extensive development, ground water that previously would have discharged to rivers, or to overlying aquifers by leakage through confining units, is intercepted by these large cones of depression. In addition to the regular recharge in areas shown by the steady-state simulation, recharge also is induced over much of Iowa, eastern Wisconsin, northeastern Illinois, and north-central Missouri because of increased or reversed head gradients.

The validity of the flow model also is supported by the transient simulation for the period 1861–1980. Simulated drawdown to 1980 compares well with observed drawdown. In a comparison of the simulated and observed 1980 potentiometric surfaces for aquifer layer 3, the root mean square difference is 63 ft, with 40 percent of the nodes having a difference of less than 25 ft. The largest differences are along the Mississippi River. A possible explanation for the difference could be the discharge from a large number of flowing wells from the late 1800's and early 1900's, which was not accounted for in the water-use inventory or in the simulations. Head gradients under pumping conditions may be relatively steep, especially near major pumping centers, causing a wide range in measured heads over a 16-mi node. Although simulated heads are higher than most measured heads within a given node, the simulated decline follows the general trend of the observed decline.

For the 1976–80 simulation period, recharge increased to 9, 65, 1,064, and 217 ft^3/s, or 0.03, 0.08, 0.45, and 0.08 in/yr, for aquifer layers 1, 2, 3, and 4, respectively. Simulated total recharge averaged 1,398 ft^3/s for 1976–80. The increase in recharge can be attributed to steeper hydraulic gradients near recharging areas than those in the steady-state simulation, or to a reduction in natural discharge from the aquifer layers. Simulated discharge to overlying streams and the glacial drift decreased to 33, 59, 178, and 15 ft^3/s, or 0.10, 0.10, 0.23, and 0.02 in/yr, for aquifer layers 1, 2, 3, and 4, respectively. Lateral discharge to dissecting rivers and streams decreased slightly, to 1, 13, and 88 ft^3/s for aquifer layers 1, 2, and 3, respectively. Discharge totals 1,619 ft^3/s, of which pumpage is 1,208 ft^3/s. Total discharge exceeds recharge, and therefore water levels are lower. Release from aquifer storage is 215 ft^3/s.

How well the regional model depicts flow conditions in the Cambrian-Ordovician aquifer system depends on how well the aquifer system is described mathematically, how it is discretized, and how accurately its hydraulic properties are estimated. The flow equation derived for this study describes lateral flow in aquifers in which ground-water density is spatially variable but time invariant and vertical flow to and from aquifers occurs through confining units and through multiaquifer wells. The flow equation does not accurately portray flow conditions where (1) flow in aquifers is not strictly lateral, such as near partially penetrating wells or streams, (2) flow in confining units is not strictly vertical, such as where confining units may be modest aquifers and horizontal hydraulic conductivity exceeds vertical hydraulic conductivity, and (3) movement of saline water has occurred. In particular, storage in the confining units is neglected. Therefore, some error in the simulation can be expected.

The Cambrian-Ordovician and Silurian-Devonian aquifers were discretized, vertically and horizontally, according to the finite-difference form of the flow equation. Adjacent geologic formations having similar hydraulic properties were combined into either aquifer layers or confining layers. The layering scheme was determined primarily on the basis of geology in the northern part of the study area. To the south, in most of Missouri, central and southern Illinois, and Indiana, the equivalent rocks contain more carbonate and are generally less important as aquifers; thus, the layers have less validity in these areas. To depict the regional characteristics of the flow system, aquifer and confining layers were discretized areally into 16- ×16-mi finite-difference blocks. Within these blocks hydraulic properties were assumed to be constant. Consequently, any variability in hydraulic properties or in the characteristics of the flow system on a scale smaller than the regional scale was not simulated.

Values of hydraulic properties were varied during the calibration process until reasonably good results were obtained for both prepumping conditions (prior to 1861) and stressed conditions (through 1980). The final set of values used in the simulation is not unique in that other combinations of hydraulic properties could give generally similar results. They are, however, representative of the

type of rocks that make up the aquifer system (Davis and De Weist, 1966; Freeze and Cherry, 1979), are consistent with available field data, and generally depict the main features of the regional flow system and trends in water-level declines.

The steady-state and transient simulations indicate that the Cambrian-Ordovician rocks constitute a regionally continuous aquifer system. Flow patterns within aquifer layers are similar, as are the locations of recharge and discharge areas. Stresses within a confined aquifer layer propagate throughout that aquifer layer and to adjacent layers. Simulated drawdown due to large-scale regional pumping creates a series of coalescing drawdown cones in the confined aquifer system. The drawdown cone produced by one pumping center is superimposed on the cones of nearby pumping centers. This is especially evident in the simulated drawdown in aquifer layer 3 (fig. 34*C*). Pumping centers in Iowa interfere with one another, as do pumping centers throughout eastern Wisconsin and northeastern Illinois. Further simulations using ever-increasing pumping rates would show further broadening and deepening of the existing regional cones.

SELECTED REFERENCES

Ackermann, W.C., and others, 1974, Feasibility study on desalting brackish water from the Mt. Simon aquifer in northeastern Illinois: U.S. Department of the Interior, Office of Saline Water, Research and Development Progress Report No. 938, Illinois State Water Survey Contract Report 153, 120 p.

Bennett, G.D., 1979, Regional ground-water systems analyses: Water Spectrum, v. 11, no. 4, p. 36–42.

———1980, Research and model development related to the Regional Aquifer-System Analysis program: American Geophysical Union Transactions, EOS, v. 61, no. 46, p. 951.

Bennett, G.D., and Giusti, E.V., 1971, Coastal ground-water flow near Ponce, Puerto Rico: U.S. Geological Survey Professional Paper 750-D, p. D206–D211.

Bennett, G.D., Kontis, A.L., and Larson, S.P., 1982, Representation of multiaquifer well effects in three-dimensional ground-water flow simulation: Ground Water, v. 20, no. 3, p. 334–341.

Bond, D.C., 1972, Hydrodynamics in deep aquifers of the Illinois basin: Illinois State Geological Survey Circular 470, 72 p.

———1973, Deduction of flow patterns in variable-density aquifers from pressure and water-level observations: International Symposium on Underground Waste Management and Artificial Recharge, 2d, New Orleans, Sept. 26–30, 1973, Preprints, v. 1, p. 357–378.

Bond, D.C., and Cartwright, Keros, 1970, Pressure observations and water densities in aquifers and their relation to problems in gas storage: Journal of Petroleum Technology, v. 22, p. 1492–1498.

Boonstra, J., and de Ridder, N.A., 1981, Numerical modeling of groundwater basins: Wageningen, The Netherlands, International Institute for Land Reclamation and Improvement Publication 29, 226 p.

Bredehoeft, J.D., Blyth, C.R., White, W.A., and Maxey, G.B., 1963, A possible mechanism for the concentration of brines in subsurface formations: American Association of Petroleum Geologists Bulletin, v. 47, no. 2, p. 257–269.

Bredehoeft, J.D., Neuzil, C.E., and Milly, P.C.D., 1983, Regional flow in the Dakota aquifer: A study of the role of confining layers: U.S. Geological Survey Water-Supply Paper 2237, 45 p.

Bredehoeft, J.D., and Pinder, G.F., 1970, Digital analysis of areal flow in multiaquifer systems: A quasi three-dimensional model: Water Resources Research, v. 6, no. 3, p. 883–888.

Cartwright, Keros, 1970, Groundwater discharge in the Illinois basin as suggested by temperature anomalies: Water Resources Research, v. 6, no. 3, p. 912–918.

Cartwright, Keros, Hunt, C.S., Hughes, G.M., and Brower, R.D., 1979, Hydraulic potential in Lake Michigan bottom sediments, *in* Back, William, and Stephenson, D.A., eds., Contemporary hydrology: The George Burke Maxey Memorial Volume, Journal of Hydrology, v. 43, p. 67–78.

Chow, V.T., 1964, Handbook of applied hydrology: New York, McGraw-Hill, chap. 7, p. 4.

Clark, S.P., Jr., 1966, Handbook of physical constants: Geological Society of America Memoir 97 (rev. ed.), 587 p.

Clayton, R.N., Friedman, Irving, Graf, D.L., Mayeda, T.K., Meents, W.F., and Shimp, N.F., 1966, The origin of saline formation waters, I. Isotopic composition: Journal of Geophysical Research, v. 71, no. 16, p. 3869–3882.

Clifford, M.J., 1973, Hydrodynamics of Mount Simon Sandstone, Ohio and adjoining areas, *in* Braunstein, J., ed., Underground waste management and artificial recharge: International Symposium on Underground Waste Management and Artificial Recharge, 2d, New Orleans, Sept. 26–30, 1973, v. 1, p. 349–356.

Davis, R.W., 1973, Quality of near-surface waters in southern Illinois: Ground Water, v. 11, no. 1, p. 11–18.

Davis, S.N., 1969, Porosity and permeability of natural materials, *in* De Weist, R.J.M., ed., Flow through porous media: New York, Academic Press, p. 53–89.

Davis, S.N., and De Weist, R.J.M., 1966, Hydrogeology: New York, Wiley and Sons, 463 p.

Davis, T.M., and Kontis, A.L., 1970, Spline interpolation algorithms for track-type survey data with application to the computation of mean gravity anomalies: U.S. Naval Oceanographic Office Technical Report 226, 50 p.

De Weist, R.J.M., ed., 1969, Flow through porous media: New York, Academic Press, p. 70.

Emmons, P.J., 1987, An evaluation of the bedrock aquifer system in northeastern Wisconsin: U.S. Geological Survey Water-Resources Investigations Report 85–4199, 48 p.

Fatt, I., and Davis, D.H., 1952, Reduction in permeability with overburden pressure: American Institute of Mining and Metallurgical Engineers, Petroleum Transactions, v. 195, p. 329.

Faust, C.R., and Mercer, J.W., 1979, Geothermal reservoir simulation: 2. Numerical solution techniques for liquid- and vapor-dominated hydrothermal system: Water Resources Research, v. 5, no. 1, p. 31–46.

Flint, R.F., Colton, R.B., Goldthwaite, R.P., and Willman, H.B., 1959, Glacial map of the United States east of the Rocky Mountains: Geological Society of America map, scale 1:1,750,000, 2 sheets.

Foley, F.C., Walton, W.C., and Drescher, W.J., 1953, Ground-water conditions in the Milwaukee-Waukesha area, Wisconsin: U.S. Geological Survey Water-Supply Paper 1229, 96 p.

Freeze, R.A., 1972, Regionalization of hydrogeologic parameters for use in mathematical models of groundwater flow: International Geological Congress, 24th, Proceedings, section 11, p. 177–190.

Freeze, R.A., and Cherry, J.A., 1979, Groundwater: Englewood Cliffs, N.J., Prentice-Hall, p. 29.

Freeze, R.A., and Witherspoon, P.A., 1967, Theoretical analysis of regional groundwater flow: 2. Effect of water table configuration

and subsurface permeability variation: Water Resources Research, v. 3, no. 2, p. 623–634.

Graf, D.L., Friedman, Irving, and Meents, W.F., 1965, The origin of saline formation waters, II: Isotopic fractionation by shale micropore systems: Illinois State Geological Survey Circular 393, 32 p.

Graf, D.L., Meents, W.F., Friedman, Irving, and Shimp, N.F., 1966, The origin of saline formation waters, III: Calcium chloride waters: Illinois State Geological Survey Circular 397, 60 p.

Guswa, J.H., Siegel, D.I., and Gillies, D.C., 1982, Preliminary evaluation of the ground-water flow system in the Twin Cities metropolitan area, Minnesota: U.S. Geological Survey Water-Resources Investigations 82–44, 65 p.

Hadley, D.W., and Pelham, J.H., 1976, Glacial deposits of Wisconsin, Sand and gravel potential: Wisconsin Geological and Natural History Survey map, scale 1:500,000.

Hansen, R.E., 1970, Geology and ground-water resources of Linn County, Iowa: Iowa Geological Survey Water-Supply Bulletin 10, 66 p.

Hershey, H.G., Wahl, K.D., and Steinhilber, W.L., 1970, Geology and ground-water resources of Cerro Gordo County, Iowa: Iowa Geological Survey Water-Supply Bulletin 9, 75 p.

Hobbs, H.C., and Goebel, J.E., 1982, Geologic map of Minnesota, Quaternary geology: Minnesota Geological Survey map, series S-1, scale 1:500,000.

Horick, P.J., and Steinhilber, W.L., 1978, Jordon aquifer of Iowa: Iowa Geological Survey Miscellaneous Map Series 6, 3 sheets.

Imes, J.L., 1985, The ground-water flow system in northern Missouri, with emphasis on the Cambrian-Ordovician aquifer: U.S. Geological Survey Professional Paper 1305, 61 p.

Kontis, A.L., and Mandle, R.J., 1980, Data-base system for Northern Midwest Regional Aquifer-System Analysis: U.S. Geological Survey Water-Resources Investigations Report 80–104, 23 p.

———1989, Modification of a three-dimensional ground-water flow model to account for variable water density and effects of multiaquifer wells: U.S. Geological Survey Water-Resources Investigations Report 87–4265.

Krohelski, J.T., 1986, Hydrogeology and ground-water use and quality, Brown County, Wisconsin, *with a section on* Bedrock geology by B.A. Brown: Wisconsin Geological and Natural History Survey Information Circular 57, 42 p.

Kuiper, L.K., 1983, A numerical procedure for the solution of the steady state variable density groundwater flow equation: Water Resources Research, v. 19, no. 1, p. 234–240.

Law, Jan, 1944, A statistical approach to the interstitial heterogeneity of sand reservoirs: American Institute of Mining and Metallurgical Engineers Transactions, Petroleum Division, v. 155, p. 202–222.

Lohman, S.W., 1972, Ground-water hydraulics: U.S. Geological Survey Professional Paper 708, 70 p.

Matthews, C.S., and Russell, D.G., 1967, Pressure buildup and flow tests in wells: Society of Petroleum Engineers of American Institute of Mining and Metallurgical Engineers, p. 158.

McDonald, M.G., and Harbaugh, A.W., 1983, A modular three-dimensional finite-difference ground-water flow model: U.S. Geological Survey Open-File Report 83–875, 528 p.

McLeod, R.S., 1975a, A digital-computer model for estimating drawdowns in the sandstone aquifer in Dane County, Wisconsin: Wisconsin Geological and Natural History Survey Information Circular 28, 91 p.

———1975b, A digital-computer model for estimating hydrologic changes in the aquifer system in Dane County, Wisconsin: Wisconsin Geological and Natural History Survey Information Circular 30, 40 p.

Meents, W.F., Bell, A.H., Rees, O.W., and Tilbury, W.G., 1952, Illinois oil field brines, their geologic occurrence and chemical composition: Illinois State Geological Survey, Illinois Petroleum 66, 38 p.

Mossler, J.H., 1983, Bedrock topography and isopachs of Cretaceous and Quaternary strata, east-central and southwestern Minnesota: Minnesota Geological Survey Miscellaneous Map Series M-42, 2 pls.

Norton, W.H., Hendrixson, W.S., Simpson, H.E., and Meinzer, O.E., and others, 1912, Underground water resources of Iowa: U.S. Geological Survey Water-Supply Paper 293, 994 p.

Norvitch, R.F., Ross, T.G., and Brietkrietz, Alex, 1973, Water resources outlook for the Minneapolis-St. Paul metropolitan area, Minnesota: Metropolitan Council of the Twin Cities Area, 219 p.

Pinder, G.F., and Bredehoeft, J.D., 1968, Application of the digital computer for aquifer evaluation: Water Resources Research, v. 4, no. 5, p. 1069–1093.

Piskin, Kemal, and Bergstrom, R.E., 1975, Glacial drift in Illinois: Thickness and character: Illinois State Geological Survey Circular 490, 35 p.

Potter, R.W., II, and Brown, D.L., 1977, The volumetric properties of aqueous sodium chloride solutions from 0° to 500° C at pressures up to 2000 bars based on a regression of available data in the literature: U.S. Geological Survey Bulletin 1421-C, 36 p.

Prickett, T.A., 1967, Designing pumped well characteristics into electric analog models: Ground Water, v. 5, p. 38–46.

Prickett, T.A., and Lonnquist, C.G., 1971, Selected digital computer techniques for groundwater resource evaluation: Illinois State Water Survey Bulletin 55, 62 p.

Siegel, D.I., 1989, Geochemistry of the Cambrian-Ordovician aquifer system in the northern Midwest, United States: U.S. Geological Survey Professional Paper 1405-D.

Steinhilber, W.L., and Horick, P.J., 1970, Ground-water resources of Iowa, *in* Horick, P.J., ed., Water resources of Iowa—A symposium: Cedar Falls, Iowa Academy of Science, p. 29–49.

Steinhilber, W.L., and Young, H.L., 1979, Plan of study for the Northern Midwest Regional Aquifer-System Analysis: U.S. Geological Survey Water-Resources Investigations 79–44, 20 p.

Suter, Max, Bergstrom, R.E., Smith, H.F., Emrich, G.H., Walton, W.C., and Larson, T.E., 1959, Preliminary report on groundwater resources of the Chicago region, Illinois: Illinois State Water Survey and Geological Survey Cooperative Groundwater Report 1, 89 p.

Theis, C.V., Brown, R.H., and Meyer, R.R., 1963, Estimating the transmissibility of aquifers from the specific capacity of a well, *in* Bentall, Ray, comp., Methods of determining permeability, transmissibility, and drawdown: U.S. Geological Survey Water-Supply Paper 1536-I, p. 331–341.

Trescott, P.C., 1975, Documentation of finite-difference model for simulation of three-dimensional ground-water flow: U.S. Geological Survey Open-File Report 75–438, 32 p.

Trescott, P.C., and Larson, S.P., 1976, Documentation of finite-difference model for simulation of three-dimensional ground-water flow, Supplement to Open-File Report 75–438: U.S. Geological Survey Open-File Report 76–591, 21 p.

Trotta, L.C., and Cotter, R.D., 1973, Depth to bedrock in Wisconsin: Wisconsin Geological and Natural History Survey map, scale 1:1,000,000.

U.S. Geological Survey and Missouri Division of Geology and Land Survey, 1976, Mineral and water resources of Missouri: U.S. 90th Congress, 1st session, Senate Document 19, 399 p.

Visocky, A.P., 1982, Impact of Lake Michigan allocations on the Cambrian-Ordovician aquifer system: Illinois State Water Survey Contract Report 292, 36 p.

Walton, W.C., 1960, Leaky artesian aquifer conditions in Illinois: Illinois State Water Survey Report of Investigations 39, 27 p.

———1962, Ground-water recharge and runoff in Illinois: Illinois State Water Survey Report of Investigations 48, 55 p.

Walton, W.C., and Csallany, S.C., 1962, Yields of deep sandstone wells in northern Illinois: Illinois State Water Survey Report of Investigations 43, 47 p.

Warren, J.E., Skiba, F.F., and Price, H.S., 1961, An evaluation of the significance of permeability measurements: Journal of Petroleum Technology, v. 13, p. 739–744.

Wattenbarger, R.A., and Thurnau, D.H., 1976, Application of SSOR to three-dimensional reservoir problems: Paper presented at Symposium on Numerical Simulation of Reservoir Performance, Society of Petroleum Engineers of American Institute of Mining and Metallurgical Engineers, 4th, Los Angeles, February 19–20, 1976.

Weidman, Samuel, and Schultz, A.R., 1915, The underground and surface water supplies of Wisconsin: Wisconsin Geological and Natural History Survey Bulletin 35, 664 p.

Weiss, E.J., 1982a, A computer program for calculating relative-transmissivity input arrays to aid model calibration: U.S. Geological Survey Open-File Report 82–447, 22 p.

———1982b, A model for the simulation of flow of variable-density ground water in three dimensions under steady-state conditions: U.S. Geological Survey Open-File Report 82–352, 66 p.

Young, H.L., 1976, Digital-computer model of the sandstone aquifer in southeastern Wisconsin: Waukesha, Southeastern Wisconsin Regional Planning Commission Technical Report 16, 42 p.

———in press, Hydrogeology of the Cambrian-Ordovician aquifer system in the northern Midwest, United States: U.S. Geological Survey Professional Paper 1405-B.

SELECTED SERIES OF U.S. GEOLOGICAL SURVEY PUBLICATIONS

Periodicals

Earthquakes & Volcanoes (issued bimonthly).
Preliminary Determination of Epicenters (issued monthly).

Technical Books and Reports

Professional Papers are mainly comprehensive scientific reports of wide and lasting interest and importance to professional scientists and engineers. Included are reports on the results of resource studies and of topographic, hydrologic, and geologic investigations. They also include collections of related papers addressing different aspects of a single scientific topic.

Bulletins contain significant data and interpretations that are of lasting scientific interest but are generally more limited in scope or geographic coverage than Professional Papers. They include the results of resource studies and of geologic and topographic investigations, as well as collections of short papers related to a specific topic.

Water-Supply Papers are comprehensive reports that present significant interpretive results of hydrologic investigations of wide interest to professional geologists, hydrologists, and engineers. The series covers investigations in all phases of hydrology, including hydrogeology, availability of water, quality of water, and use of water.

Circulars present administrative information or important scientific information of wide popular interest in a format designed for distribution at no cost to the public. Information is usually of short-term interest.

Water-Resources Investigations Reports are papers of an interpretive nature made available to the public outside the formal USGS publications series. Copies are reproduced on request unlike formal USGS publications, and they are also available for public inspection at depositories indicated in USGS catalogs.

Open-File Reports include unpublished manuscript reports, maps, and other material that are made available for public consultation at depositories. They are a nonpermanent form of publication that may be cited in other publications as sources of information.

Maps

Geologic Quadrangle Maps are multicolor geologic maps on topographic bases in 7.5- or 15-minute quadrangle formats (scales mainly 1:24,000 or 1:62,500) showing bedrock, surficial, or engineering geology. Maps generally include brief texts; some maps include structure and columnar sections only.

Geophysical Investigations Maps are on topographic or planimetric bases at various scales; they show results of surveys using geophysical techniques, such as gravity, magnetic, seismic, or radioactivity, which reflect subsurface structures that are of economic or geologic significance. Many maps include correlations with the geology.

Miscellaneous Investigations Series Maps are on planimetric or topographic bases of regular and irregular areas at various scales; they present a wide variety of format and subject matter. The series also includes 7.5-minute quadrangle photogeologic maps on planimetric bases that show geology as interpreted from aerial photographs. Series also includes maps of Mars and the Moon.

Coal Investigations Maps are geologic maps on topographic or planimetric bases at various scales showing bedrock or surficial geology, stratigraphy, and structural relations in certain coal-resource areas.

Oil and Gas Investigations Charts show stratigraphic information for certain oil and gas fields and other areas having petroleum potential.

Miscellaneous Field Studies Maps are multicolor or black-and-white maps on topographic or planimetric bases for quadrangle or irregular areas at various scales. Pre-1971 maps show bedrock geology in relation to specific mining or mineral-deposit problems; post-1971 maps are primarily black-and-white maps on various subjects such as environmental studies or wilderness mineral investigations.

Hydrologic Investigations Atlases are multicolored or black-and-white maps on topographic or planimetric bases presenting a wide range of geohydrologic data of both regular and irregular areas; principal scale is 1:24,000, and regional studies are at 1:250,000 scale or smaller.

Catalogs

Permanent catalogs, as well as some others, giving comprehensive listings of U.S. Geological Survey publications are available under the conditions indicated below from the U.S. Geological Survey, Book and Open-File Report Sales, Federal Center, Box 25425, Denver, CO 80225. (See latest Price and Availability List.)

"Publications of the Geological Survey, 1879–1961" may be purchased by mail and over the counter in paperback book form and as a set of microfiche.

"Publications of the Geological Survey, 1962–1970" may be purchased by mail and over the counter in paperback book form and as a set of microfiche.

"Publications of the U.S. Geological Survey, 1971–1981" may be purchased by mail and over the counter in paperback book form (two volumes, publications listing and index) and as a set of microfiche.

Supplements for 1982, 1983, 1984, 1985, 1986, and for subsequent years since the last permanent catalog may be purchased by mail and over the counter in paperback book form.

State catalogs, "List of U.S. Geological Survey Geologic and Water-Supply Reports and Maps For (State)," may be purchased by mail and over the counter in paperback booklet form only.

"Price and Availability List of U.S. Geological Survey Publications," issued annually, is available free of charge in paperback booklet form only.

Selected copies of a monthly catalog "New Publications of the U.S. Geological Survey" are available free of charge by mail or may be obtained over the counter in paperback booklet form only. Those wishing a free subscription to the monthly catalog "New Publications of the U.S. Geological Survey" should write to the U.S. Geological Survey, 582 National Center, Reston, VA 22092.

Note. Prices of Government publications listed in older catalogs, announcements, and publications may be incorrect. Therefore, the prices charged may differ from the prices in catalogs, announcements, and publications.